



MONASH University

**Identifying the immune function of NgR in EAE
and multiple sclerosis**

Maha Bakhuraysah

A thesis submitted for the degree of

Doctor of Philosophy

Central Clinical School

Faculty of Medicine, Nursing and Health Sciences

Monash University

June 2016

Copyright notice

© The author (2016). Except as provided in the Copyright Act 1968, this thesis may not be reproduced in any form without the written permission of the author.

Abstract

Despite clear evidence demonstrating that the deletion of Nogo-receptor 1 (NgR1) can protect against axonal degeneration and thus progression of experimental autoimmune encephalomyelitis (EAE), an immunological role for this receptor is yet to yield mechanistic evidence. However, recently NgR has been suggested as an alternate receptor for the B-cell activating factor (BAFF) in the central nervous system (CNS). Therefore our strategic aim was to define whether NgR contributes in the modulation of the adaptive immune response during EAE by promoting maturation and differentiation of BAFF-reactive B-cells within follicles that are localised within the CNS during the induction of disease. The results showed that CNS-infiltrating blood cells revealed an augmented response in the B-cell populations, which expressed NgR1 and NgR3, observed in *ngr1^{+/+}* mice with the onset and progression of the disease that could not be demonstrated within the spinal cords of EAE-induced *ngr1^{-/-}* mice. Remarkably, a cluster of B-cells-expressing NgR was present at the meninges of lumbosacral spinal cords of the *ngr1^{+/+}* EAE-induced mice at clinical score 1. Furthermore, there were significant increases of secreted immunoglobulins from these NgR1-expressing B-cells. Importantly, these cells could be directed into the synthesis phase of the cell cycle, after stimulating sorted cells by extracellular BAFF *in vitro*; however, when BAFF signalling was blocked using either rBAFF-R, or NgR1-Fc, or NgR3 peptides, the cells were observed to be into G0/G1 phase. As a consequence, when we blocked NgR1-ligand signalling using a novel hematopoietic stem cell-based delivery of a therapeutic protein, immune lineage-differentiated cells, including ZsGreen and fusion protein, were trafficking into the CNS

during acute EAE. Collectively, these data indicate that the existence of an inducible expression of NgR1 and NgR3 in specific immune lineage cells upon the induction of EAE, and that the follicular-like NgR1 and NgR3-positive B-cells in the meninges may play an active role during the induction of EAE. It is plausible that an alternate mechanism may be operative with BAFF playing a signalling role in the follicle like structures formed in the CNS of EAE mice, transduced through NgR1 and NgR3. Thus, our data reinforce the idea that blocking the interaction of BAFF and NgR1 and NgR3 may be vital for neuroprotection during inflammatory insults and this thesis presents a novel treatment paradigm, currently under investigation that may limit both adaptive immune response and neurodegenerative mechanisms during EAE.

General Declaration

I hereby declare that this thesis contains no material which has been accepted for the award of any other degree or diploma at any university or equivalent institution and that, to the best of my knowledge and belief, this thesis contains no material previously published or written by another person, except where due reference is made in the text of the thesis.

This thesis includes one original paper published in peer-reviewed journal. The core theme of the thesis is “ To identify the role of NgR in the maturation and differentiation of B-cells within the follicles that are localised within the central nervous system during neuroinflammation, exhibited in the animal model of multiple sclerosis, EAE”. The ideas, development and writing up of all the papers in the thesis was the principle responsibility of my self, the candidate, working within the Central Clinical School under the supervision of Dr. Steven Petratos.

In the case of chapter 1, my contribution to the work involved the following:

Thesis chapter	Publication title	Publication status*	Nature and extent (%) of students contribution
1	Hematopoietic stem cell transplantation for multiple sclerosis: is it a clinical reality?	Published	Key ideas and writing of article (85%)

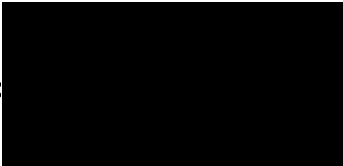
Student signature:



Date: 29/5/2016

The undersigned hereby certify that the above declaration correctly reflects the nature and extent of the student and co-authors' contributions to this work.

Main Supervisor signature:



Date: 29/5/2016

Acknowledgements

First and foremost, I would like to express my heartfelt gratitude to my supervisor, Dr. Steven Petratos, for his guidance, expertise, and unlimited support during the course of my PhD. I appreciate his inspiring suggestions for the developing of my project and thesis. I would also like to thank all of the staff of the Regenerative Neuroscience and Development Group for their suggestions, help and support, especially Sara Mokhtar, Amani Alrehaili. Also, I would like to thank Jae Lee, Melissa Biemond, Amani Alrehaili and Peimun Aui for their contributions in chapter 5 works. It is a pleasure to acknowledge Dr. William Figgett for his help and suggestions in BAFF work at chapter 4.

I would like to thank the School of Medicine at Taif University for providing me the opportunity to complete my PhD degree in Australia. I am deeply and forever indebted for their help and financial support throughout this project and through my entire studies in Australia.

I would like to thank my friends either in Saudi Arabia and Australia for helping me maintain a life and provided a wonderful environment. I sincerely appreciate their support and friendship.

Finally and most importantly, I am deeply and forever indebted to my gorgeous mother Enssaf, my husband Ahmed Alharbi, my kids Talia, Abdulmohsen, and a new baby girl, my sibling and all of my family members for their support, continues love, faith in me, and encouragement throughout my entire life. I dedicate this thesis to them, as my life would never be completed without you.

Table of contents

Abstract	3
General Declaration	5
Acknowledgements	7
List of Tables	12
List of Figures	13
List of Abbreviations	17
List of Publications and Presentations	21
Awards	25
CHAPTER 1: Literature Review	26
1.1 Multiple sclerosis	27
1.2 Immune-mediated mechanisms of MS/EAE	29
1.2.1. Mechanisms of Immune cell infiltration in MS/EAE	30
1.2.2. B-cell-dependent humoral immune mechanisms of MS/EAE	35
1.2.3. Localisation of B-cells in the CNS of MS	37
1.2.4. Mediators maintaining and attracting B-cells in MS	38
1.3 The role of MAIFs in EAE/MS	40
1.3.1. Nogo-A/NgR1 role in regulating the immune response in MS/EAE	46
1.4 BAFF and EAE	51
1.4.1 The influence of BAFF on T _{h17} -cells that aggravates EAE.....	51
1.4.2 Ability of BAFF antagonist to suppresses EAE.....	52
1.4.3 BAFF-R-deficient mice accelerate CNS autoimmunity	53
1.4.4 The effect of blocking BAFF with TACI-IgG in EAE	54
1.5 BAFF and MS	56
1.6 BAFF and NgR	58
1.7 Therapeutic approaches for MS	59
1.7.1 Hematopoietic stem cell transplantation (HSCT)	60
1.7.1.1 Isolation of HSCs.....	64

1.7.1.2	Cell surface markers of human and mice HSCs	66
1.7.1.3	HSCT in a mouse model of MS	70
1.7.1.4	HSCT as a therapeutic option for MS	72
1.7.1.5	Complications compared with the beneficial effects of HSCT in MS.....	80
1.7.1.6	Criteria to be considered in HSCT in MS patients	89
1.8	Conclusion	90
1.9	Research rationale, hypothesis and aims	92
CHAPTER 2: Methods.....		106
2.1	Mouse Breeding	111
2.2	Mouse Genotyping.....	111
2.3	Mouse EAE Induction and Clinical Assessment.....	113
2.4	Mouse Perfusion and Tissue processing	113
2.5	Isolation of immune cells and myelin from mouse tissues	114
2.5.1	Spleen and lymph node isolation.....	114
2.5.2	Spinal cord isolation.....	115
2.5.3	Myelin Isolation	116
2.6	Flow Cytometry.....	116
2.6.1	Single-labelled.....	116
2.6.2	Double-labelled.....	117
2.7	Immunohistochemistry analysis for mouse tissue.....	118
2.7.1	Paraffin sections.....	118
2.7.2	Frozen sections.....	120
2.7.3	Quantification of NgR and B-cell populations in the white matter tract of the lumbar and sacral spinal cord	121
2.7.4	Demyelination and axonal degeneration.....	122
2.8	Protein Biochemistry.....	123
2.8.1	Preparation of cell and tissue lysate for western blotting.....	123
2.8.2	Western immunoblotting.....	123
2.9	Cell Culture	125
2.10	Cell cycle analysis	125
2.11	ELISA	127
2.12	Transplantation of genetically modified hematopoietic stem cells (HSCs) 128	
2.12.1	NgR1 sub-cloning in pLVX-EF1 α -IRES-ZsGreen1	128

2.12.1	Transfection of 293T cells with pLVX-EF1 α -NgR(310)-Fc-IRES-ZsGreen1.....	129
2.12.2	Transduction of HeLa cells with LV-pLVX-EF1 α -NgR(310)-Fc-IRES-ZsGreen1 133	
2.12.3	Flow cytometric analysis of transduction of HeLa cells.....	133
2.12.4	Isolation of bone marrow and lineage negative enrichment.....	134
2.12.5	Transduction of HSCs and testing in culture	135
2.12.6	Transplantation of LV transduced HSCs in EAE	136
2.13	Statistics.....	138
CHAPTER 3: NgR expression on immune cells during CNS inflammation.....		139
3.1	Introduction	140
3.2	Results of EAE induced with MOG₃₅₋₅₅.....	141
3.2.1	<i>ngr1</i> ^{-/-} does alter the clinical course of MOG ₃₅₋₅₅ EAE.....	141
3.2.2	EAE Histopathology in the <i>ngr1</i> ^{+/+} and <i>ngr1</i> ^{-/-} mice.....	144
3.2.3	Isolation of immune cells from spleen, lymph node and spinal cord of <i>ngr1</i> ^{+/+} and <i>ngr1</i> ^{-/-} mice following EAE induction with MOG ₃₅₋₅₅	147
3.3	Results of EAE induced with rMOG immunisation.	161
3.3.1	<i>ngr1</i> ^{-/-} mice do not display an altered clinical course during rMOG-induced EAE 161	
3.3.2	Isolation of immune cells from spleen, lymph node and the spinal cord of <i>ngr1</i> ^{+/+} and <i>ngr1</i> ^{-/-} mice following EAE induction with rMOG	165
3.4	Preparation of tissue lysates for western blotting to identify NgR homologues in spleen, lymph nodes and spinal cord of <i>ngr1</i>^{+/+} and <i>ngr1</i>^{-/-} mice	175
3.5	Immunohistochemistry of NgR-positive B-cells in <i>ngr1</i>^{+/+} and <i>ngr1</i>^{-/-} spinal cord sections.....	180
3.5.1	Quantification of NgR-positive B-cells for <i>ngr1</i> ^{+/+} and <i>ngr1</i> ^{-/-} mice during EAE 195	
3.6	Co-localisation of Troy with NgR in B-cell infiltrate within spinal cord and optic nerve tissues at the disease onset during <i>ngr1</i>^{+/+} EAE-induced	198
3.7	Immune-phenotyping of cellular infiltrates expressing NgR1 during EAE in <i>ngr1</i>^{+/+} mice at clinical score 1.....	207
3.8	Discussion.....	213
CHAPTER 4: BAFF as an alternate ligand for NgR during the induction of EAE		217
4.1	Introduction	218

4.2	Expression of NgR and BAFF in the spinal cord tissue of <i>ngr1^{+/+}</i> EAE-induced mice at clinical score 1	220
4.3	Expression of BAFF-R and NgR on immune cells in the spleen.....	227
4.4	BAFF may play a role in stimulating B-cells that express NgR1 and NgR3 during the disease onset of EAE	232
4.5	Phenotype of immune cells from spleen and spinal cord isolates, during EAE at clinical score 1.....	244
4.5.1	The immunoglobulin response in isolated cells measured by ELISA	244
4.5.2	The immunoglobulin localisation detected by IHC.....	248
4.5.3	The immunoglobulin response against myelin.....	260
4.6	Discussion.....	263
CHAPTER 5: Transplantation of genetically modified HSCs to deliver the therapeutic NgR(310)-Fc protein into the active demyelinating lesion.....		268
5.1	Introduction.....	269
5.2	Production of lentivirus.....	273
5.3	Lineage negative enrichment of bone marrow cells	276
5.4	Transduction of lineage negative bone marrow cells with lentiviral vector	279
5.5	Confirmation of NgR(310)ecto-Fc protein production upon pLVX-EF1 α NgR(310)-Fc-myc-IRES-ZsGreen1 transfection	284
5.6	Transplantation of genetically manipulated HSCs to deliver therapeutic protein	287
5.7	Induce EAE post-transplantation.....	291
5.8	Peripheral localisation of vector-positive lineage differentiated cells.....	294
5.9	Infiltration of vector-positive lineage cells in the CNS post-EAE.....	300
5.10	Discussion	311
CHAPTER 6: Discussion.....		319
References.....		330
Appendix 1.....		346
Appendix 2.....		348

List of Tables

Table 1. Surface profile of HSCs in mouse and human.....	67
Table 2. Main markers used to discriminate mouse and human HSCs	68
Table 3. Antibodies and reagents used in experiments outlined in this thesis.	107
Table 4. Genotyping primers.	112
Table 5. Effect of deleting the <i>ngr1</i> gene on clinical course of MOG ₃₅₋₅₅ EAE.....	141
Table 6. Effect of deleting the <i>ngr1</i> gene on clinical course of rMOG EAE.	162
Table 7. Spinal cord section from <i>ngr1</i> ^{+/+} and <i>ngr1</i> ^{-/-} mice.....	195
Table 8. Reagents and their preparations.....	346
Table 9. rMOG purification.	348

List of Figures

Figure 1. Infiltration of immune cells into the CNS.	34
Figure 2. Nogo protein structure.	43
Figure 3. NgR signalling mechanism.	45
Figure 4. BlyS/BAFF signalling mechanism.	50
Figure 5. Hematopoietic hierarchy model.	63
Figure 6. The experimental procedure of bone marrow transplantation in EAE mice.	75
Figure 7. Autologous hematopoietic stem cell transplantation in multiple sclerosis patients.	77
Figure 8. Lentiviral vector production.	132
Figure 9. Significant delay in EAE onset and reduce in severity for the <i>ngr1</i> ^{-/-} mice.	143
Figure 10. The severity of demyelination and axonal injury reduced in the spinal cord of <i>ngr1</i> ^{-/-} EAE mice.	146
Figure 11. Flow cytometric analysis of single cell suspension from the spleen, lymph nodes and spinal cord of EAE-induced mice with MOG35-55 comparing to naive <i>ngr1</i> ^{+/+} and <i>ngr1</i> ^{-/-} mice, and adjuvant control.	151
Figure 12 Immune lineage cells that were immune-positive for NgR in the spleen, of <i>ngr1</i> ^{+/+} and <i>ngr1</i> ^{-/-} mice during the induction and course of EAE. B-cells, with NgR3 increased significantly in <i>ngr1</i> ^{+/+} mice at the disease progression and there was a significant increase of T-cell positive for NgR in <i>ngr1</i> ^{-/-} mice.	156
Figure 13. Flow cytometric analysis of double-cell suspension from the lymph nodes of <i>ngr1</i> ^{+/+} and <i>ngr1</i> ^{-/-} mice.	158
Figure 14. Double-staining of immune cells with NgR from the spinal cord of <i>ngr1</i> ^{+/+} and <i>ngr1</i> ^{-/-} mice.	160
Figure 15. Significant delay in EAE onset and reduce in severity for the <i>ngr1</i> ^{-/-} mice.	164
Figure 16. Flow cytometric analysis of single cell suspension from the spleen, lymph nodes and spinal cord of EAE-induced mice with rMOG comparing to naïve <i>ngr1</i> ^{+/+} and <i>ngr1</i> ^{-/-} mice.	167

Figure 17. Immune lineage cells that were immunopositive for NgR in the spleen, of <i>ngr1</i> ^{+/+} and <i>ngr1</i> ^{-/-} mice during the induction and course of EAE.....	170
Figure 18. Flow cytometric analysis of double-cell suspension from the lymph nodes of <i>ngr1</i> ^{+/+} and <i>ngr1</i> ^{-/-} mice.	172
Figure 19. Double-staining of immune cells with NgR from the spinal cord of <i>ngr1</i> ^{+/+} and <i>ngr1</i> ^{-/-} mice.	174
Figure 20. Western blot for the spleen, lymph nodes of naïve <i>ngr1</i> ^{+/+} and <i>ngr1</i> ^{-/-} mice.	177
Figure 21. Preparation of tissue lysates for western blotting to identify NgR homologues in the spleen and spinal cord of <i>ngr1</i> ^{+/+} and <i>ngr1</i> ^{-/-} mice.....	179
Figure 22. Double-immunostaining on the spinal cord tissue of <i>ngr1</i> ^{+/+} mice.....	184
Figure 23. Localisation of double-immunofluorescence staining (NgR1-positive B-cell clusters) on 10 µm-thick longitudinal spinal cord sections during EAE in <i>ngr1</i> ^{+/+} EAE-induced mice at clinical score 1.	186
Figure 24. A cluster of B-cell infiltrate expressing NgR around <i>ngr1</i> ^{+/+} mice blood vessel at clinical score 1 of EAE <i>ngr1</i> ^{+/+} mice.....	188
Figure 25. A massive neuroinflammation lesion appears in the chronic stage of disease in EAE-induced <i>ngr1</i> ^{+/+} mice.....	190
Figure 26. Double-staining on the spinal cord tissue of <i>ngr1</i> ^{-/-} mice.....	192
Figure 27. B-cells-positive either NgR1 or its homologues in the spleen, lymph nodes and spinal cord of <i>ngr1</i> ^{+/+} at the clinical score 1.....	194
Figure 28. Increased severity of EAE MOG ₃₅₋₅₅ peptide in <i>ngr1</i> ^{+/+} mice at the disease onset and reduced in <i>ngr1</i> ^{-/-} mice.	197
Figure 29. Expression of TROY on B-cells during <i>ngr1</i> ^{+/+} EAE-induced within spinal cord tissues at the disease onset.....	200
Figure 30. Co-localisation of TROY on B-cells during <i>ngr1</i> ^{+/+} EAE-induced within the optic nerve tissues at the clinical score 1.....	202
Figure 31. Co-localisation of TROY with NgR during <i>ngr1</i> ^{+/+} EAE-induced in immune cell infiltrates within optic nerve tissues at the disease onset.....	204
Figure 32. Co-localisation of TROY with NgR3 during <i>ngr1</i> ^{+/+} EAE-induced in immune cell infiltrates within the spinal cord tissues at the disease onset.....	206

Figure 33. Phenotype of B-cells that were immunopositive for NgR1 from the spinal cord EAE-induced at the disease onset.	210
Figure 34. Phenotype of B-cells and NgR double-positive populations from <i>ngr1</i> ^{+/+} EAE-induced at clinical score 1.	212
Figure 35. Expression of NgR in conjunction with BAFF in <i>ngr1</i> ^{+/+} EAE-induced mice at the clinical score 1.	222
Figure 36. Expression of either NgR in conjunction with BAFF or B-cells in follicles of <i>ngr1</i> ^{+/+} EAE-induced spleen at the clinical score 1.	224
Figure 37. Expression of BAFF in conjunction with NgR3 on immune cells in <i>ngr1</i> ^{+/+} EAE-induced at the clinical score 1.	226
Figure 38. Expression of BAFF-R and NgR on immune cells in the spinal cord of <i>ngr1</i> ^{+/+} EAE-induced mice at the clinical score 1.	229
Figure 39. Expression of BAFF-R and NgR on immune cells within follicle in the spleen.	231
Figure 40. The number of B-cells expressing NgR1 and NgR3 from either spleen or spinal cord of EAE mice at disease onset.	234
Figure 41. Isolated B-cells expressing NgR from spleen and spinal cord of <i>ngr1</i> ^{+/+} and <i>ngr1</i> ^{-/-} mice at clinical score 1.	236
Figure 42. The association of BAFF as a ligand for NgR in the B-cells isolated from spleens of EAE-induced mice at the disease onset, identification and modulation cell cycle events.	241
Figure 43. The association of BAFF as a ligand for NgR in the B-cells isolated from spinal cords of EAE-induced mice at clinical score 1, using cell cycle analysis. ...	243
Figure 44. The responses of immunoglobulin in the supernatant of isolated cells from the spleen and spinal cord of <i>ngr1</i> ^{+/+} and <i>ngr1</i> ^{-/-} mice at clinical score 1.	247
Figure 45. Immunostaining of secretory IgG in the supernatant from isolated cells (B-cells positive for either NgR1 or NgR3) from the spleen of <i>ngr1</i> ^{+/+} mice.	251
Figure 46. Immunostaining of secretory IgG in the supernatant from spinal cord isolates within the spinal cord and optic nerve tissues of the <i>ngr1</i> ^{+/+} mice (control).	253
Figure 47. Immunostaining of IgM in the supernatant from spinal cord isolates within the optic nerve tissues of the <i>ngr1</i> ^{+/+} mice (control).	255

Figure 48. Immunostaining of Nogo-A and IgG from the supernatant of spinal cord isolated cells within the spinal cord tissue of the <i>ngr1</i> ^{+/+} mice.....	257
Figure 49. Immunostaining of Nogo-A and IgG from the supernatant of spinal cord isolated cells within the spinal cord tissue of the <i>ngr1</i> ^{+/+} mice.....	259
Figure 50. Immunoblot analysis of secretory IgG in the supernatant from isolated cells.	262
Figure 51. Haematopoietic stem cell transplantation paradigm in EAE.....	272
Figure 52. Lentiviral vector production and quantification.....	275
Figure 53. Lineage negative enrichment of BM cells.....	278
Figure 54. Qualification of vector-transduced cells used for transplantation.....	283
Figure 55. Confirmation of NgR(310)-Fc protein production upon pLVX-EF1 α -NgR(310)-Fc-myc-IRES-ZsGreen1 bicistronic vector transfection.....	286
Figure 56. Post-HSCT monitoring.....	290
Figure 57. Clinical progression of EAE.....	293
Figure 58. Donor derived immune cells in HSC transplanted mice post-EAE.....	296
Figure 59. Donor derived immune cells in the spleen of HSC-transplanted mice post-EAE.....	299
Figure 60. Infiltration of donor derived immune cells in the spinal cord of HSC-transplanted mice post-EAE.....	306
Figure 61. Donor derived immune cell infiltrates in the optic nerve of HSC-transplanted mice post-EAE.....	308
Figure 62. Localisation of transplant derived cells in pathologically significant regions of the CNS.....	310

List of Abbreviations

ALDH	Aldehyde dehydrogenase
AF	Alexa fluor
AMREP	Alfred Medical Research and Education Precinct
APC	Allophycocyanin
7AAD	7-aminoactinomycin D
ARR	Annualized relapse rates
CAMPATH-1H	Anti-lymphocyte antibodies
APCs	Antigen-presenting cells
APRIL	A proliferation-inducing ligand
AQP4	Aquaporin4
Auto-HSCT	Autologous hematopoietic stem cell transplantation
Bp	Base pair
BAFF	B-cell activating factor
BAFF-R	B-cell activating factor -receptor
BAFF-R ^{-/-}	BAFF-R deficient
BCR	B-cell receptors
BCMA	Soluble B-cell maturation antigen
BCA	Bicinchoninic acid
BCNU	Bis-chloroethyl nitrosourea
BlyS	B-lymphocyte stimulator
BBB	Blood brain barrier
BM	Bone marrow
BSA	Bovine serum albumin
CCR-6	C-C chemokine receptor 6
CNS	Central nervous system
CSF	Cerebrospinal fluid
CHO	Chinese hamster ovarian
CSPGs	Chondroitin sulphate proteoglycan
CIS	Clinically isolated syndrome
CD	Cluster differentiation
CD40L	Cluster differentiation 40 ligand
Coll D	Collagenase D
CRMP-2	Collapsin response mediator protein-2
CFU-S	Colony-forming spleen assays
CFA	Complete Freund's adjuvant
DCs	Dendritic cells
DNA	Deoxyribonucleic acid
NMO	Devic's neuromyelitis optica
DAPI	4',6-diamidino-2-phenylindole
DMT	Disease-modifying treatments
DPX	Distyrene, a plasticizer, and xylene
DRG	Dorsal root ganglia

EV	Empty vector
eGFP	Enhanced green fluorescent protein
ELISA	Enzyme-linked immunosorbent assay
EAE	Experimental autoimmune encephalomyelitis
EDSS	Expanded disability status scale
FBS	Fetal bovine serum
FCS	Fetal calf serum
FACS	Fluorescence-activated cell sorting
FISH	Fluorescent in situ hybridisation
FITC	Fluorescein isothiocyanate
TPO	FLT3 ligand
FDCs	Follicular dendritic cells
FLS	Follicle-like structure
Gd+	Gadolinium-enhancing
GA	Glatiramer acetate
GPI	Glycosylphosphatidylinositol
GVHD	Graft versus host disease
G-CSF	Granulocyte-colony stimulating factor
G0/G1	Growth phase 0 and 1
G2/M	Growth phase 2 and mitotic phase
HRQL	Health related quality of life
HSCs	Hematopoietic stem cells
HSCT	Hematopoietic stem cell transplantation
HeLa	Henrietta Lacks
T _h	Helper T-cells
HDIT	High-dose immunosuppressive therapy
Ho	Hoechst 33342
HEK	Human embryonic Kidneys
HLA	Human leukocyte antigen
5-FU	Hydroxyurea and 5-fluorouracil
Ig	Immunoglobulin
ITP	Immune thrombocytopenic purpura
IFN- γ	Interferon
IL	Interleukin
IRES	Internal ribosomal entry site
IVMP	IV methylprednisolone
LRR	Leucine-rich repeat
LV	Lentivirus
Lin	Lineage
Lin ⁻	Lineage-depleted
LSK	Lin ⁻ , Sca-1 ⁺ and c-Kit ⁺
LM	Littermates
LINGO-1	Leucine-rich repeat and Ig domain containing 1
LT	Long-term
LVN	Low viscosity nitrocellulose

LFB	Luxol fast blue
MACS	Magnetic activated separation
MRI	Magnetic resonance imaging
MHC	Major Histocompatibility
MAG	Myelin associated glycoprotein
MAIFs	Myelin associated inhibitory factors
MTX	Mitoxantrone
MOI	Multiple of infection
MS	Multiple sclerosis
MBP	Myelin basic protein
MOG	Myelin oligodendrocyte glycoprotein
NKT	Natural killer T-cells
NgR1	Nogo-66 receptor
<i>ngR1^{-/-}</i>	NgR1 deficient
OCBs	Oligoclonal bands
OMgp	Oligodendrocyte-myelin glycoprotein
OCT	Optimal cutting temperature compound
PFA	Paraformaldehyde
Pen/Strep	Penicillin and streptomycin
PBS	Phosphate buffered saline
PE-Cy7	Phycoerythrin Cyanine7
PE	Phycoerythrin
PCR	Polymerase chain reaction
PerCP-Cy5.5	Peridinin chlorophyll protein complex
P	Peptide
PAS	Periodic acid-Schiff
PB	Peripheral blood
PBCS	Peripheral blood stem cells
PNM	Peripheral nervous system myelin
PVDF	Polyvinylidene fluoride
PP	primary progressive
PLP	Proteolipid protein
PR	progressive relapsing
rATG	Rabbit anti-thymocyte globulin
RIPA	Radioimmunoprecipitation assay
rBAFF	recombinant B-cell activating factor
rMOG	recombinant myelin oligodendrocyte glycoprotein
T _{reg}	Regulatory T
RR	Relapsing remitting
Rtn 4A	Reticulon family
Rho	Rhodamine-123
SP	Secondary progressive
ST	Short-term
SP	Side population
siRNA	Small interfering RNA
SDS-PAGE	Sodium dodecyle sulphate polyacrylamide gels

SEM	Standard error of the mean
SCA-1	Stem cell antigen-1
S phase	synthesis phase
TBI	Total body irradiation
TAC1	Transmembrane activator and CAML-interactor
TM	Transmembrane
c-Kit	Transmembrane tyrosine-protein kinase
TBST	Tris-buffered saline-Tween
TNF	Tumour necrosis factor
WM	White matter
WT	Wild-type
ZsGreen	<i>Zoanthus sp.</i> Green1 fluorescent protein

List of Publications and Presentations

1. BAKHURAYSAH, M. M., SIATSKAS, C. & PETRATOS, S. 2016. Hematopoietic stem cell transplantation for multiple sclerosis: is it a clinical reality? *Stem Cell Res Ther*, 7, 12.
2. ALREHAILI A, LEE JY, TAGHIAN K, MAHABAKHURAYSAH, THOMAS SPEROS, PETRATOS S. 2014. Microglial mechanisms governing axonal degeneration in multiple sclerosis. *J Neurol Neurophysiol*. 5:206.
3. MOKHTAR, S. H., BAKHURAYSAH, M. M., CRAM, D. S. & PETRATOS, S. 2013. The Beta-amyloid protein of Alzheimer's disease: communication breakdown by modifying the neuronal cytoskeleton. *Int J Alzheimers Dis*, 2013, 910502.
4. LITWAK, S. A., PAYNE, N. L., CAMPANALE, N., OZTURK, E., LEE, J. Y., PETRATOS, S., SIATSKAS, C., BAKHURAYSAH, M. & BERNARD, C. C. 2013. Nogo-receptor 1 deficiency has no influence on immune cell repertoire or function during experimental autoimmune encephalomyelitis. *PLoS One*, 8, e82101

Conference (Poster) Presentations

2013-Australian Society for Medical Research (ASMR; Melbourne, AUS)

Identifying the immune function of NgR1 in EAE and multiple sclerosis. Maha Bakhuraysah¹, Peimun Aui¹, Steven Petratos²

¹Department of Anatomy and developmental Biology, Monash University, Clayton 3800, Australia

²Department of Medicine, Central Clinical School, The Alfred Centre, Monash University, Prahran 3004, Australia

2014-Australian Neuroscience Society (ANS; Adelaide, AUS)

A possible novel immune role for NgR1 in B-cell populations localised in the CNS during EAE. Maha Bakhuraysah¹, Jae Young Lee¹, Peimun Aui¹, Steven Petratos¹

¹Department of Medicine, Central Clinical School, Monash University, Prahran 3004, Australia

2015-International Society of Neurochemistry / Australian Neuroscience Society (ISN/ANS; Cairns, AUS)

Nogo-receptor 1 expression on B-cell populations in the central nervous system during experimental autoimmune encephalomyelitis. Maha Bakhuraysah¹, Amani Alrehaili¹, Sara Mokhtar, Jae Young Lee¹, Peimun Aui¹, Steven Petratos¹.

¹Department of Medicine, Central Clinical School, Monash University, Prahran, VIC, Australia.

2015 Multiple Sclerosis Research Australia (MSRA; Melbourne)

Nogo-receptor 1 expression on B-cell populations in the central nervous system during experimental autoimmune encephalomyelitis. Maha Bakhuraysah¹, Amani Alrehaili¹, Sara Mokhtar, Jae Young Lee¹, Peimun Aui¹, Steven Petratos¹.

¹Department of Medicine, Central Clinical School, Monash University, Prahran, VIC, Australia.

2016 The Americas Committee for Treatment and Research in Multiple Sclerosis (ACTRIMS; New Orleans, USA)

Identifying the role of Nogo-receptor on B-cell populations in the central nervous system during experimental autoimmune encephalomyelitis. Maha Bakhuraysah¹, Amani Alrehaili¹, Jae Young Lee¹, Peimun Aui¹, Steven Petratos¹.

¹Department of Medicine, Central Clinical School, Monash University, Prahran, VIC, Australia.

Oral Presentations

2012 Monash Immunology and Stem cell laboratory Student Symposium (MISCL; Melbourne, AUS)

Identifying the immune function of NgR1 in EAE and multiple sclerosis. Maha Bakhuraysah¹, Peimun Aui¹, Steven Petratos²

¹Department of Monash Immunology and Stem cell laboratory, Monash University, Clayton 3800, Australia

²Department of Medicine, Central Clinical School, The Alfred Centre, Monash University, Prahran 3004, Australia

2013 Anatomy and developmental Biology Symposium (ADB; Melbourne, AUS)

Identifying the immune function of NgR1 in EAE and multiple sclerosis. Maha Bakhuraysah¹, Peimun Aui¹, Steven Petratos²

¹Department of Anatomy and developmental Biology, Monash University, Clayton 3800, Australia

²Department of Medicine, Central Clinical School, The Alfred Centre, Monash University, Prahran 3004, Australia

2015 Central Clinical School postgraduate Symposium (CCS; Melbourne, AUS)

Identifying the immune role of NgR in EAE and MS. Maha Bakhuraysah¹, Amani Alrehaili¹, Jae Young Lee¹, Peimun Aui¹, Steven Petratos¹.

¹Department of Medicine, Central Clinical School, Monash University, Prahran, VIC, Australia.

Awards

Travel grant for a young investigator from the Americas Committee for Treatment and Research in Multiple Sclerosis (ACTIMS, New Orleans, USA) in 2016.

CHAPTER 1: Literature Review

1.1 Multiple sclerosis

Although the aetiology of multiple sclerosis (MS) has not been clearly elucidated, it is generally agreed that autoreactive T-cells, activated by either self or cross-reactive antigens, migrate through the blood brain barrier (BBB), trigger an inflammatory cascade, that ultimately leads to demyelination and progressive neurodegeneration of the central nervous system (CNS) (Villar et al., 2010). Pathologically, the brain tissue of autopsy patients exhibit inflammatory infiltrates with the degeneration of myelin, reactive gliosis and axonal degeneration (Vosoughi and Freedman, 2010, Fassas and Mancardi, 2008). Neurological disability is manifest in a number of symptoms, including blurred vision and diplopia, sensory disturbances (e.g. paresthesia and dysaesthesia), heat intolerance, hemiparesis or paraparesis, vertigo and dizziness, lack of coordination, limb spasticity, bowel and bladder incontinence, cognitive impairment and memory loss.

As with most autoimmune disorders, MS predominately affects young females between 20 and 40 years of age with the prevalence being 80–120/100,000 population with a lifetime risk of 1 in 400 (Weinshenker et al., 1989, Compston and Coles, 2002). MS is classified into four main subtypes: relapsing remitting (RR), secondary progressive (SP), primary progressive (PP), and progressive relapsing (PR) (Vosoughi and Freedman, 2010). Over 80% of patients with MS begin with a RR course characterized by relapses that result from inflammation, followed by incomplete or complete remission. This form of MS commonly presents in Europeans and Caucasian Americans but not African Americans, Asian and South American populations (Martinez et al., 2012, Vosoughi and

Freedman, 2010). Epidemiological data have shown that between 5-15 years from its onset, 50% of RR-MS patients convert to the SP-MS, where pre-existing neurological deficits gradually worsen from the onset with subsequent superimposed relapses (Fassas and Nash, 2004, Fassas and Mancardi, 2008). The later is characterized by axonal degeneration and loss, leading to gliosis and brain atrophy. MS can manifest also as the PP-MS phase in approximately 15% of individuals, in which disability accumulates faster than in the classical early RR course. PR-MS is the least frequent form of MS and is characterized by a steady neurological decline with superimposed attacks experienced by the patient (Fassas and Nash, 2004, Fassas and Mancardi, 2008).

1.2 Immune-mediated mechanisms of MS/EAE

The malfunction of the immune system in MS leads to an attack of CNS myelin, which induces an increase in several cytokines and immune effector cells. During a pro-inflammatory response, helper T-cells (T_{h1} -) and (T_{h2} -) cells are elevated during relapses exhibited in MS models of disease, while during an anti-inflammatory response, T_{h2} -cells, natural killer T-cells (NKT) and regulatory T (T_{reg}) are more active during remissions (Martinez et al., 2012). Therefore, MS is thought to be a T_{h1} -mediated disease in the inflammatory animal model of MS, which is experimental autoimmune encephalomyelitis (EAE) (Martinez et al., 2012). It is induced by immunisation with the myelin oligodendrocyte glycoprotein (MOG), proteolipid protein (PLP) or myelin basic protein (MBP) (Bettelli, 2007, Van Wijmeersch et al., 2008).

EAE can be induced in C57Bl/6 mice by immunising with the MOG₃₅₋₅₅ peptide emulsified in complete Freund's adjuvant (CFA), resulting in a progressive paralysis ascending from the tail to the forelimbs. Thus, the disease progression in this model can be scored accordingly and the immune-mediated pathology within the CNS can be measured accurately. Furthermore, myelin damage and CNS inflammation in this mouse model can be quantified and visualized using histological analysis, in addition to immunological assays to measure autoantibody reactivity and specific T-cells which can be used to validate certain immune responses to the different myelin components (Chan et al., 2008). Furthermore, in EAE, myelin-specific T_{h1} -cells can be adoptively transferred to induce EAE into recipient animals and are directly related to immunopathology of the disease (Martinez et al., 2012).

1.2.1. Mechanisms of Immune cell infiltration in MS/EAE

Briefly, B-cells migrate into the site of inflammation and they may encounter specific antigens and lymphokines, which aid their differentiation. B-cells produce anti-myelin antibodies that may contribute to the transition of the disease from relapses into progression (Hemmer et al., 2002). The malfunctions of the immune system in MS may be responsible for initiating an attack on myelin, (involving oligodendrocytes), caused by a complex interaction among B-cells, macrophages, cytotoxic CD8⁺ T-cells, and cytokines (interleukin (IL-17) and interferon (IFN- γ)) (Weber and Hemmer, 2010). The responses of B- and T-cells are primed in the peripheral lymphoid organs by cross-reactive foreign antigens or by antigens released from the CNS. B-cells are efficient antigen-presenting cells (APCs) for intact antigens of myelin (Weber and Hemmer, 2010). Following the activation of the pro-inflammatory cascade, cytokines are released, leading the endothelial cells lining blood vessels of the CNS to express adhesion molecules, potentiating T- and B-cell binding to these molecules and subsequently infiltrating through the BBB after clonal expansion. Clonally expanded B- and T-cells invade the brain and the former re-attach to their particular antigens, maturing to plasma cells and then releasing great numbers of IgG antibodies (Weber and Hemmer, 2010). In addition, Cytotoxic CD8⁺ T-cells encounter their particular ligands, presented by neuronal or glial cells, expressed on major histocompatibility (MHC) I, leading to direct damage to the antigen expressing cells. Furthermore, T_h-cells encounter antigens of microglial cells on MHC II within the CNS. Once reactivated, the production of

inflammatory cytokines is leading to activation of other types of immune cells that damage the myelin sheath (Weber and Hemmer, 2010) (Figure 1).

CD8⁺ cytotoxic T-cells are considered as major effector T-cells because they can participate in direct/indirect early axonal damage in MS; directly by cytotoxicity or indirectly by the induction of microglial cell activation (Figure 1) (Babbe et al., 2000, Magliozzi et al., 2010). Moreover, these cells greatly outnumber CD4⁺ T-cells in MS lesions, and several data showed clonal expansion of cytotoxic CD8⁺ T-cells within blood, CSF, and MS lesions (Babbe et al., 2000, Crawford et al., 2004, Skulina et al., 2004). Therefore, the plausible mechanism for by which cytotoxic CD8⁺ T-cells can mediate axonal damage in MS may be through granule exocytosis. The cytolytic protein, perforin and a serine protease, granzyme B, are the main molecules that have been extensively studied. Perforin emanating from CD8⁺ cytotoxic T-cells can disrupt the membrane of targeted cells by forming transmembrane pores, causing cell lysis (Waterhouse et al., 2006, Lee et al., 2015). It has been identified that perforin from cytotoxic CD8⁺ T-cells can induce neuronal damage in both embryonic mouse neuronal cell culture and in mouse brain slice, by using live cell imaging (Nitsch et al., 2004, Meuth et al., 2009, Miller et al., 2013). In addition, liberation of granzyme B-dependent neurotoxicity from cytotoxic CD8⁺ T-cells has been showed in neuronal cell culture experiments (Wang et al., 2006a, Haile et al., 2011, Wang et al., 2012).

However, the subsets of B-cells have variable effects on the differentiation of T-cells, which can relate to antigen specificity, activation status, B-cell phenotype, and the

immunological environment where B-cells recognise naïve T-cells. Under certain circumstances, antigen primed B-cells can switch the isotype of immunoglobulin (Ig) to become plasma cells as mentioned above, or enter the germinal centre to develop into memory B-cells, under the control of activated T_h-cells. Therefore, both T- and B-cells may support the MS pathogenesis in both a regulatory and an inflammatory manner (Weber and Hemmer, 2010). To date, it is not clear if antigen experienced B-cells are shared between the compartments of the peripheral blood (PB) and CNS (Von Büdingen et al., 2012).

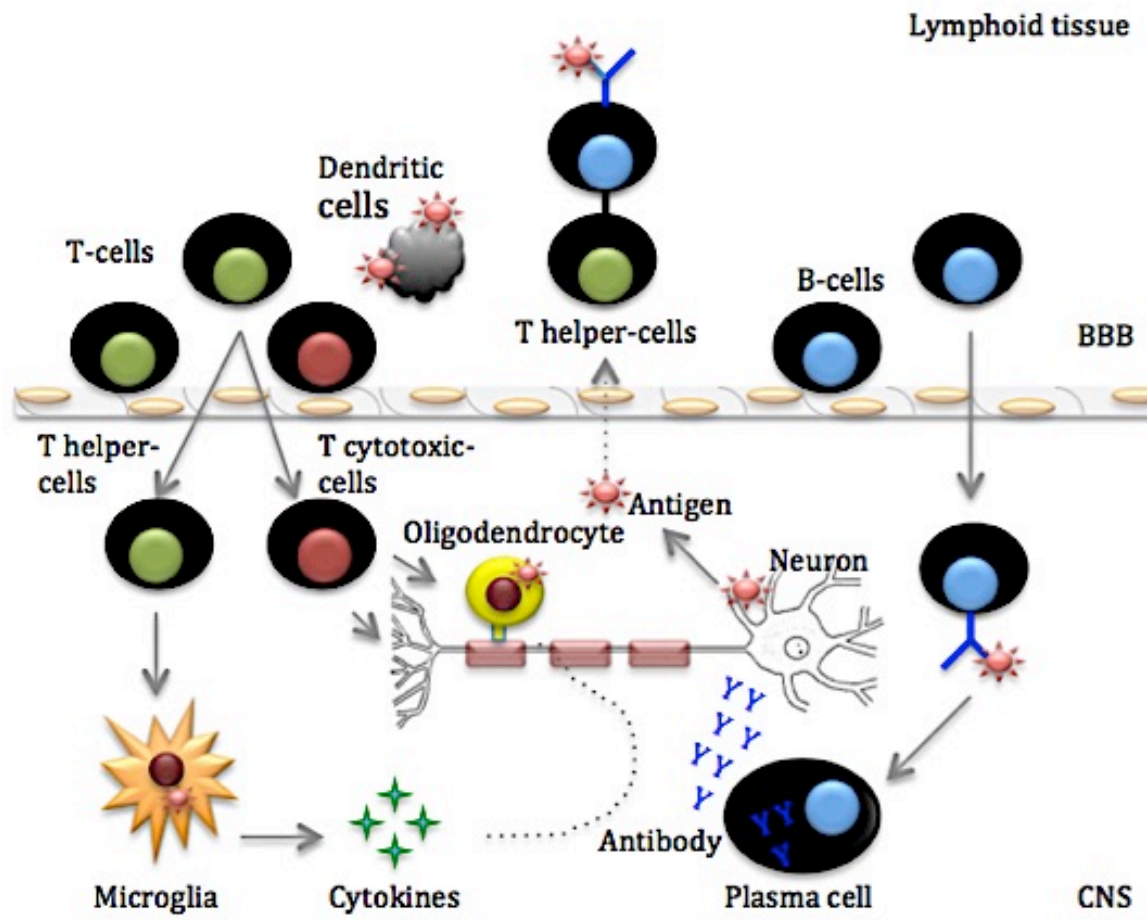


Figure 1. Infiltration of immune cells into the CNS. Autoimmune T-cells and B-cells migrate from the periphery into the CNS via BBB, causing inflammation, demyelination, and damage to oligodendrocytes, axons and neurons by activating other types of immune cells (Villar et al., 2010, Weber and Hemmer, 2010)

1.2.2. B-cell-dependent humoral immune mechanisms of MS/EAE

Data from both animal models and results from clinical trials provide evidence for a specific role of B-cells in the MS pathology (Pikor and Gommerman, 2012). Normally, the development of humoral immune responses to T-cell dependent antigens occurs at secondary lymphoid organs, such as the lymph nodes and spleen. The interaction of B-cells and effector T-cells occur after their migration to the edges of their respective follicular zones (Huntington et al., 2006). CD4⁺ T-cells express CD40 ligand (CD40L), also known as tumour necrosis factor (TNF), this ligand and cytokine can stimulate B-cells to proliferate and differentiate, leading to either their entry into follicles to initiate the reaction within the germinal centre or short-lived foci. B-cells are capable of entering germinal centres via signalling from both CD40 and B-cell receptors (BCR) (Huntington et al., 2006). B-cells, therefore, give rise to antibody-producing cells upon maturation and have an effect on the inflammatory response. B-lymphocytes can produce cytokines, which may be either anti-inflammatory which block T-cells and macrophages, or pro-inflammatory which activate macrophages and T-cells (Krumbholz et al., 2012, Martinez et al., 2012)

The interest in B-cells and autoantibodies in MS pathophysiology has been reintroduced due to identification of humoral constituents in certain EAE types and due to the presence of a prominent humoral pathology in MS patients within their active lesions. This is primarily due to the presence of perivascular Ig deposition and complement proteins in

several active lesions of Devic's neuromyelitis optica (NMO). In the past decade, aquaporin-4 (AQP4) has been identified as a target of autoantibodies in NMO (Jarius and Wildemann, 2010, Mader et al., 2011). In specific MS patients, the role of IgG in the destruction of tissue components has been investigated by identifying demyelination and axopathic IgG in patient sera, observing complement activation and Ig deposition in some MS patients, and successful plasma exchange treatment in patient subsets (Keegan et al., 2005, Dau, 1995). However, the role of complement staining and Ig in MS remains a controversial issue. Recently, Howell *et al.* (2011) showed that B-cells are a prominent feature in the neurodegenerative process; these were characterised as CNS B-cell-like follicles with germinal centres in the meninges of SP-MS patients (Howell et al., 2011), as mentioned previously. These results coincide with a previous study (Serafini et al., 2004).

One of the most reliable markers for MS immunodiagnosis is oligoclonal bands (OCBs), which are present in CSF in combination with elevated intrathecal IgG production in around 90% of MS patients at the first clinical event, and approximately 40% demonstrate oligoclonal IgM (Villar et al., 2010, Krumbholz et al., 2012). In fact, Villar *et al.* (2010) have reported that B-cells responsible for the secretion of intrathecal IgM in MS may relate to the aggressive course of MS. Therefore, both the clinicopathological picture from MS patients and fundamental scientific data generated from animal models advocate a central role for antibody-dependent neurodegeneration during progressive MS and may during trials now directed to limit B-cell/antibody-dependent neural damage.

1.2.3. Localisation of B-cells in the CNS of MS

Based on the histological analysis of MS active lesions, B-cells are located primarily in the perivascular space, throughout white matter (WM) lesions, and the meninges (Kutzelnigg et al., 2005, Pikor and Gommerman, 2012). In SP-MS patients, infiltration of B-cells and plasma cells has also been identified within the FLS as aggregates found within the meninges. This later finding may support the role of antibodies in the progression of the disease (Serafini et al., 2004, Pikor and Gommerman, 2012). Meningeal inflammation is associated with the pathology of cortical demyelination; MS is initiated with limited plaques of demyelination in the cortex and the white matter, followed by its progression to diffuse inflammation across the brain, in association with band-like subpial demyelination (Kutzelnigg et al., 2005). It has been highlighted that the presence of clonally specific B-cells in the meninges, demyelinating lesions and CSF, may implicate a local expansion of B-lymphocyte clones persisting and occurring over time within the CNS in MS patients (Howell et al., 2011). There exists evidence to support the role of the meninges in the inflammatory response initiated during MS. Firstly, B-cell FLS's exist in the cerebral meninges of MS patients (Magliozzi et al., 2010, Lovato et al., 2011). Meningeal B-cell structures consist of proliferating B-cells with the follicular dendritic cells (FDCs) network that are present in the meninges and paranchyma. Secondly, T_{h17}-cells enter the CNS through a specific port, C-C chemokine receptor 6 (CCR-6), throughout the choroid plexus that initiate the inflammatory response documented in the EAE model (Reboldi et al., 2009). The interaction of antigen-specific T- and B-cells with APCs, which include dendritic cells (DCs), FDCs, and macrophages,

lead to proliferation, and differentiation into effector and memory cells (Lovato et al., 2011, Pikor and Gommerman, 2012). However, it is still unclear whether B-cells present within the meninges associate with those that populate the CNS parenchyma and contribute to the MS pathology.

1.2.4. Mediators maintaining and attracting B-cells in MS

There are specific mediators, such as chemokines, that direct the migration of B-cells. There are two types of chemokines that regulate this process; lymphoid chemokines, which are vital for lymphoid organ maintenance and development, and inflammatory chemokines, which attract immune cells to the sites of inflammation. MS is associated mainly with inflammatory chemokines; however, in the CSF and MS lesions, lymphoid chemokines are increased (Pashenkov et al., 2003, Krumbholz et al., 2006). For example, B-cell-attracting chemokine CXCL13 levels, which are produced by the resident cells of the brain, are elevated in the CSF of MS. This chemokine is associated with either the production of intrathecal IgG, the number of cells in the CSF circulating in MS patients or with the development of MS seen in patients with clinically isolated syndrome (CIS) (Pashenkov et al., 2003, Krumbholz et al., 2006). Meningeal FLS's consist of host plasma cells, T- and B-cells, regulated through B-cell chemokines or FDC, which participate in responses of germinal centres in the spleen and lymph node (Pikor and Gommerman, 2012).

Since B-cells play a vital role in the pathogenesis of MS, being involved in the activation of pro-inflammatory T-cells, secretion of pro-inflammatory cytokines, and production of autoantibodies directed against myelin, the usage of B-cell-depleting monoclonal antibodies targeting CD20 as therapy for MS is of major clinical importance (Sorensen and Blinkenberg, 2016). The first anti-CD20 monoclonal antibody to be used successfully for MS treatment was Rituximab (Maloney et al., 1994, Hauser et al., 2008); then, ocrelizumab, a second-generation anti-CD20 monoclonal antibody, explored in a large phase II, placebo-controlled randomised, multicentre trial in RR-MS (Kappos et al., 2011). More details will be discussed in Section 1.7.

There are currently several anti-inflammatory and disease modifying therapeutic agents for patients living with MS but these cannot cure the disease. Although these agents can decrease the inflammation within the CNS, the disease progression remains unabated in a large percentage of patients. In particular, chronic-active forms of MS, such as PP-MS and SP-MS, do not respond to treatment, since there is propagation of neurodegeneration evident in patients (Fitzner, 2010). Several studies have demonstrated that insufficient myelin clearance contributes to the failure of axonal regeneration in the CNS after acute injury (David and Lacroix, 2003, Buss and Schwab, 2003). Due to the fact that myelin includes several growth inhibitory molecules, such as Nogo-A, which exhibit inhibitory effects on axonal regrowth (Schwab, 2004), a novel therapeutic approach for progressive MS may consist of strategies targeting the Nogo-A protein, which has been well characterised in the inflammatory mouse model of MS, namely EAE.

1.3 The role of MAIFs in EAE/MS

Several integral components of the CNS are responsible for inhibiting re-growth at the distal end of the axon, culminating in a regeneration/sprouting failure. Most important are the myelin components or the myelin associated inhibitory factors (MAIFs), including Nogo-A. The Nogo-A protein, a member of the reticulon family (Rtn 4A), is a potent neurite outgrowth inhibitor that is expressed by numerous neural populations (Karnezis et al., 2004). It plays a major role both in neuroarchitecture and plasticity in the CNS, along with its role during development and disease during the limitation of axonal regeneration after injury. The pathophysiological characteristics of EAE lesions can be improved by either immunisation against the Nogo-A protein or deletion of the nogo gene (Yang et al., 2010, Karnezis et al., 2004, Petratos et al., 2012). This gene is spliced to create three isoforms, Nogo-A, -B, -C. Among these isomers, Nogo-A has a longer N-terminal sequence and has two transmembrane (TM) domains in the C-terminal portion that are disconnected by a short extracellular (Nogo-66) domain (Petratos et al., 2010) (Figure 2). MAIFs that include Nogo-A, myelin associated glycoprotein (MAG), oligodendrocyte-myelin glycoprotein (OMgp), bind with high affinity to NgR1, which is a glycosylphosphatidylinositol (GPI)-anchored protein, expressed in conjunction with a leucine-rich repeat and Ig domain containing 1 (LINGO-1) and either TROY or p75^{NTR} signalling receptors (Mi et al., 2007). Therefore, NgR1 is able to transduce its signals inside the cell via activating the intracellular RhoA-GTPase, causing inhibition of axonal outgrowth, or modulation of motility and cell adhesion (Pernet and Schwab, 2012, Fournier et al., 2003) (Figure 3). Nogo receptor 3, which is a homologue of NgR1, may

act as a NgR1 co-receptor for Nogo-66. Both paralogues of NgR1, NgR2 and NgR3 are expressed in the developing and adult CNS, and they share similar protein structures with NgR1, including the GPI-anchored domain and leucine-rich repeat (LRR) motif (Zhang et al., 2011) (Figure 3). Dickendesher *et al.* (2012) demonstrated that NgR1 and NgR3 are novel chondroitin sulphate proteoglycan (CSPGs) receptors, which are a diverse class of extracellular matrix molecules that influence of developing neurons and axonal growth, and contribute to glial scar formation after injury to the adult CNS (Dickendesher et al., 2012). Furthermore, there is a functional redundancy among these receptors because they bind with high-affinity to CSPG and contribute in the inhibition of GSPG in cultured neurons (Dickendesher et al., 2012). These results highlighted vital information with regards to sharing common mechanisms of CSPG and MAIFs regulating regeneration failure in the CNS. According to Giger *et al.* (2010), some axonal regeneration *in vivo* has been promoted by acute blockade of NgR1 functions (Giger et al., 2010). Despite clear evidence demonstrating that the deletion of NgR1 can protect against axonal degeneration and thus progression of EAE (Petratos et al., 2012), an immunological role for this receptor is yet to yield mechanistic evidence.

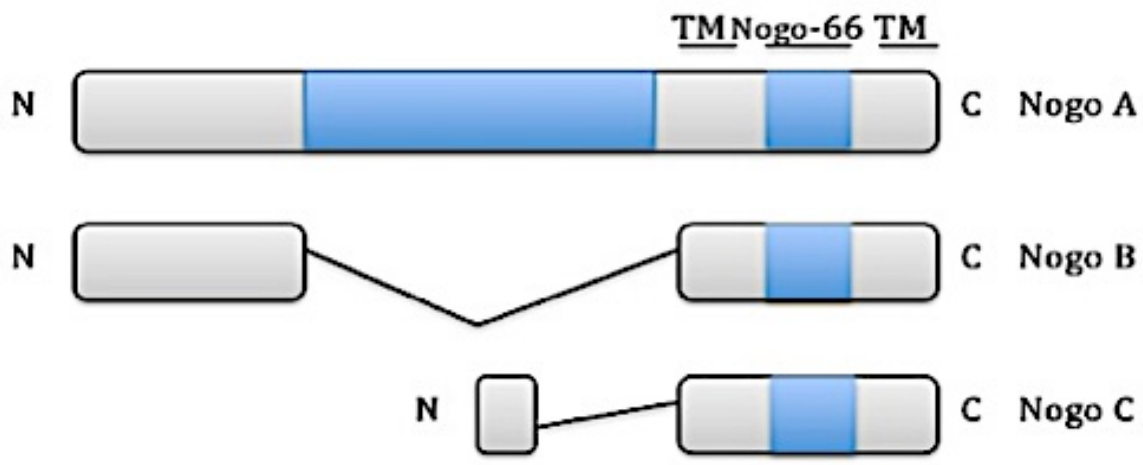


Figure 2. Nogo protein structure. Three forms of Nogo, -A, -B-, and -C, including two transmembrane (TM) domains separated by Nogo-66 (Petratos et al., 2010).

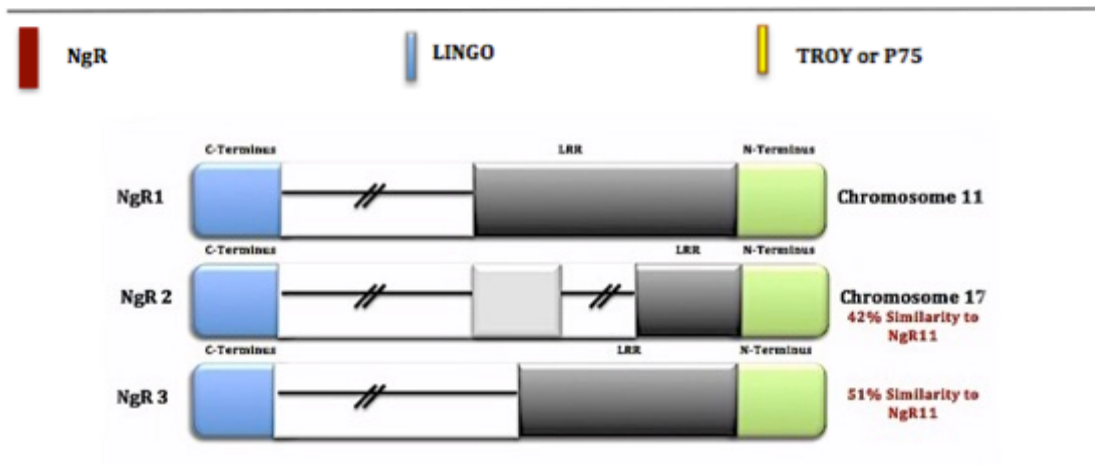
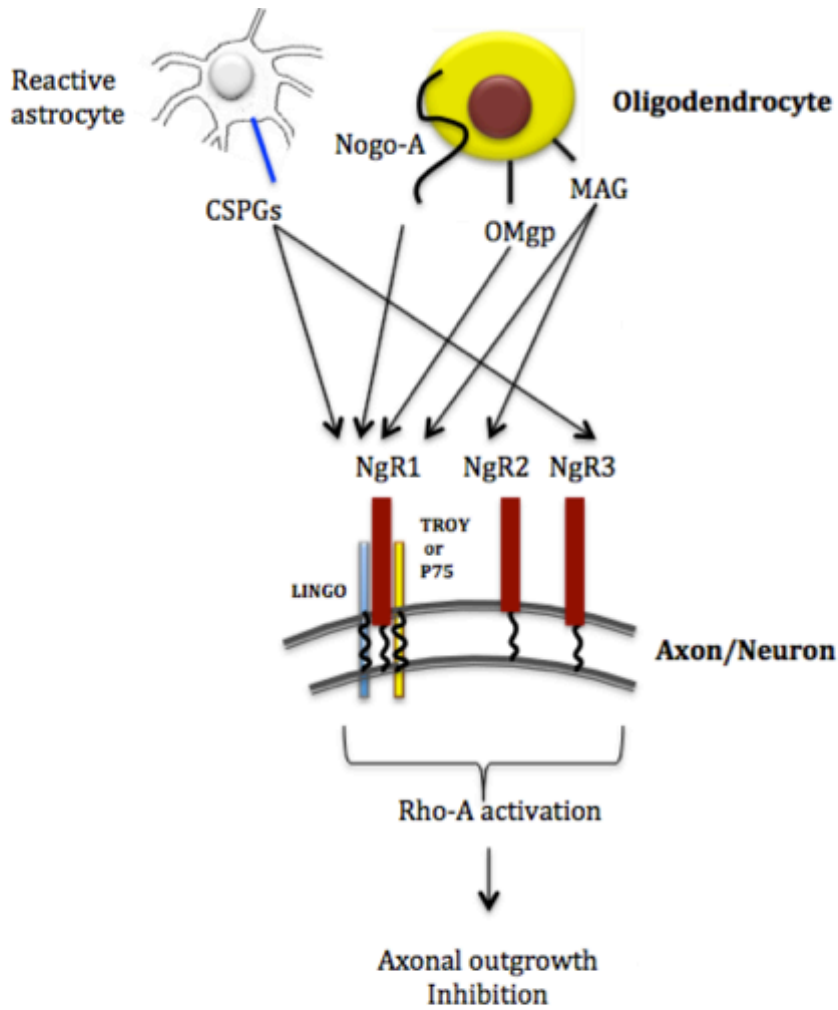


Figure 3. NgR signalling mechanism. NgR1 is able to transduce its signals inside the cell via activating the intracellular RhoA-GTPase causing inhibition of axonal outgrowth, when Nogo-A binds with a high affinity to NgR1, expressed in conjunction with the leucine rich repeat and Ig domain containing 1 (LINGO-1) and either, TROY or p75NTR signalling receptors (Mi et al., 2007, Pernet and Schwab, 2012, Fournier et al., 2003). NgR2 and NgR3 share similar protein structures with NgR1, including the GPI-anchored domain and leucine-rich repeat (LRR) motif (Zhang et al., 2011).

1.3.1. Nogo-A/NgR1 role in regulating the immune response in MS/EAE

Reindl *et al.* (2003) have recently identified that anti-Nogo-A antibodies are present in the cerebrospinal fluid (CSF) and the serum of MS patients, particularly in RR-MS, rather than in the chronic forms of MS (Reindl *et al.*, 2003). These investigators suggested that such antibodies may play a role in the disease's clinical remission; however, this has since been dismissed as a hypothesis (Reindl *et al.*, 2003). In chronic demyelinating lesions of MS, Nogo-A expression in oligodendrocytes was also illustrated to be up-regulated. This expression of Nogo-A in the MS lesions was demonstrated to associate with the progression of the disease (Theotokis *et al.*, 2012, Petratos *et al.*, 2012).

However, it has been shown that NgR may play a role in the efflux of macrophages from the injured peripheral nerve to terminate inflammation at the end of the Wallerian degeneration process, and so this effect may contribute to the regeneration capacity of transected peripheral nerve axons (Fry *et al.*, 2007, David *et al.*, 2008). By extension, it is plausible that the expression of NgR may play a role in the efflux of macrophages from the CNS, after an inflammatory insult or injury within the CNS. In addition, it has recently been reported that the immune response of B- and T-cells were stimulated after injecting SJL mice with peptides from various peptide-specific domains of Nogo-66, where EAE was either suppressed or induced, depending on the injected Nogo-66-specific epitope to which the peptide corresponded (Fontoura *et al.*, 2004). These investigators also found that Nogo-66-specific T-cell lines ameliorate EAE, via a T_{h2}

dependent response within the CNS (Fontoura et al., 2004). Furthermore, the spreading of antibody responses (epitope spreading) increased against other myelin antigens after immunisation with a certain peptide, Nogo 45-66, increasing paralysis and demyelination in the SJL mice. The data show that Nogo-66 can be encephalitogenic and potentiate neurodegeneration. Conversely, a recent study indicated that using a DNA vaccine to generate an antibody response to full-length Nogo-A was not encephalitogenic and they could not stimulate inflammatory disease and demyelination in naïve mice (Bourquin et al., 2008).

Emerging evidence suggests that, NgR1 has an effect on the immune cells behaviour, in addition to its role in preventing axonal regrowth. Indeed, the role of B-lymphocyte stimulator (BlyS) or B-cell activating factor (BAFF), which is known stimulator of B-cell activation, is investigated during NgR activation (Mackay et al., 1999, Schneider et al., 1999, Thompson et al., 2000). Over last sixteen years, the potential role of BlyS/BAFF (TNF superfamily protein involved in the development of B-cells) has been extensively investigated for its role in autoimmunity (Mackay et al., 1999, Schneider et al., 1999). It is expressed by bone marrow (BM)-derived radiation resistant stromal cells, myeloid-lineage cells and T-cells (Moore et al., 1999, Schneider et al., 1999). It has the ability to bind to variable receptors, such as BCMA, TACI and BR3 (also known as BAFF-R) on the B-cell surface, when it is cleaved at the cell surface by furin proteases to release BAFF as a soluble, biologically active molecule (17 kDa) (Schneider et al., 1999, Zhou et al., 2011). It has been identified that BAFF, which is known as the best B-cell survival factor, plays a vital role in B-cell differentiation, in Ig production, and in Ig class

switching (Thompson et al., 2000, Castigli et al., 2005) (Figure 4). The activity of BAFF during the pathogenesis of MS may be an important paradigm shift in the search for candidate therapeutic targets during the progression of the disease.

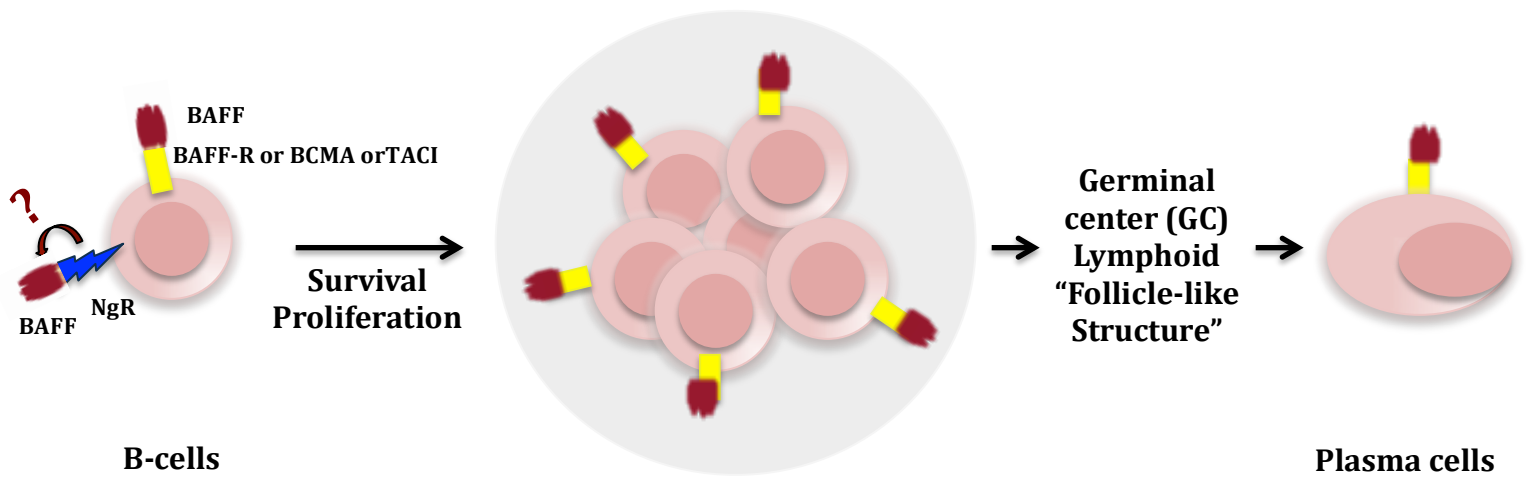


Figure 4. BlyS/BAFF signalling mechanism. BAFF has been suggested to signal through BAFF-R, BCMA and TACI receptors for B-cell proliferation and maturation (Thompson et al., 2000, Castigli et al., 2005), and it may act as a ligand for NgR1.

1.4 BAFF and EAE

1.4.1 The influence of BAFF on T_{h17}-cells that aggravates EAE

Recently, BAFF has been identified to contribute significantly to pathogenic T_{h17}-cell responses in the MOG₃₅₋₅₅ EAE model of MS, where BAFF (BAFF-tg) mice exhibited increased percentages of B- and T-cells in the spleen and lymph nodes when compared to wild-type (WT) mice but these immune cell populations were decreased sharply in BAFF^{-/-} mice (Zhou et al., 2011). Importantly, T_{h17}-cells were markedly elevated in BAFF-tg mice (which over express soluble BAFF and express membrane BAFF) and declined in BAFF^{-/-} mice *in vivo*, demonstrating that the effect of BAFF is not limited to T_{h1}- and T_{h2}-cells responses, but it also affects the generation of T_{h17}-responses (Zhou et al., 2011). Indeed, T_{h17}-cells enter the CNS throughout the choroid plexus that initiate the inflammatory response documented in EAE (Reboldi et al., 2009), and also memory T-cells produce IL-22 and IL-17 that infiltrate into MS lesion (Kebir et al., 2007), thus T_{h17}-cells may play vital roles in MS pathology. Furthermore, the development of EAE was significantly delayed and severity of disease was reduced in BAFF^{-/-} mice when compared to WT mice. Conversely, EAE duration was prolonged in BAFF-tg mice. These results are supported by an earlier study, which identified the association between BAFF up-regulation in the CNS with EAE development (Magliozzi et al., 2004). Thus, BAFF may be a therapeutic target in T_{h17}-cell dependent autoimmune disease (Zhou et al., 2011), with significant interest in the mechanisms during MS pathogenesis.

1.4.2 Ability of BAFF antagonist to suppresses EAE

Further evidence supporting the pathogenic role of BAFF is from a study that targeted this ligand and similar receptor interacting proteins such as, a proliferation-inducing ligand (APRIL). Instances of delayed onset and decreased severity of disease in mice treated prior to EAE induction with a fusion protein that neutralized both BAFF and APRIL evaluated the critical role of BAFF for B-cell homeostasis and T-cell co-stimulation by exploring the efficacy of preventing BAFF signalling in order to suppress B-cell antigen presentation and antibody production, as well as co-stimulator of T-cell activation in the induction and effector phase of EAE (Huntington et al., 2006). This was achieved by using a BAFF/APRIL antagonist (soluble B-cell maturation antigen; BCMA) fused to the constant region of human IgG1 (hBCMA-Fc) in EAE immunized with recombinant (rMOG). BCMA is one of the three main receptors of BAFF found on the surface of B-cells (transmembrane activator and CAML-interactor (TACI), BAFF-receptor (BAFF-R))(Gross et al., 2000, Thompson et al., 2001). Interestingly, BAFF-R was found to mediate BAFF co-stimulation of T-cells due to its co-expression on activated and memory T-cells, as well as in B-cells; while TACI and BCMA do not have the ability to express on activated and memory T-cells (Ng et al., 2004). Consequently, Huntington and co-workers found a significant delay in EAE onset and reduction in disease severity for the mice pre-treated with hBCMA-Fc, however they also observed a significant improvement in the clinical course of the mice treated with hBCMA-Fc after

the disease onset; This improvement seemed to be confirmed by the histopathological analysis that demonstrated the treated mice with hBCMA-Fc had a reduction in inflammation in the pons, forebrain, cerebellum and medulla, and they also had multiple demyelinating plaque-like lesions, which appeared to be older with little infiltration in the cerebellum and spinal cord of treated mice. Along with the modulation of the B-cell population in the therapeutically treated mice, titres of the MOG-specific auto-antibodies, and the responses seen in T_h-cell subtypes were reduced dramatically in both treatment groups, suggesting the vital role of BAFF in the pathogenesis of EAE when BCMA ligands were targeted to inhibit B-cell survival. Thus, targeting both humoral and cell-mediated immune responses may be an important therapeutic approach in acquired demyelinating diseases, such as MS. These results coincide with results from a previous study which found that B-cell deficient mice are resistant to EAE immunized with rMOG (Svensson et al., 2002).

1.4.3 BAFF-R-deficient mice accelerate CNS autoimmunity

The regulation of B-, T-cells and macrophages in the T-cell dependent model of EAE induced by MOG₃₅₋₅₅, has recently been elucidated in BAFF-R deficient (BAFF-R^{-/-}) mice (Kim et al., 2011). The investigators observed that an earlier onset of clinical disease was induced in the BAFF-R^{-/-} mice with higher severity scores manifest. More

extensive inflammation was histopathologically seen in the spinal cords of these mice with the inflammatory foci exhibiting large numbers of activated macrophages that expressed BAFF, and this was associated with elevated systemic BAFF secretion. Interpretations of this specific study were that the effect of BAFF upon the regulation of T-cells may relate to changes imposed in the function of macrophages, rather than through the promotion of B-cell survival. In support of this contention is derived from studies that have shown BAFF-R is expressed in macrophages and T-cells (Jeon et al., 2010, Sasaki et al., 2004). Furthermore, Kim *et al.* (2011) reported that the number of mature B-cells decreased significantly and antibody production was impaired in BAFF-R^{-/-} mice, suggesting that the effect of BAFF on the survival of B-cells can be governed through BAFF-R (Kim et al., 2011). Thus, a potential role for BAFF-R to mediate its effect on T-cell regulation and macrophage function in EAE exists. This seems to occur independently of mature B-cells through the generation of high levels of BAFF, which may act through other receptors (e.g. TACI or BCMA) to promote the responses of pro-inflammatory T-cells and macrophages in MS.

1.4.4 The effect of blocking BAFF with TACI-IgG in EAE

A more recent study undertaken by Wang *et al.* (2015) evaluated the effect of blocking BAFF with TACI-IgG in an attempt to reduce the mature B-cell populations in EAE mice induced by MOG₃₅₋₅₅ (Wang et al., 2015). It has been reported previously that the BAFF inhibitor atacicept (TACI-IgG) can block the effect of BAFF and APRIL by binding a

portion of the receptor TACI, causing a reduction in circulating B-cells and plasma cells, and in the bone marrow and spleen, with reported inhibition of T-cell activation, but not memory B-cells (Carbonatto et al., 2008). The effect of BAFF on T-cell activation, with the promotion of T_{h17}-cells, thereby aggravating EAE, has been mentioned previously (Zhou et al., 2011). Wang *et al.* (2015) recently found that the pathogenicity of T_{h1}- and T_{h17}-cells reduced significantly in the spleen and lymph nodes when BAFF blockade was achieved in EAE mice at day 21 after TACI-IgG treatment (Wang et al., 2015). Nonetheless, memory T-cells (CD62L⁺ CD44^{hi} CD8⁺) were up-regulated in the spleen in EAE mice, treated with TACI-IgG (Wang et al., 2015). These results were consistent to a previous finding that TACI-IgG is efficient in decreasing circulating B-cells, and interleukin 15 (IL-15), [an important cytokine sustaining expansion and survival of memory T-cells] was up-regulated in TACI-IgG treated EAE mice (Ma et al., 2014b, Ma et al., 2014a). As a consequence, Wang and co-workers blocked IL-15 in TACI-IgG treated EAE mice and they found that these memory cells were reduced markedly in the spleen and lymph nodes of this group of treated mice (Wang et al., 2015). This study suggested that a combination of BAFF and IL-15 blocking agent will be vital for autoimmune disease treatment, with possible implications for MS, by suppressing the effect of B- and T-cells, including memory cells (Wang et al., 2015). This study will be more convincing if the investigators identified the levels of immune cells in the spinal cord of TACI-IgG treated EAE mice, along with secondary lymphoid organs.

1.5 BAFF and MS

BAFF has been pointed as a potential target in MS because it is produced endogenously in the CNS by astrocytes during the pathogenesis and importantly associated closely with BAFF-R expressing cells, up-regulated within the meninges in ectopic lymphoid follicles (Krumbholz et al., 2005, Magliozzi et al., 2004). Furthermore, Ragheb *et al.* (2011) showed in their study that MS patients had higher BAFF levels in the CSF during RR and SP disease (Ragheb et al., 2011). A more recent study undertaken by Kannel *et al.* (2015) addressed the association of BAFF levels with the clinical course of RR-MS, and the efficiency of short-term steroid treatment and disease-modifying treatments (DMT) (Kannel et al., 2015). These investigators measured the levels of BAFF in the blood of 170 stable MS patients along with those of 186 with relapses after 2.3 years follow-up. Although, they found that there was a significant increase in the levels of BAFF in MS patients compared to healthy controls, BAFF levels were significantly higher in stable MS patients without relapses than those of relapsing patients (Kannel et al., 2015). In addition, they found that treatment with immunosuppressants and IFN- β increased BAFF levels in the blood without causing a more severe course of MS and this result confirmed similar previous reports (Krumbholz et al., 2008, Hedegaard et al., 2011). These clinical data may suggest that BAFF is not of relevance in the pathogenesis of RR-MS. Over the last 20 years, there were numerous therapeutic options for relapse rates in MS patients, including glatiramer acetate (GA) and IFN- β therapies. Although the earlier DMTs are mainly used to treat MS patients only, 3 studies have explored the effect of IFN- β therapy on BAFF levels in the peripheral blood of MS patients. Krumbholz *et al.* (2008) found

that BAFF levels were up-regulated in blood leucocytes and serum from MS patients were modulated following IFN- β therapy (Krumbholz et al., 2008). Furthermore, other groups investigated the effect of IFN- β therapy on circulating BAFF and autoantibodies to MBP in 23 RR-MS patients who were followed longitudinally for 26 months (Hedegaard et al., 2011). This type of treatment led to the identification of elevated BAFF levels after 3-6 months of therapy. Nevertheless, there were decreases in IgM and IgG anti-MBP reactive antibodies in the order of 11-33% respectively (Hedegaard et al., 2011). These results are consistent with those previously reported using this therapeutic approach for MS patients (Vaknin-Dembinsky et al., 2010). These findings support the concept that the effectiveness of MS treatments is associated with how the elevation of BAFF levels in the peripheral blood modulate disease, and it may be debated that B-cell-mediated immune responses may be affected differently with variable DMTs in a heterogeneous disease (Kannel et al., 2015). This study may emphasize the importance of how MS treatments alter BAFF levels, thereby modulating MS pathogenesis.

Other immunomodulatory types of MS therapeutics, such as the anti-CD52 monoclonal antibody alemtuzumab, have also been reported to coincide with elevated BAFF levels (Thompson et al., 2010). Significant increases in serum BAFF levels were documented in 78 RR-MS patients after treatment with alemtuzumab, up to 12 months of follow up investigation. However, no change in the serum levels of APRIL, TACI and BCMA, could be demonstrated after treatment with alemtuzumab (Thompson et al., 2010).

Using a soluble BAFF receptor and its related ligand APRIL (Atacicept) may be a promising clinical trial being pursued in MS therapeutics, due to the B-cell-promoting effect of BAFF. However, this treatment has been shown to worsen MS outcomes due to unclear reasons. This may indicate a function for BAFF/APRIL beyond the regulation of B-cell survival (Hartung and Kieseier, 2010). The failure of this therapy needs to be explained and considered. Indeed, the function of BAFF in CNS physiology has recently been investigated by targeting the Nogo-66 receptor (NgR1), which may also be of importance in understanding its regulatory role during the course of MS (Zhang et al., 2009).

1.6 BAFF and NgR

It was recently reported by Pool *et al* (2009) that NgR1 can be expressed on circulating immune cells from MS patients and may be involved in the induction of pro-inflammatory cytokines, demonstrating that an alternate signalling mechanism may play a role in driving neuroinflammation (Pool et al., 2009). Furthermore, Zhang *et al.* (2009) have illustrated that BlyS or BAFF may act as a ligand for NgR1 to inhibit dorsal root ganglion outgrowth (at least *in vitro*), thereby signalling independently of the putative MAIFs (Zhang et al., 2009). Several integral components of the adult mammalian CNS are responsible for inhibiting re-growth at the distal end of the axon, culminating in a regeneration/sprouting failure, initiated through MAIFs and CSPGs (Dickendesher et al., 2012). However, it is plausible that an alternate mechanism may be also operative with BAFF playing a role in the purported FLS formed in the CNS of MS patients and EAE

mice, regulated through NgR1 and NgR3 interactions (Serafini et al., 2004, von Budingen et al., 2011). If so, therefore, blocking either NgR1 or NgR3 may be a viable therapeutic approach to be trialled in MS

1.7 Therapeutic approaches for MS

Currently there is no cure for MS, however a number of therapeutic agents are being used to treat specific symptoms and sequelae of the disease, with most designed to prevent relapse rates thereby potentially limiting the progression to disability, ostensibly by targeting immune activation and inflammation (Fassas and Mancardi, 2008). Conventionally, MS can be treated by chemotherapeutic agents for chronic immunosuppression, corticosteroids for the management of acute inflammatory relapses and immunotherapeutic interventions for immunomodulation, through the use of biological agents such as natalizumab, interferon- β , glatiramer acetate, alemtuzumab, and small molecule such as dimethyl fumarate and fingolimod (Fassas and Mancardi, 2008). These treatments are used to diminish the patient's relapses both in frequency (e.g. glatiramer, interferon- β , and more recent types of monoclonal antibodies given regularly) and in severity (e.g. corticosteroids taken acutely) (Scolding, 2011). Rituximab is one such biological agent that is a monoclonal antibody of the IgG1 isotype targeting CD20 having the ability to trigger rapid complement and natural killer cell-mediated CD20 depletion (Maloney et al., 1994). Thus anti-CD20 treatment is considered as a paradigm shift for MS disease activity in the attempt to reduce autoreactive and demyelinating antibodies (Maloney et al., 1994). It has the ability to deplete peripheral B-cells, and partially deplete CSF B-cells but no change in the serum and CSF Ig titres and

OCB have been reported primarily due to the long life of Ig and/or the persistence of CD20-negative plasma cells (Hauser et al., 2008, Nesbeth et al., 2009). Compared with rituximab, a second-generation anti-CD20 monoclonal antibody with a humanised IgG1 tail, ocrelizumab, induces a reduced immune response to foreign antigens, due to the fact that it is derived mostly from human antibodies (Dorner and Burmester, 2008). Hence, given that it is thought to be less immunogenic than rituximab and expected to bind more avidly to CD20, it might be more advantageous regarding MS risk profile (Dorner and Burmester, 2008). However, what the clinical data emphasise is that both antibody-dependent and antibody-independent mechanisms of B-cells are involved in the MS disease process.

Among the most promising strategies used in regenerative medicine, hematopoietic stem cell transplantation (HSCT) prevails as an excellent but controversial therapeutic regime to limit the deleterious pathology following an autoimmune attack. It has been posited that HSCT may in fact be useful for improving the neurological function of MS patients by the replacement of auto-reactive cells with healthy cells potentially removing the patient's genetic susceptibility to propagate MS pathology (Van Wijmeersch et al., 2008).

1.7.1 Hematopoietic stem cell transplantation (HSCT)

HSCT has been harnessed for more than 40 years in the clinic as an effective therapeutic approach. In 1995, the first transplantation of hematopoietic stem cells (HSCs) was suggested as a treatment for MS after hypothesizing that an immune-mediated attack on myelin causes pathologic events in MS (Burt et al., 1995). Two years later in Greece, HSCT

was performed in 15 MS patients with progression (Fassas A et al., 1997). HSCs capable of self-renewal when effectively transplanted and engrafted in the human, can differentiate into all of the cells constituting the hematopoietic system. They are divided into two different types: long and short-term subtypes (Figure 5). Long-term (LT)-HSCs have the ability to self-renew and provide all hematopoietic lineages during the life of an individual. Short-term (ST)-HSCs, as the name suggests, are incapable of long-term self-renewal under normal conditions, however they do provide the ability to reconstitute hematopoiesis of certain lineages over a finite period (Filip et al., 2009).

HSCs represent rare cell populations that exist in the BM and constitute approximately 0.01 % of total nucleated cells (Challen et al., 2009). They can afford the complete restoration of all blood-cell lineages after BM ablation *in vivo* and the improvement of the MS patients' immunity. Based on this definition, several xenogenic and congenic assays have been established to quantitate and detect human and mouse HSCs (Wognum et al., 2003).

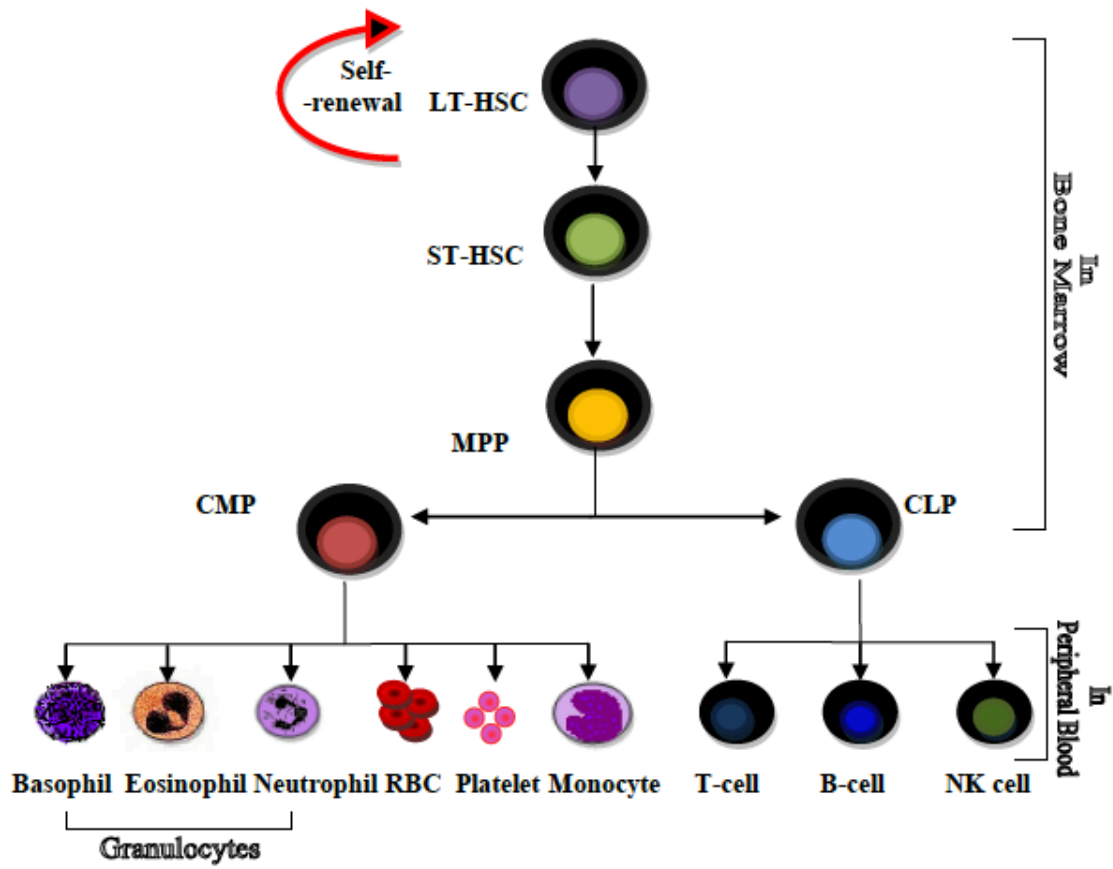


Figure 5. Hematopoietic hierarchy model. Hematopoietic stem cells (HSCs) are divided into long-term (LT)-HSC and short-term (ST)-HSC types. A LT-HSC with long-term self-renewal activity is converted into a ST-HSC and then HSCs give rise to a multipotent progenitor (MPP). A MPP commits in bone marrow to become either common myeloid progenitor (CMP) or common lymphoid progenitor (CLP). The CMP and CLP give rise to mature blood cells in peripheral blood, such as granulocytes, red blood cells (RBC), platelets, monocytes, T-cells, B-cells and NK cells (Scolding, 2011).

1.7.1.1 Isolation of HSCs

HSC populations isolated from their stem cell niche, differ morphologically. Therefore, they can be separated using several methods based on their physical, physiological properties or using specific cell surface markers (Challen et al., 2009). The study of HSCs has been expedited in the last 20 years by the development of various isolation techniques such as flow cytometry and the availability of newly developed monoclonal antibodies more specific to HSCs, with the most successful approaches varying in selectivity, choice of separation parameters and capacity (Wognum et al., 2003). These methods are classified into non-antibody and antibody-based HSC selection methods.

I. Non-antibody based methods

The most common technique for separating HSCs, based on differences in their cell size and density, is density gradient centrifugation (Wognum et al., 2003, Juopperi et al., 2007). HSC suspensions are centrifuged through a density medium such as percoll or a mixture of ficoll and hypaque, resulting in the separation of denser mature cells such as granulocytes and erythrocytes. However, this method results in loss of HSCs due to overlapping densities of lymphocytes and stem cells. Cytotoxic drugs, such as hydroxyurea and 5-fluorouracil (5-FU), can be used to selectively kill mature cells which are undergoing cell division and this approach has been used to enrich mouse HSCs before other selection techniques. Hydroxyurea inhibits the activity of ribonucleotide reductase, whereas 5-FU inhibits thymidylate synthase, the end result being decreased

production of deoxyribonucleotides, which are used in replication. Since most of HSCs are quiescent under steady-state conditions, they are resistant to cytotoxic drugs. Alkylating agents such as phosphamide, can interfere with DNA replication and can also be used to eliminate dividing cells. In addition, HSCs express aldehyde dehydrogenase (ALDH), which is an intracellular enzyme that confers resistance against phosphamides (Wognum et al., 2003). It has been demonstrated that fraction 25, lineage depleted, ALDH bright cells are stable for long-term reconstitution of lymphohematopoietic cells at 10 cells per animal. These techniques can be utilized to distinguish primitive HSCs from multiprogenitors demonstrated through colony-forming spleen assays (CFU-S) (Juopperi et al., 2007). Furthermore, HSCs are enriched by the activity of ALDH; the expression of this enzyme overlaps with the expression of CD34 in the BM cells of adult humans, demonstrating that the activity of this enzyme is a marker for primitive HSCs as well as lineage committed progenitor cells (Wognum et al., 2003).

II. Antibody-based HSC selection methods

The antibody-dependent methods for the isolation of HSCs rely on the availability of monoclonal antibodies directed against specific cell surface markers followed by isolation using either fluorescence-activated cell sorting (FACS) or magnetic activated separation (MACS) (Wognum et al., 2003). Utilizing flow cytometry, fluorescently-tagged antibodies are used to identify surface proteins, which are expressed at specific stages of development, permitting distinctions among phenotypically homogenous cell populations. By using MACS, antibodies directed against a surface antigen of interest are coated with magnetic

nanoparticles. The cells are separated by placing the cell suspension into a magnetic field following antibody incubation. Both FACS and MACS use positive and negative selection. These techniques are typically applied to provide a sufficient yield and purity of HSCs for clinical transplantation purposes by eliminating the vast majority of mature cells. Furthermore, these techniques can be adapted for either positive or negative selection of HSCs (Wognum et al., 2003).

1.7.1.2 Cell surface markers of human and mice HSCs

Although there are several shared biological similarities between human and mouse HSCs, there are differences with the purification strategies implemented for human HSCs as opposed to the experimental isolation of mouse HSCs when utilized for therapeutic applications. Although the human cord blood or adult BM side population (SP) showed very low HSC activity *in vitro*, the mouse BM SP represents significant enrichment for hematopoietic activity. Another disparity is that positive selection through the enrichment of human CD34⁺CD38⁻ cells has been readily utilized for clinical purposes enriching the populations of progenitors and HSCs (Wognum et al., 2003). However, it has been shown that only low levels of CD34 are expressed on mouse LT-HSCs (Challen et al., 2009). An outline of readily utilized markers for both human and mouse HSCs is described in Table 1. The main HSC markers that distinguish mouse and human cells are shown in Table 2.

Table 1. Surface profile of HSCs in mouse and human (Fassas A et al., 1997).

CD marker	Synonym	Main expression	Function
CD3	T3, leu-4	T-cell	Mediated T-cell signals transduction and used in Lin cocktail
CD4	T4, leu3	MHC-II, T-cell, Macrophage/monocytes, dendritic cells	Initiate early phase of T-cell activation and used in Lin cocktail
CD8	T8	MHC-I, T-cell subsets	T-cell mediated killing, and used in Lin cocktail
CD11b	CR3,MAC 1	Macrophage/monocytes, dendritic cells, granulocytes, NK cells	Phagocytosis, adhesion interaction of Macrophage/monocytes, granulocytes, and used in Lin cocktail
CD11c	CR4	Macrophage/monocytes, granulocytes, NK cells	Similar to CD11b , cell-cell interaction during inflammatory response, and used in Lin cocktail
CD34	Gp105/120, Mucosialin	Precursor of hematopoietic cells, Endothelial cells	Cell adhesion
CD38	T10	Lymphoid cells, macrophage/monocytes	Cell adhesion and transduction
CD45R	B220, Ly-5	T-cells and mostly B-cells	T and B cell antigen receptor mediated signalling, and used in Lin cocktail
CD59	MIRL	T-cells, NK cells, granulocytes, erythroid, macrophage/monocytes,	Complement cascade regulation
CD117	c-Kit	HSCs / progenitor cells and mast cells	Survival of mast cells, activation, proliferations, and chemotaxis
CD161	NK1.1	NK cells	NK cell mediated cytotoxicity, proliferation, and used in Lin cocktail
SCA-1	Ly6A/E	HSCs, HPCs, some lymphoid and myeloid cells	Mice HSCs are positive
Gr1	Ly-6G	Monocytes and granulocytes	used in Lin cocktail
Ter119	Ly76	Erythroid cells	used in Lin cocktail

CD; Cluster of Differentiation, **CR**; Complement Receptor, **MAC1**; Macrophage 1 antigen, **NK**; Natural Killer, **leu**; Leucine, **MHC**; Major Histocompatibility Complex, **HPC**; Haematopoietic progenitor cells, **MIRL**; Membrane Inhibitor of Reactive Lysis, **Sca-1**; Stem Cell Antigen-1, **c-Kit**; Tyrosine-protein kinase receptor, **lin**; Lineage markers, **Ly**; Lymphocyte activation protein.

Table 2. Main markers used to discriminate mouse and human HSCs (Wognum et al., 2003).

	Cell surface markers
Mouse	Lin⁻, CD34^{-/low}, CD38⁺, Sca-1⁺, c-Kit⁺, Thy-1, FGFR, CD201, CD105,
Human	Lin⁻, CD34⁺, CD38^{-/low}, CD133, c-Kit^{-/low}, Thy-1⁺, CDCPI, VEGFR1

Thy-1; Thymocytes, **FGFR;** Fibroblast Growth Factor Receptor, **CDCPI;** Cubdomain Containing Protein, **VEGFR1;** Vascular Endothelial Growth Factor Receptor.

In mouse HSCs, most of the purification approaches revolve around the positive selection markers, such as stem cell antigen-1 (SCA-1) or the transmembrane tyrosine-protein kinase receptor (c-Kit or CD117) and negative markers for mature HSC lineages (e.g., CD3e, CD4, CD8a, CD45R/B220, CD11b, CD11c, NK1.1, TER119, and Gr-1). Removal of mature cells that express lineage (lin) markers using an antibody cocktail leads to the enrichment of blast cells, HSCs and progenitor cells from bone marrow and blood (Wognum et al., 2003). Therefore, about 10% of Lin⁻, Sca-1⁺ and c-Kit⁺ (LSK) cells are bona fide LT-HSCs, which are self-renewing cells and can grow in culture, along with being able to be transduced *ex vivo* using lentiviral vectors (Maetzig et al., 2011). However, CD34⁺ cells from mouse BM are expressed on ST-HSCs, which rapidly die *ex vivo* and then cannot be cultured (Tsiftoglou et al., 2009), hence LSK cells are those selected for sorting by FACS for long-term culture experiments.

In addition to the cell surface markers, SP has been used to further enrich BM for mouse or human HSCs based on their capability to efflux the Hoechst nuclear dye via a membrane transport pump (ATP-binding cassette family). The dye is reserved at low levels in these cells in a highly active form when compared directly with other types of BM cells (Challen et al., 2009, Wognum et al., 2003). Rhodamine-123 (Rho) and Hoechst 33342 (Ho) are examples of effluxing specific fluorescent dyes. Rho-/low presents the majority of HSCs from adult mouse and human, while this phenotype of Rho-/low is regulated correspondingly to CD34 in murine HSCs (Wognum et al., 2003). According to Pearce *et al.* (Pearce and Bonnet, 2007), it has been suggested that there is no long-term reconstitution established by utilizing either human HSC or cord blood SP, although there is a significant

HSC enrichment when using mouse stem cell SP, which are primarily CD34⁺, highlighting differences in the transplantation of HSCs in experimental models when compared with those performed in the clinical setting.

1.7.1.3 HSCT in a mouse model of MS

HSCT was clinically pursued in MS based on strong data obtained from mouse models of autoimmune encephalomyelitis investigating the outcome of the therapy. A series of experiments conducted in the early 1990s used the classical EAE model, which has been widely used to understand the mechanism of MS disease.

Recent research in autoimmune conditions is now also investigating gene therapy as a possible option to correct the defective HSCs present prior to transplantation (Alderuccio et al., 2011). The experimental procedure includes the isolation of BM stem cells from donor mice that are transduced with retrovirus encoding a specific antigen after culturing these cells *ex vivo*. Transduced stem cells are then transferred to conditioned recipient mice; following total body irradiation (TBI), leaving them to engraft and regenerate the hematopoietic system, including dendritic cells, B- and T- cells, all lineages being identified by flow cytometry (Figure 6). By using this model, mice were resistant to EAE induction after transferring transduced BM cells with retrovirus encoding MOG (Alderuccio et al., 2011).

The rationale of autologous hematopoietic stem cell transplantation (auto-HSCT) for MS is based on using chemotherapy to induce immunoablation, with subsequent reconstitution of the impaired immune system through renewed self-tolerant cells (Burt RK, 2008). A report in 1996 by van Gelder & van Bakkum explored the use of auto-HSCT in EAE demonstrating that lymphocytes, which are present in the autologous cells, might lead to the occurrence of relapse after transplantation (van Gelder M and van Bakkum DW., 1996). An additional report by van Bakkum in 2004 explored the efficacy of auto-HSCT with TBI in Buffalo rats with EAE and absence of disease relapse was seen in 70% of cases. The treatment was found to be most effective at the early stages of autoimmune disease, whereas no effect was seen in the later stages. High-dose TBI led to a better response; however, TBI can lead to severe carcinogenic events at a later stage. The use of cyclophosphamide and busulfan also proved less effective than TBI (van Bakkum, 2004).

In addition, the animal model study was conducted to supplement the conventional non-specific-dose immunosuppression efforts. It involved the administration of a high dose of an immunosuppressant (myeloablative chemotherapy) followed by HSCT, which reduced morbidity and mortality effectively in this model. The transplant experiments showed that EAE remissions were attained in animals after high dose TBI. Therefore, the use of high-dose immunosuppressive agents in EAE led to a better response as compared to TBI (Bowen et al., 2012).

1.7.1.4 HSCT as a therapeutic option for MS

Over the last 20 years, HSCT was anticipated as a treatment for MS patients by ablating or suppressing the endogenous immune system. It is likely to beneficially affect the inflammatory stage of the disease (Burt et al., 2005). In the 1990s, auto-HSCT was suggested for the management of refractory and severe autoimmune disease, including MS. Only a few HSCT trials have implemented the use of donor-derived HSC grafts, or human leukocyte antigen (HLA)-matched allogeneic cell transplants because of the higher rate of mortality and morbidity with GVHD than auto-HSCT. The role of HLA proteins is to direct the response of T-cells and they are important in the selection of donors for allo-HSCT (Farge et al., 2010, Pasquini et al., 2012).

Recently, several MS patients were treated with auto-HSCT after exposure to high doses of immunosuppressive drugs by using different procedures of HSC harvesting and conditioning regimens (Openshaw, 2000, Farge et al., 2010, Pasquini et al., 2012). In a BM graft, around 3-5% of the cells are HSCs and the graft of peripheral blood HSCs are rich in lymphocytes, granulocytes and monocytes. The procedure of transplantation is initiated after collecting HSCs from the patient's BM through several aspirations performed under general or regional anesthesia (Atkins and Freedman, 2013). Otherwise, peripheral blood stem cells (PBCS) can be mobilized from the BM into blood circulation in large amounts by using chemotherapy and/or a specific cytokine, such as granulocyte-colony stimulating factor (G-CSF), and FLT3 ligand (TPO). In HSCT, this cytokine is injected into the donor prior to

harvesting stem cells to maximize HSC collection. During the apheresis process, the donor's blood is passed through a device whereby CD34+ (a cluster of differentiation mixture of HSCs, progenitor cells and WBCs) is expunged, and then RBCs are returned to the donor. By using this method, 5-20% of the extracted HSCs are suitable for treating patients with MS (Atkins and Freedman, 2013). These purified HSCs can be cryopreserved until the patients are ready to undergo transplantation, estimated to be between 2-6 weeks. In this process, administration of chemotherapy with or without immune depleting biological agents is vital for destroying the patient's mature immune lineage cells before infusing the cryopreserved HSCs. Hematopoietic engraftment and recovery from chemotherapy may take between 3 to 6 months (Atkins and Freedman, 2013) (Figure 7).

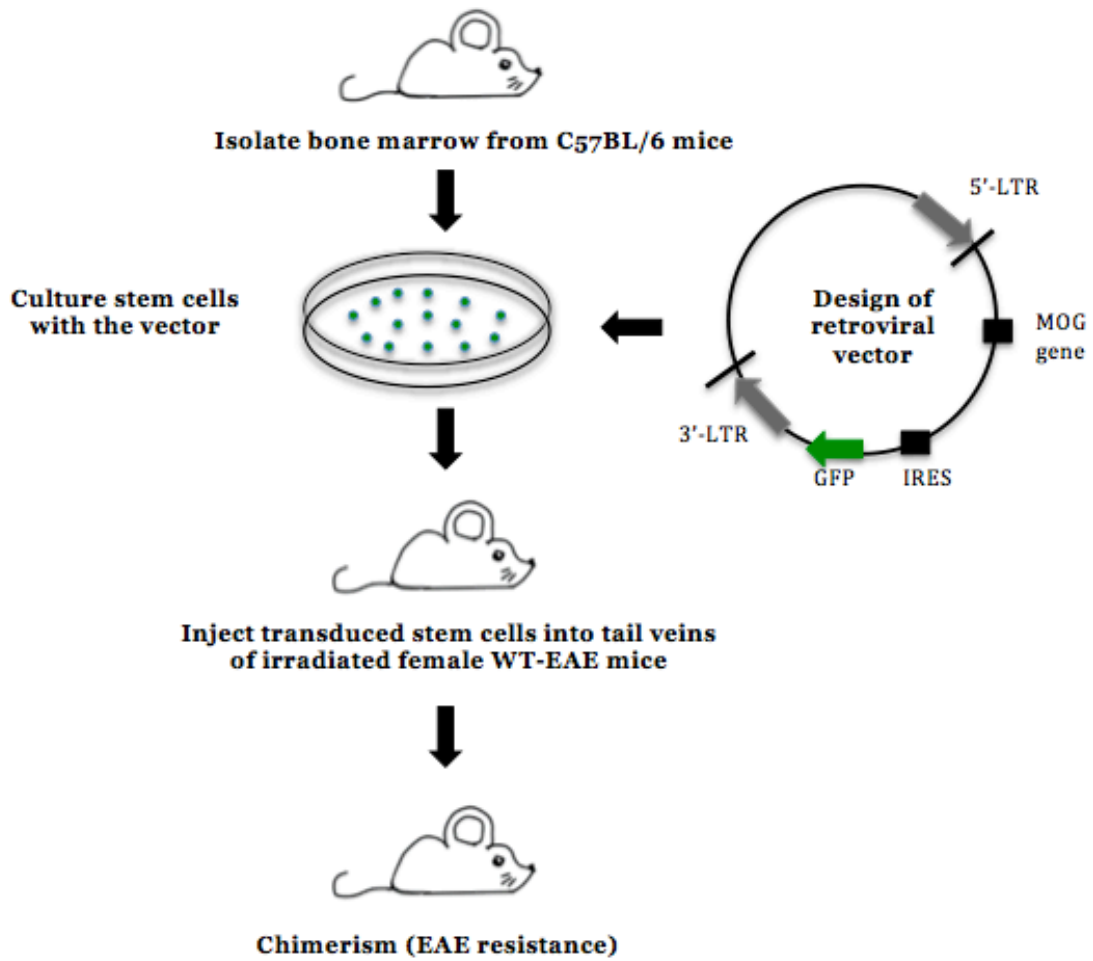


Figure 6. The experimental procedure of bone marrow transplantation in EAE mice.

Isolated bone marrow cells from 6-10 week old donor mice (C57Bl/6) are cultured *ex vivo* transduced with a retroviral vector, which encodes the MOG gene and green fluorescent protein (GFP) driven by an internal ribosomal entry site (IRES) to assist enumeration and tracking of these cells. Transplanted GFP-expressing cells into irradiated mice following their immunization with MOG₃₅₋₅₅, to induce EAE are assessed in their development or protection of disease, as well as chimerism (Alderuccio et al., 2011).

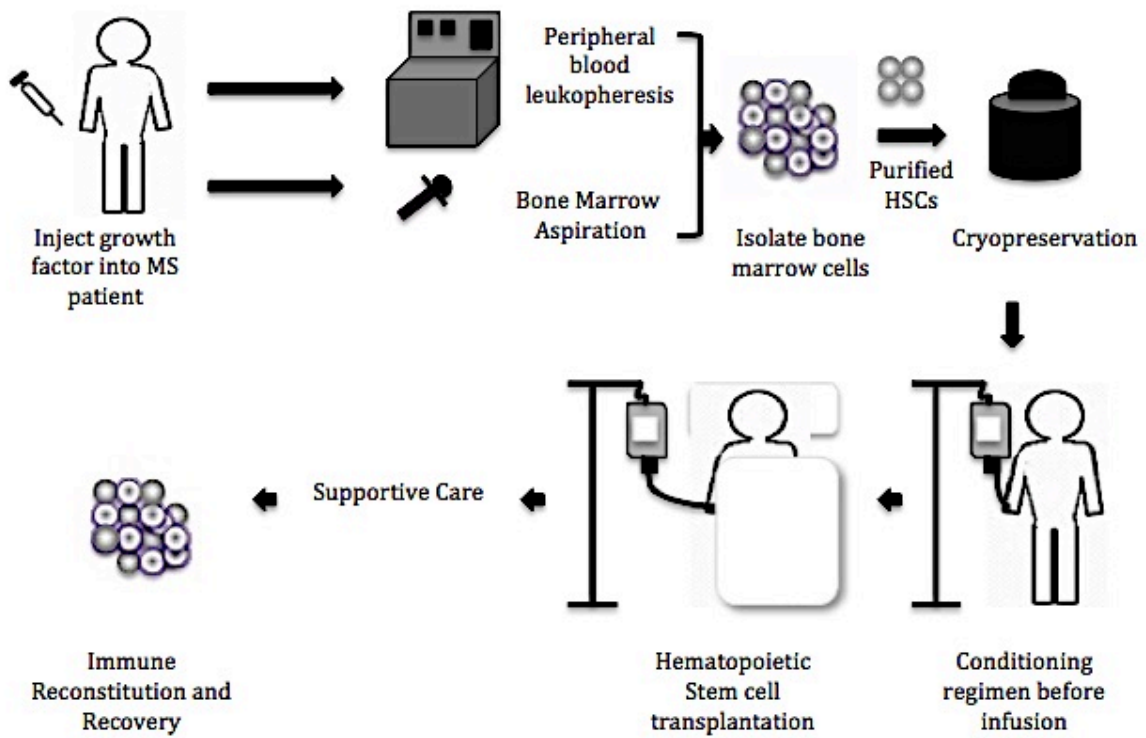


Figure 7. Autologous hematopoietic stem cell transplantation in multiple sclerosis patients. The technique is initiated after collecting HSCs from the patient's BM through BM aspiration or peripheral blood leukopheresis achieved under general or regional anesthesia (Atkins and Freedman, 2013). The collected HSC grafts are cryopreserved in liquid nitrogen until they are required for transplantation (Atkins and Freedman, 2013). The patient's immune cells will be destroyed after high dose chemotherapy along with immune ablative conditioning regimens. The cryopreserved HSCs will be infused into the patient intravenously, then the reconstitution of the hematopoietic system will occur following 10 to 14 days after transplantation, with full recovery from chemotherapy occurring between 3 to 6 months (Atkins and Freedman, 2013).

Immune reconstitution occurs by two key mechanisms; homeostatic expansion of mature T- and B-cells comprised in the graft, and de novo lymphopoiesis of new engrafted HSCs (Gress et al., 2010). In theory, on-going MS activity after HSCT may be caused by the expansion of autoreactive lymphocytes. Procedures to diminish the immune cell load in the graft may improve the outcome. Therefore, the effect of using immune ablative conditioning regimens to deplete lymphocytes in the graft may be apparent following HSCTs (Atkins and Freedman, 2013). However, when adopting or developing pre-existing HSCT regimens for novel indications, such as MS, consideration needs to be given to: 1) cytogenetic abnormalities, 2) the patient's medical condition (e.g. age, status of performance and status of disease), 3) an existing graft source, and 4) disease specific prognostic factors (Sureda et al., 2015).

Muraro *et al.* (2005) showed in their study that by using the auto-HSCT myeloablative regimen can re-configure the immune system in mature MS patients by reconstituting the CD4⁺ T cell lineage population (Muraro et al., 2005). In myeloablative conditioning regimens, patients are given chemotherapy with or without TBI before transplantation. The purpose of this process is to eliminate disease in the patient before HSC infusion and suppression of the immune system and it requires stem cell support to rescue marrow function and avoid aplasia related death. However, the process is restricted to patients less than 50 years old due to its toxic effect on non-bone marrow organs (e.g., liver, heart and lung) (Atkins and Freedman, 2013).

On the other hand, Burt *et al.* (Burt et al., 2005) confirmed in their study that the purpose of conditioning regimens in MS is lymphoablative because the rationale of auto-HSCT is to revive an antigen-naïve immune system from the patient's HSCs; thus, myeloablative regimens are lethal to HSCs. In addition, the rationale of non-myeloablative HSCT in MS is to suppress relapses by intervening prior to the onset of irreversible progressive axonal degeneration, to prevent inflammation, and to reduce toxicity in the older patient population. Such a regimen, being immunosuppressive in nature but without the myeloablative side effects, can be designed to dampen the activity of the immune system by using cyclophosphamide, fludarabine, rabbit anti-thymocyte globulin (rATG) or CAMPATH-1H (anti-lymphocyte antibodies), and/or by using the graft selection of CD34⁺ (Burt et al., 2005, Gosselin and Rivest, 2011). This *ex vivo* cell selection or depletion technology can change the composition of graft cells but it may lead to an elevated risk of treatment-related infection for an intense conditioning regime (Burt et al., 2005). Furthermore, the intensity of conditioning regimes may exert a toxic effect on the CNS and this neurotoxicity has been associated with radiation and busulfan treatment. Therefore, it may stand to reason that moderating conditioning regimes may provide a less toxic outcome for MS patients when treated through HSCT (Burt et al., 2005).

Recently, powerful conditioning regimens followed by auto-HSCT have been applied to aggressive MS. An example of this is alemtuzumab, which is a monoclonal antibody that targets the B- and/or T-cell compartment. Alemtuzumab contributed to the depletion of circulating lymphocytes that lead to the control of the autoimmune response in MS patients after transplantation, as well as to prevent the development of graft versus host disease

(GVHD) by diminishing cytotoxic effector cells (Burt RK, 2008). However, it has been noted that using this drug may lead to the induction of secondary autoimmune sequelae (Loh et al., 2007). Around 10% of patients undergoing HSCT for autoimmune illness have been observed to develop a secondary autoimmune disease unrelated to their induction for auto-HSCT within the first two years after HSCT, although the primary autoimmune illness may have been suppressed following the HSC graft (Daikeler et al., 2011). Secondary autoimmune disease was found to be less common in patients who undertook HSCT for MS but more frequent in patients who undertook HSCT for systemic lupus erythematosus (Loh et al., 2007). Furthermore, immune thrombocytopenic purpura (ITP), immune cytopenia, may occur after many years of HSCT. This may occur as a result of the lymphocyte-depleting antibodies administered during the conditioning of the HSC graft (Cuker et al., 2011). Secondary autoimmune disease occurred in around 4% of patients without having a lymphocyte-depleting agent during the HSCT conditioning regimen, although 9% of patients suffered from secondary autoimmune disease after using ATG (Cuker et al., 2011).

1.7.1.5 Complications compared with the beneficial effects of HSCT in MS

A specific study identifying the toxicity and feasibility of auto-HSCT in 15 patients with SP-MS and RR-MS with a median expanded disability status scale (EDSS) of 6 (range 4.5-6.5) measured that in 2 patients, neurological deterioration with high fever continued, 1 sustained a transient neural deterioration, 3 patients exhibited transient engraftment syndrome, 1 patient had unsuccessful mobilization and reactivation of cytomegalovirus in 1 patient. The EDSS had improved in 3 patients assessed at a one-year follow-up after transplantation but

remained constant in 9 patients and had worsened in 2 patients. According to magnetic resonance imaging (MRI), enhanced T1 lesion disappeared in patients. This study demonstrated that the feasibility and acceptable toxicity of using auto-HSCT to reduce the progression of MS. Long-term follow-up after transplantation is vital for the health management of MS patients (Carreras et al., 2003).

A more recent study conducted by Shevchenko *et al.* (Shevchenko et al., 2015) set out to determine the long-term effectiveness and safety of auto-HSCT in conjunction with high-dose immunosuppressive therapy (HDIT), along with decreased intensity BEAM condition regimen of different types of MS patients. Fassas *et al.* (Fassas A et al., 2000) pioneered BEAM as conditioning regimen for auto-HSCT, which includes carmustine (BCNU: bis-chloroethyl nitrosourea), etoposide, cytosine arabinoside, and melphalan. Investigators of this study used 99 MS patients (39 male and 60 female with mean age 35 years old); 43 of the patients were RR-MS, 35 SP-MS, 18 PP-MS, and 3 PR-MS with EDSS prior to graft was 3.5. Ninety eight patients had a neurological improvement or stabilization after 6 months of transplantation (Shevchenko et al., 2015). There were not transplanted deaths observed and cumulative incidence of disease progression was 16.7 % at 8 years post-transplantation. These studies were very favorable because 47 % of the patients improved on their EDSS scale (at least 0.5), as compared to the baseline, and 45 % of MS patients were stable at the median long-term follow-up for more than 5 years in both RR-MS and progressive MS group. Besides, the patient's quality of life improved in MS by using auto-HSCT with this specific regimen (Shevchenko et al., 2015). The consistency of these results of long-term clinical and quality of life with a previous study published by Bowen *et al.*

(2012), advocates for the safety and efficiency of this treatment approach in MS patients (Bowen et al., 2012). In addition, a clinical study was conducted by Guimaraes *et al.* (Guimarães FA, 2010) to determine the impact of auto-HSCT on health related quality of life (HRQL) in patients with PP-MS and SP-MS in Brazil (Guimarães FA, 2010). Approximately, 79% of patients enrolled in these trials (27 patients) revealed neurological improvement one year after transplantation with significant improvement in the HRQL indicating that although HSCT involves complicated procedures, it impacts positively in MS patients by improving their HRQL. Progression-free survival after treatment with HSCT has been reported in 81% of SP-MS patients after three years and 67% of PP-MS patients (Guimarães FA, 2010).

On the other hand, researchers in Greece released long-term results from a single center phase I/II trial of auto-HSCT (Fassas et al., 2011). According to clinical and MRI data from 35 patients with progressive MS treated with auto-HSCT, researchers demonstrated that HSCT is a therapy for aggressive cases but not recommended for the vast majority of MS patients with more common relapsing-remitting presentations. Moreover, HSCT has a sustained and impressive effect in suppressing disease activity after a medium follow-up period of 11 (range 2-15) years. At 15 years, disease (progression-free) survival was 44% for patients with active CNS disease and 10% for those without. There was an improvement in EDSS scores in 16 patients by 0.5-5.5 for a median of 2 years. However, EDSS from 9 patients did not progress above baseline scores and 2 patients died from transplant related complications. MRI data identified a significant reduction of gadolinium enhancing lesions

after mobilization, became maximal post-transplantation (Fassas et al., 2011). This study is consistent with Saccardi *et al.* (Saccardi et al., 2006) on 178 patients from 45 centers.

Several studies have shown the ineffectiveness of using HSCT for young patients with highly aggressive, malignant forms of MS. This type of MS is rare and characterized by abnormally localized autoimmune processes in the brain stem or upper cervical cord and/or intense inflammation resulting in rapid development of significant disability or death in the early stages of the disease course. Marburg variant MS is another demyelinating disease with an equally ominous prognosis with malignant MS, although it may differ histologically (Atkins et al., 2012, Kimiskidis et al., 2008). Since 2011, researchers in the United Kingdom evaluated the effect of using pulsed cyclophosphamide and non-myeloablative auto-HSCT in the case of a severely disabled 21 years of age female patient presenting with malignant MS, after auto-HSCT. This kind of treatment led to the improvement in the patient, who suffered from a disturbance of sensorimotor function in all four limbs. The results of her neuro-imaging showed demyelination with enhancement, cerebrospinal fluid (CSF) was positive to oligoclonal bands and demonstrated 47 lymphocytes, and serum was negative for aquaporin4 (Aq4) antibodies. Although she experienced several treatments, such as alemtuzumab with pulsed IV methylprednisolone (IVMP) and plasma exchange, she continued to deteriorate. The patient underwent auto-HSCT after 2 months of treatment with cyclophosphamide. The patient's EDSS was 8.5 at the time of transplantation but it decreased to 6.5 one year after the treatment, and she was able to walk. According to this case report, using cyclophosphamide prior to auto-HSCT is crucial for clinical

improvement, suppression of relapses, and stabilization of lesion burden, especially in highly active RR-MS patients (Alix et al., 2013). This study is consistent with the Fagius *et al.* (Fagius et al., 2009) study on 9 patients with malignant RR-MS who underwent auto-HSCT with BEAM condition followed by cyclophosphamide, resulting in 1 relapse in 280 patients/months following HSCT. All patients had their disability improve or stabilize, and most of the patients showed no enhanced lesions during follow-up. Furthermore, Kimiskidis *et al.* (Kimiskidis et al., 2008) reported an improvement and long-lasting clinical and radiological response in the case with malignant MS who was treated with high dose chemotherapy plus ATG followed by auto-HSCT.

Results from several studies recommend non-myeloablative HSCT to treat SP-MS and RR-MS mainly due to the fact that HSCT has immunosuppressive and immunomodulatory effects, evident by a more diverse T-cell clonal population in post-HSCT patients (Holloman, 2013). This occurs due to the ability of HSCT to modulate autoimmunity without the requirement to eradicate the full patient's hematopoietic cells (myeloablation regimen). In 2015, a study by Burt *et al.* (Burt et al., 2015) focused on improving of neurological disabilities and other clinical results of RR-MS patients using non-myeloablative HSCT. This study included 191 MS patients; 123 patients had a RR course of the disease and 28 had SP-MS, with mean age at 36 years old. Patients were treated at a single United States institution between 2003 and 2014, and the researchers followed-up with patients for 5 years. At year 4 post-transplantation, 64 % of patients demonstrated improvement in EDSS score from a pre-transplant median of 4.0 to 2.5 and neurological rating scale scores increased from a pre-transplant median of 74 to 87.5 in

34 patients and the MS functional composite scores were 0.45 (0.04 to 0.60) with p value 0.02. Brain T2 lesion volume reduced significantly from a pre-transplant median of 8.57 cm³ to 5.74 cm³ ($p < 0.001$) at the last post-transplant assessment on MRI scans in 128 patients with a mean follow-up of 27 months. In this study, the quality of life short form based upon the 36 questionnaire score, was improved significantly in 132 patients from a pre-transplant median of 46 to 64 at year 2 post-transplant as compared to the previous results of the AFFIRM and SENTINEL trials. In addition, there were no early or late infectious cases of fungal, *P. jirovecii*, JC virus, Epstein-Barr virus, or cytomegalovirus, and there was no treatment related mortality (Burt et al., 2015). Altogether, using non-myeloablative HSCT was crucial in improving neurological disabilities in RR-MS patients.

A major pathological complication of auto-HSCT may be the effects reported on brain volume. Saiz *et al* (Saiz et al., 2001) focused on monitoring the evolution of inflammatory disease activity by suppressing the relapses and Gd+ MRI lesions post auto-HSCT. Four out of five patients had a constant or improved EDSS after three and 12 months post-transplantation, but the fifth patient suffered deterioration in their condition during the treatment. For all the patients post auto-HSCT, there was no enhancement of T1 lesions and no enlargement of or new T2 lesions (median: 11.8% appearing). In addition, the corpus callosum area decreased in all patients at one-year follow-up (median declines: 12.4%) and for two patients, there was no progress at two-years post-HSCT. These results suggest a positive impact of auto-HSCT on active inflammation that corresponds with the clinical stabilization of the five patients at one-year post-HSCT.

Although the five patients showed improvements in other MRI variables, the atrophy of the corpus callosum increased. The relationship between the development of brain atrophy and inflammatory activity is uncertain. This study indicates the effectiveness of using auto-HSCT in arresting the inflammatory activity; however, the pathological process responsible for brain atrophy was not reversed (Saiz et al., 2001).

Rapid loss of brain volume has been measured a few months after treatment (Burt et al., 2003). Auto-HSCT has seemingly detrimental effects on the integrity of the brain tissue that leads to rapid loss of about 1.92% of brain volume. A study on SP-MS patients showed that brain atrophy after auto-HSCT is not constant but declines for the first two years after treatment. The reduction in brain volume may be a result of the significant inflammation seen before stem cell transplantation is performed. The pathological evidence for this is through the large number of transected axons seen in MS lesions, marked axonal injury, cortical demyelination and diffuse inflammation of the brain observed after histopathological analysis (Burt et al., 2003). Histopathological studies have also been carried out on brain tissue obtained at autopsy from deceased who had been treated with auto-HSCT and they indicate ongoing active demyelination. Metz *et al.* (Metz et al., 2007) have interrogated brain tissue samples from 5 patients with chronic lesions where they investigated 53 individual white matter lesions through immunohistochemical and routine staining techniques. They were able to characterize damaged axons, activated macrophages/microglial cells, inflammatory infiltrates and demyelinating activity in these lesions. Limited numbers of T-cells, which were dominated by CD8⁺ cytotoxic T-cells in the inflammatory infiltrate, could be observed

within the lesions while plasma cells, and B-cells were completely absent. Macrophages/microglial cells were found on the injured tissue and high numbers of damaged axons were present in the active lesion areas. The study concluded that axonal degeneration and demyelination remain a constant feature even after auto-HSCT, despite effective immunosuppression associated with transplantation (Metz et al., 2007). Their data were supported by other clinical studies, which indicate that there is continued clinical disease progression in MS patients with high EDSS despite their special auto-HSCT therapy (Sainaghi PP, 2013). The clinical efficacy of intense immunosuppression with auto-HSCT does not appear to avoid further progression in MS patients with high EDSS (> 6.0) (Metz et al., 2007). Thus, future HSCT trials should consider inclusion criteria to be early stage of disease course with active relapses of MS, as well as combinatorial new therapeutic strategies that may prevent ongoing neurodegeneration and demyelination in progressive MS (Metz et al., 2007).

A more recent study undertaken by Mancardi *et al.* (Mancardi et al., 2015) in Italy evaluated the effect of a highly intense conditioning regimen followed by auto-HSCT compared to the immunosuppressive therapy, mitoxantrone (MTX; EMD Serono, Novatrone) on the disease activity of 21 MS patients. This controlled, randomized, multicenter phase II trial of auto-HSCT led to a significant reduction in T2-weighted lesions, gadolinium-enhancing (Gd⁺) areas, and annualized relapse rates (ARR) as compared to MTX. 9 patients (4 SP-MS with relapses, 3 SP-MS, 2 RR-MS) were assigned to the auto-HSCT group and 12 patients ended up in the MTX-treatment group (5 RR-MS, 3 SP-MS, 3 SP-MS with relapses, 1 RP-MS). The first group was given 4

g/m² of cyclophosphamide and 5 µg/kg body weight of filgrastim, along with a high-dose chemotherapy conditioning regimen, BEAM. Patients treated with MTX received a 20 mg MTX dose intravenously and 1 g of methylprednisolone diluted in 250 mL 0.9 saline every month for 6 months. The researchers found that 79% of patients who experienced auto-HSCT had fewer new T2 lesions on MRI scans as compared to the MTX-treated patients by using an intention-to-treat analysis. However, due to patient dropout and technical problems, only 17 of the 21 patients had MRI scans. Furthermore, there was a complete suppression of active inflammatory lesions, as demonstrated by the absence of new Gd⁺ lesions in the auto-HSCT group during a 4-year follow up, although 56% of MTX-treated patients had inflammatory activity. In regards to the effect of ARR over 4 years, ARR reduced in the auto-HSCT patients with 0.19 as compared to MTX patients (ARR=0.6). Nevertheless, only 48% of MTX patients demonstrated progression while 57% of auto-HSCT patients had progressed at the end of follow up. There were no observable differences in EDSS scores between the two groups. This study demonstrated that for patients with severe progressive MS, treatment with auto-HSCT is superior to treatment with MTX. The effect is related to the intensity of the conditioning regimen, which was used to reset the immune system in MS patients before performing HSCT, compared to the Nash *et al.* (Nash et al., 2015) and Burt *et al.* (Burt et al., 2015) trials that were reported earlier in 2015. Although this randomized and controlled study yielded promising results, the sample size was small. In addition, the clinical results of Mancardi *et al.* (Mancardi et al., 2015) study were lackluster in comparison to other studies in auto-HSCT, especially when compared with the reduction in EDSS among MS patients, who enrolled in the Burt *et al.* (Burt et al., 2015) study in 2015 as well as the information on

quality of life and brain atrophy, not investigated in this study.

1.7.1.6 Criteria to be considered in HSCT in MS patients

There are several criteria that may play a crucial role in using HSCT as a therapeutic option in the management of MS, including proposed international multicenter, randomized clinical trials of HSCT compared to the best standard of care treatment, MS patients' selection in studies and long-term follow-up studies of patients from international registries (Atkins and Freedman, 2013). Although recent studies provide a significant improvement in various types of MS patients' lives, several vital limitations have been reported (Shevchenko et al., 2015, Burt et al., 2015). Firstly, the inferences deducted of HSCT effects cannot be made because most studies were observational for the treated cohorts without appropriate control groups. Secondly, there has not been enough information about the disease activity before the disease course and its treatment (and there has been no long-term follow-up available for certain patients). In addition, the studies were mostly performed at a single institution, which may implicate bias.

In this review, we hypothesised that NgR may play a role in the modulation of the adaptive immune response during the progression of EAE in the maturation and differentiation of BAFF-reactive B-cells within follicles that are localized within the CNS during EAE due to the fact that NgR1 is expressed on specific immune cells, as well as its role well documented in limiting axonal regrowth. (Pool et al., 2009, David et al., 2008, Fry et al., 2007). Interestingly, B-cells present within FLS are considered culprits

in MS grey matter lesion due to the fact that B-cells have several effector functions, including antigen presentation to T-cells, antigen uptake and transport, cytokine and chemokine production, and migration to inflammatory sites, and they can also produce pathogenic autoantibodies (Moisini and Davidson, 2009). Additionally, BAFF, which stimulates B-cell activation, interacts with NgR1 *in vitro* (Zhang et al., 2009). Therefore, BAFF signalling in B-cells may be targeted for inactivation by binding to the Nogo-receptor ectodomain fused to the mouse Fc peptide of IgG1 (NgR(310)-Fc), using a novel HSC-based delivery of a therapeutic protein to limit the immune-mediated degeneration of axons in EAE.

1.8 Conclusion

MS is a neuroinflammatory disease of the spinal cord, brain and optic nerve manifesting as demyelination and progressive neurodegeneration (Vosoughi and Freedman, 2010). Chronic-active forms of MS, such as primary progressive (PP-MS) and secondary progressive (SP-MS), do not respond to treatment (Fitzner, 2010). Thus, a novel therapeutic approach for progressive MS may consist of strategies targeting the Nogo-A protein, which has been well characterised in the inflammatory mouse model of MS, namely EAE. Recently, data from our laboratory have clearly demonstrated that deletion of the cognate receptor for Nogo-A, NgR1, can protect against axonal degeneration, and thus progression of disease, in EAE-induced mice. Moreover, it has been identified *in vitro* that BAFF may act as a ligand for NgR1 to inhibit neurite outgrowth (Zhang et al., 2009). Therefore, this study indicates that there may exist a strong correlation between

NgR1 and BAFF. It is tantalising to hypothesise that NgR1 localised on B-cells may interact with BAFF on neighbouring B-cells within a follicular structure stimulating their development, thereby propagating the neurodegenerative disease through the development of immunocompetent B-cells that target neural autoantigens. Thus, in the current series of experiments, we have targeted the NgR1-specific ligands using a novel HSC-based delivery of a therapeutic protein that utilises the Nogo-receptor ectodomain fused to the mouse Fc peptide of IgG1 (NgR(310)-Fc) as a means of limiting the immune-mediated degeneration of axons in a MS model. As a corollary, we have investigated whether the NgR1-Fc can bind and inactivate BAFF signalling in B-cells to localised in spinal cord during EAE. HSCT is a plausible treatment paradigm for MS patients. However, auto-HSCT is considered to be a ‘sledgehammer’ approach at treating MS patients, one that will be astoundingly effective when used on appropriately selected patients. The reasons for this promising therapy’s success are its lower toxicity and its ability to replace the immune system. The future of HSCT trials should discover novel therapeutic strategies that prevent ongoing neurodegeneration and demyelination in progressive MS. The trial designs should consider the reproducibility of HSCs with sufficient yield and purity, select MS patients with active inflammatory disease and use appropriate conditioning agents. We are now assuming the question whether NgR1-Fc delivered to the lesion site can not only be beneficial to limit the neurodegenerative ligands such as the MAIFs and CSPG but also other soluble ligands such as BAFF that can perpetrate the inflammatory nature of the disease governed by meningeal B-cells.

1.9 Research rationale, hypothesis and aims

Research Rationale

The current proposal aims to answer a critical question in neuroimmunology regarding the existence of a prominent immunological role for NgR, which may in fact potentiate the axonal degeneration commonly seen following EAE induction. We will systematically dissect the immune function of NgR1 and NgR3 during CNS inflammation, initially in *ngr1*^{+/+} wild-type mice following EAE induction. We will then compare this repertoire with the *ngr1*^{-/-} mutant mice, to elucidate how the expression of NgR1 and NgR3 on specific immune cell lineages can effect their infiltration and activation in the CNS. In particular, we plan on identifying how NgR1 and NgR3 can propagate neurodegeneration and we will also attempt to block the inflammatory-mediated effect of degeneration in the CNS by virtue of a novel gene delivery system of the therapeutic fusion protein NgR1-Fc.

Hypothesis

NgR1 and NgR3 may play a role in the maturation and differentiation of BAFF-reactive B-cells within the follicles that are localised within the CNS during neuroinflammation, exhibited in the animal model of MS, EAE.

Aims

Aim 1: To define the immune function of NgR during CNS inflammation.

Aim 2: To identify BAFF as an alternate ligand for NgR during the induction of EAE.

Aim 3: Transplantation of genetically modified hematopoietic stem cells (HSCs) to deliver the therapeutic NgR(310)-Fc protein in to the active demyelinating lesion.

REVIEW

Open Access



Hematopoietic stem cell transplantation for multiple sclerosis: is it a clinical reality?

Maha M. Bakuraysah, Christopher Siatskas and Steven Petratos*

Abstract

Hematopoietic stem cell transplantation (HSCT) is a treatment paradigm that has long been utilized for cancers of the blood and bone marrow but has gained some traction as a treatment paradigm for multiple sclerosis (MS). Success in the treatment of patients with this approach has been reported primarily when strict inclusion criteria are imposed that have eventuated a more precise understanding of MS pathophysiology, thereby governing trial design. Moreover, enhancing the yield and purity of hematopoietic stem cells during isolation along with the utility of appropriate conditioning agents has provided a clearer foundation for clinical translation studies. To support this approach, preclinical data derived from animal models of MS, experimental autoimmune encephalomyelitis, have provided clear identification of multipotent stem cells that can reconstitute the immune system to override the autoimmune attack of the central nervous system. In this review, we will discuss the rationale of HSCT to treat MS by providing the benefits and complications of the clinically relevant protocols, the varying graft types, and conditioning regimens. However, we emphasize that future trials based on HSCT should be focused on specific therapeutic strategies to target and limit ongoing neurodegeneration and demyelination in progressive MS, in the hope that such treatment may serve a greater catchment of patient cohorts with potentially enhanced efficiency and lower toxicity. Despite these future ambitions, a proposed international multicenter, randomized clinical trial of HSCT should be governed by the best standard care of treatment, whereby MS patients are selected upon strict clinical course criteria and long-term follow-up studies of patients from international registries are imposed to advocate HSCT as a therapeutic option in the management of MS.

Background

Multiple sclerosis (MS) has been defined as an autoimmune disease of the central nervous system (CNS). Although the etiology of MS has not been clearly elucidated, it is generally agreed that autoreactive T cells, activated by either self-reactive or cross-reactive antigens, migrate through the blood–brain barrier (BBB) and trigger an inflammatory cascade that ultimately leads to demyelination and progressive neurodegeneration of the CNS [1]. Pathologically, the brain tissue of autopsy patients exhibits inflammatory infiltrates with the degeneration of myelin, reactive gliosis, and axonal degeneration [2, 3]. Neurological disability is manifest in a number of symptoms, including blurred vision and diplopia, sensory disturbances (e.g., paresthesia and dysesthesia), heat intolerance, hemiparesis or paraparesis, vertigo and dizziness, lack

of coordination, limb spasticity, bowel and bladder incontinence, cognitive impairment, and memory loss.

As with most autoimmune disorders, MS predominantly affects young females between 20 and 40 years of age with the prevalence being 80–120/100,000 population with a lifetime risk of 1 in 400 [4, 5]. MS is classified into four main subtypes: relapsing remitting (RR), secondary progressive (SP), primary progressive (PP), and progressive relapsing (PR) [2]. Over 80 % of patients with MS begin with a RR course characterized by relapses that result from inflammation, followed by incomplete or complete remission. After 5–15 years from its onset, 50 % of patients enter SP-MS, where pre-existing neurological deficits gradually worsen from the onset with subsequent superimposed relapses. The latter is characterized by axonal degeneration and loss, leading to gliosis and brain atrophy. MS follows the PP phase in 15 % of individuals, in which disability accumulates faster than in the early RR course. PR-MS is the least frequent form of MS and is characterized by a steady

* Correspondence: [REDACTED]
Department of Medicine, Central Clinical School, Monash University, Prahran, VIC 3004, Australia



© 2016 Bakuraysah et al. **Open Access** This article is distributed under the terms of the Creative Commons Attribution 4.0 International License (<http://creativecommons.org/licenses/by/4.0/>), which permits unrestricted use, distribution, and reproduction in any medium, provided you give appropriate credit to the original author(s) and the source, provide a link to the Creative Commons license, and indicate if changes were made. The Creative Commons Public Domain Dedication waiver (<http://creativecommons.org/publicdomain/zero/1.0/>) applies to the data made available in this article, unless otherwise stated.

neurological decline with superimposed attacks experienced by the patient [3, 6].

Currently there is no cure for MS, but a number of therapeutic agents are used to treat specific symptoms and sequelae of the disease, with most designed to prevent the progression of disability by targeting immune activation and inflammation [3]. Conventionally, MS can be treated by chemotherapeutic agents for chronic immunosuppression, corticosteroids for the management of acute inflammatory relapses, and immunotherapeutic interventions for immunomodulation, using drugs such as natalizumab, interferon beta, glatiramer acetate, dimethyl fumarate, alemtuzumab, and fingolimod [3]. These treatments are used to diminish the patient's relapses both in frequency (e.g., glatiramer, interferon beta, and more recent types of monoclonal antibodies given regularly) and in severity (e.g., corticosteroids taken acutely) [7]. Among the most promising strategies used in regenerative medicine, hematopoietic stem cell transplantation (HSCT) prevails as an excellent but controversial therapeutic regime to limit the deleterious pathology following an autoimmune attack. It has been posited that HSCT may in fact be useful for improving the neurological function of MS patients by the replacement of autoreactive cells with healthy cells, potentially removing the patient's genetic susceptibility to develop MS [8].

Hematopoietic stem cell transplantation

HSCT has been harnessed for more than 40 years in the clinic as an effective therapeutic approach. In 1995, the first transplantation of hematopoietic stem cells (HSCs) was suggested as a treatment for MS after hypothesizing that an immune-mediated attack on myelin causes pathologic events in MS [9]. Two years later in the United States, HSCT was performed in 15 MS patients with a progressive form [10]. HSCs capable of self-renewal when effectively transplanted and engrafted in the human can differentiate into all of the cells found in the hematopoietic system. They are divided into two different types: long-term (LT) and short-term (ST) subtypes (Fig. 1). LT-HSCs have the ability to self-renew and provide all hematopoietic lineages during the life of an individual. ST-HSCs, as the name suggests, are incapable of long-term self-renewal under normal conditions, but they do provide the ability to reconstitute hematopoiesis of certain lineages over a finite period [11].

Isolation of HSCs

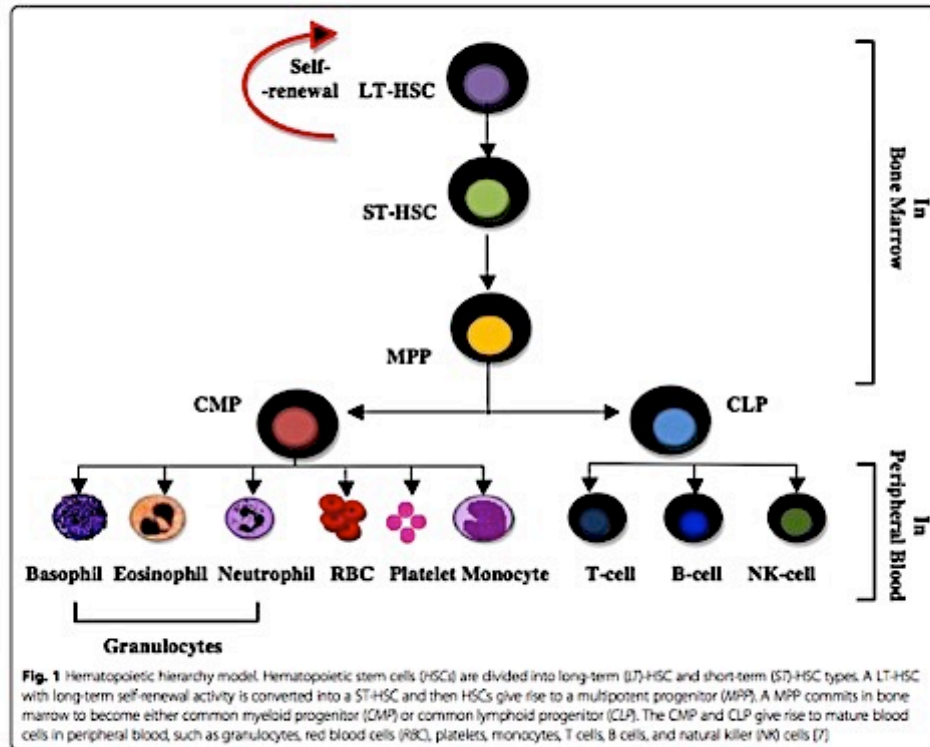
HSCs represent rare cell populations that exist in the bone marrow (BM) and constitute approximately 0.01 % of total nucleated cells [12]. They can afford the complete restoration of all blood-cell lineages after BM ablation *in vivo* and the improvement of the MS patients' immunity. Based on this definition, several xenogenic and congenic assays

have been established to quantitate and detect human and mouse HSCs [13].

HSC populations isolated from their stem cell niche differ morphologically. They can therefore be separated using several methods based on their physical properties, on their physiological properties, or using specific cell surface markers [12]. The study of HSCs has been expedited in the last 20 years by the development of various isolation techniques such as flow cytometry and the availability of newly developed monoclonal antibodies more specific to HSCs, with the most successful approaches varying in selectivity, choice of separation parameters, and capacity [13]. These methods are classified into nonantibody-based and antibody-based HSC selection methods.

HSC selection methods without the need of antibodies

The most common technique for separating HSCs, based on differences in their cell size and density, is density gradient centrifugation [13, 14]. HSC suspensions are centrifuged through a density medium such as Percoll (GE Healthcare life Sciences, Uppsala, Sweden) or a mixture of Ficoll (GE Healthcare life Sciences) and Hypaque (GE Healthcare life Sciences), resulting in the separation of denser mature cells such as granulocytes and erythrocytes. However, this method results in loss of HSCs due to overlapping densities of lymphocytes and stem cells. Cytotoxic drugs, such as hydroxyurea and 5-fluorouracil (5-FU), can be used to selectively kill mature cells which are undergoing cell division and this approach has been used to enrich mouse HSCs before other selection techniques. Hydroxyurea inhibits the activity of ribonucleotide reductase, whereas 5-FU inhibits thymidylate synthase, the end result being decreased production of deoxyribonucleotides, which are used in replication. Since most HSCs are quiescent under steady-state conditions, they are resistant to cytotoxic drugs. Alkylating agents such as phosphamide can interfere with DNA replication and can also be used to eliminate dividing cells. In addition, HSCs express aldehyde dehydrogenase (ALDH), which is an intracellular enzyme that confers resistance against phosphamides [13]. It has been demonstrated that fraction 25, lineage-depleted, ALDH bright cells are stable for long-term reconstitution of lymphohematopoietic cells at 10 cells per animal. These techniques can be utilized to distinguish primitive HSCs from multiprogenitors demonstrated through colony-forming spleen assays (CFU-S) [14]. Furthermore, HSCs are enriched by the activity of ALDH; the expression of this enzyme overlaps with the expression of CD34 in the BM cells of adult humans, demonstrating that the activity of this enzyme is a marker for primitive HSCs as well as lineage-committed progenitor cells [13].



Antibody-based HSC selection methods

The antibody-dependent methods for the isolation of HSCs rely on the availability of monoclonal antibodies directed against specific cell surface markers followed by isolation using either fluorescence-activated cell sorting (FACS) or magnetic-activated separation (MACS) [13]. Utilizing flow cytometry, fluorescently tagged antibodies are used to identify surface proteins, which are expressed at specific stages of development, permitting distinctions among phenotypically homogeneous cell populations. Using MACS, antibodies directed against a surface antigen of interest are coated with magnetic nanoparticles. The cells are separated by placing the cell suspension into a magnetic field following antibody incubation. Both FACS and MACS use positive and negative selection. These techniques are typically applied to provide a sufficient yield and purity of HSCs for clinical transplantation purposes by eliminating the vast majority of mature cells. Furthermore, these techniques can be adapted for either positive or negative selection of HSCs [13].

Cell surface markers of human and mice HSCs

Although there are several shared biological similarities between human and mouse HSCs, there are differences in the purification strategies implemented for human HSCs as opposed to the experimental isolation of mouse HSCs when utilized for therapeutic applications. Although the human cord blood or adult BM side population showed very low HSC activity *in vitro*, the mouse BM side population represents significant enrichment for hematopoietic activity. Another disparity is that positive selection through the enrichment of human CD34⁺CD38⁻ cells has been readily utilized for clinical purposes enriching the populations of progenitors and HSCs [13]. However, it has been shown that only low levels of CD34 are expressed on mouse LT-HSCs [12]. An outline of readily utilized markers for both human and mouse HSCs is presented in Table 1. The main HSC markers that distinguish mouse and human cells are presented in Table 2.

Table 1 Surface profile of HSCs in mouse and human [7]

CD marker	Synonym	Main expression	Function
CD3	T3, leu4	T cell	Mediated T-cell signal transduction and used in Lin cocktail
CD4	T4, leu3	MHC-II, T cell, macrophage/monocytes, dendritic cells	Initiate early phase of T-cell activation and used in Lin cocktail
CD8	T8	MHC-I, T-cell subsets	T-cell-mediated killing, and used in Lin cocktail
CD11b	CR3, MAC 1	Macrophage/monocytes, dendritic cells, granulocytes, NK cells	Phagocytosis, adhesion interaction of macrophage/monocytes, granulocytes, and used in Lin cocktail
CD11c	CR4	Macrophage/monocytes, granulocytes, NK cells	Similar to CD11b, cell-cell interaction during inflammatory response, and used in Lin cocktail
CD34	Gp105/120, Mucosalin	Precursor of hematopoietic cells, endothelial cells	Cell adhesion
CD38	T10	Lymphoid cells, macrophage/monocytes	Cell adhesion and transduction
CD45R	B220, Ly-5	T cells and mostly B cells	T-cell and B-cell antigen receptor-mediated signaling and used in Lin cocktail
CD59	MIRL	T cells, NK cells, granulocytes, erythroid, macrophage/monocytes	Complement cascade regulation
CD117	c-Kit	HSCs/progenitor cells and mast cells	Survival of mast cells, activation, proliferation, and chemotaxis
CD161	NK1.1	NK cells	NK cell-mediated cytotoxicity, proliferation, and used in Lin cocktail
SCA-1	Ly6A/E	HSCs, HPCs, some lymphoid and myeloid cells	Mouse HSCs are positive
Gr1	Ly-6G	Monocytes and granulocytes	Used in Lin cocktail
Ter119	Ly76	Erythroid cells	Used in Lin cocktail

CD cluster of differentiation, c-Kit tyrosine-protein kinase receptor, CR complement receptor, HPC hematopoietic progenitor cell, HSC hematopoietic stem cell, leu leucine, Lin lineage markers, Ly lymphocyte activation protein, MAC1 macrophage 1 antigen, MHC major histocompatibility complex, MIRL membrane inhibitor of reactive lysis, NK natural killer, SCA-1 stem cell antigen-1

In mouse HSCs, most of the purification approaches revolve around the positive selection markers, such as stem cell antigen-1 (SCA-1) or the transmembrane tyrosine-protein kinase receptor (c-Kit or CD117) and negative markers for mature HSC lineages (e.g., CD3e, CD4, CD8a, CD45R/B220, CD11b, CD11c, NK1.1, TER119, and Gr-1). Removal of mature cells that express lineage (lin) markers using an antibody cocktail leads to the enrichment of blast cells, HSCs, and progenitor cells from BM and blood [13]. Therefore, about 10 % of Lin⁻, Sca-1⁺, and c-Kit⁺ (LSK) cells are bona fide LT-HSCs, which are self-renewing cells and can grow in culture, along with being able to be transduced ex vivo using lentiviral vectors [15]. However, CD34⁺ cells from mouse BM are expressed on ST-HSCs, which rapidly die ex vivo and then cannot be cultured [16]. Hence LSK

cells are those selected for sorting by FACS for long-term culture experiments.

In addition to the identification of cell surface markers, the side population has been used to further enrich BM for mouse or human HSCs based on their capability to efflux the Hoechst nuclear dye via a membrane transport pump (ATP-binding cassette family). The dye is reserved at low levels in these cells in a highly active form when compared directly with other types of BM cells [12, 13]. Rhodamine-123 (Rho) and Hoechst 33342 (Ho) are examples of effluxing specific fluorescent dyes. Rho^{-low} presents the majority of HSCs from adult mouse and human, while this phenotype of Rho^{-low} is regulated correspondingly to CD34 in murine HSCs [13]. According to Pearce and Bonnet [17], it may be that there is no long-term reconstitution established by utilizing either human HSCs or the cord blood side population, although there is a significant HSC enrichment when using the mouse stem cell side population, which are primarily CD34⁺, highlighting differences in the transplantation of HSCs in experimental models when compared with those performed in the clinical setting.

HSCT in a mouse model of MS

HSCT was clinically pursued in MS based on strong data obtained from mouse models of autoimmune

Table 2 Main markers used to discriminate mouse and human HSCs [10]

	Cell surface markers
Mouse	lin ⁻ , CD34 ^{low} , CD38 ⁺ , Sca-1 ⁺ , c-Kit ⁺ , Thy-1, FGFR, CD201, CD105
Human	lin ⁻ , CD34 ⁺ , CD38 ^{low} , CD133, c-Kit ^{low} , Thy-1 ⁺ , CDOP1, VEGFR1

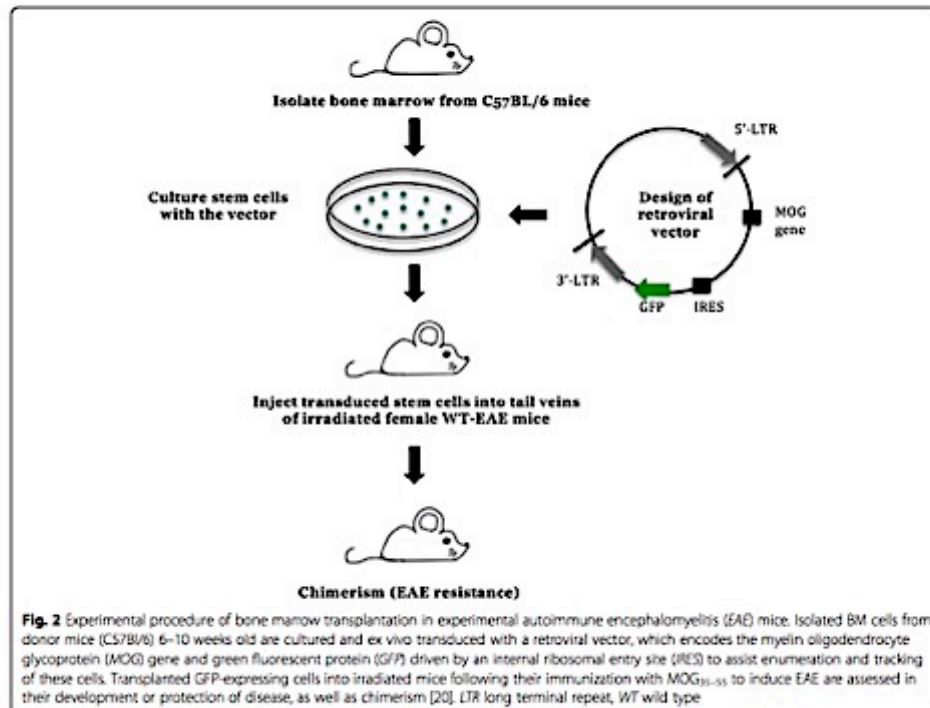
CD cluster of differentiation, CDOP cubdomain-containing protein, c-Kit tyrosine-protein kinase receptor, FGFR fibroblast growth factor receptor, HSC hematopoietic stem cell, lin lineage markers, Sca-1 stem cell antigen-1, Thy-1 thymocytes, VEGFR1; vascular endothelial growth factor receptor 1

encephalomyelitis investigating the outcome of the therapy. A series of experiments conducted in the early 1990s used the classical experimental autoimmune encephalomyelitis (EAE) model, which has been widely used to understand the mechanism of MS disease. It is induced by immunization with the myelin oligodendrocyte glycoprotein (MOG), proteolipid protein (PLP), or myelin basic protein (MBP) [8, 18].

EAE can be induced in C57BL/6 mice by immunizing with the MOG₃₅₋₅₅ peptide emulsified in complete Freund's adjuvant (CFA), resulting in a progressive paralysis ascending from the tail to the forelimbs. The disease progression in this model can thus be scored accordingly and the immune-mediated pathology within the CNS can be measured accurately. Furthermore, myelin damage and CNS inflammation in this mouse model can be quantified and visualized using histological analysis, in addition to immunological assays to measure autoantibody reactivity and specific T cells which can be used to validate certain immune responses to the different myelin components [19]. Recent research in autoimmune conditions is now also investigating gene therapy as a possible option to

correct the defective HSCs present prior to transplantation [20]. The experimental procedure includes the isolation of BM stem cells from donor mice that are transduced with retrovirus encoding a specific antigen after culturing these cells *ex vivo*. Transduced stem cells are then transferred to conditioned recipient mice, following total body irradiation (TBI), leaving them to engraft and regenerate the hematopoietic system, including dendritic cells, B cells, and T cells, all lineages being identified by flow cytometry (Fig. 2). Using this model, mice were resistant to EAE induction after transferring transduced BM cells with retrovirus encoding MOG [20].

The rationale of autologous hematopoietic stem cell transplantation (auto-HSCT) for MS is based on using chemotherapy to induce immunoablation, with subsequent reconstitution of the impaired immune system through renewed self-tolerant cells [21]. A report in 1996 by van Gelder and van Bekkum [22] explored the use of auto-HSCT in EAE, demonstrating that lymphocytes, which are present in the autologous cells, might lead to the occurrence of relapse after transplantation. An additional report by van Bekkum in 2004 [23] explored the



efficacy of auto-HSCT with TBI in Buffalo rats with EAE, and absence of disease relapse was seen in 70 % of cases. The treatment was found to be most effective at the early stages of autoimmune disease, whereas no effect was seen in the later stages. High-dose TBI led to a better response; however, TBI can lead to severe carcinogenic events at a later stage. The use of cyclophosphamide and busulfan also proved less effective than TBI [23].

In addition, the animal model study was conducted to supplement the conventional nonspecific-dose immunosuppression; it involved the administration of high-dose immunosuppressant (myeloablative chemotherapy) followed by HSCT, which effectively reduced morbidity and mortality in this model. The transplant experiments showed that EAE remissions were attained in animals after high-dose TBI. Therefore, the use of high-dose immunosuppressive agents in EAE led to a better response as compared with TBI [24].

HSCT as a therapeutic option for MS

Over the last 20 years, HSCT was anticipated as a treatment for MS patients by ablating or suppressing the endogenous immune system. It is likely to beneficially affect the inflammatory stage of the disease [25]. In the 1990s, auto-HSCT was suggested for the management of refractory and severe autoimmune disease, including MS. Only a few HSCT trials have implemented the use of donor-derived HSC grafts or HLA-matched allogeneic cell transplants because of the higher rate of mortality and morbidity with graft versus host disease (GVHD) than auto-HSCT. The role of HLA proteins is to direct the response of T cells and they are important in the selection of donors for allo-HSCT [26, 27].

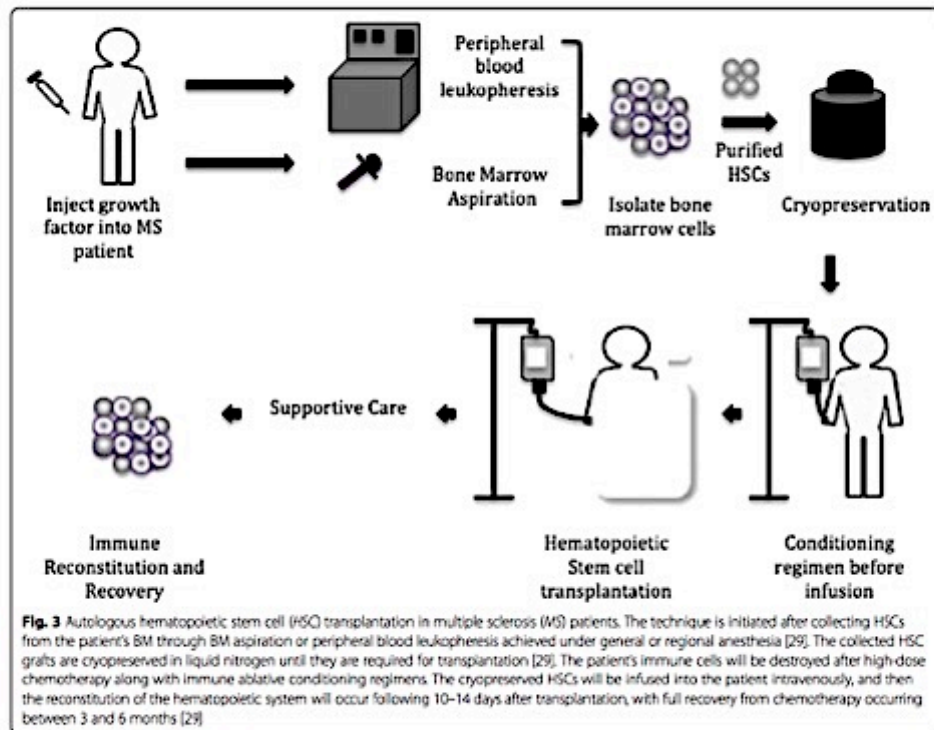
Recently, several MS patients were treated with auto-HSCT after exposure to high doses of immunosuppressive drugs by using different procedures of HSC harvesting and conditioning regimens [26–28]. In a BM graft, around 3–5 % of the cells are HSCs and the graft of peripheral blood HSCs are rich in lymphocytes, granulocytes, and monocytes. The procedure of transplantation is initiated after collecting HSCs from the patient's BM through several aspirations performed under general or regional anesthesia [29]. Otherwise, peripheral blood stem cells (PBSCs) can be mobilized from the BM into blood circulation in large amounts by using chemotherapy and/or a specific cytokine, such as granulocyte colony-stimulating factor (G-CSF), and FLT3 ligand thyroid peroxidase (TPO). In HSCT, this cytokine is injected into the donor prior to harvesting stem cells to maximize HSC collection. During the apheresis process, the donor's blood is passed through a device whereby CD34⁺ (a cluster of differentiation mixture of HSCs, progenitor cells, and white blood cells) is expunged, and then red blood cells are returned to the donor. By using this method, 5–20 % of the

extracted HSCs are suitable for treating patients with MS [29]. These purified HSCs can be cryopreserved until the patients are ready to undergo transplantation, estimated to be between 2 and 6 weeks. In this process, administration of chemotherapy with or without immune-depleting biological agents is vital for destroying the patient's mature immune lineage cells before infusing the cryopreserved HSCs. Hematopoietic engraftment and recovery from chemotherapy may take between 3 and 6 months [29] (Fig. 3).

Immune reconstitution occurs via two key mechanisms: homeostatic expansion of mature T cells and B cells comprised in the graft; and de novo lymphopoiesis of new engrafted HSCs [30]. In theory, ongoing MS activity after HSCT may be caused by the expansion of autoreactive lymphocytes. Procedures to diminish the immune cell load in the graft may improve the outcome. Therefore, the effect of using immune ablative conditioning regimens to deplete lymphocytes in the graft may be apparent following HSCTs [29]. However, when adopting or developing pre-existing HSCT regimens for novel indications, such as MS, consideration needs to be given to cytogenetic abnormalities, to the patient's medical condition (e.g., age, status of performance and status of disease), to an existing graft source, and to disease-specific prognostic factors [31].

Muraro et al. [32] showed that using the auto-HSCT myeloablative regimen can reconfigure the immune system in mature MS patients by reconstituting the CD4⁺ T-cell lineage population. In myeloablative conditioning regimens, patients are given chemotherapy with or without TBI before transplantation. The purpose of this process is to eliminate disease in the patient before HSC infusion and suppression of the immune system, and it requires stem cell support to rescue marrow function and avoid aplasia-related death. However, the process is restricted to patients younger than 50 years old due to its toxic effect on non-BM organs (e.g., liver, heart, and lung) [29].

On the other hand, Burt et al. [25] confirmed in their study that the purpose of conditioning regimens in MS is lymphoablative because the rationale of auto-HSCT is to revive an antigen-naïve immune system from the patient's HSCs; thus, myeloablative regimens are lethal to HSCs. In addition, the rationale of nonmyeloablative HSCT in MS is to suppress relapses by intervening prior to the onset of irreversible progressive axonal degeneration, to prevent inflammation, and to reduce toxicity in the older patient population. Such a regimen, being immunosuppressive in nature but without the myeloablative side effects, can be designed to dampen the activity of the immune system by using cyclophosphamide, fludarabine, rabbit anti-thymocyte globulin (ATG), or CAMPATH-1H (anti-lymphocyte antibodies), and/or by using the graft



selection of CD34⁺ [25, 33]. This ex vivo cell selection or depletion technology can change the composition of graft cells but may lead to an elevated risk of treatment-related infection for an intense conditioning regime [25]. Furthermore, the intensity of conditioning regimens may exert a toxic effect on the CNS and this neurotoxicity has been associated with radiation and busulfan treatment. Therefore, it may stand to reason that moderating conditioning regimens may provide a less toxic outcome for MS patients when treated through HSCT [25].

Recently, powerful conditioning regimens followed by auto-HSCT have been applied to aggressive MS. An example of these is alemtuzumab, which is a monoclonal antibody that targets the B-cell and/or T-cell compartment. Alemtuzumab contributed to the depletion of circulating lymphocytes that lead to the control of the autoimmune response in MS patients after transplantation, as well as preventing the development of GVHD by diminishing cytotoxic effector cells [21]. However, it has been noted that using this drug may lead to the

induction of secondary autoimmune sequelae [34]. Around 10 % of patients undergoing HSCT for autoimmune illness have been observed to develop a secondary autoimmune disease unrelated to their induction for auto-HSCT within the first 2 years after HSCT, although the primary autoimmune illness may have been suppressed following the HSC graft [35]. Secondary autoimmune disease was found to be less common in patients who undertook HSCT for MS but more frequent in patients who undertook HSCT for systemic lupus erythematosus [34]. Furthermore, immune thrombocytopenic purpura (immune cytopenia) may occur many years after HSCT. This may occur as a result of the lymphocyte-depleting antibodies administered during the conditioning of the HSC graft [36]. Secondary autoimmune disease occurred in around 4 % of patients without having a lymphocyte-depleting agent during the HSCT conditioning regimen, although 9 % of patients suffered from secondary autoimmune disease after using ATG [36].

Complications compared with the beneficial effects of HSCT in MS

A specific study identifying the toxicity and feasibility of auto-HSCT in 15 patients with SP-MS and RR-MS with a median Expanded Disability Status Scale (EDSS) of 6 (range 4.5–6.5) determined that in two patients neurological deterioration with high fever continued, one patient sustained a transient neural deterioration, three patients exhibited transient engraftment syndrome, one patient had unsuccessful mobilization, and reactivation of cytomegalovirus occurred in one patient. The EDSS improved in three patients assessed at 1-year follow-up after transplantation but remained constant in nine patients and worsened in two patients. According to magnetic resonance imaging (MRI), enhanced T1 lesion disappeared in patients. This study demonstrated the feasibility and acceptable toxicity of using auto-HSCT to reduce the progression of MS. Long-term follow-up after transplantation is vital for the health management of MS patients [37].

A more recent study conducted by Shevchenko et al. [38] set out to determine the long-term effectiveness and safety of auto-HSCT in conjunction with high-dose immunosuppressive therapy (HDIT), along with a decreased intensity BEAM condition regimen, for different types of MS patients. Fassas et al. [39] pioneered BEAM (BCNU (carmustine), cytarabine, etoposide, melphalan) as a conditioning regimen for auto-HSCT, which includes carmustine (bis-chloroethyl nitrosourea), etoposide, cytosine arabinoside, and melphalan. This study involved 99 MS patients (39 male and 60 female, mean age 35 years); 43 of the patients were RR-MS, 35 were SP-MS, 18 were PP-MS, and three were PR-MS with EDSS prior to graft of 3.5. Ninety-eight patients had a neurological improvement or stabilization after 6 months of transplantation [38]. There were no transplanted deaths observed and the cumulative incidence of disease progression was 16.7 % at 8 years post-transplantation. These studies were very favorable because 47 % of the patients improved in their EDSS score (at least 0.5), as compared with the baseline, and 45 % of MS patients were stable at median long-term follow-up for more than 5 years in both the RR-MS and progressive MS groups. Besides, the patient's quality of life improved in MS by using auto-HSCT with this specific regimen [38]. The consistency observed in these long-term clinical results associated with the quality of life enhancement for these patients reported by Bowen et al. [24] advocates for the safety and efficiency of this treatment approach in MS patients. In addition, a clinical study was conducted by Guimarães et al. [40] to determine the impact of auto-HSCT on health-related quality of life (HRQL) in patients with PP-MS and SP-MS in Brazil [40]. Approximately 79 % of patients enrolled in these trials (27 patients) revealed neurological improvement 1 year after

transplantation with significant improvement in the HRQL, indicating that although HSCT involves complicated procedures it impacts positively in MS patients by improving their HRQL. Progression-free survival after treatment with HSCT has been reported in 81 % of SP-MS patients after 3 years and in 67 % of PP-MS patients [40].

On the other hand, researchers in Greece released long-term results from a single-center phase I/II trial of auto-HSCT [41]. According to clinical and MRI data from 35 patients with progressive MS treated with auto-HSCT, researchers demonstrated that HSCT is a therapy for aggressive cases but is not recommended for the vast majority of MS patients with more common RR presentations. Moreover, HSCT has a sustained and impressive effect in suppressing disease activity after a medium follow-up period of 11 (range 2–15) years. At 15 years, disease (progression-free) survival was 44 % for patients with active CNS disease and 10 % for those without. There was an improvement in EDSS scores in 16 patients by 0.5–5.5 for a median of 2 years. However, the EDSS from nine patients did not progress above baseline scores and two patients died from transplant-related complications. MRI data identified a significant reduction in gadolinium-enhancing (Gd⁺) lesions after mobilization, becoming maximal post-transplantation [41]. This study is consistent with Saccardi et al. [42] on 178 patients from 45 centers.

Several studies have shown the effectiveness of using HSCT for young patients with highly aggressive, malignant forms of MS. This type of MS is rare and characterized by abnormally localized autoimmune processes in the brain stem or upper cervical cord and/or intense inflammation resulting in rapid development of significant disability or death in the early stages of the disease course. Marburg variant MS is another demyelinating disease with an equally ominous prognosis with malignant MS, although it may differ histologically [43, 44]. Since 2011, researchers in the United Kingdom have evaluated the effect of using pulsed cyclophosphamide and nonmyeloablative auto-HSCT in the case of a severely disabled 21-year-old female patient presenting with malignant MS. This treatment led to improvement in the patient, who suffered from a disturbance of sensorimotor function in all four limbs. The results of her neuroimaging showed demyelination with enhancement. cerebrospinal fluid (CSF) was positive to oligoclonal bands and demonstrated 47 lymphocytes, and serum was negative for aquaporin4 (Aq4) antibodies. Although the patient experienced several treatments, such as alemtuzumab with pulsed intravenous methylprednisolone (IVMP) and plasma exchange, she continued to deteriorate. The patient underwent auto-HSCT after 2 months of treatment with cyclophosphamide. The patient's EDSS score was 8.5

at the time of transplantation but 1 year after treatment the score decreased to 6.5, and she was able to walk. According to this case report, using cyclophosphamide prior to auto-HSCT is crucial for clinical improvement, suppression of relapses, and stabilization of the lesion burden, especially in highly active RR-MS patients [45]. This study is consistent with the study of Faguis et al. [46] on nine patients with malignant RR-MS who underwent auto-HSCT with BEAM condition followed by cyclophosphamide, resulting in one relapse in 280 patient-months following HSCT. All patients had their disability improve or stabilize, and most of the patients showed no enhanced lesions during follow-up. Furthermore, Kimiskidis et al. [44] reported an improvement and long-lasting clinical and radiological response in a case with malignant MS who was treated with high-dose chemotherapy plus ATG followed by auto-HSCT.

Results from several studies recommend nonmyeloablative HSCT to treat SP-MS and RR-MS mainly due to the fact that HSCT has immunosuppressive and immunomodulatory effects, evident from a more diverse T-cell clonal population in post-HSCT patients [47]. This occurs due to the ability of HSCT to modulate autoimmunity without the requirement to eradicate the full patient's hematopoietic cells (myeloablation regimen). In 2015, a study by Burt et al. [48] focused on improving neurological disabilities and other clinical results of RR-MS patients using nonmyeloablative HSCT. This study included 191 MS patients; 123 patients had a RR course of the disease and 28 had SP-MS, with mean age of 36 years. Patients were treated at a single US institution between 2003 and 2014, and the researchers followed-up with patients for 5 years. At year 4 post-transplantation, 64 % of patients demonstrated improvement in the EDSS score from a pre-transplant median of 4.0 to 2.5, neurological rating scale scores increased from a pretransplant median of 74 to 87.5 in 34 patients, and the MS functional composite scores were 0.45 (0.04–0.60) ($p = 0.02$). The brain T2 lesion volume reduced significantly from a pretransplant median of 8.57 cm³ to 5.74 cm³ ($p < 0.001$) at the last post-transplant assessment of MRI scans in 128 patients with a mean follow-up of 27 months. In this study, the quality-of-life short form based upon the 36 questionnaire score was improved significantly in 132 patients from a pretransplant median of 46 to 64 at year 2 post-transplant as compared with the previous results of the AFFIRM (The Natalizumab Safety and Efficacy in Relapsing Remitting Multiple Sclerosis) and SENTINEL (The Safety and Efficacy of Natalizumab in Combination with Interferon Beta-1a in Patients with Relapsing Remitting Multiple Sclerosis) trials. In addition, there were no early or late infectious cases of fungal, *Pneumocystis jirovecii*, JC virus, Epstein-Barr virus, or cytomegalovirus, and there was no treatment-related mortality [48]. Altogether,

using nonmyeloablative HSCT was crucial in improving neurological disabilities in RR-MS patients.

A major pathological complication of auto-HSCT may be the effects reported on brain volume. Saiz et al. [49] focused on monitoring the evolution of inflammatory disease activity by suppressing the relapses and Gd⁺ MRI lesions post-auto-HSCT. Four out of five patients had a constant or improved EDSS after 3 and 12 months post-transplantation, but the fifth patient suffered deterioration in their condition during the treatment. For all of the patients post-auto-HSCT, there was no enhancement of T1 lesions and no enlargement of or new T2 lesions (median: 11.8 % appearing). In addition, the corpus callosum area decreased in all patients at 1-year follow-up (median declines: 12.4 %) and for two patients there was no progress at 2 years post-HSCT. These results suggest a positive impact of auto-HSCT on active inflammation that corresponds with the clinical stabilization of the five patients at 1 year post-HSCT. Although the five patients showed improvements in other MRI variables, the atrophy of the corpus callosum increased. The relationship between the development of brain atrophy and inflammatory activity is uncertain. This study indicates the effectiveness of using auto-HSCT in arresting the inflammatory activity; however, the pathological process responsible for brain atrophy was not reversed [49].

Rapid loss of brain volume has been measured a few months after treatment [50]. Auto-HSCT has seemingly detrimental effects on the integrity of the brain tissue that leads to rapid loss of about 1.92 % of brain volume. A study of SP-MS patients showed that brain atrophy after auto-HSCT is not constant but declines for the first 2 years after treatment. The reduction in brain volume may be a result of the significant inflammation seen before stem cell transplantation is performed. The pathological evidence for this is through the large number of transected axons seen in MS lesions, marked axonal injury, cortical demyelination, and diffuse inflammation of the brain observed after histopathological analysis [50]. Histopathological studies have also been carried out on brain tissue obtained at autopsy from deceased patients who had been treated with auto-HSCT, and they indicate ongoing active demyelination. Metz et al. [51] interrogated brain tissue samples from five patients with chronic lesions where they investigated 53 individual white matter lesions through immunohistochemical and routine staining techniques. They were able to characterize damaged axons, activated macrophages/microglial cells, inflammatory infiltrates, and demyelinating activity in these lesions. Limited numbers of T cells, which were dominated by CD8⁺ cytotoxic T cells in the inflammatory infiltrate, could be observed within the lesions while plasma cells and B cells were completely absent. Macrophages/microglial cells were found on the injured tissue and

high numbers of damaged axons were present in the active lesion areas. The study concluded that axonal degeneration and demyelination remain a constant feature even after auto-HSCT, despite effective immunosuppression associated with transplantation [51]. Their data were supported by other clinical studies, which indicate that there is continued clinical disease progression in MS patients with high EDSS despite their special auto-HSCT therapy [52]. The clinical efficacy of intense immunosuppression with auto-HSCT does not appear to avoid further progression in MS patients with high EDSS score (>6.0) [51]. Thus, future HSCT trials should consider inclusion criteria to be an early stage of disease course with active relapses of MS, as well as combinatorial new therapeutic strategies that may prevent ongoing neurodegeneration and demyelination in progressive MS [51].

A more recent study undertaken by Mancardi et al. [53] in Italy evaluated the effect of a highly intense conditioning regimen followed by auto-HSCT compared with the immunosuppressive therapy mitoxantrone (MTX, Novantrone; EMD Serono, Rockland, MA USA) on the disease activity of 21 MS patients. This controlled, randomized, multicenter phase II trial of auto-HSCT led to a significant reduction in T2-weighted lesions, Gd⁺ areas, and annualized relapse rates (ARR) as compared with MTX. Nine patients (four SP-MS with relapses, three SP-MS, two RR-MS) were assigned to the auto-HSCT group and 12 patients ended up in the MTX-treatment group (five RR-MS, three SP-MS, three SP-MS with relapses, one RP-MS). The first group was given 4 g/m² cyclophosphamide and 5 µg/kg body weight filgrastim, along with a high-dose chemotherapy conditioning regimen, BEAM. Patients treated with MTX received a 20 mg MTX dose intravenously and 1 g methylprednisolone diluted in 250 ml 0.9 % saline every month for 6 months. The researchers found that 79 % of patients who experienced auto-HSCT had fewer new T2 lesions on MRI scans as compared with the MTX-treated patients by using an intention-to-treat analysis. However, due to patient drop-out and technical problems, only 17 of the 21 patients had MRI scans. Furthermore, there was a complete suppression of active inflammatory lesions, as demonstrated by the absence of new Gd⁺ lesions in the auto-HSCT group during a 4-year follow-up, although 56 % of MTX-treated patients had inflammatory activity. Regarding the effect of ARR over 4 years, ARR reduced in the auto-HSCT patients (ARR = 0.19) as compared with MTX patients (ARR = 0.6). Nevertheless, only 48 % of MTX patients demonstrated progression while 57 % of auto-HSCT patients had progressed at the end of follow-up. There were no observable differences in EDSS scores between the two groups. This study demonstrated that for patients with severe progressive MS, treatment with auto-HSCT is superior to

treatment with MTX. The effect is related to the intensity of the conditioning regimen, which was used to reset the immune system in MS patients before performing HSCT, compared with the Nash et al. [54] and Burt et al. [48] trials that were reported earlier in 2015. Although this randomized and controlled study yielded promising results, the sample size was small. In addition, the clinical results of the study by Mancardi et al. [53] were lackluster in comparison with other studies in auto-HSCT, especially when compared with the reduction in EDSS among MS patients who enrolled in the Burt et al. [48] study in 2015 as well as the information on quality of life and brain atrophy, not investigated in this study.

Criteria to be considered in HSCT in MS patients

There are several criteria that may play a crucial role in using HSCT as a therapeutic option in the management of MS, including proposed international multicenter, randomized clinical trials of HSCT compared with the best standard of care treatment, MS patient selection in studies, and long-term follow-up studies of patients from international registries [29]. Although recent studies provide a significant improvement in various types of MS patients' lives, several vital limitations have been reported [38, 48]. Firstly, the inferences deduced from HSCT effects cannot be made because most studies were observational for the treated cohorts without appropriate control groups. Secondly, there has not been enough information about disease activity before the disease course and its treatment (and there has been no long-term follow-up available for certain patients). In addition, the studies were mostly performed at a single institution, which may implicate bias.

Conclusion

HSCT is a plausible treatment paradigm for MS patients. However, auto-HSCT is considered to be a sledgehammer approach for treating MS patients, one that will be astoundingly effective when used on appropriately selected patients. The reasons for this promising therapy's success are its lower toxicity and its ability to replace the immune system. The future of HSCT trials should discover novel therapeutic strategies that prevent ongoing neurodegeneration and demyelination in progressive MS. The trial designs should consider the reproducibility of HSCs with sufficient yield and purity, select MS patients with active inflammatory disease, and use appropriate conditioning agents.

Abbreviations

5-FU: 5-Fluorouracil; ALDH: Aldehyde dehydrogenase; ARR: Annualized relapse rates; ATG: Anti-thymocyte globulin; auto-HSCT: Autologous hematopoietic stem cell transplantation; BBB: Blood-brain barrier; BM: Bone marrow; CFA: Complete Freund's adjuvant; CFU-S: Colony-forming spleen assays; CNS: Central nervous system; CSF: Cerebrospinal fluid; EAE: Experimental autoimmune encephalomyelitis; EDSS: Expanded Disability Status Scale.

FACS: Fluorescence-activated cell sorting; G-CSF: Granulocyte colony-stimulating factor; Gd³⁺: Gadolinium-enhancing; GVHD: Graft versus host disease; HDCT: High-dose immunosuppressive therapy; HRQL: Health-related quality of life; HSC: Hematopoietic stem cell; HSCT: Hematopoietic stem cell transplantation; IMiP: Intravenous methylprednisolone; LSK: Lin⁻¹, Sca-1⁺, and c-Kit⁺; LT: Long term; MACS: Magnetic-activated separation; MBP: Myelin basic protein; MOG: Myelin oligodendrocyte glycoprotein; MRI: Magnetic resonance imaging; MS: Multiple sclerosis; MTK: Mitoxantrone; PBSCs: Peripheral blood stem cells; RLP: Proteolipid protein; PP: Primary progressive; PR: Progressive relapsing; RR: Relapsing remitting; SP: Secondary progressive; ST: Short term; TB: Total body irradiation.

Competing interests

The authors declare that they have no competing interests.

Authors' contributions

MMB wrote the manuscript and contributed to its conceptual framework. CS helped to draft and edited the manuscript. SP conceptualized and edited the manuscript. All authors read and approved the final manuscript.

Acknowledgements

The authors acknowledge the contribution of Ms Sara Mokhtar and Ms Amari Alreihani for their proofreading of the manuscript. MMB was supported by a Taf University postgraduate scholarship, and SP was supported by National Multiple Sclerosis Society (USA) Project Grant ID #RG43981/1 and International Progressive Multiple Sclerosis Alliance Project ID#PA0065.

Published online: 16 January 2016

References

1. Villar LM, Espino M, Cavanillas ML, Roldan E, Urcelay E, de la Concha EG, et al. Immunological mechanisms that associate with oligoclonal IgM band synthesis in multiple sclerosis. *Clin Immunol*. 2010;137(1):51–9.
2. Vossoughi R, Freedman MS. Therapy of MS. *Clin Neurol Neurosurg*. 2010;112(3):366–85.
3. Fassas A, Mancardi GL. Autologous hemopoietic stem cell transplantation for multiple sclerosis: is it worthwhile? *Autoimmunity*. 2008;41(8):901–10.
4. Weinstenker BG, Bass B, Rice GP, Noseworthy J, Carriere W, Baskerville J, et al. The natural history of multiple sclerosis: a geographically based study. I. Clinical course and disability. *Brain*. 1989;112(Pt 1):133–46.
5. Compston A, Coles A. Multiple sclerosis. *Lancet*. 2002;359(9313):1221–31.
6. Fassas A, Nash R. Multiple sclerosis. *Best Pract Res Clin Haematol*. 2004;17(2):247–62.
7. Scolding N. Adult stem cells and multiple sclerosis. *Cell Prolif*. 2011;44 Suppl 1:35–8.
8. Van Wijnenersch B, Sprangers B, Dubois B, Waer M, Billiau AD. Autologous and allogeneic hematopoietic stem cell transplantation for multiple sclerosis: perspective on mechanisms of action. *J Neuroimmunol*. 2008;197(2):89–98.
9. Butt RK, Burns W, Hess A. Bone marrow transplantation for multiple sclerosis. *Bone Marrow Transplant*. 1995;16(1):1–6.
10. Fassas A, Anagnostopoulos A, Kizis A, Kapinas A, Sakellari L, Kimiskidis V, et al. Peripheral blood stem cell transplantation in the treatment of progressive multiple sclerosis: first results of a pilot study. *Bone Marrow Transplant*. 1997;20(8):631–8.
11. Filip S, Meky J, Vávrová J, Cizková D, Sinkorová Z, Topolenská V, et al. Homing of lin⁻¹CD117⁺ hematopoietic stem cells. *Transfus Apher Sci*. 2009;41(3):183–90.
12. Challen GA, Boles N, Lin KK, Goodell MA. Mouse hematopoietic stem cell identification and analysis. *Cytometry A*. 2009;75(1):14–24.
13. Wognum AW, Eaves AC, Thomas TE. Identification and isolation of hematopoietic stem cells. *Arch Med Res*. 2003;34(6):461–75.
14. Juopperi TA, Schuler W, Yuan X, Collector M, Dang CV, Shariq S. Isolation of bone marrow-derived stem cells using density-gradient separation. *Exp Hematol*. 2007;35(2):335–41.
15. Maestzig T, Brugman MH, Bartels S, Heinz N, Kudikova OS, Modlich U, et al. Polyclonal fluctuation of lentiviral vector transduced and expanded murine hematopoietic stem cells. *Blood*. 2011;117(11):3053–64.
16. Tsiptsoglou AS, Bonavolas ID, Tsiptsoglou SA. Multilevel targeting of hematopoietic stem cell self-renewal, differentiation and apoptosis for leukemia therapy. *Pharmacol Ther*. 2009;122(3):264–80.
17. Pearce DJ, Bonnet D. The combined use of Hoechst efflux ability and aldehyde dehydrogenase activity to identify murine and human hematopoietic stem cells. *Exp Hematol*. 2007;35(9):1437–46.
18. Bettelli E. Building different mouse models for human MS. *Ann N Y Acad Sci*. 2007;1103:11–8.
19. Chan J, Ban E, Chun K, Wang B, Backstrom B, Bernard C, et al. Transplantation of bone marrow transduced to express self-antigen establishes deleterious tolerance and permanently remits autoimmune disease. *J Immunol*. 2008;181:7571–80.
20. Alderuccio F, Nasa Z, Chung J, Ko HJ, Chan J, Toh BH. Hematopoietic stem cell gene therapy as a treatment for autoimmune diseases. *Mol Pharm*. 2011;8(5):1488–94.
21. Butt RK, Testori A, Craig R, Cohen B, Suffit R, Bar W. Hematopoietic stem cell transplantation for autoimmune diseases: what have we learned? *J Autoimmun*. 2008;30(3):116–20.
22. van Gelder M, van Bekkum DW. Effective treatment of relapsing experimental autoimmune encephalomyelitis with pseudoautologous bone marrow transplantation. *Bone Marrow Transplant*. 1996;18(6):1029–34.
23. van Bekkum D. Stem cell transplantation for autoimmune disorders. Preclinical experiments. *Best Pract Res Clin Haematol*. 2004;17(2):201–22.
24. Bowen J, Kraft GH, Wundes A, Guan Q, Maravilla KR, Gooley TA, et al. Autologous hematopoietic cell transplantation following high-dose immunosuppressive therapy for advanced multiple sclerosis: long-term results. *Bone Marrow Transplant*. 2012;47(7):946–51.
25. Butt RK, Cohen B, Rose J, Petersen F, Oyama Y, Stefanski D, et al. Hematopoietic stem cell transplantation for multiple sclerosis. *Arch Neurol*. 2005;62(6):860–4.
26. Farge D, Labopin M, Tyndall A, Fassas A, Mancardi GL, Van Laar J, et al. Autologous hematopoietic stem cell transplantation for autoimmune diseases: an observational study on 12 years' experience from the European Group for Blood and Marrow Transplantation Working Party on Autoimmune Diseases. *Haematologica*. 2010;95(2):284–92.
27. Pasquini MC, Voltarelli J, Atkins HL, Hamerschlak N, Zhong X, Ahn KW, et al. Transplantation for autoimmune diseases in North and South America: a report of the Center for International Blood and Marrow Transplant Research. *Biol Blood Marrow Transplant*. 2012;18(10):1471–8.
28. Openshaw H, Stuve O, Antel JP, Nash R, Lund BT, Weiner LP, et al. Multiple sclerosis flares associated with recombinant granulocyte colony-stimulating factor. *Neurology*. 2000;54(11):2147–50.
29. Atkins HL, Freedman MS. Hematopoietic stem cell therapy for multiple sclerosis: top 10 lessons learned. *Neurotherapeutics*. 2013;10(1):66–76.
30. Gress RG, Emerson SG, Drobyski WR. Immune reconstitution: how it should work, what's broken, and why it matters. *Biol Blood Marrow Transplant*. 2010;16(1 Suppl):S133–7.
31. Suredu A, Bader P, Cesaro S, Dreger P, Duarte RF, DuFour C, et al. Indications for allo- and auto-SCT for hematological diseases, solid tumours and immune disorders: current practice in Europe, 2015. *Bone Marrow Transplant*. 2015;50(3):1037–56.
32. Muraro PA, Douek DC, Packer A, Chung K, Guenaga FJ, Cassiani-Ingoni R, et al. Thymic output generates a new and diverse TCR repertoire after autologous stem cell transplantation in multiple sclerosis patients. *J Exp Med*. 2005;201(5):805–16.
33. Gosselin D, Rivest S. Immune mechanisms underlying the beneficial effects of autologous hematopoietic stem cell transplantation in multiple sclerosis. *Neurotherapeutics*. 2011;8(4):643–9.
34. Loh Y, Oyama Y, Starkute L, Traynor A, Satkus J, Quigley K, et al. Autologous hematopoietic stem cell transplantation in systemic lupus erythematosus patients with cardiac dysfunction: feasibility and reversibility of ventricular and valvular dysfunction with transplant-induced remission. *Bone Marrow Transplant*. 2007;40(1):47–53.
35. Dalkeler T, Labopin M, Di Gioia M, Abinun M, Alexander T, Mirlati L, et al. Secondary autoimmune diseases occurring after HSCT for an autoimmune disease: a retrospective study of the EBMT Autoimmune Disease Working Party. *Blood*. 2011;118(6):1693–8.
36. Cuker A, Coles AJ, Sullivan H, Fox E, Goldberg M, Oyuela P, et al. A distinctive form of immune thrombocytopenia in a phase 2 study of alemtuzumab for the treatment of relapsing remitting multiple sclerosis. *Blood*. 2011;118(24):6299–305.
37. Carreras E, Saiz A, Marin P, Martinez C, Rovira M, Vilamor N, et al. CD34⁺ selected autologous peripheral blood stem cell transplantation for multiple

- sclerosis: report of toxicity and treatment results at one year of follow-up in 15 patients. *Haematologica*. 2003;88(3):306–14.
38. Shevchenko JL, Kumetsov AN, Ionova TI, Melnichenko VY, Fedorenko DA, Kurbatova KA, et al. Long-term outcomes of autologous hematopoietic stem cell transplantation with reduced-intensity conditioning in multiple sclerosis: physician's and patient's perspectives. *Ann Hematol*. 2015;94(7):1149–57.
 39. Fassas A, Anagnostopoulos A, Kazis A, Kapinas K, Sakellari I, Kimiskidis V, et al. Autologous stem cell transplantation in progressive multiple sclerosis—an interim analysis of efficacy. *J Clin Immunol*. 2000;20(1):24–30.
 40. Guimarães FA, Oliveira-Carlos EA, Mastroianni AP, Voltarelli JC, Santos MA. Impact of autologous hematopoietic stem cell transplantation on the quality of life of patients with multiple sclerosis. *Arg Neuropsiquiatr*. 2010;68(4):522–7.
 41. Fassas A, Kimiskidis VK, Sakellari I, Kapinas K, Anagnostopoulos A, Tsimourou V, et al. Long-term results of stem cell transplantation for MS: a single-center experience. *Neurology*. 2011;76(2):1066–70.
 42. Saccardi R, Kozak T, Bocelli-Lyndal C, Fassas A, Kazis A, Havrdova E, et al. Autologous stem cell transplantation for progressive multiple sclerosis: update of the European Group for Blood and Marrow Transplantation autoimmune diseases working party database. *Mult Scler*. 2006;12(6):814–23.
 43. Atkins HL, Muzio PA, van Laar JM, Pavletic SZ. Autologous hematopoietic stem cell transplantation for autoimmune disease—is it now ready for prime time? *Biol Blood Marrow Transplant*. 2012;18(1 Suppl):S177–83.
 44. Kimiskidis V, Sakellari I, Tsimourou V, Kapina V, Papagiannopoulos S, Kazis D, et al. Autologous stem-cell transplantation in malignant multiple sclerosis: a case with a favorable long-term outcome. *Mult Scler*. 2008;14(2):278–83.
 45. Alix JJ, Blackburn DJ, Sokhi D, Craven I, Sharack B, Snowden JA. Autologous hematopoietic stem cell transplantation following pulsed cyclophosphamide in a severely disabled patient with malignant multiple sclerosis. *J Neurol*. 2013;260(3):914–6.
 46. Fagius J, Lundgren J, Öberg G. Early highly aggressive MS successfully treated by hematopoietic stem cell transplantation. *Mult Scler*. 2009;15(2):229–37.
 47. Holloman J, Ho CC, HAJAKI A, Hurlley JL, Galiccano GI. The development of hematopoietic and mesenchymal stem cell transplantation as an effective treatment for multiple sclerosis. *Am J Stem Cells*. 2013;2(2):95–107.
 48. Burt RK, Balabanov R, Han X, Sharack B, Morgan A, Quigley K, et al. Association of nonmyeloablative hematopoietic stem cell transplantation with neurological disability in patients with relapsing-remitting multiple sclerosis. *JAMA*. 2015;313(3):275–84.
 49. Saiz A, Cereas E, Berenguer J, Yague J, Martinez C, Marin P, et al. MRI and CSF oligoclonal bands after autologous hematopoietic stem cell transplantation in MS. *Neurology*. 2001;56(8):1084–9.
 50. Burt RK, Cohen BA, Russell E, Spero K, Joshi A, Oyama Y, et al. Hematopoietic stem cell transplantation for progressive multiple sclerosis: failure of a total body irradiation-based conditioning regimen to prevent disease progression in patients with high disability scores. *Blood*. 2003;102(7):2373–8.
 51. Metz J, Lucchinetti CF, Opershaue H, Garcia-Merino A, Lassmann H, Freedman MS, et al. Autologous haematopoietic stem cell transplantation fails to stop demyelination and neurodegeneration in multiple sclerosis. *Brain*. 2007;130(5):1254–62.
 52. Sainaghi PP, Collimedaglia L, Aicardi F, Molinari R, Sola D, Ranza E, et al. Growth arrest specific gene 6 protein concentration in cerebrospinal fluid correlates with relapse severity in multiple sclerosis. *Mediators Inflamm*. 2013;2013:406483.
 53. Mancardi GL, Sormani MP, Gualandi F, Saiz A, Cereas E, Merelli E, et al. Autologous hematopoietic stem cell transplantation in multiple sclerosis: a phase II trial. *Neurology*. 2015;84(10):981–8.
 54. Nash RA, Hutton GI, Racke MK, Popat U, Devine SM, Griffith LM, et al. High-dose immunosuppressive therapy and autologous hematopoietic cell transplantation for relapsing-remitting multiple sclerosis (HALT-MS): a 3-year interim report. *JAMA Neurol*. 2015;72(2):159–69.

CHAPTER 2: Methods

Materials

All antibodies and reagents are listed below in Table 3. For more information on how solutions were prepared, see Appendix 1.

Table 3. Antibodies and reagents used in experiments outlined in this thesis.

Techniques	Name	Catalogue	Company/Supplier	Dilution	Size
Induction of EAE	Freund's Adjuvant, Complete	F5881-6X10ML	Sigma Aldrich		6 x 10 mL
	Hamilton syringe 5 μ L, Model 175 RN SYR, Small Removable NDL, 32G, 2 in, point style 3	80016	Biostrategy		
	Myelin Oligodendrocyte Glycoprotein (MOG) ₃₅₋₅₅	MOG (35-55)	Purar Chemicals		50 mg
	Pertussis Toxin (salt free)	181	Sapphire Bioscience		0.05 mg
	Tuberculosis, H37RA, Dessicated	231141	BD Bioscience		6 /sp
	recombinant MOG	See Appendix 2			
Polymerase chain reaction (PCR)	Agarose gel	16500-500	Invitrogen		500 g
	BlueJuice Gel Loading buffer (10x)	10816-015	Life Technologies		1 mL
	Extract-N-AMP for tissue	XNAT2	Sigma Aldrich		kit
	Extract-N-AMP PCR reaction mix	E3004-12ML	Sigma Aldrich		12 mL
	Sybr Safe DNA Gel Stain	S33102	Life Technologies		0.4 mL
	1kb Plus DNA Ladder	10787026	Life Technologies		1 mg
Flow Cytometry	Anti-mouse CD3e PE-Cy7	25-0031-81	Jomar	1:200	0.05 mg
	Anti-mouse CD45/B220 PE	553090	BD Pharmigen	1:200	0.2 mg
	Anti-mouse CD11c APC	550261	BD Pharmigen	1:50	0.1 mg
	Anti-mouse NgR purified	MAB1659	R&D system	1:10	0.05 mg
	Anti-Mouse/Rat Ki-67 eFluor® 450	48-5698-80	Affymetrix-eBioscience	1:200	0.1 mg
	Anti-mouse IgG-Biotin	13-4013-85	affymetrix-eBioscience	1:200	0.5 mg
	Anti-mouse IgD APC	405714	BioLegend	1:200	0.1 mg
	Anti-mouse IgM PerCP/Cy5.5	406512	BioLegend	1:400	0.1 mg
	Anti-NgR2antibody	sc-168752	Santa Cruz Biotechnology	1:100	0.2 mg/mL
	Anti-NgR3 antibody	sc-165108	Santa Cruz Biotechnology	1:100	0.2 mg/mL
	Anti-goat Alexa fluor 488 (2mg/uL)	A11055	Life Technologies	1:200	0.5 mL
	Anti-goat Alexa fluor 555 (2mg/uL)	A21432	Life Technologies	1:200	0.5 mL
	Anti-rat Alexa fluor 488	A11006	Life technologies	1:200	2 mg/mL
	Armenian hamster IgG, PE-Cy7	25-4888-81	Jomar	1:200	
	Isotype control				0.5 mg
	Hamster IgG1, λ 1 APC Isotype control	553956	BD pharmingen	1:200	0.1 mg
	Rat IgG2b, k PE Isotype control	553989	BD Pharmigen	1:200	0.1 mg
	Purified rat IgG2b, k Isotype control	559478	BD Pharmigen	1:200	0.25 mg
Streptavidin APC	17-4317-82	Affymetrix-eBioscience	1:300	0.1 mg	

	Bovine Serum Albumin (BSA)	A2153	Sigma Aldrich		100 g
	Collagenase D	11088866001	Roche		500 mg
	Corning 96-well plates round bottom, P/S, non-treated	CLS3795 - 100EA	Sigma Aldrich		100/box
	Fixation/Permeabilisation Solution Kit	554714	BD Biosciences		250 tests
	Normal Rat Serum	10710C	Life Technologies		10 mL
	DAPI	D3571	Molecular Probes	1:2000	10 mg
	DMEM F12	11320-033	Life Technologies		500 mL
	Dnase I from Bovine Pancreas	11284932001	Roche		100 mg
	DPBS Ca -, Mg-	14190-250	Life Technologies		500 mL
	DPBS Ca+ Mg+	14040-182	Life Technologies		500 mL
	Fetal bovine serum (FBS) tetracycline-free	631105	Clontech		50 mL
	Ficoll Paque PLUS	7957	Stemcells Technologies		500 mL
	Lymphoprep	7861	Stem Cells Technologies		500 mL
	RC lysis buffer (10x)	9803S	Genesearch		15 mL
	RPMI-1640	R0883-500ML	Sigma Aldrich		500 mL
	Trypan Blue	T8154	Sigma Aldrich		100 mL
	5ml Polystyrene round bottom tube with cell strainer cap	FAL352235	In Vitro tech		500/case
Immunohistochemistry (IHC)	Anti- CD45/B220 FITC	553087	BD Pharmigen	1:200	0.5 mg/mL
	Anti-CD45/B220	bs-4818R	BIOSS	1:200	0.1 mL
	Anti-CD11c	bs-2508R	BIOSS	1:200	0.1 mL
	Anti-CD3e	PAB 9003	Abnova	1:200	0.1 mg
	Anti- NgR	MAB1659	R&D system	1:100	0.5 mg
	Anti-NgR2	sc-168752	Santa Cruz Biotechnology	1:100	0.2 mg/mL
	Anti-NgR3	sc-165108	Santa Cruz Biotechnology	1:100	0.2 mg/mL
	Anti-NgR3 (B-7)	sc-398584	Santa Cruz Biotechnology	1:100	0.2 mg/mL
	Anti-BAFF Antibody	IMG-247	Imgenex	1:100	0.1 mg
	Anti-BLyS TNFSF13B	NB100-56310	Sapphire Biosciences	1:100	0.1 mg
	Anti-TROY/TNFRSF19	AF723	R&D systems		0.1 mg
	Anti-TROY	ab138502	Abcam	1:50	0.1 mL
	Anti-GFP	AB3080	Merck Millipore	1:200	
	Anti-GFP	A11120	Thermo fisher	1:200	0.1 mg
	Anti-myc (71D10)	2278S	Cell signalling tech	1:8000	0.1 mL
	Anti-Nogo-A	AB5888	Merck Millipore	1:200	0.1 mg
	Anti-goat Alexa fluor 488 (2mg/uL)	A11055	Life Technologies	1:200	0.5 mL
	Anti-goat Alexa fluor 555 (2mg/uL)	A21432	Life Technologies	1:200	0.5 mL
	Anti-rabbit Alexa fluor 488 (2mg/uL)	A11008	Life Technologies	1:200	0.5 mL
	Anti-rabbit Alexa Fluor 555 (2mg/uL)	A21428	Life Technologies	1:200	0.5 mL
	Anti-rat Alexa Fluor 555 (2mg/uL)	A21434	Life Technologies	1:200	0.5 mL
	Anti-mouse Alexa Fluor 488 (2mg/uL)	A11001	Life Technologies	1:200	0.5 mL
	Anti-mouse Alexa Fluor 546 (2mg/uL)	A11003	Life Technologies	1:200	0.5 mL
	Anti-mouse 647 Antibody (2mg/uL)	A21235	Life Technologies	1:200	0.5 mL
	Dako Mounting media	S3023	Dako		15 mL
	NgR2 peptide	sc-168752 P	Santa Cruz Biotechnology	1:100	0.2 mg/mL

	NgR3 peptide	sc-165108 P	Santa Cruz Biotechnology	1:100	0.2 mg/mL
	Proteinase K	19133	Qiagen	1:1000	10 mL
	Recombinant mouse NgR/Fc chimera protein	1440-NG	Bioscientific		0.05 mg
Western blot (WB)	Cell lysis buffer (10X)	9803S	Genesearch		15 mL
	RIPA buffer (10X)	9806S	Genesearch		15 mL
	Phosphatase Inhibitor Cocktail Set III	524627	Merck Millipore		1 mL
	Anti-NgR	AB15138	Millipore		0.1 mg
	Anti-NgR	MAB1659	R&D system		0.05 mg
	Anti-NgR2	sc-168752	Santa Cruz Biotechnology		0.2 mg/mL
	Anti-NgR3	sc-165108	Santa Cruz Biotechnology		0.2 mg/mL
	Anti-myelin basic protein	Ab40390	Sapphire Bioscience	1:10000	0.1 mg
	Anti-actin clone c4 (β -actin)	MAB1501	Millipore	1:15000	0.1 mL
	Anti-Alpha-Tubulin	05-829	Merck Millipore	1:15000	0.2 mg
	Anti-goat IgG (H+L) HRP conjugate	81-1620	Life Technologies	1:10000	1.5 mg
	Anti-mouse IgG (H+L) HRP conjugate	402335-2ML	Merck	1:10000	2 mL
	Anti-rat IgG (H+L) HRP conjugate	62-9520	Life Technologies	1:10000	1 mL
	NgR2 peptide	sc-168752 P	Santa Cruz Biotechnology		0.2 mg/mL
	NgR3 peptide	sc-165108 P	Santa Cruz Biotechnology		0.2 mg/mL
	BCA Protein Assay Kit	PIE23225	Thermo Scientific		500 tests
	GE Amersham ECL prime kit	VWR/GE	VWR/GE healthcare		1000 cm ² membrane
	Gel loading pipette tips	NAAU3640	Merck Millipore		Box
	Luminata Forte Western Reagent	WBLUF0100	Millipore		100 mL
	Protein G magnetic beads	LSKMAGG10	Millipore		10 mL
	Tracker Tape	RPN2050	GE Healthcare		10 x 15 cm
	Super RX Films	4741019236	Fujifilm		100 sheets
	Protease Inhibitor Cocktail Set III, EDTA Free	539134	Merck Millipore		1 mL
	Recombinant Mouse NgR/Fc chimera	1440-NG	R&D systems		0.2 μ g
	Methanol GR	1060099025	Merck Millipore		25 L
	NuPage Antioxidant	NP0005	Life Technologies		15 mL
	NuPage 4-12% Bis Tris 10 well gel	NP0335BOX	Life Technologies		10 gels
	NuPage 4-12% Bis Tris 15 well gel	NP0336BOX	Life Technologies		10 gels
NuPage MOPS SDS Running Buffer	NP0001	Life Technologies		500 ml	
NuPage Sample reducing agent (10x)	NP0009	Life Technologies		10 mL	
1X see Blue Plus 2 prestained	LC 5925	Life Technologies		0.5 mL	
Cell culture	BAFF (soluble) mouse recombinant	ALX-522-052	Sapphire Bioscience		0.01 mg
	BAFF (Soluble) mouse recombinant	ALX-522-052	Enzo		0.01 mg
	BAFF-R/TNFRSF13C Fc Chimera Protein, mouse recombinant	1357-BR-050	In Vitro Technology		0.05 mg
	Beta-meracptoethanol (55 nM)	21985023	Gibco		50 mL
	BrdU APC flow kit	552598	BD Bioscience		50 tests
	L-glutamine	25030-081	Life Technologies		100 mL
	Penicillin and streptomycin (Pen/Strep)	15140-122	Life Technologies		100 mL
	RNase free DNase set	79254	Qiagen		50 set
	RPMI-1640	R0883-500ML	Sigma		500 mL

Enzyme-linked immunosorbent assay (ELISA)	384-well plate	3700	Corning		100
	Anti-mouse Ig (H+L)	1010-01	Southern Biotech		2 mg
	Anti-IgM-AP conjugated	1020-04	Southern Biotech	1:2000	1 mL
	Anti-IgA-AP conjugated	1040-04	Southern Biotech	1:2000	1 mL
	Anti-IgG1-AP conjugated	1070-04	Southern Biotech	1:2000	1 mL
	Anti-IgG2b-AP conjugated	1090-04	Southern Biotech	1:2000	1 mL
	Anti-IgG2c-AP conjugated	1079-04	Southern Biotech	1:2000	1 mL
	Anti-IgE-AP conjugated	1110-04	Southern Biotech	1:2000	1 mL
	Anti-IgG-AP conjugated	1030-04	Southern Biotech	1:2000	1 mL
	Mouse IgM-AP	0101-01	Southern Biotech		1 mL
	Mouse IgA-AP	0106-01	Southern Biotech		1 mL
	Mouse IgE-AP	01114-01	Southern Biotech		1 mL
	Mouse IgG1-AP	0102-05	Southern Biotech		1 mL
	Mouse IgG2b-AP	0104-04	Southern Biotech		1 mL
	Mouse IgG2c-AP	0106-04	Southern Biotech		1 mL
	Mouse IgG3-AP	0105-04	Southern Biotech		1 mL
Sigma fast OPD tablet	P9187	Sigma Aldrich		50 set	
Haematopoietic stem cell transplantation (HSCT)	Anti-rat BioMag beads	310107	Qiagen		
	Anti-mouse CD117-PE	60025PE	Stem cell Technologies	1:50	0.2 mg
	Anti-mouse Ly-6A/E (Sca-1) PE-Cy7	25-5981	eBioscience	1:400	0.1 mg
	Anti-mouse CD3e PE-Cy7	25-0031-81	Jomar	1:200	0.05 mg
	Anti-mouse CD3e	PAB 9003	Abnova	1:200	0.1 mg
	Anti-mouse CD45/B220 PE	553090	BD Pharmigen	1:200	0.2 mg
	Anti-mouse CD45/B220	bs-4818R	BIOSS	1:200	0.1 mL
	Anti-mouse CD11c APC	550261	BD Pharmigen	1:50	0.1 mg
	Anti-mouse CD11c biotin	553800	BD Pharmigen	1:100	0.1 mg
	Anti-mouse CD11c	bs-2508R	BIOSS	1:200	0.1 mL
				1:10 FC	
	Anti-mouse NgR	MAB1659	R&D system	1:100 IHC	0.05 mg
	Anti-GFP	A11120	Thermo fisher	1:200	0.1 mg
	Anti-GFP	AB3080	Merck Millipore	1:200	
	Anti-myc (71D10)	2278S	Cell signalling tech	1:8000	0.1 mL
	Anti-Iba1	NBP2-16908	In vitro Tech	1:500	0.1 mL
	Anti-goat Alexa Fluor 488 (2mg/uL)	A11055	Life Technologies	1:200	0.5 mL
	Anti-goat Alexa Fluor 555 (2mg/uL)	A21432	Life Technologies	1:200	0.5 mL
	Anti-rabbit Alexa Fluor 488 (2mg/uL)	A11008	Life Technologies	1:200	0.5 mL
	Anti-rabbit Alexa Fluor 555 (2mg/uL)	A21428	Life Technologies	1:200	0.5 mL
	Anti-rat Alexa Fluor 555 (2mg/uL)	A21434	Life Technologies	1:200	0.5 mL
	Anti-mouse Alexa Fluor 488 (2mg/uL)	A11001	Life Technologies	1:200	0.5 mL
	Anti-Mouse Alexa Fluor 546 (2mg/uL)	A11003	Life Technologies	1:200	0.5 mL
	Anti-mouse Alexa Fluor 647 (2mg/uL)	A21235	Life Technologies	1:200	0.5 mL
	Biotin lineage panel	559971	BD bioscience		
	Costar 6-well clear TC-treated multiple well plates (sterile)	3516	Corning		50 plates
	Costar 24-well clear TC-treated multiple well plates (sterile)	3524	Corning		100 plates
	DMEM, high glucose, pyruvate	11995065	Life Technologies		500 mL
	DPBS Ca+ Mg+	14040-182	Life Technologies		500 mL
	DPBS Ca -, Mg-	14190-250	Life Technologies		500 mL
	Fetal Bovine Serum (Tetracycline-free)	631106	CloneTech		500 mL
L-glutamine	25030-081	Life Technologies		100 mL	

Normal Rat Serum	10710C	Life Technologies		10 mL
Penicillin and streptomycin (Pen/Strep)	15140-122	Life Technologies		100 mL
StemSpan Serum-Free Expansion Medium	9655	Stem cell Technologies		500 mL
Streptavidin APC	17-4317-82	Affymetrix-eBioscience	1:200	0.1 mg

2.1 Mouse Breeding

All experiments were implemented in accordance with the guidelines of the Australia code of practice for the use and care of animals for scientific purposes and approved by the Monash University Animal Ethic Committee (Alfred Medical Research and Education Precinct; AMREP) and office of the Gene Technology Regulator of Australia (AEC AMREP Approval number E/1532/2015/M). Female *ngr1*^{-/-} mice (aged 8-12 weeks) and their *ngr1*^{+/+} littermates (LM) were bred and maintained at AMREP and PAC Animal Services. The exon 2 of the *ngr1* gene was a double targeted allele on a C57Bl/6 background mice and backcrossed more than 10 generations as mentioned previously (Kim et al., 2004).

2.2 Mouse Genotyping

Tail samples (2-3 mm) were obtained and DNA extraction was performed using the SIGMA Aldrich Kit according to manufacturer's specifications. All samples were stored at 4°C, polymerase chain reaction (PCR) amplification was performed using 2 µL of PCR water, 10 µL of extract N Amp PCR reaction mix, then 1 µL of each of the following

primers (NgR Forward (Fwd), NgR Reverse (Rev), Neo Fwd, Neo Rev) (Table 4). Following this, 4 μ L of the sample was added, then mixed gently before start cycling.

Cycling conditions

1x 94 °C for 3 min

34x 94°C for 20 sec

57°C for 30 sec

68°C for 60 sec

1x 68°C for 5 min

1x 4°C hold

All samples were then loaded into Agarose gels (1g with 100 mL of TAE buffer with SYBER safe (Life Technologies; CA, USA)) after mixing with BlueJuice Gel Loading buffer (10x) (Life Technologies; CA, USA). The gels were run at 95 V for 45 min.

Table 4. Genotyping primers.

Name of Primer	Gene Target	Sequence
NgR Fwd	NgR	5'- CAGTACCTGCGACTCAATGACAACCCC-3'
NgR Rev.	NgR	5'- CTTCCGGGAACAACCTGGCCTCC-3'
Neo Fwd	NgR	5'- CTATTCGGCTATGACTGGGCACAACAGAC-3'
Neo Rev.	NgR	5'- GAACTCGTCAAGAAGGCGATAGAAGGCGAT-3'

2.3 Mouse EAE Induction and Clinical Assessment

To induce EAE, 8-12 week old C57Bl/6 (*ngr1*^{+/+} or *ngr1*^{-/-}) mice were subcutaneously injected in the lower flanks with either 200 µg MOG₃₅₋₅₅ (Purac Chemical, China) or rMOG (see Appendix 2), emulsified in 200 µL of complete Freund's Adjuvant (CFA, Sigma-Aldrich, MO, USA) supplemented with 4 µg/mL *Mycobacterium tuberculosis* (BD Biosciences, CA, USA). On the same day, immunised mice had an intraperitoneal injection of 350 ng pertussis toxin; a second dose of pertussis toxin was injected into the mice two days later (57). Post-MOG-induced mice were scored for disease progression, consistent with well documented disease stages as previously described, classically these included (Petratos et al., 2012); pre-onset (score 0; day 7 after injection), onset (score 1; day 12 after injection), peak (score 2; day 18 after injection) and chronic (> score 3; day 30 after injection) in *ngr1*^{+/+} and *ngr1*^{-/-} female mice. In addition to the un-injected mice used as controls in *ngr1*^{+/+} and *ngr1*^{-/-}, we injected *ngr1*^{+/+} and *ngr1*^{-/-} mice with Adjuvant alone serving as a non-specific injection control. The major aim in this experiment was to perform an in-depth immunological analysis of the EAE peripheral immune arm from *ngr1*^{+/+} LM and *ngr1*^{-/-} mice.

2.4 Mouse Perfusion and Tissue processing

These mice were euthanised at variable stages of disease (maximum clinical score 3) via CO₂ inhalation according to ethical guidelines. Once the mice were unconscious and lacked neurological reflex to a paw pinch, then the chest cavity was opened to access the

heart. In order to drain out the blood, a small hole was cut in the right atrium. Filtered PBS was slowly injected into the left ventricle using a 27 gauge needle to ensure all blood was drain out. Approximately 20 to 25 mL of filtered PBS was used for each mouse, then spleen, axillary and inguinal lymph nodes and spinal cord were dissected to isolate immune cells for immunophenotyping analysis. Otherwise, an equal amount of 4% paraformaldehyde (PFA) fixative was injected into the left ventricle and tissues were then processed for immunohistochemistry. Longitudinal spleen, lymph node and spinal cord sections were cut into 10 μ m serial sections on a conventional microtome and processed for immunohistochemistry, performed in Histology platform, Monash University.

2.5 Isolation of immune cells and myelin from mouse tissues

2.5.1 Spleen and lymph node isolation

T-cells, B-cells and DCs were isolated from the tissues of induced mice (n=222 female mice; n=137 *ngr1*^{+/+} and n=85 *ngr1*^{-/-}), immunised with either MOG₃₅₋₅₅ or rMOG at variable clinical stages of EAE disease progression, including non-immunised *ngr1*^{+/+} (n=11) and *ngr1*^{-/-} (n=11) LM mice. Spleen and lymph node tissues were placed into two different cell strainers (BD Falcon), and then mashed into the petri dish using the plunger end of the syringe. The cell strainers were rinsed with 5 mL warmed RPMI 1640 (Sigma-Aldrich), and the suspended cells were transferred to a 15 mL conical tube for each tissue. The cells were spun at 800 xg for 3 min, the supernatant was discarded and the pellet was re-suspended in 1 mL of warm red cell lysis buffer (Sigma-Aldrich), an

incubated for 10 min at room temperature. Next, 9 mL of a cold FACS wash buffer [0.02% sodium azide (100 mg/mL), 1% bovine serum albumin (BSA) (100 mg/mL), phosphate buffered saline (1X PBS)] were added and spun as previously described. The supernatant was discarded and the pellet re-suspended in a 3 mL FACS wash buffer (see appendix), filtered through a blue top FACS tube. The cells were counted manually using a haemocytometer (10 μ L of cell suspension were diluted in 10 μ L of trypan blue).

2.5.2 Spinal cord isolation

Spinal cord tissue was chopped into fine pieces in a petri dish using a scalpel blade with 1X PBS, and then transferred into 20 mL collagenase D (Roche) / Dnase I (Roche) (250 μ L Coll D (100 mg/mL), 200 μ L of diluted Dnase I (100 mg/mL), 19.55 mL 1X PBS). Cells were then spun at 800 xg for 5 min after incubating at 37°C for 30 min. The supernatant was discarded, and then re-suspended in 3 mL PBS then placed in a 40 μ m cell strainer (BD Falcon). The cells were meshed through the strainer with a plunger and collected into a tube after being washed with DPBS (Life Technologies). They were spun at 800 xg for 5 min, then re-suspended in 20 mL DMEM F12 (Life Technologies) layered on top of 15 mL of Ficol (Stem cells Technologies) to perform a cell gradient. After spinning at 800 xg for 30 minutes at 20°C, the interference layer was collected, and 20 mL DPBS were added. Afterward, the cells were spun twice at 400 xg for 10 min at 20°C. The cells were re-suspended in a 2 mL FACS wash buffer, filtered and counted.

2.5.3 Myelin Isolation

Purification of peripheral nervous system myelin (PNM) was described previously (Geczy et al., 1984). Sciatic nerves were obtained from both *ngr1^{+/+}* and *ngr1^{-/-}* mice, immunised with MOG₃₅₋₅₅ at variable clinical stages of EAE disease progression, including non-immunised *ngr1^{+/+}* and *ngr1^{-/-}* LM mice. The nerves were then ground to a fine powder in liquid nitrogen that were homogenised in 0.29 mol/L of sucrose solution (5% w/v). After preparing a discontinuous sucrose gradient by layering 15 mL aliquots of the homogenate over 11 mL of 0.85 mol/L sucrose, this was spun for 45 min at 90000 xg. The interface, including crude myelin, was collected and diluted 1:1 with 0.24 mol/L sucrose. Then it was spun for 30 min at 17000 xg to collect the pellet, which was resuspended in dH₂O (osmotic shock), and re-spun again for 30 min at 17000 xg. Afterword, a second discontinuous sucrose gradient were used again for further myelin purification, and to remove any immunoglobulin contamination that may provide a false positive. The purified myelin was treated with diethylamine-HCl (50 mmol/L, pH=11.5), then pelleted in a microfuge, and thoroughly washed with dH₂O to become lyophilised.

2.6 Flow Cytometry

2.6.1 Single-labelled

Isolated cells (n=222 female mice; n=137 *ngr1^{+/+}* and n=85 *ngr1^{-/-}*) were analysed using flow cytometry to determine whether there existed disparate populations within disease-

originating organ sites. Briefly, cells were washed with 1 mL FACS wash buffer, centrifuged (3x) at 1500 rpm for 5 min. Each cell staining involved a phycoerythrin (PE)-labelled antibody, a fluorescein isothiocyanate (FITC)-labelled antibody, Allophycocyanin (APC)-labelled antibody, a peridinin chlorophyll protein complex (perCP-Cy5.5)-labelled antibody, and phycoerythrin Cyanine7 (PE-Cy7)-labelled antibody. Mouse immune cell antigens were detected using the following fluorescently labelled antibodies: CD45/B220-PE (BD Pharmigen) and its isotype control (BD Pharmigen; PE labelled rat IgG 2b kappa); CD11c-APC (BD Pharmigen) and its isotype control (BD Pharmigen; APC labelled rat IgG 2a kappa); CD3e-Pe-Cy7 (eBioscience) and its isotype control (eBioscience; PE-Cy7 labelled hamster IgG); mouse Nogo Receptor/NgR antibody (R&D systems) and its isotype control (BD Pharmigen; rat IgG 2b kappa); IgM-PerCP/Cy5.5 (BioLegend); IgD-APC (BioLegend), IgG-Biotin (affymetrix-eBioscience); Streptavidin APC (affymetrix-eBioscience); and Ki-67-eFluor®450 (affymetrix-eBioscience).

2.6.2 Double-labelled

In addition to the previous single staining, each immune cell antigen was stained with an anti-NgR antibody (R&D system), using an indirect method, in order to determine whether NgR is expressed on these isolated immune cells. The fluorescently labelled antibodies were added to the cells according to the specific dilution (as recommended by the manufacturer), mixed well and then incubated on ice for 30 min in the dark. The cells were washed (3x), then centrifuged at 1500 rpm for 5 min at 4°C. Fluorescent staining of dead cells was performed by 4',6-diamidino-2-phenylindole (DAPI) (1:2000) (Molecular

Probes), labelling all cells with a disrupted cell membrane for 5 to 10 min before analysis.

Normal rat serum (Life Technologies, CA, USA) was added into all tubes that contained the mouse NgR and incubated on ice for 15-30 min in the dark. The cells were then washed (3x) and centrifuged at 1500 rpm for 5 min at 4°C, and the secondary antibody (Alexa fluor 488 goat anti-rat IgG (H+L); Invitrogen) for mouse NgR was added into all samples, and incubated for 30 min on ice in the dark. After washing as previously described, the following primary antibodies (PE-CD45/B220, APC-CD11c, PE-Cy7-CD3e, and cocktail of PE-CD45/B220, PE-Cy7-IgG, APC-IgD and PerCP/Cy5.5-IgM) were added into double-labelled staining tubes. Similarly, the cells were washed (3x) by centrifugation at 1500 rpm for 5 min at 4°C. DAPI was added into each sample for 5 to 10 min before analysis. Finally, all tubes were analysed by using the BD FACS Canto II (BD Biosciences, MD, USA).

2.7 Immunohistochemistry analysis for mouse tissue

2.7.1 Paraffin sections

Standard immunohistochemistry of several EAE spinal cord tissue sections (n=34 *ngr1*^{+/+} mice; 108 sections, n=15 *ngr1*^{-/-} mice; 40 sections) with varying clinical scores (0; day 7 after injection, 1; day 12 after injection, 3; day 21-30 after injection) for severity was performed to identify demyelination and inflammatory cell infiltration, as well as to demonstrate the existence and localisation of B-cells that express NgR1 and its

homologues within the CNS tissue. This was performed to correlate the *in vivo* analysis steriologically with *ex vivo* flow cytometric data generated for immune cells during disease and to indicate the location of B-cells that express NgR1 and its homologues in the spinal cord. Initially, fixed, paraffin-embedded tissues were cut into 10 µm serial sections on a conventional microtome and processed for immunohistochemistry. The sections were de-waxed then they were incubated with proteinase K (20 µg/mL) (Qiagen) for 1 hour at 37°C. then washed (3x 10 min) with PBS. All sections were post-fixed with 4% PFA for 30 min at room temperature, followed by three washes with PBS. Tissues were then incubated in the blocking buffer (5% goat serum (v/v), 5% fetal bovine (v/v) serum, 0.1% triton X-100 (v/v) in PBS) at 4°C overnight. All sections were incubated with a primary antibody (Rabbit anti-CD45/B220 polyclonal antibody; BIOSS) or (polyclonal antibody to BLyS; IMGENEX) or (anti-TROY antibody; Sapphire Bioscience) or (polyclonal anti-NgR2 antibody; Santa Cruz Biotechnology) or (polyclonal anti-NgR3 antibody; Santa Cruz Biotechnology), in addition to anti-mNgR antibody for 2 hours at room temperature, followed by washing (3x) in PBS (pH=7.4) for 10 min. Appropriate secondary antibodies (Alexa Fluro® 488 goat anti-rabbit IgG (H+L) antibody; Life technologies, Alexa Fluro® 488 goat anti-rat IgG (H+L) antibody; Life technologies, Alexa Fluro® 555 goat anti-rabbit IgG (H+L) antibody; Life technologies, Alexa Fluro® 555 goat anti-rat IgG (H+L) antibody; Life technologies, Donkey anti-Goat 488 antibody; Life technologies, Donkey anti-Goat 555 antibody; Life technologies) were placed on all slides, and incubated for 1-2 hours at room temperature. DAPI was added after washing in PBS for 15 min to visualise inflammatory infiltrates, then washed and cover-slipped using Dako, fluorescent mounting medium. Subsequently, all tissue

specimens were captured by the three-channel fluorescence imaging, using a confocal Nikon C1 upright microscope with 40x and 60x UPlanApo objective lens. The image files were saved as TIFF and ND2, then modified using Adobe Photoshop C3 software and saved as JPEG 2000.

2.7.2 Frozen sections

Freshly dissected spinal cord, cerebellum and optic nerve blocks from EAE-induced and control were placed onto a pre-labelled tissue base mold. The blocks were completely covered with Optimal Cutting Temperature compound (OCT), then the mold was placed into liquid nitrogen until submerged the entire tissue block into liquid nitrogen, to ensure that the tissue was completely frozen. The tissue blocks were then cut into 10 μm serial sections on a cryostat (Leica Microsystems; Wetzlar, Germany), mounted on SuperFrost[®] Plus microscope slides (Menzel-Gläser; Braunschweig, Germany) and allowed to dry at 20 °C (minimum 2hours). The sections were post-fixed with 4% PFA for 30 min at room temperature, followed by three washes with PBS. Tissues were then incubated in the blocking buffer (5% goat serum (v/v), 5% fetal bovine serum (v/v), 0.1% triton X-100 (v/v) in PBS) for 1 hour at room temperature. All sections were incubated with a primary antibody (Rabbit anti-CD45/B220 polyclonal antibody; BIOSS) or (polyclonal antibody to CD3e; Abnova) or (anti-CD11c antibody; BIOSS) or (anti-Myc antibody; Cell Signalling Tech) or (anti-GFP antibody; Merck Millipore), or (anti-mouse/Rat Ki-67 eFluor[®] 450), in addition to anti-mNgR antibody at 4°C overnight, followed by washing (3x) in PBS (pH=7.4) for 10 min. Appropriate secondary antibodies

(Alexa Fluro® 488 goat anti-rabbit IgG (H+L) antibody; Life technologies, Alexa Fluro® 488goat anti-rat IgG (H+L) antibody; Life technologies, Alexa Fluro® 555 goat anti-rabbit IgG (H+L) antibody; Life technologies, Alexa Fluro® 555 goat anti-rat IgG (H+L) antibody; Life technologies, anti-mouse 647 antibody) were placed on all slides, and incubated for 1-2 hours at room temperature. DAPI was added after washing in PBS for 15 min to visualise inflammatory infiltrates, then washed and cover-slipped using Dako, fluorescent mounting medium. Subsequently, all tissue specimens were captured by the three-channel fluorescence imaging, using a confocal Nikon C1 upright microscope with 40x and 60x UPlanApo objective lens. The image files were saved as TIFF and ND2, then modified using Adobe Photoshop C3 software and saved as JPEG 2000.

2.7.3 Quantification of NgR and B-cell populations in the white matter tract of the lumbar and sacral spinal cord

Analysis of cell numbers localised within specific tissue areas were performed on all spinal cord sections (n=148) of both *ngr1^{+/+}* and *ngr1^{-/-}* mice after immunohistochemistry preparation. The number of double stained cells (NgR that is expressed on B-cells) was counted per unit area (per μm^2) of spinal cord longitudinal-sections in all genotypes (3 different sections per mouse > 50 μm apart). The mean and standard error was calculated for each group of mice at different clinical stages of the disease.

2.7.4 Demyelination and axonal degeneration

Post-tissue processing, luxol fast blue and periodic acid-Schiff (LFB/PAS) and Bilshowsky staining were used on spinal cord sections of *ngr1^{+/+}* and *ngr1^{-/-}* mice at different clinical scores (Histology platform, Monash University) in order to demonstrate areas of demyelination and axonal injury in EAE mice respectively. LFB was performed by hydrating the tissue sections using 95% ethanol, then placed in Low Viscosity Nitrocellulose (LVN) for 1 min. the sections were then placed into 0.1 % LFB solution (w/v) overnight at 40°C incubator (cover staining dish in cling wrap to avoid excessive evaporation of the solution). Excess stain was rinsed off in 70% ethanol, then was washed in dH₂O. With very quick dip, the sections were placed in dilute lithium carbonate (0.5 mg/mL), then differentiated in 50-70% ethanol. Immediately, all sections were washed in dH₂O (to stop the differentiation but if it over differentiated, place back into LFB solution for 5-6 hours or overnight). The sections were counterstained with periodic acid-Schiff for 5 seconds, then dehydrated rapidly through ethanol into xylene, mount in DPX (a mixture of distyrene, a plasticizer, and xylene). Bilshowsky staining were performed by adding sections into 20% silver nitrate (w/v), incubated for 20 mins at 40°C incubator. All sections were then washed with dH₂O, and returned into silver nitrate again. Ammonium hydroxide was added drop-by-drop until the precipitate formed had completely dissolved. Then drops of developer stock solution (37-40% formaldehyde, 0.5 g of citric acid (5 mg/mL), 2 drops of 20% nitric acid, and 100 mL of dH₂O) were added

to 20% of ammoniacal silver, then reduced to a visible metallic silver. The sections were dehydrated rapidly through ethanol and then xylene.

2.8 Protein Biochemistry

2.8.1 Preparation of cell and tissue lysate for western blotting

Spleen, lymph nodes and spinal cord samples were ground and lysed from both naïve *ngr1^{+/+}* and *ngr1^{-/-}* mice using radioimmunoprecipitation assay (RIPA) buffer (Cell Signaling Technology), including PhosSTOP phosphatase inhibitors cocktail (Roche Applied Science) and 1% protease inhibitor (v/v) (Sigma-Aldrich) in a dounce homogenizer. The protein supernatants were collected from homogenates, after centrifuging them at 13,000 xg for 15 min at 4°C. By using the bicinchoninic acid (BCA) protein assay kit (Thermo Fisher Scientific, USA), the protein concentrations were determined.

2.8.2 Western immunoblotting

10 µg of protein isolated from spleen, lymph nodes, spinal cord and myelin samples were loaded into 4-12% graded sodium dodecyl sulphate polyacrylamide gels (SDS-PAGE) (Invitrogen). The proteins were blocked with 5% skim milk powder (w/v) in Tris-buffered saline-Tween (TBST) for 30 min at room temperature after transferring onto polyvinylidene fluoride (PVDF) membranes. The membranes were then incubated with primary anti-NgR antibody (Millipore and R&D system), anti-NgR2 antibody (Santa

Cruz Biotechnology), anti-NgR3 antibody (Santa Cruz Biotechnology), and anti-myelin basic protein antibody (Sapphire Bioscience) in 5% skim milk (50 mg/mL) at 4°C, overnight. The membranes were then washed (3x) with 0.1% TBST (v/v) for 10 minutes, followed by adding the secondary anti-rabbit antibody (HRP-conjugated; Calbiochem), anti-rat antibody (HRP-conjugated; Calbiochem), and anti-mouse antibody (HRP-conjugated; Calbiochem) diluted in 5% skim milk or TBST and incubated for 2 hours at room temperature; washed longer for more than (3x) by 0.1% TBST (v/v). The membranes were then incubated with 2 mL of Luminata Forte Western Reagent (Millipore) or Luminata ECL chemiluminescence (Merck-Millipore, CA) for 3-5 min at room temperature for development. Using the Alpha Imager (Alpha Innotech, San Leandro), the films were scanned and the intensities of the bands were determined using ImageQuant TL v2003 software (Nonlinear Dynamics Ltd, All Saints, Newcastle, UK). Some of the membranes were stained with coomassie blue (8 mg/mL) dye for 30 mins to 1 hour, and they were scanned after de-staining.

Testing the specificity of the polyclonal NgR antibody using 100 µg of spleen and lymph node lysates of naïve *ngr1^{+/+}* and *ngr1^{-/-}* mice with 1 µL of anti-NgR antibody at 4°C overnight. 50 µL of a 50% slurry of Protein A-Sepharose beads (Merck Millipore) was washed (3x) with 500 µL 1X PBS in Tween-20 then it was added into each sample and incubated for 2 hours at 4°C. 25 µL of denaturing solution (RIPA buffer, beta mercap and loading dye) were added into each sample after washing them (3x) using a magnetic stand (Merck Millipore). The samples were incubated at 70-90°C for 10 minutes in a heat block. Three gels were performed and were loaded with; 1) all samples, 2) secondary

anti-rabbit HRP-conjugated antibody alone, 3) the supernatant that was collected from the last wash. All gels were loaded with 1 μ L of NgR1-Fc peptide (0.1 mg/mL) (as a positive control).

2.9 Cell Culture

Immune cells were isolated from spleen and spinal cords of EAE mice (n=26 *ngR1*^{+/+} and n=10 *ngR1*^{-/-}), as previously described. The cells were suspended into 2 mL FACS buffer (2% heat inactivated fetal calf serum (FCS) and DPBS) in 5 mL polypropylene round bottom tubes, then stained as mentioned in page 121-123, using only anti-CD45/B220-PE antibodies and either anti-NgR or anti-NgR3 antibodies. The double-positive cells were stained with DAPI, then sorted using either BD FACS ARIA or BD Influx sorter at FLOW core (AMREP). The sorted cells were collected and cultured for 2-3 days in RPMI medium supplemented with 10% heat inactivated FCS (Clontech), 50 mM β -mercaptoethanol, L-glutamine (2 mM), 100 U/ml penicillin, and 100 U/ml streptomycin (Gibco) at 37 °C with 5% CO₂ in a humidified atmosphere.

2.10 Cell cycle analysis

In order to test the cell cycle progression within cultured cells, 50 ng/mL of BAFF (soluble) mouse recombinant (rBAFF; Enzo) was added into all B-cells cultures and incubated 24 hours at 37 °C with 5% CO₂ in a humidified atmosphere. To identify NgR

interactions with BAFF, rBAFF was blocked with an excess amount of either rBAFF-R, NgR1-Fc or NgR3-P by incubating them for 30 min at 37 °C. Then the supernatant was collected after spinning for 5 min with 16,000 xg and added into cultured cells by incubating for 24 hours at 37 °C with 5% CO₂ in a humidified atmosphere. We collected 100 µL of supernatant for all samples before and after stimulation with rBAFF, or following inhibition of rBAFF activity with either NgR1-Fc or NgR3-P peptides. The following day, the cell cycle was tested using a BrdU APC flow kit (BD Bioscience). First, 1 mM solution of BrdU was added for 1 hour to a culture and treated cells. Second, BrdU-pulsed cells were transferred into FACS tubes and their counts were measured. Extracellular antibodies (CD45/B220, NgR and NgR3) were used to stain cells, as mentioned previously. Cells were fixed and permeabilised with a BD Cytofix/Cytoperm Buffer for 20 min on ice, then washed with 1X BD Perm/Wash Buffer and spun for 5 min at 300 xg. Then the supernatant was discarded. Cells were next incubated with BD Cytoperm Permeabilisation Buffer Plus for 10 min on ice and washed with 1X BD Perm/Wash Buffer again. Cells were re-fixed with BD Cytofix/Cytoperm Buffer for 5 min on ice, then washed as described. Dnase was added into treated cells and incubated for 1 hour at 37 °C, then washed with 1X BD Perm/Wash Buffer. Finally, cells were stained using an anti-BrdU antibody for 20 min. These were stained with total DNA for cell cycle analysis, 7-aminoactinomycin D (7AAD), after washing it with 1X BD Perm/Wash Buffer. Stained cell counts were acquired from BD LSR II.

2.11 ELISA

Supernatant was collected from sorted and cultured cells of *ngr1^{+/+}* and *ngr1^{-/-}* mice and Ig phenotype was measured by Enzyme-linked immunosorbent assay (ELISA) at clinical score 1 and 3, with supernatant diluted as follows: 1:10, 1:100 and 1:1000 for anti-IgM, -IgA, -IgE, -IgG AP conjugated secondary antibodies (Southern Biotech) and its subtypes; anti-IgG1, -IgG2b, -IgG2c and -IgG3 antibodies (Southern Biotech). The 384-well assay plate (Corning) was coated with 20 μ l/well of 2 μ g/ml coating reagent (goat anti-mouse Ig (H+L)) (Southern Biotech) and incubated overnight at 4 $^{\circ}$ C. The plate was washed (2x) with wash buffer (0.1% Tween-20 (w/v), PBS) and (1x) with PBS. 100 μ l/well of Block buffer (4% BSA (w/v), PBS) was added and incubated 30 min at room temperature, followed by two washes with wash buffer and one wash with PBS. 40 μ l of diluted samples (supernatant collected from sorted and cultured cells) or control antibodies in a dilution buffer (0.5% (w/v) BSA, PBS) were added into the plate into serial dilution (1:10, 1:100 and 1:1000) for the sample and (1:2) for control antibodies (Southern Biotech). At the same time, 20 μ l of a dilution buffer was added to other wells. Then the plate was incubated for 30 min at room temperature on the plate shaker, followed by two washes with wash buffer and one wash with PBS. 20 μ l/well of secondary antibody (diluted 1:2000 in a dilution buffer) (Southern Biotech) was added and incubated for 30 min at room temperature on the plate shaker. Then the plate was washed (4x) with wash buffer and (2x) with PBS. 20 μ l/well of 1 mg/ml Substrate solution (PNPP tablets dissolved in M.H₂O; one 20 mg tablet per 20 ml M.H₂O) (Sigma).

Once the yellow colour developed the absorbances were measured at 405 nm using microplate reader (Bio-Rad Laboratories, CA, USA).

2.12 Transplantation of genetically modified hematopoietic stem cells

(HSCs)

2.12.1 NgR1 sub-cloning in pLVX-EF1 α -IRES-ZsGreen1

We have successfully able to transplant LV-modified HSCs encoding the ectodomain of NgR1 fused to the mouse IgG Fc portion (Figure 8A). Briefly, the NgR(310)ecto cDNA was cloned from the adult mouse brain Marathon-Ready cDNA (Cloneteck Laboratories, CA, USA) and inserted into pFUSE-mIgG1-Fc1 plasmid (InvivoGen, San Diego, CA, USA) to add the Fc component. The insertion of NgR(310) (1654 base pair (bp)) has been amplified, using a designed PCR primer with 15 bp extensions (5') that are complementary to the end of the linearised vector (obtained from Cloneteck Laboratories, CA, USA). After amplification of NgR(310)ecto-Fc1 portion, it was inserted into the pCMV-Tag 5 plasmid (Agilent Technologies, CA, USA) to add a myc-tag for tracking purpose. The total NgR(310)ecto-Fc-myc cDNA was confirmed by DNA sequencing (5'-TATTTCCGGTGAATTCTTAATGAAGAGGGCGTCCT-3') (Fwd) and (5'-TAGTCTCGAGGAATTCGCCCTACAGATCCTCTTC-3') (Rev) (Micromon, Monash University). An In-Fusion HD Cloning Kit reaction was used, including an enzyme premix, linearised vector, insert, and dH₂O, followed by a short incubation for 15 min at 50°C on ice. The reaction mixture was then transformed with a competent mixture.

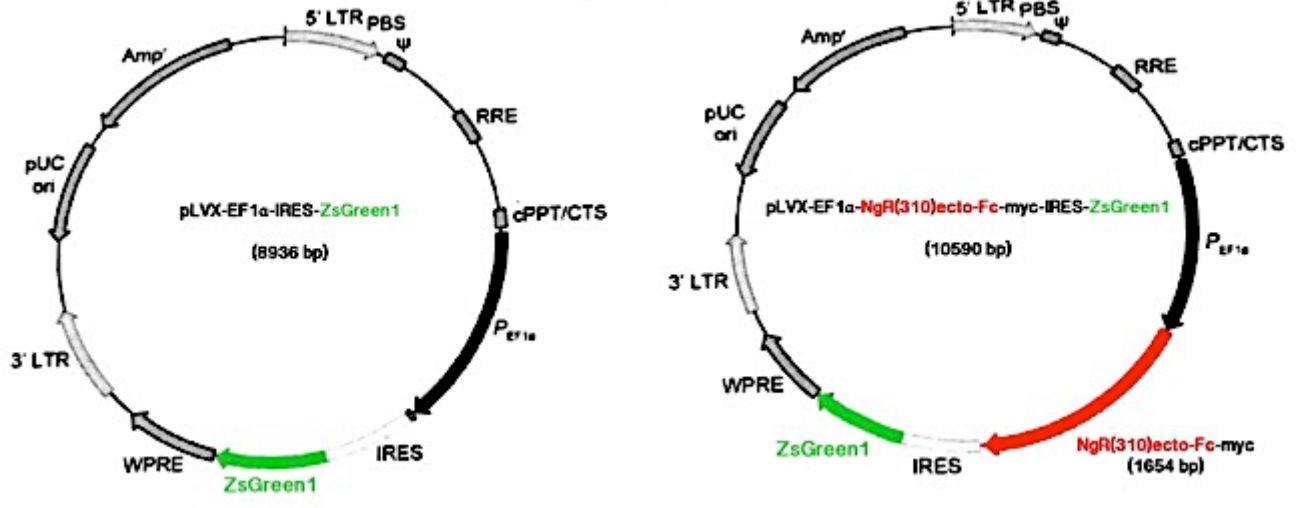
Consequently, this yielded pLVX-EF1 α -NgR(310)ecto-Fc-myc-IRES-ZsGreen1, as shown in Figure 8A, confirmed by DNA sequencing.

2.12.1 Transfection of 293T cells with pLVX-EF1 α -NgR(310)-Fc-IRES-ZsGreen1

In order to produce functional Lentiviral (LV) vectors for *ex vivo* transductions of mouse lin⁻ BM cells and transplantation (Figure 8B), 293T cells, which is isolated from human embryonic Kidneys (HEK), were propagated in 8 x 10 cm tissue culture dishes with media (DMEM, 10% FCS (Clontech), L-glutamate, penicillin, and streptomycin (tetracycline free, antibiotic) at 37 °C with 5% CO₂ in a humidified atmosphere. Cells were harvested, then counted and re-suspended at 5 x 10⁶ cells/mL. 1 mL of cell suspension was aliquoted into 20, 10 cm tissue culture dishes, then 9 mL of media was added into each dish and incubated overnight at 37°C with 5% CO₂ in a humidified atmosphere. On the day of transfection, the medium was aspirated and overlaid with 6 mL of fresh medium, then incubated for 2 hours. The DNA cocktail was prepared; x 1 reaction (2.73 μ L pWLVX clone G (1168.8 ng/ μ L), 3.73 μ L psPAX2 clone (1071 ng/ μ L), 0.42 μ L pMD2.G clone (941.6 ng/ μ L), 33.12 μ L ddH₂O) and x 21 reaction (57.33 μ L pWLVX clone G, 78.33 μ L psPAX2 clone, 8.82 μ L pMD2.G clone, 695.52 μ L ddH₂O). Twenty sterile eppendorfs were set up for each transfection and 160 μ L of DMEM (did not include, serum, L-glutamate, penicillin, and streptomycin) and 24 μ L Fugene HD (pipetted gently for 4-5x) were added. Afterward, 40 μ L of DNA cocktail was added gently into tubes and incubated for 20-30 min at room temperature. The

cocktail mix was added into the plate, then transfected 293T cells were incubated for 72 hours at 37°C with 5% CO₂ in a humidified atmosphere. Viral supernatant was then collected and filtered by passing through a 0.45 µm filter (low protein binding). Subsequently, vector prep was concentrated before being tested on HeLa cells by following the concentration protocols. Firstly, vector supernatant was concentrated by ultracentrifugation. ~ 20 mL of vector supernatant was added to six V-bottom Beckman Coulter canonical tubes (Brea, CA, USA), then tubes were placed into a JS-24.38 rotor (Beckman) and centrifuged for 140 min at 20,000 rpm (~ 72,000 x g) at 16°C in a Beckman Avanti-J-301 centrifuge. After centrifugation, supernatant was discarded and re-suspended viral pellet with 50 µL of DPBS and 0.5% BSA (~ 50x) on ice and frothing was avoided. All tubes were then incubated on ice for 30 min. each pellet was re-suspended again (~ 20x) and 50 µL of the supernatant was pooled into 7 sterile eppendorfs. Besides, 3 µL of the supernatant was stored at -80°C (Figure 8B).

A



B

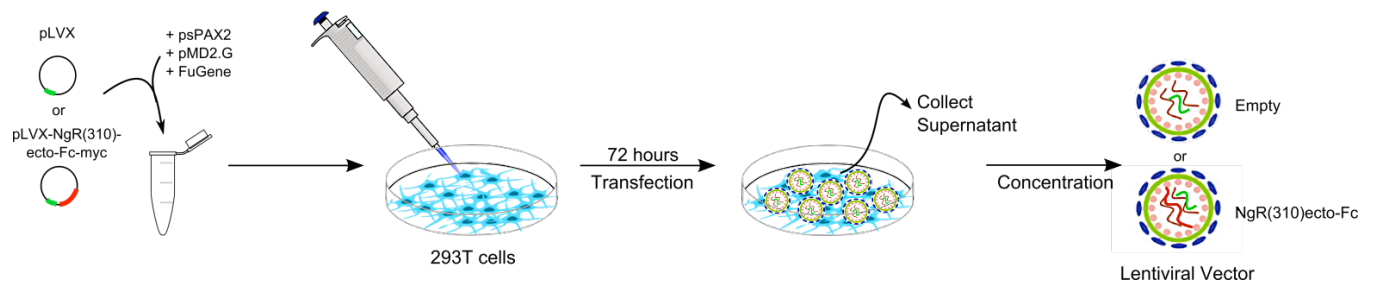


Figure 8. Lentiviral vector production. **A.** Sub-cloning of NgR1 in pLVX-EF1 α -IRES-ZsGreen1. The expression of ZsGreen is controlled by an internal ribosomal entry site (IRES). NgR(310)ecto-Fc-myc insert (1654 (bp) into pLVX-EF1 α -IRES-ZsGreen1. **B.** Production of lentiviral vectors in 293T cells.

2.12.2 Transduction of HeLa cells with LV-pLVX-EF1 α -NgR(310)-Fc-IRES-ZsGreen1

Twenty-four hours prior transduction, 1×10^5 Henrietta Lacks (HeLa) cells (epithelia cells from human) were aliquoted into 6-well plate (Corning), harvested, counted and re-suspended at 1×10^6 cells/mL. Then, 100 μ L of cell suspension was aliquoted into 6 wells of a 6-well plate and 2 mL of media was added into these wells and incubated overnight at 37°C with 5% CO₂ in a humidified atmosphere. Serial 10-fold dilutions of the viral prep were prepared and 1.8 mL of medium was added into a 24-well plate (Corning) (A2-A6). 2 mL of media and 2 μ L of vector supernatant prep were added into the A1 well. We serially diluted this medium across the plate by removing 200 μ L of diluted viral supernatant and transferred across to the adjacent well (until A5 but A6 had medium only). 4 mg/mL media (25 mL DMEM, 50 μ L protamine sulphate (4 μ g/mL)) was prepared. The supernatant of HeLa cells was aspirated and 1 mL of medium was added into each well. 1 mL of viral supernatant was added into each well and incubated for 16 hours. After 16 hours, the medium from each well was aspirated, then HeLa cells were overlaid with 2 mL fresh medium (DMEM, 10% FCS, 1% L-glutamate, 1% penicillin and streptomycin).

2.12.3 Flow cytometric analysis of transduction of HeLa cells

Medium was aspirated from each well and 1 mL detach buffer (PBS, 5 mM EDTA, 0.1% D-glucose (w/v)) was added to remove cells off plate substratum, then cells were

incubated 5-10 min at 37°C with 5% CO₂ in a humidified atmosphere. 1 mL pipettor (Gilson) was used to flush cells from the plate, then cell suspension was passed through 70 µm sieve. Cells were centrifuged for 5 min at 350 x g at 4°C. supernatant was aspirated and cell pellets were re-suspended in 1 mL FACS buffer (PBS, 1% FCS (Clontech), 0.02% sodium azide (w/v)), then 25 µL of 7AAD was added (25 µg/mL). The virus titre is given as equation below:

$$(\text{Number of cells} \times \% \text{ ZsGreen}^+) / \text{Viral Dilution}(\text{mL/mL}) \times 10^{-3}.$$

2.12.4 Isolation of bone marrow and lineage negative enrichment

Hematopoietic stem cells (HSCs) were isolated from 6-10 week old male mice (C57Bl/6), then injected with 150 mg/kg 5-FU (Sigma Aldrich, USA) and humanely killed after 3 days with CO₂. HSCs were harvested by flushing mouse tibias and femurs with FACS buffer (PBS, 2% FCS (Clontech, USA)) using a 10 mL syringe with 26 G needle. Cells were filtered through 40 µm mesh into a 50 mL centrifuge tube, and centrifuged for 5 min at 1300 rpm at 4°C, then cells were counted. Afterword, the BM cells were re-suspended at 4 x 10⁶ cells/mL of blocking buffer (PBS, 2% FCS, 1% normal rat serum). BioMag beads (Qiagen, Germany) were pre-cleaned by applying 8 mL thoroughly re-suspended beads to the magnet for min, then supernatant was removed and re-suspended in 8 mL FACS buffer (repeated 2x). Lineage antibodies (BD Bioscience, USA) were added at 1.5 µL/1 x 10⁶ cells and incubated on ice for 30 min. Cells were washed, then centrifuged at 1300 rpm for 5 min at 4°C. Cells were re-suspended with 1 mL pre-cleaned BioMag beads/20x 10⁶ cells and incubated on roller at 4°C for 45 min in

the dark. Tubes containing the cells were installed into magnet stand and incubated 5 min at room temperature, then the supernatant was collected into a new tube (repeated for 2x to remove the maximum of beads-coupled cells). Lineage-depleted (Lin^-) cells were counted and flow cytometry was performed as page 121-123, using lineage cocktail (CD3e, CD4, CD8a, CD45R/B220, CD11b, CD11c, NK1.1, TER119 and Gr-1) and SA-APC, Sca-1 (PE-Cy7-conjugated), c-Kit (PE-conjugated). Lin^- , Sca-1^+ and c-Kit^+ (LSK) cells represent a highly enriched population of HSCs.

2.12.5 Transduction of HSCs and testing in culture

One million cells were placed on 20 μg retronectin-coated 35 mm plates for transduction, then incubated for at least 2 hours at room temperature or overnight at 4°C. The supernatant was aspirated, then blocked with 2 mL 2% BSA in PBS for 30 min at room temperature. 30 multiple of infection (MOI) of concentrated virus of recombinant LV (10^8 HeLa transducing units/ml) was added into a 2 mL of the total volume of HSC medium (StemSpan Serum-Free Expansion Medium (StemCell Technologies), 1% L-glutamine, 1% penicillin and streptomycin with 1 ng/mL human IL-6, 50 ng/mL murine SCF, 5 ng/mL mouse IL-3, and 50 ng/mL human Flt kinase 3 ligand). The plates were spun for 2 hours at 1200 x g at 32°C. The supernatant was aspirated and 1.5×10^6 lin^- cells was added into 2 mL HSC medium to the plates, the plates were then spun for 1 hour at 1200 rpm at 32°C. 1 mL media was added and incubated for 72 hours at 37 °C with 5% CO_2 in a humidified atmosphere. The ability for the overexpressed NgR1-Fc protein to functionally block Nogo-A was tested in culture by FACS before the

transplantation of LV-transduced HSCs, using a vector containing enhanced green fluorescent protein (eGFP) alone as control, or NgR1-Fc and eGFP construct, and the efficacy demonstrated in mouse dorsal root ganglia (DRG, day 7 postnatal) neurons in culture with MAIF substrates. Specifically, we used bovine CNS myelin substrate to assess the ability of the cells to increase neurite outgrowth of these DRG neurons. NgR1-Fc purity was evaluated by SDS-PAGE and NgR(310)ecto-Fc binding directly to AP-Nogo-66 by ELISA.

2.12.6 Transplantation of LV transduced HSCs in EAE

We were recently able to successfully transplant eGFP-expressing HSCs into mice following their immunisation with MOG₃₅₋₅₅, to induce EAE. We found that many of these cells were localised to the spinal cord specifically within inflammatory lesions. The next step was to inject LV- (include NgR1-Fc and eGFP) or control empty-vector transduced male HSCs (10^6 cells/mouse) into the tail vein of 8-12 week old irradiated mice. We performed three different transplantation; in the first transplant, *ngR1*^{+/+} female mice were transplanted with *lin*⁻ enriched *ngR1*^{+/+} BM cells either transduced with empty or NgR(310)ecto-Fc vectors or non-transduced. To prepare for transplantation, the mice were irradiated with 950 cGy caesium source gamma irradiation to ablate their endogenous BM. Then, the mice were intravenously injected with 2.5×10^5 sorted cells in 200 μ L PBS containing 2% FBS (v/v) after 3 hours period of recovery. In the second transplant, *ngR1*^{+/+} female mice were transplanted with *lin*⁻ enriched *ngR1*^{-/-} BM transduced with empty LV vector. The mice were then irradiated with (2x 550 cGy in 2

administrations). Following 3 hours recovery, the mice were intravenously injected with 1.0×10^6 unsorted cells in 200 μ L PBS containing 2% FBS (v/v). The third transplant was performed as the second one but *ngr1*^{+/+} female mice were transplanted with lin⁻ enriched *ngr1*^{+/+} BM transduced with empty or NgR(310)ecto-Fc vectors.

Post-transplantation, all mice were monitored daily and the engraftment was monitored by sub-mandibular blood sample after 4 and 8 weeks. The blood samples were analysed by flow cytometry, as page 121-123. Then, we induced EAE in mice, using either MOG₃₅₋₅₅ or adjuvant alone, as a control (Section 2.3). After scoring, they were killed at 2, 4, and 8 weeks after EAE induction, and their spinal cords, optic nerves and spleens were collected for protein analysis, immunohistochemistry and flow cytometry. Chimerism levels in the peripheral circulation were assessed using flow cytometry, analysing the number of positive cells in the blood (e.g. B220-positive, CD3-positive, CD11c-positive, myc-positive and eGFP-positive cells). We used same antibodies along with anti-Iba antibody (macrophage/microglial marker) to stain both paraffin and frozen sections. Using fluorescent in situ hybridisation (FISH) analysis will be an essential tool to determine the HSC transplantation efficiency in female recipient mice from male donors, by detecting *in vivo* the Y-chromosomes of donor HSCs, as a backup to eGFP tracking. This will be performed in spinal cord sections from female recipient mice hybridized with the FITC-labelled DNA probe in next transplantation cohort.

2.13 Statistics

Data were analysed was performed using Prism 6 (Graph Pad Software). Clinical progression data are presented as mean \pm standard error of the mean (SEM). One-way ANOVA and a one-tailed student's t-test were used to compare the percentage of CNS-infiltrating immune cells between *ngr1*^{-/-} and *ngr1*^{+/+} mice. Two-way ANOVA was used to analyse repeated measures (for all EAE scores). A $p < 0.05$ was considered as statistically significant.

**CHAPTER 3: NgR expression on immune cells during CNS
inflammation**

3.1 Introduction

Our laboratory has recently demonstrated that mice bred to retain the gene deletion in NgR1 are protected against severe clinicopathological manifestations of EAE exhibited in wild-type C57Bl/6 mice induced by MOG₃₅₋₅₅ (Petratos et al., 2012). These data were further supported with signal transduction evidence to show that NgR1 may ultimately potentiate neurodegeneration in EAE via a direct neurobiological mechanism. Despite clear evidence demonstrating that the deletion of NgR1 can protect against axonal degeneration and thus progression of EAE, an immunological role for this receptor is yet to yield mechanistic evidence (McDonald et al., 2011). Importantly, it has recently been identified by Pool *et al.* (2009) that NgR1 can be expressed on circulating immune cells from MS patients and may be involved in the induction of pro-inflammatory cytokines, demonstrating that an alternate signalling mechanism may be at play driving neuroinflammation (Pool et al., 2009). Therefore, this thesis investigates the immunological mechanisms in EAE by cellular phenotyping to partially identify the role of NgR in particular during B-cell maturation and differentiation, along with the identification of follicle-like structures localised in the CNS during inflammation.

3.2 Results of EAE induced with MOG₃₅₋₅₅

3.2.1 *ngr1*^{-/-} does alter the clinical course of MOG₃₅₋₅₅ EAE

In order to assess a potential role of NgR1 in the development of the inflammatory response in the CNS, EAE was induced by immunisation with MOG₃₅₋₅₅ peptide in both *ngr1*^{+/+} and NgR1 deficient (*ngr1*^{-/-}) mice. There are several steps to understanding the effect of NgR1 on the development of EAE; firstly we compared EAE development and severity in *ngr1*^{+/+} and *ngr1*^{-/-} mice. Figure 9 showed a significant delay in the onset of disease in the NgR1 deficient mice compared to the *ngr1*^{+/+} mice (p<0.0001). The disease's clinical manifestations in these mice were determined by daily scoring. Furthermore, There was a significant difference between *ngr1*^{+/+} and *ngr1*^{-/-} mice when analysed with respect to mean day of disease onset (*ngr1*^{+/+} day 13.9±0.3 vs *ngr1*^{-/-} day 16.4±0.7; n=60-99) or maximum clinical score (*ngr1*^{+/+} 2.4±0.1 vs *ngr1*^{-/-} 2.3±0.1), as shown in Table 5.

Table 5. Effect of deleting the *ngr1* gene on clinical course of MOG₃₅₋₅₅ EAE.

	<i>ngr1</i> ^{+/+}	<i>ngr1</i> ^{-/-}
Incidence	76/99	32/60
Mean day of onset of diseased mice only	13.9±0.3	16.4±0.7
Maximum score	2.4±0.1	2.3±0.1
Mean score	1±0.1	0.6±0.1
Median score	1.0	0.4
Mortality rate	0/99	0/60

Disease parameters of clinical course of EAE in *ngr1*^{-/-} and *ngr1*^{+/+} mice as shown in Figure 9. Data represent mean ± SEM and medians.

Clinical scores of MOG35-55 EAE immunised female *ngr1*^{+/+} and *ngr1*^{-/-}

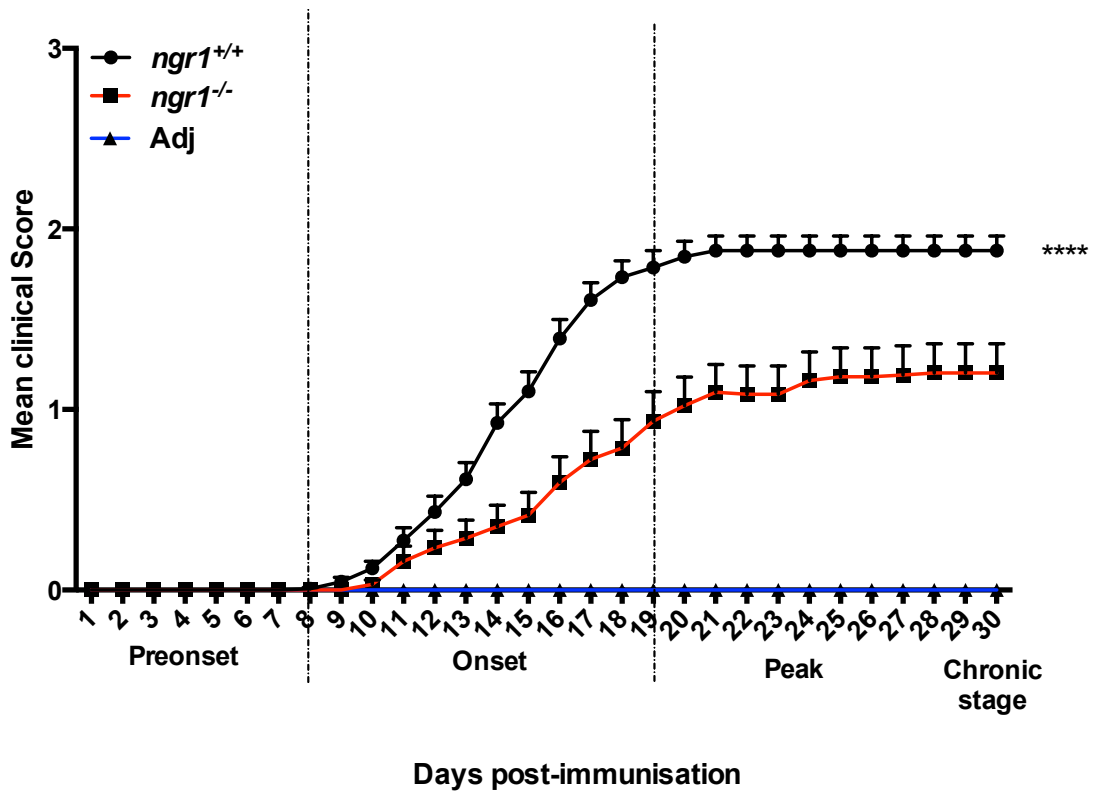


Figure 9. Significant delay in EAE onset and reduce in severity for the *ngr1*^{-/-} mice.

EAE was induced with MOG₃₅₋₅₅ peptide consistent with disease stages; pre-onset (score 0; day 7 after injection), onset (score 1; day 12 after injection), peak (score 2; day 18 after injection) and chronic (score 3; day 30 after injection) in *ngr1*^{+/+} C57Bl/6 mice (circles, n=99), *ngr1*^{-/-} mice (n=60, squares) and adjuvant-injected-only (control) group (n=10, triangle). Their disease clinical manifestations were determined by daily scoring. The severity of MOG₃₅₋₅₅ peptide-induced EAE reduced in *ngr1*^{-/-} mice in comparison to *ngr1*^{+/+} mice. Clinical scores represent mean \pm SEM of diseased mice, **** p<0.0001, two-way ANOVA.

3.2.2 EAE Histopathology in the *ngr1*^{+/+} and *ngr1*^{-/-} mice

Blind histopathological examination was performed with Luxol fast blue and periodic acid-Schiff (LFB/PAS) and Bielschowsky stained spinal cord sections of *ngr1*^{+/+} and *ngr1*^{-/-} mice with different clinical score of the diseases, in order to demonstrate the demyelination and axonal injury, respectively in EAE-induced mice. Figure 10A and 2B illustrated a significantly reduced demyelination in *ngr1*^{-/-} mice at disease onset and significantly decreased axonal damage at the chronic stage of disease, in comparison to *ngr1*^{+/+} mice.

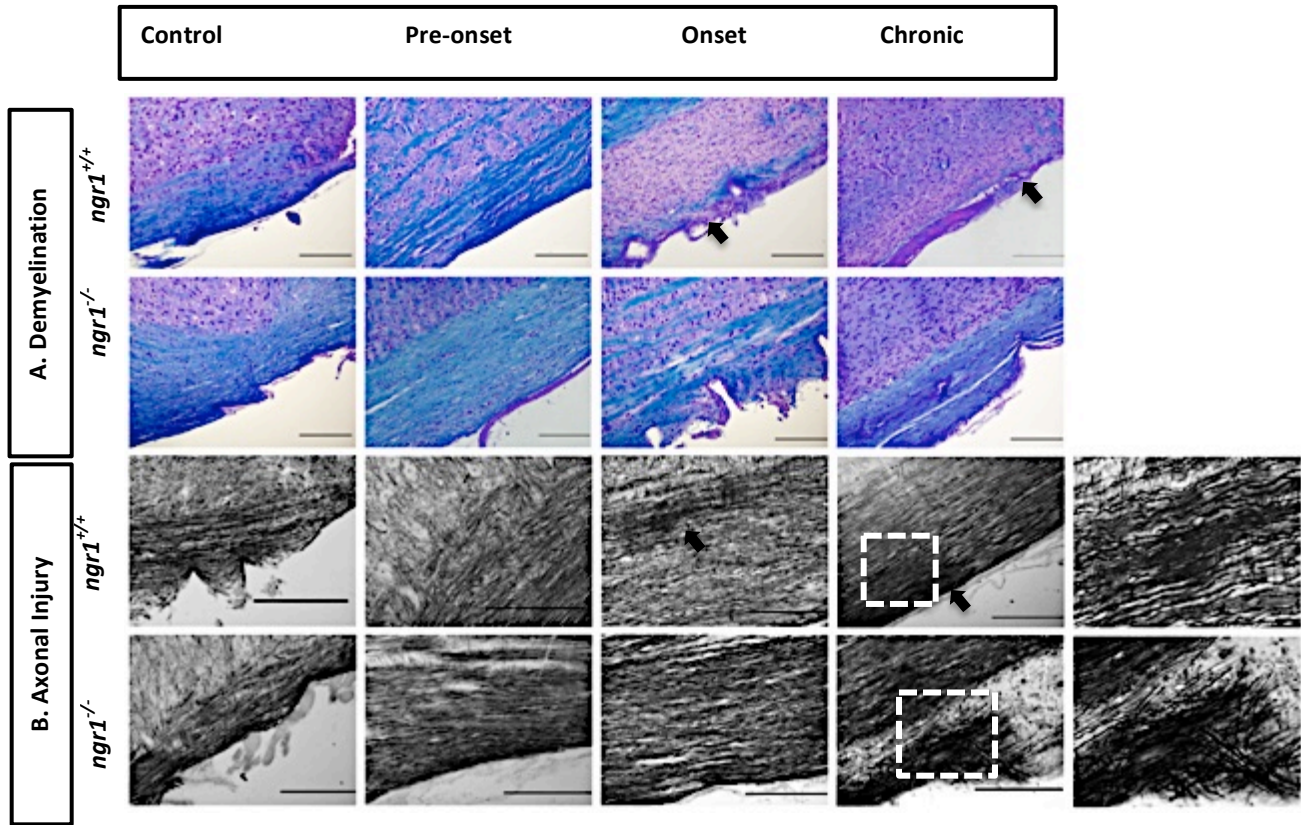


Figure 10. The severity of demyelination and axonal injury reduced in the spinal cord of *ngr1*^{-/-} EAE mice. **A.** Luxol fast blue (LFB)/Periodic acid Schiff (PAS) stained lumbar-thoracic spinal cord sections of *ngr1*^{+/+} and *ngr1*^{-/-} EAE mice for demyelination (magnification 20x, scale bar = 200 μm). **B.** Representative spinal cord sections stained with Bielschowsky for axonal injury (scale bar = 500 μm). Histological analysis was performed at different clinical score of the diseases.

3.2.3 Isolation of immune cells from spleen, lymph node and spinal cord of *ngr1*^{+/+} and *ngr1*^{-/-} mice following EAE induction with MOG₃₅₋₅₅

NgR1 was shown to be expressed on circulating immune cells in MS patients and may be involved in the induction of pro-inflammatory cytokines, demonstrating that an alternate signalling mechanism may be at play in driving neuroinflammation (Pool et al., 2009). Therefore, we next investigated the immunological mechanisms in EAE by cellular phenotyping in order to partially identify the role of NgR specifically in regulating B-cell maturation and differentiation, within follicle-like structures localised in the CNS during inflammation. There were several markers used to define each population of cells: B220 for B-cells, CD3 for T-cells and CD11c for dendritic cells. The percentages of all of these immune cells in the spleen, lymph nodes and spinal cord of *ngr1*^{+/+} and *ngr1*^{-/-} mice following EAE induction, as well as in the un-injected controls, and adjuvant-injected-only (control) group, are shown in Figure 11. In the spleen, B-cell populations made up around 40% of the total in the controls and during the disease progression in *ngr1*^{+/+} mice, however, they were significantly decreased at the onset in *ngr1*^{-/-} mice (Figure 11). In addition, T-cells were increased during the chronic phase of the disease in *ngr1*^{+/+} and *ngr1*^{-/-} mice due to immunisation with MOG. T helper 1 (T_{h1}) cells are well documented to help cellular immunity and are capable of producing pro-inflammatory responses during the active disease phase of EAE (Martinez et al., 2012). However, dendritic cells (DCs) declined significantly at clinical score 3 in *ngr1*^{+/+} mice and they were approximately similar in the percentages during disease progression in the NgR1 deficient mice (Figure 11). Indeed, B-cells may play a role as antigen-presenting cells

(APCs) in disease development by presenting antigens along with DCs during EAE pathogenesis. Mature DCs in secondary lymphoid organs are known to stimulate T-cell proliferation and differentiation by cytokine secretion and direct cell-cell interactions, initiating the immune response (Guermontprez, 2002).

In the lymph nodes of *ngr1*^{+/+} mice, the cells expressing B220 made up around 30% of the cells in the control mice, and these cells were then elevated significantly at clinical score 1 (Figure 11). This may be because of the ability of B-cells to expand in the lymph node and potentiate differentiation at clinical score 1. However, the cells expressing either B220, CD3e or CD11c dropped significantly in the lymph node during clinical score 3 (Figure 11). The finding demonstrated for lymph nodes highlights the ability of these cells to egress out of the secondary lymphoid organs, and infiltrate into the CNS, with autoaggressive lymphocytes initiating inflammation, demyelination, axonal damage and eventually profound neurodegeneration. This may correlate with a key feature of MS pathology thought to be an activator of autoimmune cells in the periphery (Dev, 2008, Chun, 2010). There was no statistical difference in the percentages of DCs, B-cells and T-cells from lymph nodes between the adjuvant injected or naïve control and clinical score 0 in the EAE-induced *ngr1*^{-/-} mice. However, B-cells along with T-cells increased significantly at disease onset in *ngr1*^{-/-} mice at the induction of EAE (Figure 11).

We next identified the percentage of immune cells in the spinal cord of *ngr1*^{+/+} mice, the B-cells and DCs that were activated during disease onset and the chronic phase, shown in

Figure 11. This is consistent with the study of McMahon *et al.* (2005) that demonstrated the important role of DCs during EAE in the late effector phase; such cells are reported to participate in epitope-spreading in the relapsing-remitting forms of EAE within the CNS (Figure 11) (McMahon, 2005). In the *ngr1*^{-/-} mice, the percentage of B-cells remained constant in the spinal cord during the disease progression, but T-cell populations and DCs increased significantly at the disease onset, and DCs were again elevated at clinical score 3 (Figure 11).

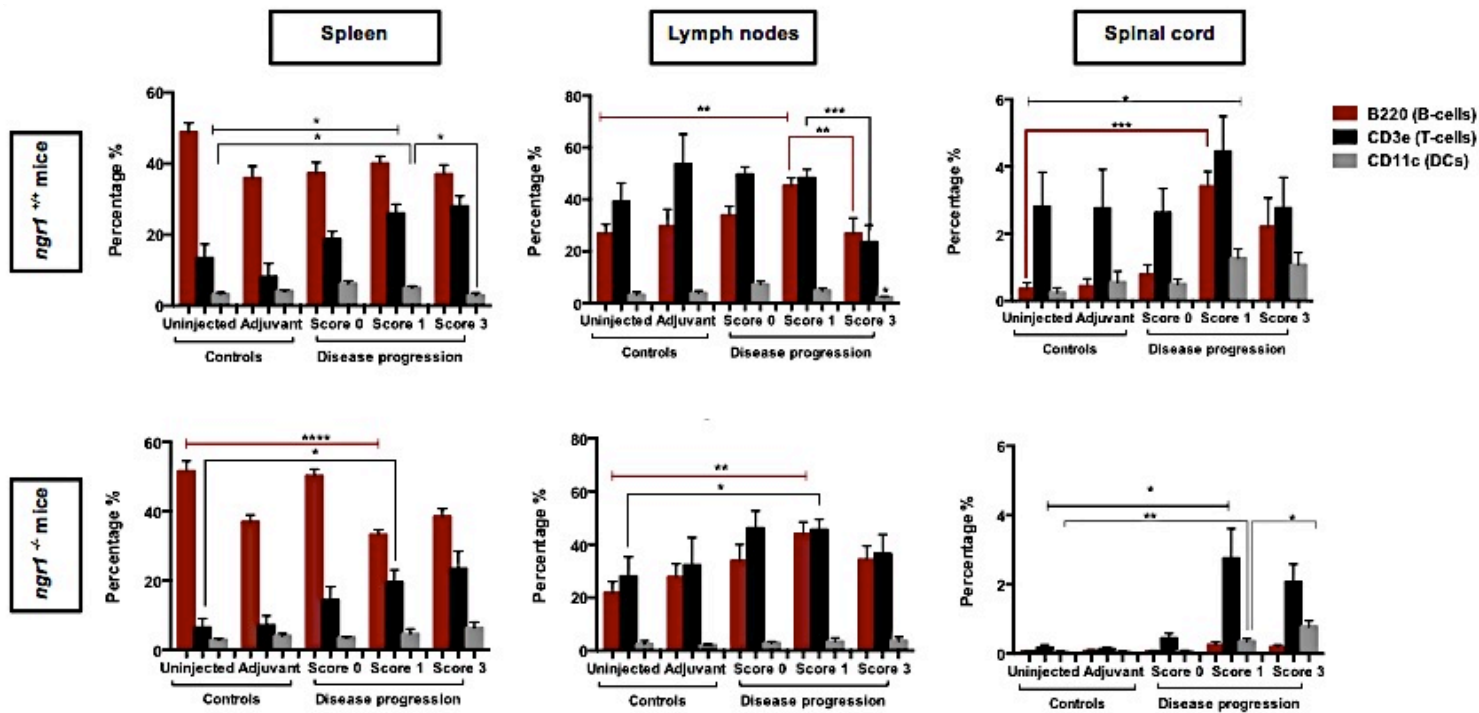


Figure 11. Flow cytometric analysis of single cell suspension from the spleen, lymph nodes and spinal cord of EAE-induced mice with MOG35-55 comparing to naive *ngr1*^{+/+} and *ngr1*^{-/-} mice, and adjuvant control. Percentage of B220+B-cells, CD3+ T-cells, and CD11+ dendritic cells are illustrated. Results represent mean \pm SEM, * P<0.05, ** P<0.01, * P<0.001, **** p<0.0001, performed by multiple t-tests.**

To determine the expression profile of NgR1 and its homologues in the various immune cell phenotypes during the progression of EAE, double staining was performed on isolated cells from the spleen, lymph nodes and spinal cord. These data show for the first time the double-staining of immune cells and NgR homologues during the propagation of the disease. In the spleen of *ngr1^{+/+}* and *ngr1^{-/-}* mice, B-cells, T-cells, and DCs with NgR and NgR3 increased with the disease progression (Figure 12), illustrating that these cells stay in the spleen to perform their physiological role of immune expression during acute phase. Figure 12 showed, the double-positive labelling of immune cell lineages and NgR in the spleen of *ngr1^{-/-}* mice; surprisingly B220 cells co-expressing NgR accounted for around 4% of the double-positive cells observed in the control mice and at disease pre-onset, then increased significantly with disease progression (to around 7%). These data suggest that the anti-NgR antibody can bind to and detect the other NgR homologues (NgR2 and NgR3) that may aid in signalling but are not as effective as NgR1, through alternate ligands (Steinbach et al., 2011). Therefore, specific antibodies for NgR2 and NgR3 were used in addition to their isotypes and secondary antibodies alone as negative controls. However, their affinities are different as anti-NgR2 and anti-NgR3 antibodies are polyclonal antibodies but anti-NgR antibody is monoclonal.

Double-positive labelling of T-cells expressing NgR2 decreased significantly at the chronic stage of the disease in the lymph nodes of the *ngr1^{+/+}* mice (Figure 13). The percentage of T-cells expressing NgR3 also decreased at clinical score 3 in *ngr1^{+/+}* and *ngr1^{-/-}* mice. However, in *ngr1^{-/-}* mice, B-cells expressing NgR (detecting NgR2 and NgR3 homologues) increased significantly during disease progression (Figure 13).

Furthermore, there was a significant increase of T-cells positive for NgR3 at clinical score 1, which then decreased significantly at clinical score 3 (Figure 13). B-cells positive for NgR3 also declined at clinical score 3 in *ngr1^{-/-}* mice. These data indicates that in the absence of NgR1, NgR2 and NgR3 homologues may compensate in these immune lineages during the disease propagation and may be targeted to limit EAE progression. However, breakouts of NgR1 and NgR2 had an effect in DC maturation that is important for myelin adhesion and axon damage when are not expressed (McDonald et al., 2011, Steinbach et al., 2011).

Interestingly, the B-cell populations positive for NgR1 in the spinal cord of the *ngr1^{+/+}* mice were elevated sharply at disease onset and did not increase in *ngr1^{-/-}* mice (less than 0.5%) (Figure 14). Thus, knocking out the NgR1 gene in mice results in no change in the infiltration of B-cells during disease progression; this may emphasise the role of NgR1 as a signalling molecule in regulating B-cells during EAE induction. Correspondingly, there was a similar dramatic increase in B-cells expressing NgR3 at clinical score 1 in *ngr1^{+/+}* and *ngr1^{-/-}* mice, raising the question as to whether there exists an association between NgR1 and NgR3 for the signal transduction through MAIFs, (or alternate ligands). In addition, the percentage of T-cells expressing NgR2 also increased with the progression of the disease at clinical score 1 in the *ngr1^{+/+}* and the *ngr1^{-/-}* mice (Figure 14). Moreover, there was a significant elevation of T-cell positive for NgR3 at clinical score 1 in *ngr1^{-/-}* mice, which then decreased significantly at clinical score 3 (Figure 14). On the basis of these findings, further investigations are now required in order to elucidate the roles of NgR2 or NgR3 in T-cells during EAE. These data indicate that there is an

inducible expression of NgR1 along with NgR3 in specific immune lineage cells upon the induction of EAE, and thus both of these receptors may influence these cells' migratory behaviour in the CNS.

Spleen
Double staining of immune cells with NgR, NgR2 or NgR3

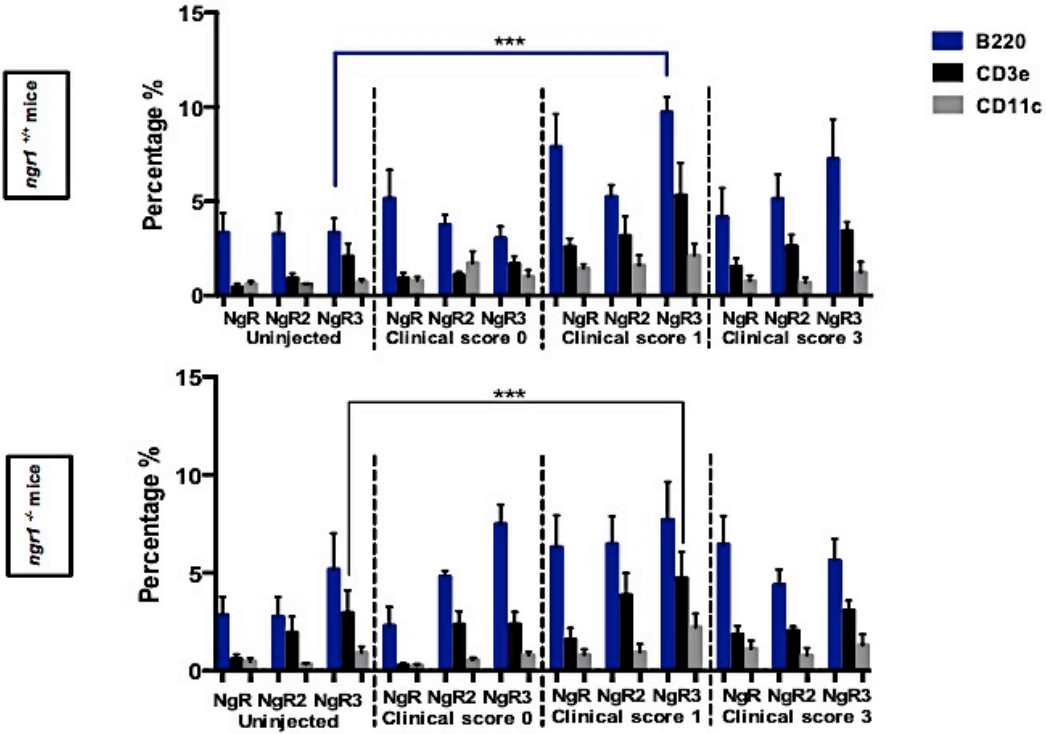


Figure 12 Immune lineage cells that were immune-positive for NgR in the spleen, of *ngr1*^{+/+} and *ngr1*^{-/-} mice during the induction and course of EAE. B-cells, with NgR3 increased significantly in *ngr1*^{+/+} mice at the disease progression and there was a significant increase of T-cell positive for NgR in *ngr1*^{-/-} mice. Results represent mean ± SEM, *** P<0.001, performed by multiple t-tests.

Lymph nodes
Double staining of immune cells with NgR, NgR2 or NgR3

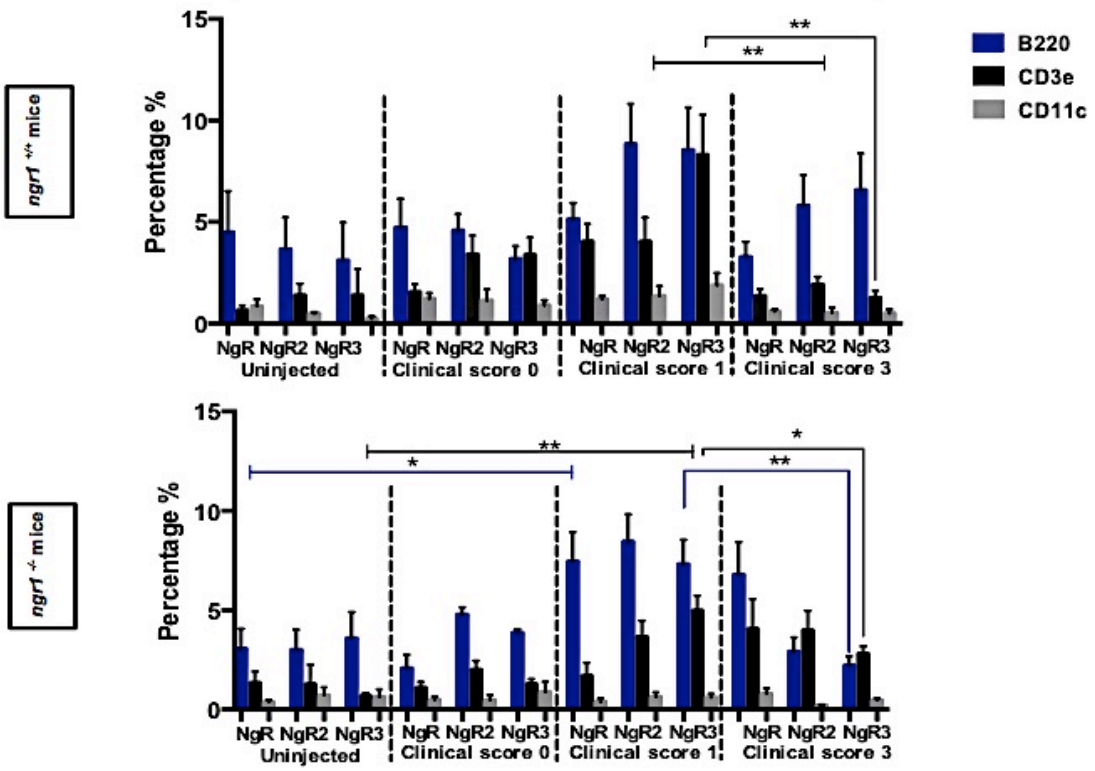
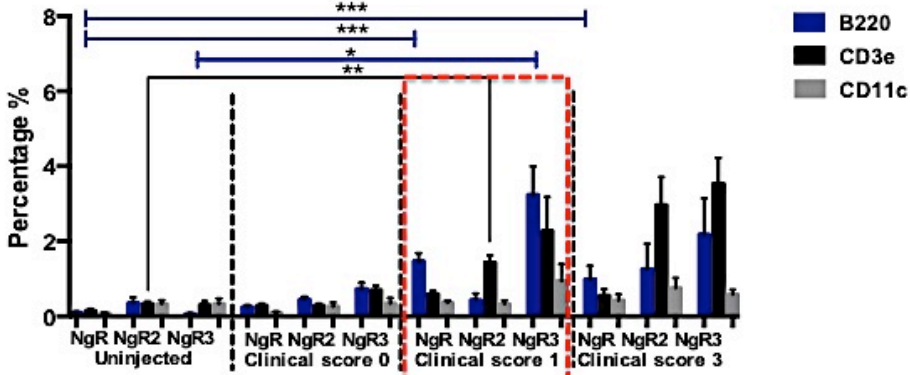


Figure 13. Flow cytometric analysis of double-cell suspension from the lymph nodes of *ngr1*^{+/+} and *ngr1*^{-/-} mice. Double-positive labelling of T-cells and NgR2 decreased significantly at the chronic stage of the disease in *ngr1*^{+/+} mice and T-cells expressing NgR3 also decreased at clinical score 3 of *ngr1*^{-/-} mice. Results represent mean \pm SEM, * P<0.05, ** P<0.01, performed by multiple t-tests.

Spinal cord
Double staining of immune cells with NgR, NgR2 or NgR3

ngr1^{+/+} mice



ngr1^{-/-} mice

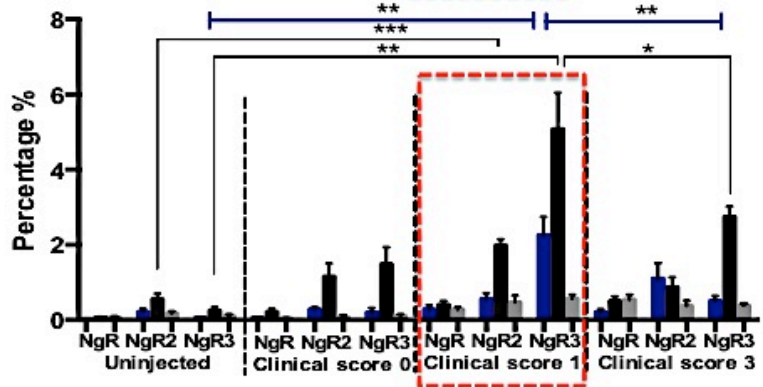


Figure 14. Double-staining of immune cells with NgR from the spinal cord of *ngr1*^{+/+} and *ngr1*^{-/-} mice. In spinal cord of *ngr1*^{-/-} mice, there were no expressions of NgR on B-cells comparing to *ngr1*^{+/+} mice, although these immune cells were within spinal cord of NgR3 *ngr1*^{-/-} mice. The B-cell populations positive for NgR1 in the spinal cord of the *ngr1*^{+/+} mice were elevated sharply at disease onset and did not increase in *ngr1*^{-/-} mice (less than 0.5%). Results represent mean \pm SEM, * P<0.05, ** P<0.01, *** P<0.001, performed by multiple t-tests.

3.3 Results of EAE induced with rMOG immunisation.

3.3.1 *ngr1*^{-/-} mice do not display an altered clinical course during rMOG-induced EAE

We next considered whether using rMOG to induce EAE may influence the development of the disease in both *ngr1*^{+/+} and *ngr1*^{-/-} mice due to the nature of the antigen processing being different to the MOG₃₅₋₅₅ peptide (Weber et al., 2010, Bettadapura et al., 1998, Payne et al., 2012). rMOG consists of the full-length protein and requires intracellular processing for its encephalitogenic activity (Weber et al., 2010, Bettadapura et al., 1998), thus potentiating a strong response of B-cell dependency. Figure 15 showed a significant delay in EAE onset and reduced severity in the *ngr1*^{-/-} mice ($p < 0.0001$). EAE was induced with the rMOG peptide consistent with the disease stages, and the mice were scored daily for clinical manifestations of the disease. These results were similar to those for mice that were induced with MOG₃₅₋₅₅ at the disease onset and peak phase but not at the chronic stage in the *ngr1*^{-/-} mice, again suggesting that NgR1 may not play a role in B-cells at the chronic stage of disease. In addition, the mean day of the disease onset was (14.3 ± 0.6 for *ngr1*^{+/+} day vs. 21.1 ± 1.8 for *ngr1*^{-/-} day; $n = 12-22$) and maximum clinical score was (2.8 ± 0.2 for *ngr1*^{+/+} mice vs. 2.1 ± 0.2 for *ngr1*^{-/-} mice), as shown in Table 6.

Table 6. Effect of deleting the *ngr1* gene on clinical course of rMOG EAE.

	<i>ngr1</i> ^{+/+}	<i>ngr1</i> ^{-/-}
Incidence	21/22	10/12
Mean day of onset of diseased mice only	14.3±0.6	21.1±1.8
Maximum score	2.8±0.2	2.1±0.2
Mean score	1.2±0.2	0.5±0.2
Median score	1.5	0.3
Mortality rate	1/22	1/12

Disease parameters of clinical course of EAE in *ngr1*^{-/-} and *ngr1*^{+/+} mice as shown in Figure 15. Data represent mean ± SEM and medians.

Clinical scores of rMOG EAE immunised female *ngr1*^{+/+} and *ngr1*^{-/-}

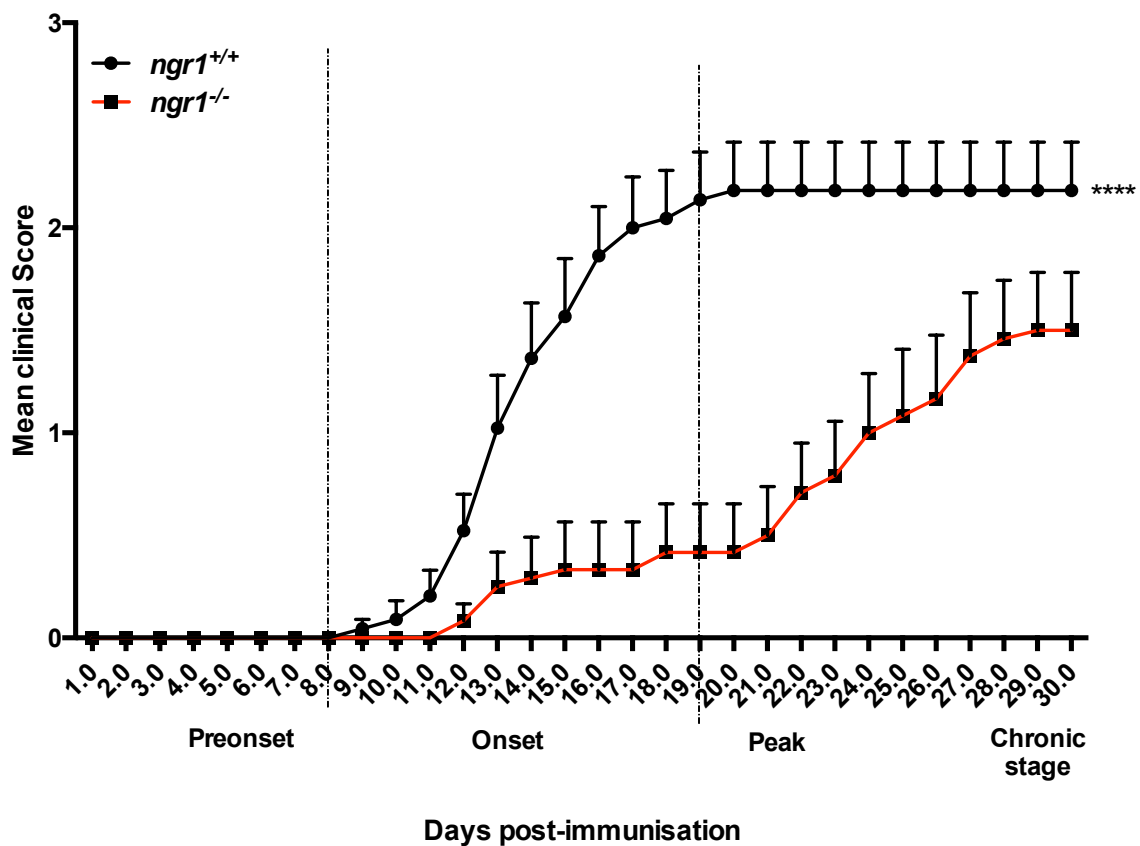


Figure 15. Significant delay in EAE onset and reduce in severity for the *ngr1*^{-/-} mice.

EAE was induced with rMOG peptide consistent with disease stages; pre-onset (score 0; day 7 after injection), onset (score 1; day 12 after injection), peak (score 2; day 18 after injection) and chronic (score 3; day 30 after injection) in *ngr1*^{+/+} C57Bl/6 mice (circles, n=22) and *ngr1*^{-/-} mice (n=12, squares). Their disease clinical manifestations were determined by daily scoring. The severity of rMOG peptide EAE reduced in *ngr1*^{-/-} mice in comparison to *ngr1*^{+/+} mice. Clinical scores represent mean \pm SEM of diseased mice, **** p<0.0001, two-way ANOVA.

3.3.2 Isolation of immune cells from spleen, lymph node and the spinal cord of *ngr1*^{+/+} and *ngr1*^{-/-} mice following EAE induction with rMOG

Next, we examined the subset of immune cells present in the spleen, lymph nodes and spinal cord harvested from *ngr1*^{+/+} and *ngr1*^{-/-} mice, at various clinical scores (1, 2, 3), compared to un-injected (naïve) controls (Figure 16). In the spleen, B-cells decreased significantly at the chronic stage in the *ngr1*^{+/+} mice, compared to the un-injected controls. Furthermore, T-cells increased significantly at clinical score 1 in both *ngr1*^{+/+} and *ngr1*^{-/-} mice; however, T- and B-cells decreased significantly at the chronic stage of the disease in *ngr1*^{+/+} mice (Figure 16). In the spleens of *ngr1*^{-/-} mice, B-cells decreased significantly at clinical score 1. In the lymph nodes, there was a significant increase of B-cells at the onset phase (clinical score 1) in both *ngr1*^{+/+} and *ngr1*^{-/-} mice, as shown in Figure 16. There were no significant differences in any of the immune cells in the spinal cord of *ngr1*^{+/+} mice; however, DCs increased significantly at the disease onset and the chronic stage in *ngr1*^{-/-} mice (Figure 16). These results were similar to what we observed in mice that were immunised with MOG₃₅₋₅₅, although given differences in the pathogenesis of EAE induced by the encephalitogenic MOG₃₅₋₅₅ peptide against rMOG-induced EAE (Weber et al., 2010, Bettadapura et al., 1998).

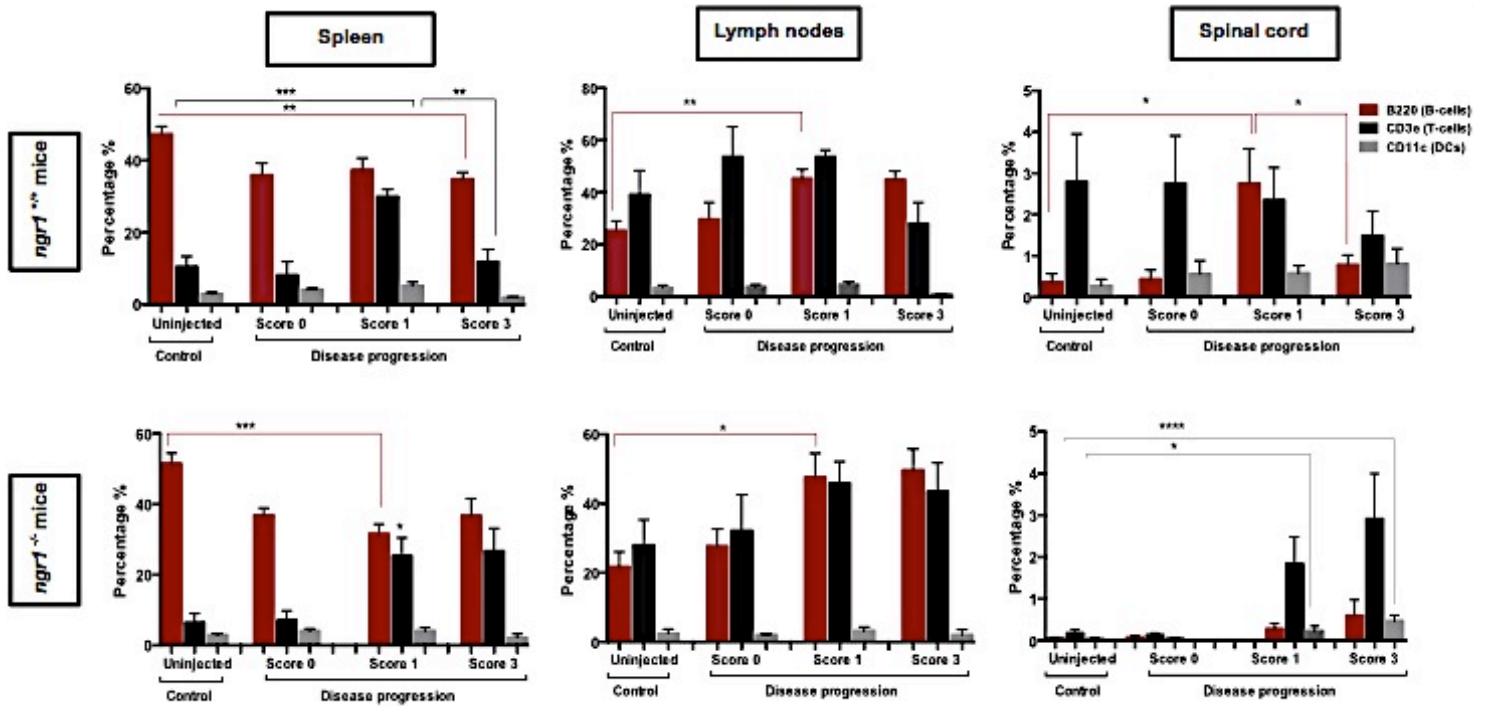
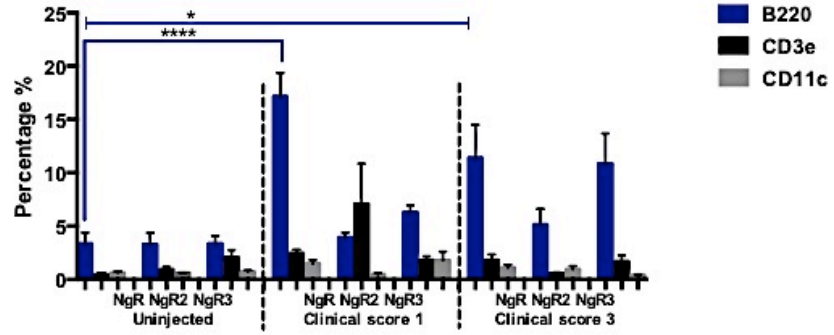


Figure 16. Flow cytometric analysis of single cell suspension from the spleen, lymph nodes and spinal cord of EAE-induced mice with rMOG comparing to naïve *ngr1*^{+/+} and *ngr1*^{-/-} mice. Percentage of B220+B-cells, CD3+ T-cells, and CD11+ dendritic cells are illustrated. Results represent mean \pm SEM, * P<0.05, ** P<0.01, *** P<0.001, **** p<0.0001, performed by multiple t-tests.

Double-positive labelling of isolated cells from various lymphoid organs was performed in order to determine the expression profile of NgR1 and its homologues during the progression of EAE (as performed during MOG₃₅₋₅₅ induced EAE), immunised with rMOG. In the spleen, B-cells expressing NgR increased significantly at clinical score 1 in the *ngr1*^{+/+} and *ngr1*^{-/-} mice (Figure 17). Comparably, there was a significant increase of B-cells positive for NgR in the lymph nodes of the *ngr1*^{+/+} and *ngr1*^{-/-} mice (Figure 18). Crucially, the B-cells expressing NgR1 in the spinal cord of *ngr1*^{+/+} mice were elevated sharply at the disease onset (about 2 fold) and about 0.5% in the *ngr1*^{-/-} mice (Figure 19), these results were coincide with our earlier finding in this chapter 3 in MOG₃₅₋₅₅-induced EAE. Furthermore, B-cells positive for NgR3 were elevated significantly in the spinal cord of the *ngr1*^{+/+} and *ngr1*^{-/-} mice, as shown in Figure 19. Taken together, these results demonstrated that both MOG₃₅₋₅₅- and rMOG-induced EAE have the same influence on the leukocyte subsets, which express NgR1 and its homologues, in the spleen, lymph nodes and spinal cord, while Weber *et al.* (2010) demonstrated that B-cells can play a role as sophisticated and highly selective antigen-presenting cells that promote the differentiation of pro-inflammatory T_{h1}- and T_{h17}- cells in EAE-induced by rMOG.

Spleen
Double staining of immune cells with NgR, NgR2 or NgR3

ngR1^{+/+} mice



ngR1^{-/-} mice

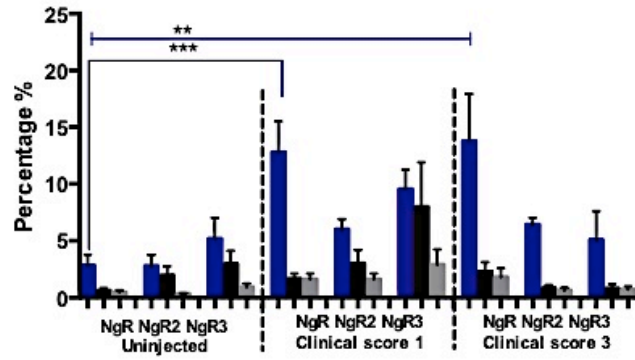
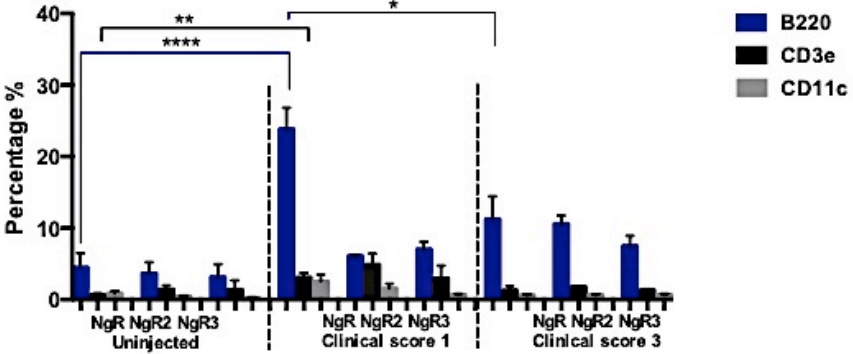


Figure 17. Immune lineage cells that were immunopositive for NgR in the spleen, of *ngr1^{+/+}* and *ngr1^{-/-}* mice during the induction and course of EAE. B-cells expressing NgR increased significantly with the disease progression at clinical score 1 in the *ngr1^{+/+}* and *ngr1^{-/-}* mice. Results represent mean \pm SEM, * P<0.05, ** P<0.01, *** P<0.001, **** p<0.0001, performed by multiple t-tests.

Lymph nodes
Double staining of immune cells with NgR, NgR2 or NgR3

ngR1^{+/+} mice



ngR1^{-/-} mice

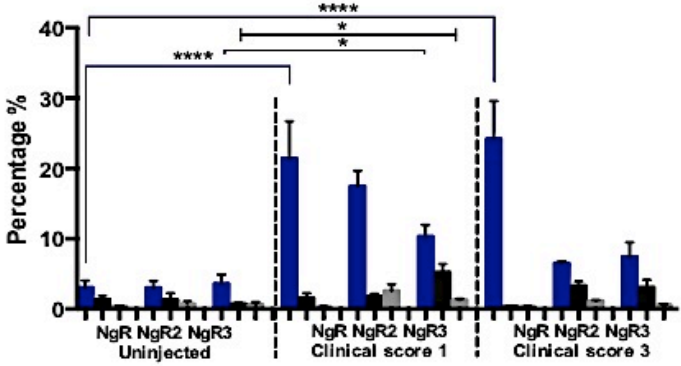


Figure 18. Flow cytometric analysis of double-cell suspension from the lymph nodes of *ngr1*^{+/+} and *ngr1*^{-/-} mice. There was a significant increase of B-cells positive for NgR in the *ngr1*^{+/+} and *ngr1*^{-/-} mice. Results represent mean \pm SEM, * P<0.05, ** P<0.01, performed by multiple t-tests.

Spinal cord
Double staining of immune cells with NgR, NgR2 or NgR3

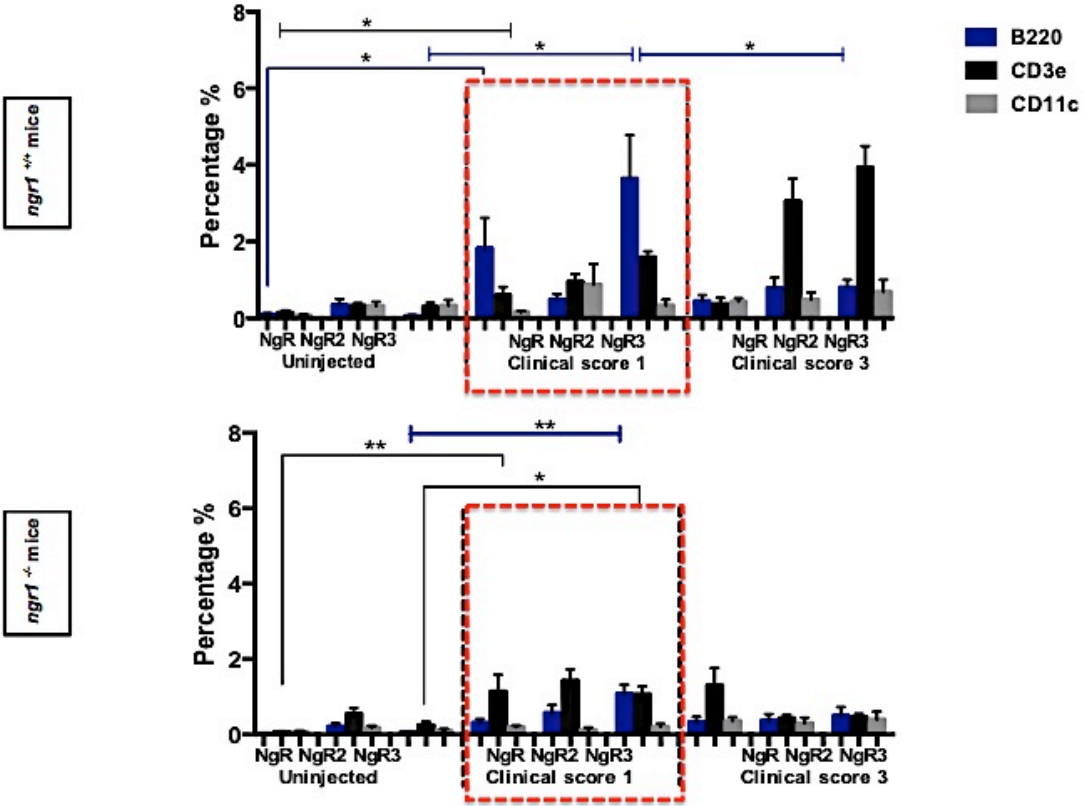


Figure 19. Double-staining of immune cells with NgR from the spinal cord of *ngr1*^{+/+} and *ngr1*^{-/-} mice. In spinal cord of *ngr1*^{-/-} mice, the B-cells expressing NgR1 in the spinal cord of *ngr1*^{+/+} mice were elevated sharply at the disease onset (about 2-fold) and about 0.5% in *ngr1*^{-/-} mice. B-cells positive for NgR3 raised significantly in the spinal cord of the *ngr1*^{+/+} and *ngr1*^{-/-} mice. Results represent mean \pm SEM, * P<0.05, ** P<0.01, * P<0.001, performed by multiple t-tests.**

3.4 Preparation of tissue lysates for western blotting to identify NgR homologues in spleen, lymph nodes and spinal cord of *ngr1*^{+/+} and *ngr1*^{-/-} mice

In order to identify the NgR homologues in spleen, lymph nodes and spinal cord, samples were ground and lysed from both naïve *ngr1*^{+/+} and *ngr1*^{-/-} mice (n=5 mice/group), as well as from EAE mice, as shown in Figure 20. The specificity of the polyclonal NgR antibody was tested using NgR-Fc peptide to block the NgR activity as a control. There were no immunoreactive bands detected for both naïve *ngr1*^{+/+} and *ngr1*^{-/-} mice in the spleen and lymph nodes when we probed with NgR, secondary alone antibodies or following the pre-absorption of the anti-NgR antibodies with the NgR-Fc peptide added in excess (Figure 20). This data demonstrates the specificity of anti-NgR antibody, that can not be detected in naïve mice. In addition, there was expression of NgR2 and NgR3 in the spleen of both naïve *ngr1*^{+/+} and *ngr1*^{-/-} mice (Figure 21A). Furthermore, there was expression of NgR2 and NgR3 in the spinal cord of *ngr1*^{+/+} and *ngr1*^{-/-} mice at different clinical scores (Figure 21B), suggesting that NgR1 and its homologues bound directly to the spinal cord lysate that actively play a role in the disease progression. Thus, further analysis, such as liquid chromatography mass spectrometry, is required to confirm which homologue of NgR was expressed in immune cells.

W.Blot: anti-NgR antibody

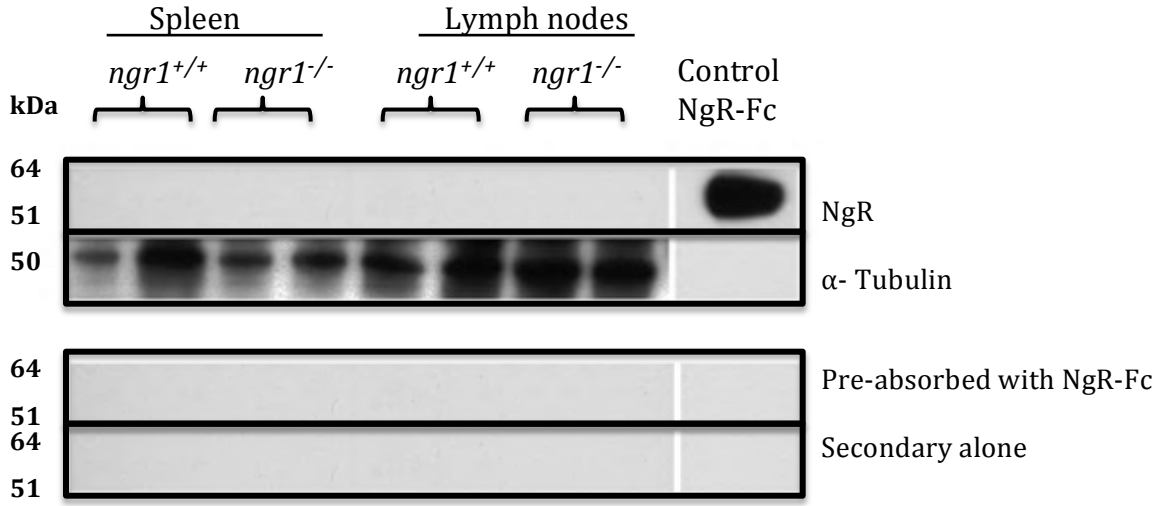
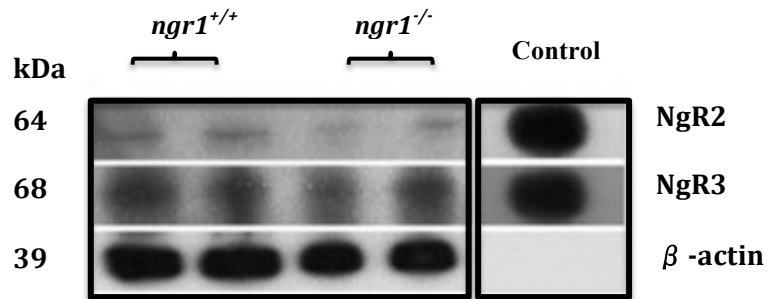


Figure 20. Western blot for the spleen, lymph nodes of naïve *ngr1*^{+/+} and *ngr1*^{-/-} mice.

There were no bands for both naïve *ngr1*^{+/+} and *ngr1*^{-/-} mice in the spleen and lymph nodes when we used anti-NgR antibody, secondary alone, and pre-absorbed with NgR-Fc (control). The specificity of the polyclonal NgR antibody was tested using NgR-Fc peptide as a control.

W. Blot: polyclonal anti-NgR2 antibody and polyclonal anti-NgR3 antibody

A. Spleen



B. Spinal cord

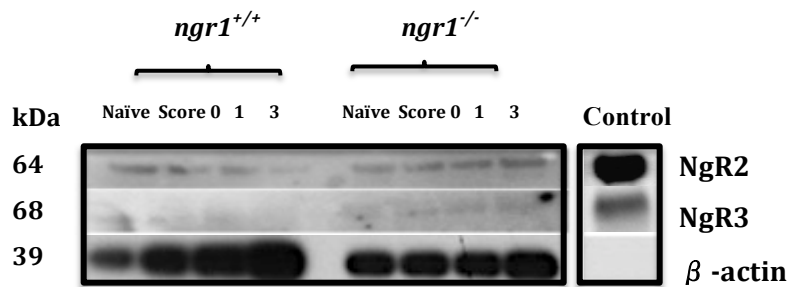


Figure 21. Preparation of tissue lysates for western blotting to identify NgR homologues in the spleen and spinal cord of *ngr1*^{+/+} and *ngr1*^{-/-} mice. **A.** There was a protein expression of NgR2 and NgR3 in the spleen of both naïve *ngr1*^{+/+} and *ngr1*^{-/-} mice. **B.** NgR2 and NgR3 can be expressed in the lysate from the spinal cord of *ngr1*^{+/+} and *ngr1*^{-/-} mice at different clinical score, comparing to un-injected littermate (naïve) mice.

3.5 Immunohistochemistry of NgR-positive B-cells in *ngr1*^{+/+} and *ngr1*^{-/-} spinal cord sections.

In order to quantify the NgR1-positive B-cells present within the CNS during neuroinflammation, immunohistochemistry was performed on 10 µm-thick longitudinal spinal cord sections. The sections were obtained from several naïve *ngr1*^{+/+} and *ngr1*^{+/+} mice and following EAE-induction at clinical scores 0, 1 and 3, in order to identify the existence and location of the B-cells that express NgR1. Immunostaining of B-cells for NgR was performed using anti-B220 antibody (green fluorescence) and anti-mouse NgR antibody (red fluorescence). The naïve *ngr1*^{+/+} and adjuvant-injected control mice showed few inflammatory cells within the spinal cord (Figure 22A and B). There were also few inflammatory cells present in *ngr1*^{+/+} mice following EAE induction at clinical score 0 (Figure 22C); this result correlates with the flow cytometry analysis which determined that B-cells expressing NgR were less than 0.2% of the cells within the *ngr1*^{+/+} mouse spinal cord (Figure 14). There was no double-positive immunostaining of B-cells for NgR in spinal cord tissue that was stained with Alex Fluor 488 (green) and 555 (red) secondary antibodies, negative controls (Figure 22D).

Remarkably, there was a cluster of B-cells expressing NgR, present at the meninges of the *ngr1*^{+/+} mice, during EAE at clinical score 1, as shown in Figure 23. This is reminiscent of the histological analysis of active MS lesions, the B-cells were located primarily in the perivascular spaces, WM lesions and meninges (Krumbholz, 2012, Pikor and Gommerman, 2012). Our outcome is consistent with that of Magliozzi *et al*

(Magliozzi, 2007), who have identified that in secondary progressive (SP-MS) post-mortem tissues have B-cell follicle-like structure (FLS) aggregates within meninges that host plasma cells, B-cells and T-cells over a network of follicular dendritic cells (FDCs) and B-cell chemokines (e.g. CXCL 13). This finding may support the role of B-cell-dependent disease progression in EAE and, by extension, in MS. Furthermore, there was a cluster of B-cells expressing NgR around the blood vessels in the *ngr1*^{+/+} mice at clinical score 1, as shown in Figure 24. This shows the infiltration of immune cells expressing NgR into the CNS during neuroinflammation in EAE. In the chronic stage of EAE, massive neuroinflammatory lesions could be observed in the *ngr1*^{+/+} mice (Figure 25).

There were cellular infiltrates in the spinal cord sections of the *ngr1*^{-/-} mice at clinical score 0 and only a few NgR-immunostained B-cells could be identified (Figure 26A and B). Figures 26 C and D showed some of the double-positive immunostaining of B-cells for NgR at the disease onset and the chronic stage in the *ngr1*^{-/-} mice.

We then stained B-cells-positive for NgR expression, for the NgR1's homologues (NgR2 and NgR3) in the spleen, lymph nodes and spinal cord of *ngr1*^{+/+} at the clinical score 1. Figure 27 showed that B-cell populations (green fluorescence) and either NgR1, NgR2, or NgR3 (red fluorescence) in all organs of *ngr1*^{+/+} mice at the disease onset. There were more double-positive B-cells and either NgR1 or NgR3 than NgR2 in all of these organs at this stage of the disease. The tissue was stained with NgR2 and NgR2-peptide as a

control. These data may provide a platform to determine how the expression of NgR1 in B-cells localised within the CNS, may initiate signalling through NgR3 during EAE.

Spinal cord

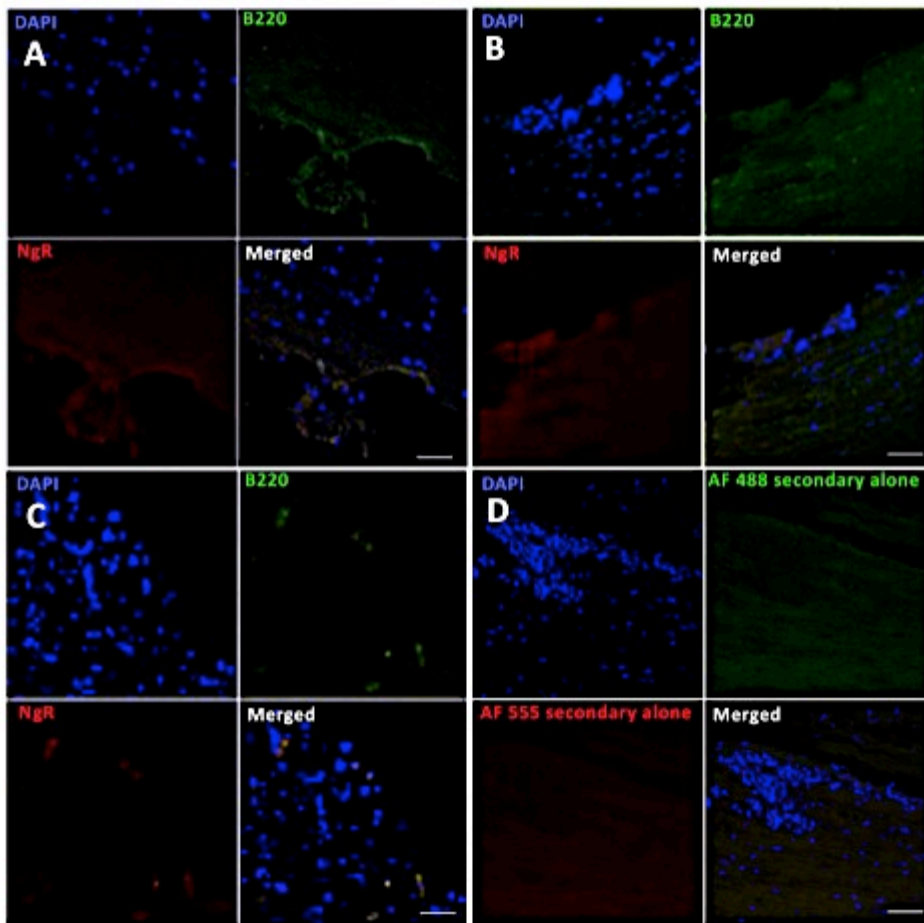


Figure 22. Double-immunostaining on the spinal cord tissue of *ngr1*^{+/+} mice. A-C. There were few inflammatory cells resident within the spinal cord of un-injected mice, adjuvant control and *ngr1*^{+/+} EAE-induced mice at clinical score 0. **D.** Negative control. The nuclei of cells stained with DAPI. CD45/B220 labelled B-cells (green fluorescence) and NgR was expressed in red fluorescence. Magnification 40x, scale bar= 50 μ m.

Spinal cord

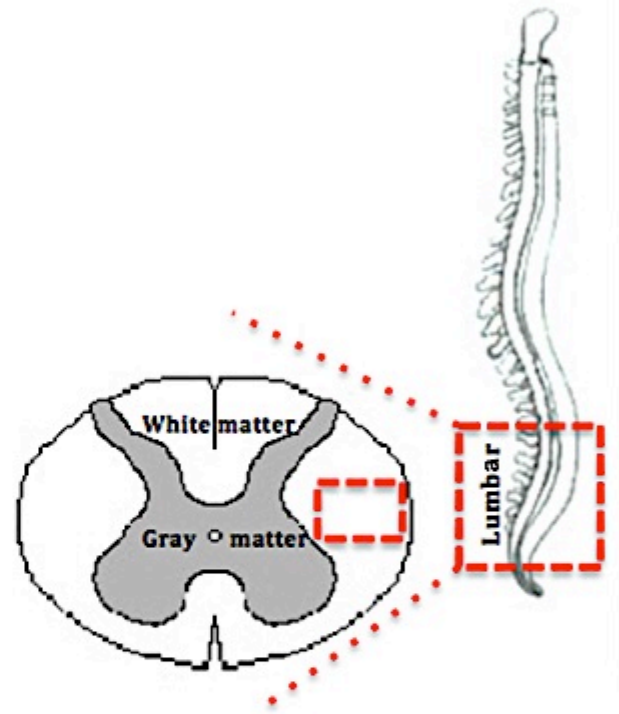
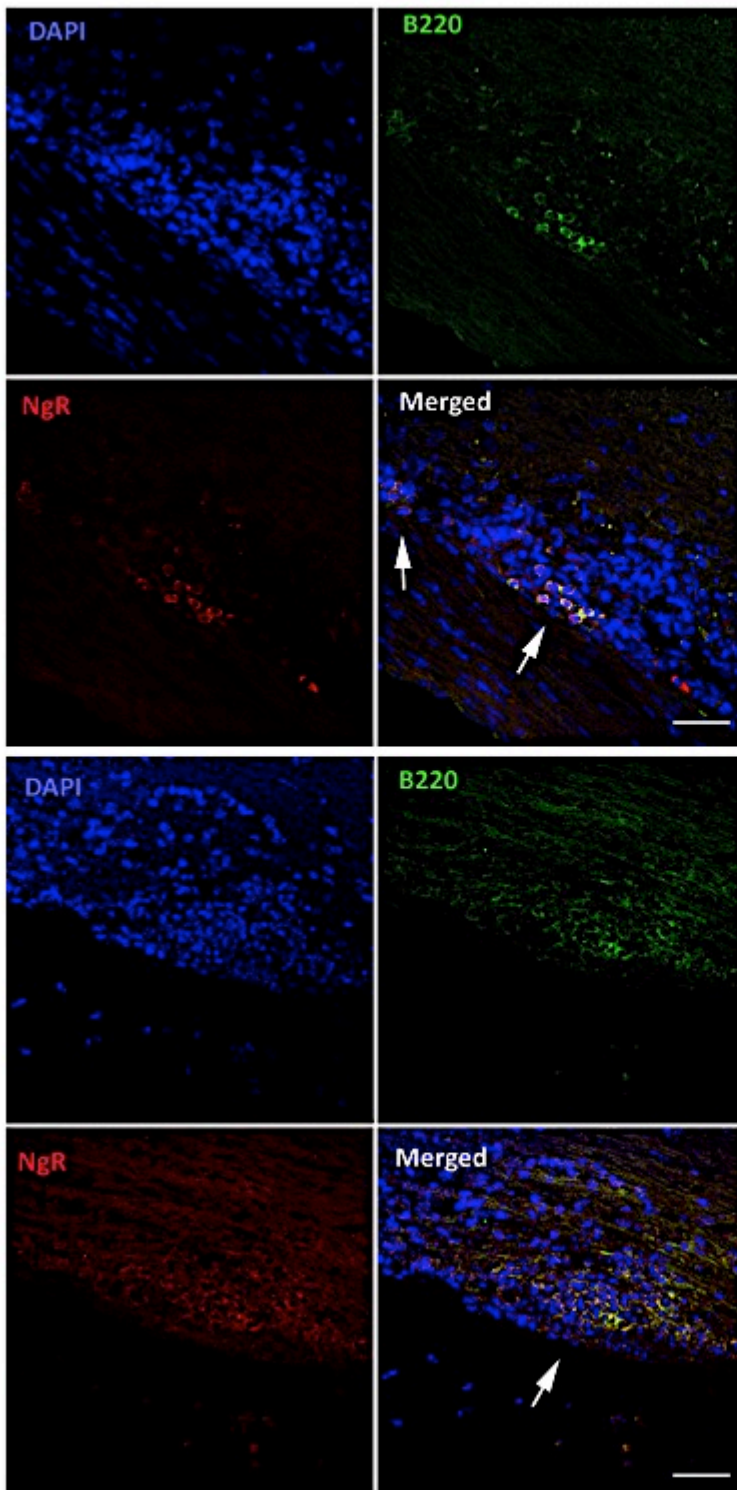


Figure 23. Localisation of double-immunofluorescence staining (NgR1-positive B-cell clusters) on 10 µm-thick longitudinal spinal cord sections during EAE in *ngr1*^{+/+} EAE-induced mice at clinical score 1. Anti- B220 and anti-NgR antibodies have been used to stain B-cells (green fluorescence) and NgR (red fluorescence) respectively. Infiltrate cells were present at the meninges of *ngr1*^{+/+} mice during disease onset. Double-positive cells were aggregated and presented in follicles at the meninges (the white arrows), magnification 40x, scale bar= 50 µm.

Spinal cord

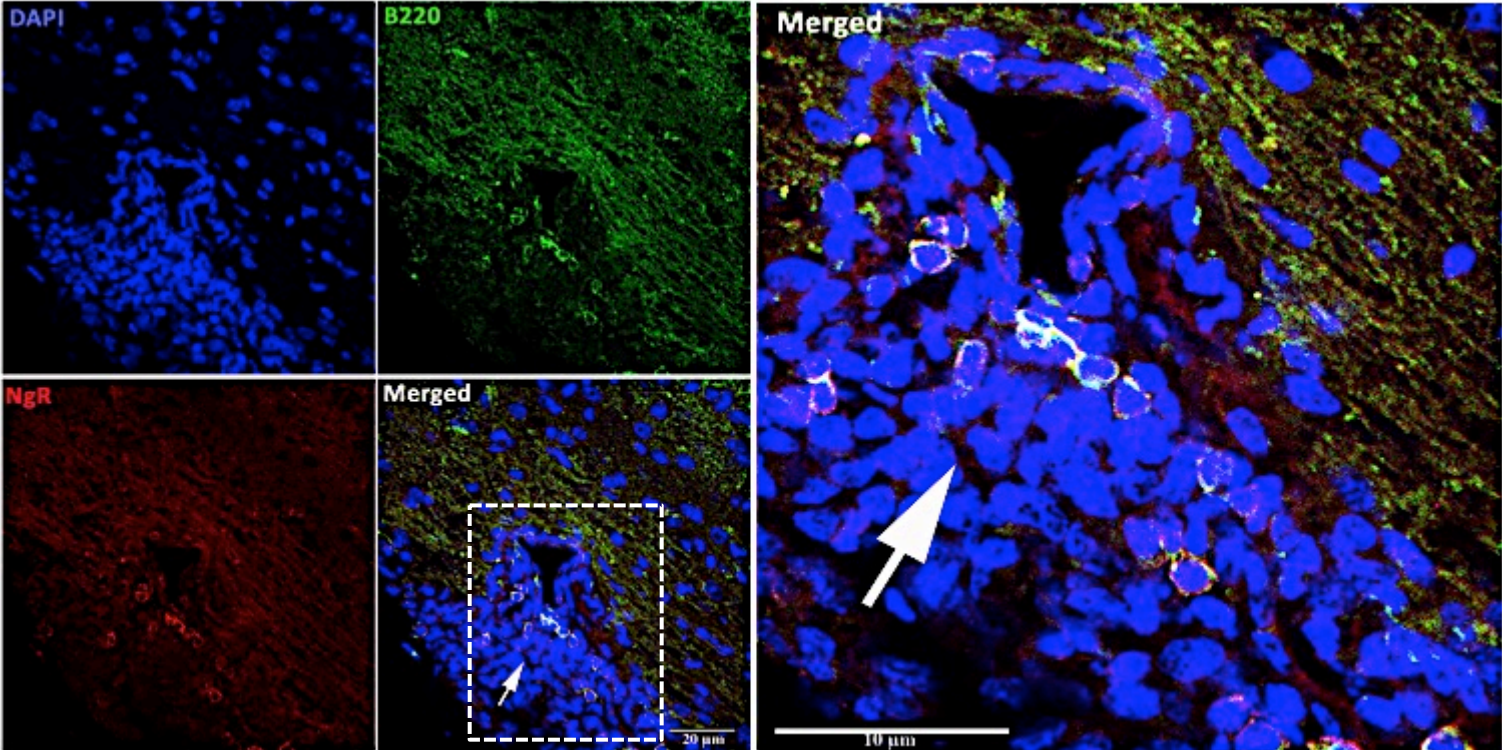


Figure 24. A cluster of B-cell infiltrate expressing NgR around *ngr1*^{+/+} mice blood vessel at clinical score 1 of EAE *ngr1*^{+/+} mice. B220 labelled B-cells (green fluorescence) and NgR was expressed in a red fluorescence. White arrows showed the cluster of B-cells expressing NgR. The nuclei of cells stained with DAPI. Magnification 40x, scale bar = 20 μm and 10 μm .

Spinal cord

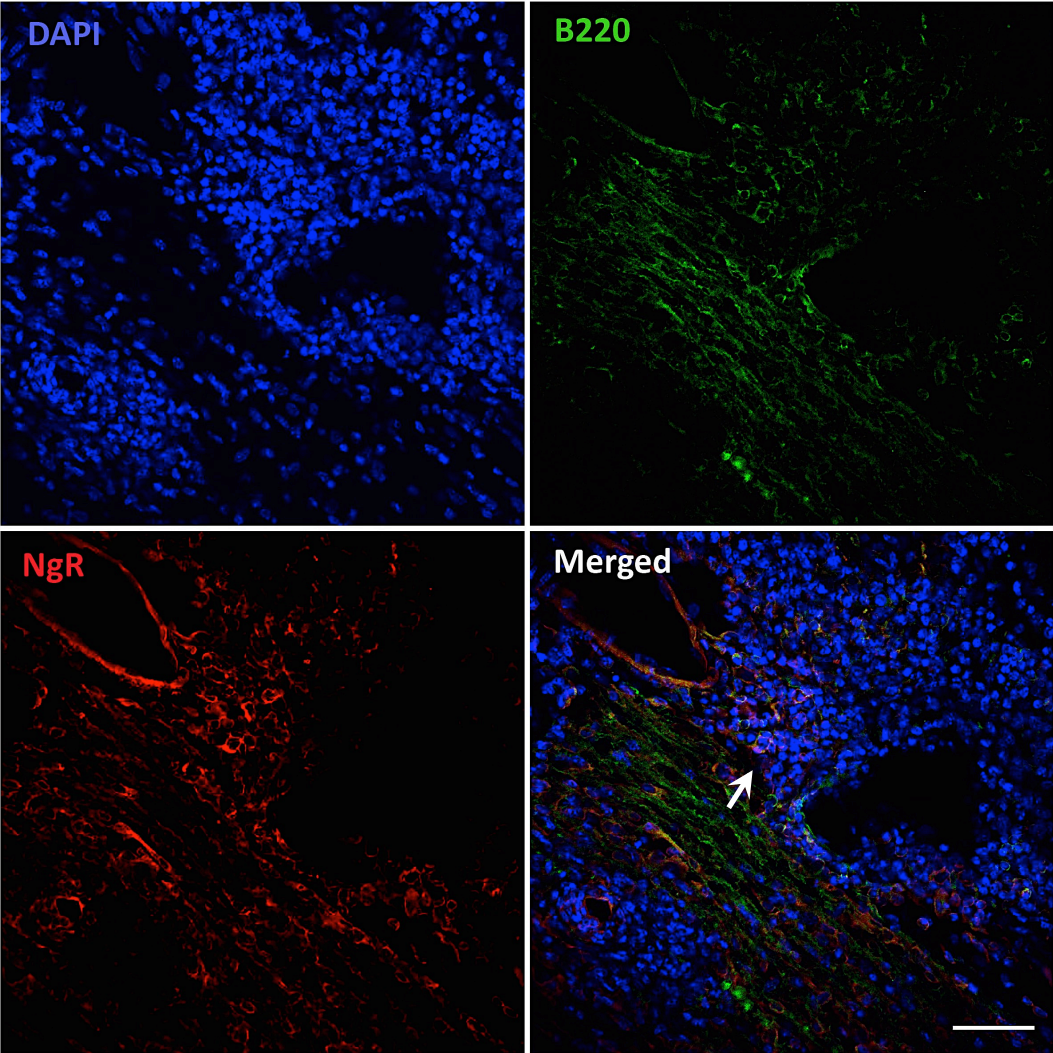


Figure 25. A massive neuroinflammation lesion appears in the chronic stage of disease in EAE-induced *ngr1*^{+/+} mice. There was an occasional double-positive immunofluorescence of B220 labelled B-cells (green fluorescence) and NgR (red fluorescence) within the spinal cord of the *ngr1*^{+/+} mice at clinical score 3 (the white arrow). The nuclei of cells stained with DAPI. Magnification 40x, scale bar= 50 μ m.

Spinal cord

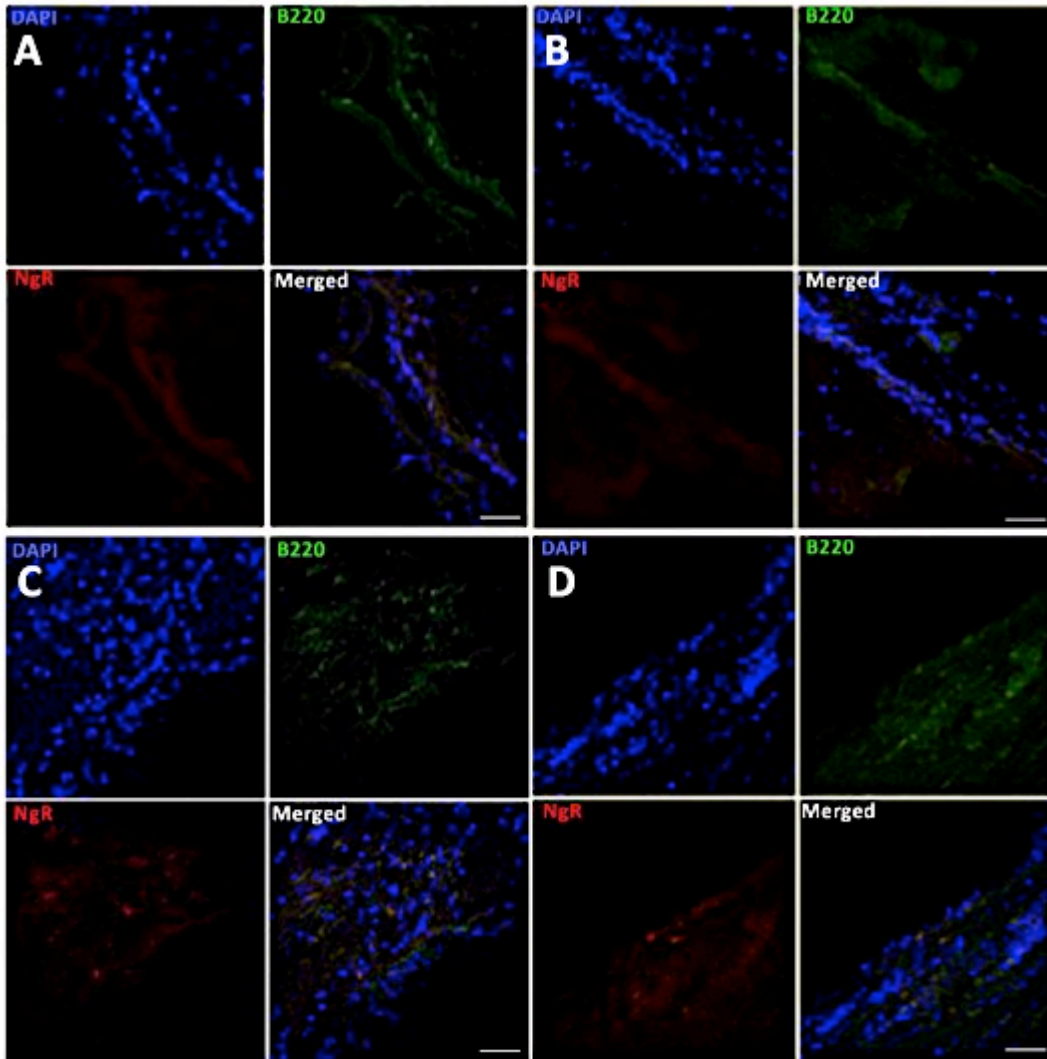


Figure 26. Double-staining on the spinal cord tissue of *ngr1*^{-/-} mice. A-B. There was cellular infiltrates in the spinal cord section and there was few NgR staining of B-cell populations of naïve *ngr1*^{-/-} mice EAE-induced at the clinical score 0. **C-D.** There was some of double-positive immunostaining of B-cells and NgR at the disease onset and chronic stage. The nuclei of cells stained with DAPI. B220 labelled B-cells (green fluorescence) and NgR was expressed in a red fluorescence. Magnification 40x, scale bar= 50 µm.

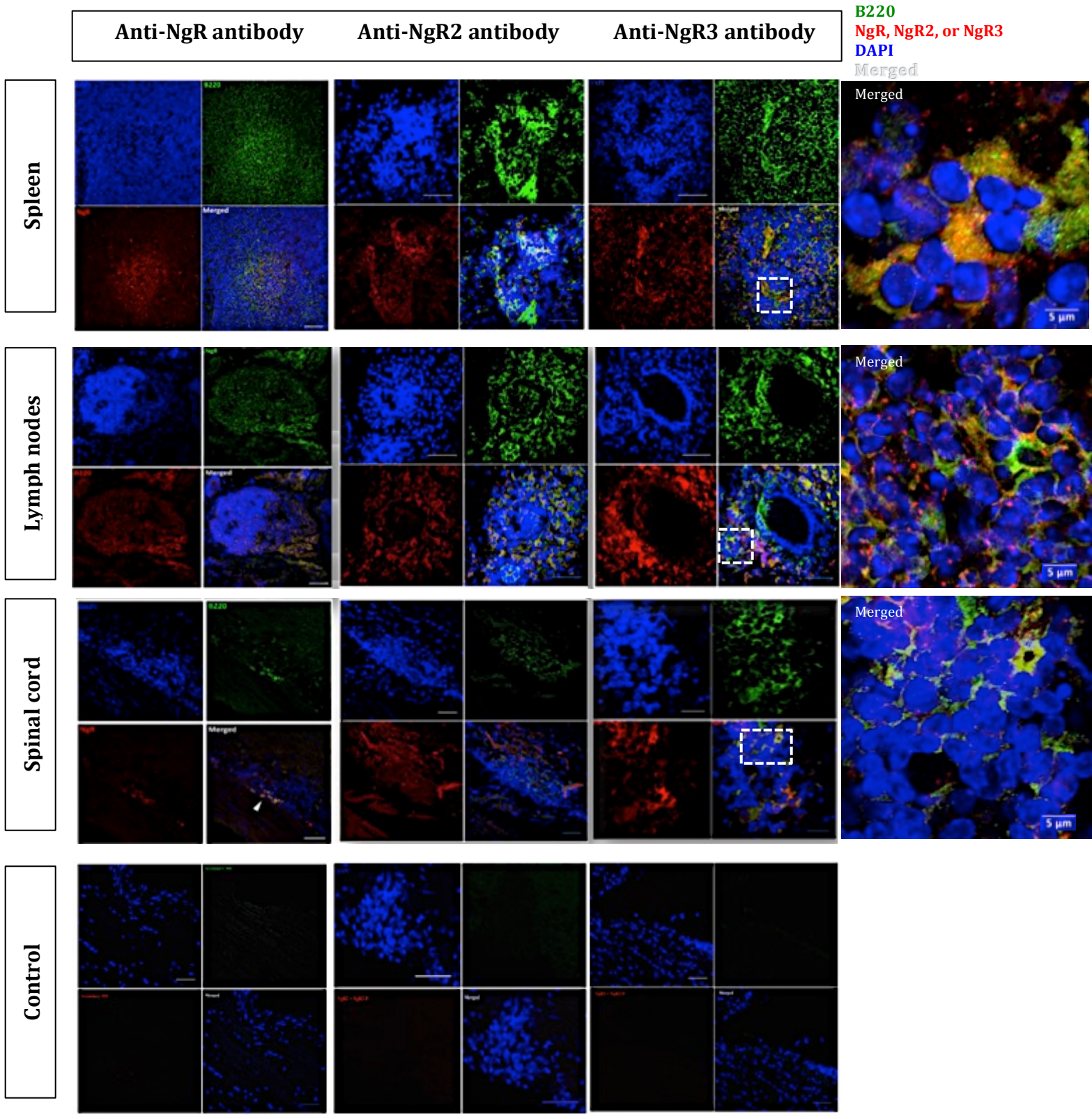


Figure 27. B-cells-positive either NgR1 or its homologues in the spleen, lymph nodes and spinal cord of *ngr1*^{+/+} at the clinical score 1. B-cell populations were expressed in a green fluorescence and either NgR1, NgR2, or NgR3 were expressed in a red fluorescence in all organs of *ngr1*^{+/+} at the disease onset. There were more double-positives of B-cells and either NgR1 or NgR3 than NgR2 in all organs at this stage of the disease. The tissue was stained with NgR2 and its peptide as a control. The nuclei of cells stained with DAPI. Magnification 40x, scale bar= 50 μ m.

3.5.1 Quantification of NgR-positive B-cells for *ngr1*^{+/+} and *ngr1*^{-/-} mice during EAE

Quantification of NgR-positive B-cells per unit area (mm²) of inflammatory lesions for the *ngr1*^{+/+} and *ngr1*^{-/-} mice (n=34 *ngr1*^{+/+} mice; 108 sections, n=15 *ngr1*^{-/-} mice; 40 sections) during EAE was performed to define the number of these cells localised within the inflammatory lesions (Table 7). The severity of EAE induced by the MOG₃₅₋₅₅ peptide increased significantly in the *ngr1*^{+/+} mice at disease onset and was reduced at the chronic stage (Figure 28A), which is consistent with the flow cytometric analysis. However, there was no statistical difference documented following double-immunofluorescence staining (NgR-positive B cells) in the *ngr1*^{-/-} mice (Figure 28B).

Table 7. Spinal cord section from *ngr1*^{+/+} and *ngr1*^{-/-} mice.

Mice Type	Number of mice used	Number of sections analysed
<i>ngr1</i> ^{+/+}	34	108
<i>ngr1</i> ^{-/-}	15	40

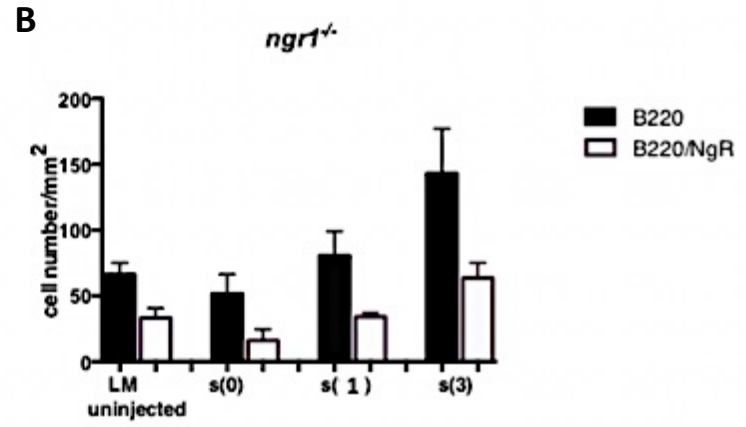
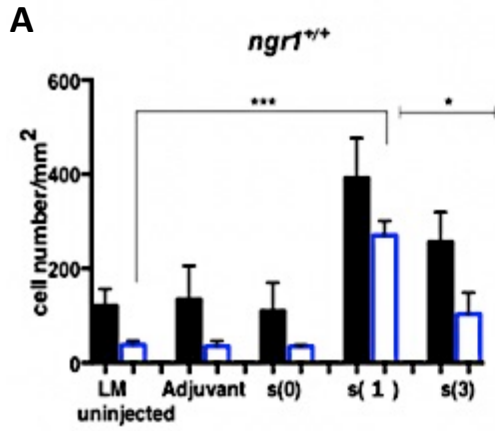


Figure 28. Increased severity of EAE MOG₃₅₋₅₅ peptide in *ngr1*^{+/+} mice at the disease onset and reduced in *ngr1*^{-/-} mice. **A. Quantification of NgR-positive B-cells per unit area (mm²) of inflammatory lesions for *ngr1*^{+/+} mice, **B.** *ngr1*^{-/-} mice. *p<0.05, **p<0.01, t-test.**

3.6 Co-localisation of Troy with NgR in B-cell infiltrate within spinal cord and optic nerve tissues at the disease onset during *ngr1*^{+/+} EAE-induced

In order to examine the role of NgR1 on B-cell populations in the spinal cord of *ngr1*^{+/+} mice at disease onset, an anti-TROY antibody was used in conjunction with either anti-NgR or anti-NgR3 or anti-B220 antibodies. TROY, a signalling co-receptor of NgR1, was expressed on B-cell clusters at the meningeal surface of the spinal cord tissue and was expressed with NgR in the *ngr1*^{+/+} EAE-induced mice (Figure 29A and B respectively).

In addition, there was significant double-positive immunofluorescence of B-cells (B220-positive) and TROY within the optic nerve of the *ngr1*^{+/+} mice at disease onset (Figure 30). Figure 31 showed the co-localisation of TROY with NgR in the immune cell infiltrates within the optic nerve of EAE-induced *ngr1*^{+/+} mice at disease onset.

Figure 32 shows the double-labelling of TROY and NgR3 in the spinal cord of the *ngr1*^{+/+} mice at disease onset; this may indicate the ability of TROY to be a functional signalling co-receptor for NgR3 but this hypothesis requires elucidation.

Spinal cord

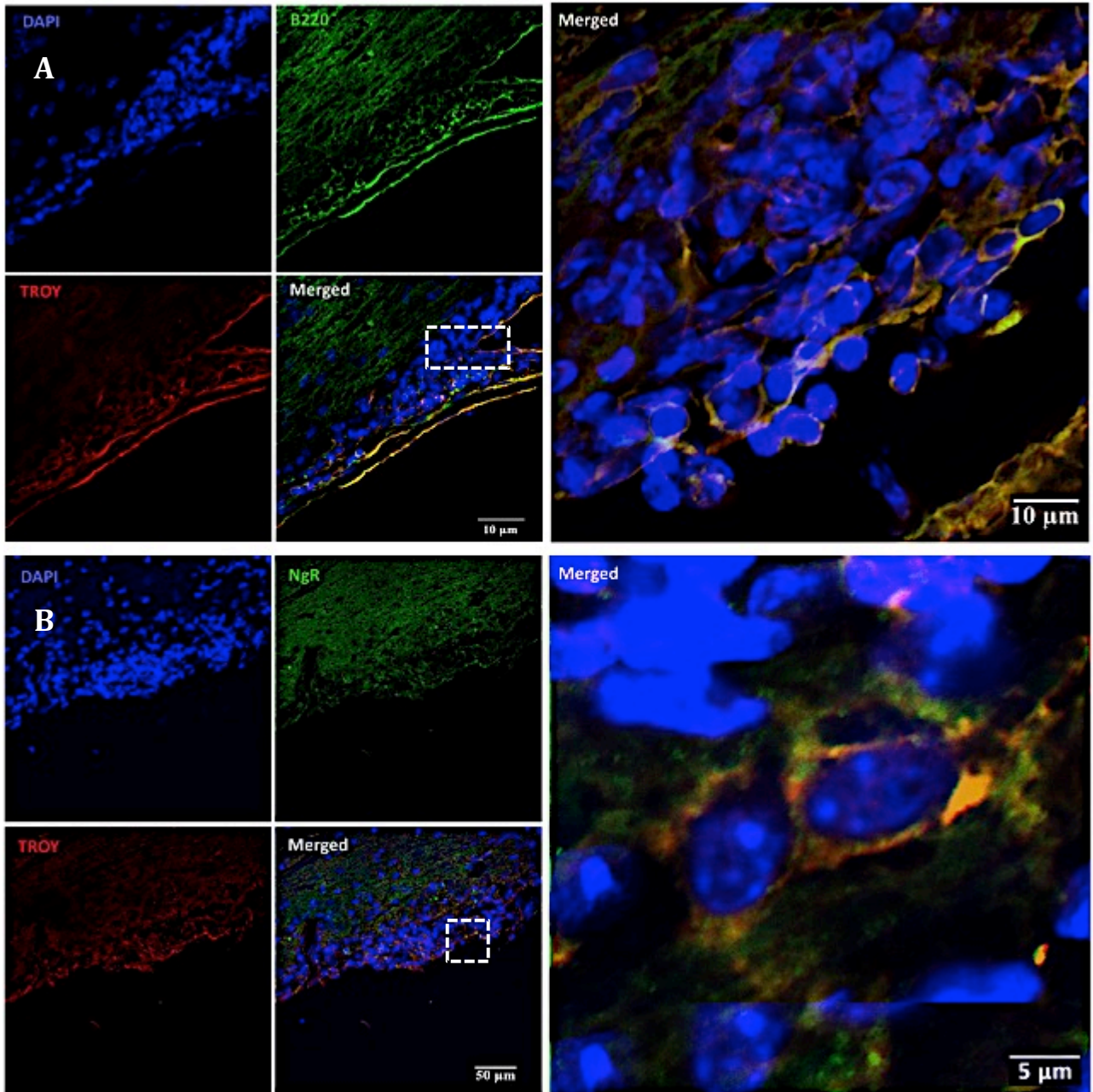


Figure 29. Expression of TROY on B-cells during *ngr1*^{+/+} EAE-induced within spinal cord tissues at the disease onset. A. TROY was expressed on B-cells in the clusters localised to the meninges of the spinal cord tissue. **B.** Double-labelling of NgR and TROY was expressed at the meninges. Magnification 40x, scale bar= 50 μm , 10 μm , and 5 μm .

Optic nerve

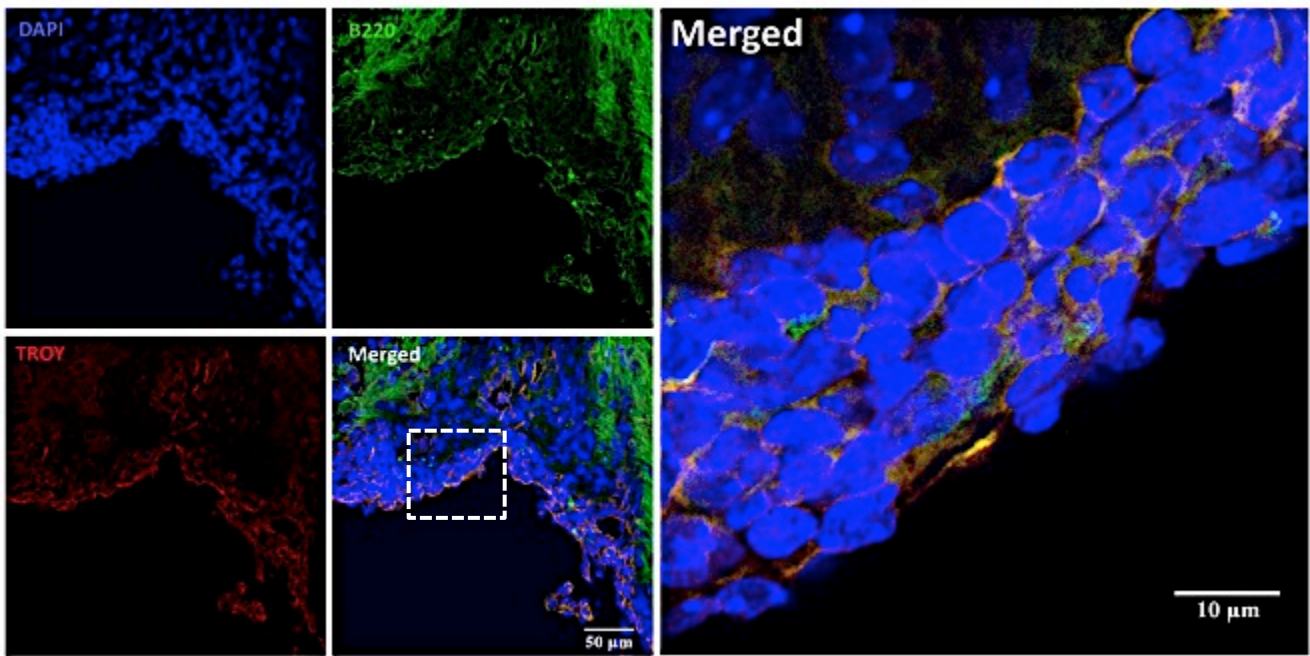


Figure 30. Co-localisation of TROY on B-cells during *ngr1*^{+/+} EAE-induced within the optic nerve tissues at the clinical score 1. There was a double-labelling of B220 labelled B-cells (green fluorescence) and Troy (red fluorescence) within the optic nerve of the *ngr1*^{+/+} mice at disease onset. The nuclei of cells stained with DAPI. Magnification 40x, scale bar= 50 μ m and 10 μ m.

Optic nerve

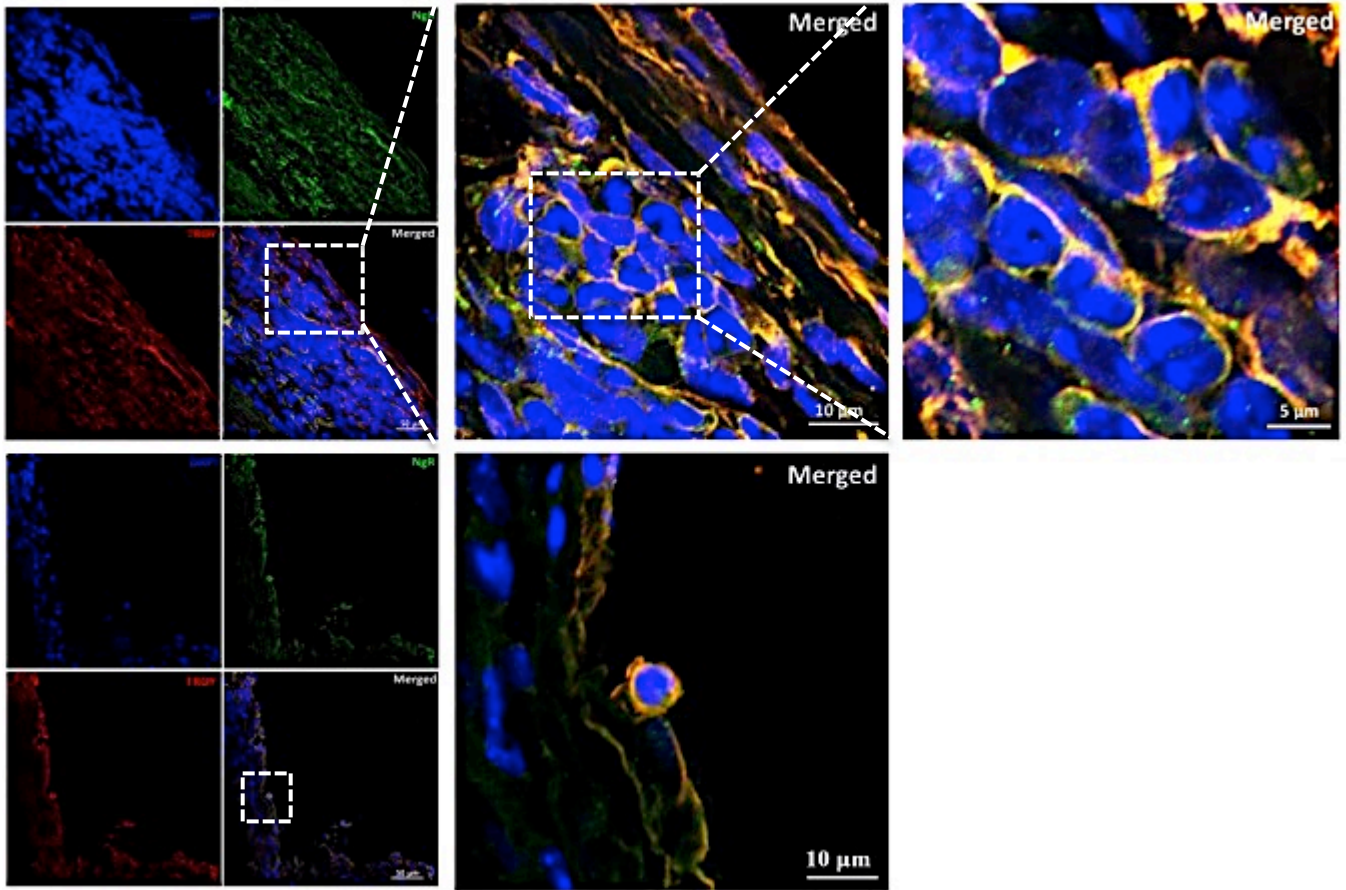


Figure 31. Co-localisation of TROY with NgR during *ngr1*^{+/+} EAE-induced in immune cell infiltrates within optic nerve tissues at the disease onset. There was a co-expression of TROY (red fluorescence) and NgR (green fluorescence) in the immune cell infiltrates within the optic nerve of EAE-induced *ngr1*^{+/+} mice at disease onset. The nuclei of cells stained with DAPI. Magnification 40x, scale bar= 50 μm , 10 μm , and 5 μm .

Spinal cord

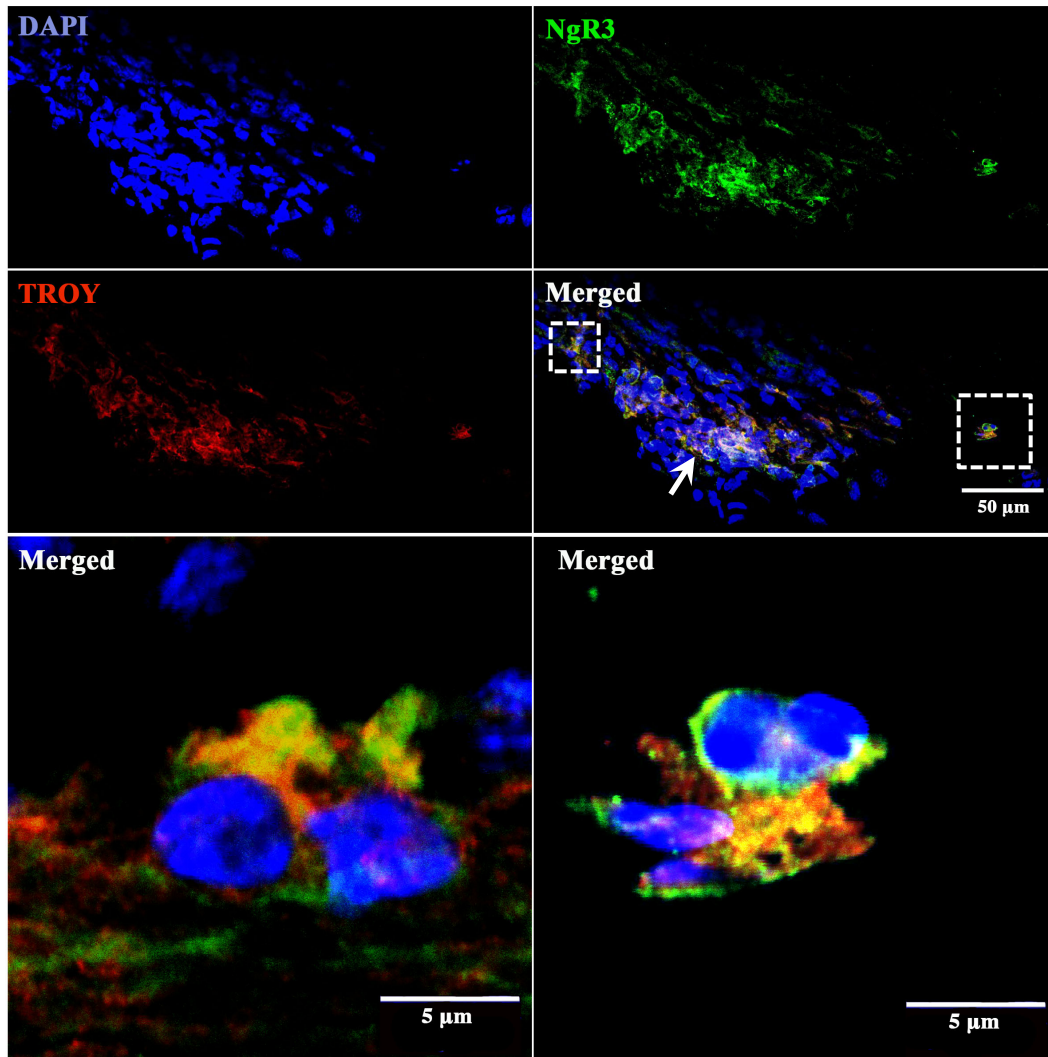


Figure 32. Co-localisation of TROY with NgR3 during *ngr1*^{+/+} EAE-induced in immune cell infiltrates within the spinal cord tissues at the disease onset. NgR3 was expressed in a green fluorescence and TROY was expressed in a red fluorescence. The double-positive of NgR3 and TROY was aggregated and presented at the meninges (the white arrow). The nuclei of cells stained with DAPI. Magnification 40x, scale bar= 50 μm , and 5 μm .

3.7 Immune-phenotyping of cellular infiltrates expressing NgR1 during EAE in *ngr1*^{+/+} mice at clinical score 1

In order to phenotype double-labelled cell suspensions of B-cells and NgR from the spleen, lymph nodes and spinal cord of the *ngr1*^{+/+} mice at disease onset, a cocktail of antibodies directed against B220, NgR, IgM and IgD was prepared and analysed using flow cytometry. The analysis was initially gated based on the forward scatter (measures cell size), and side scatter (correlates with granularity and structure complexity) of the negative control (unstained cells) to exclude small cells. DAPI-label was added to all cell suspensions in order to exclude dead cells. All samples were run in the scatter plot of B220-PE (red colour) against NgR-AF-488 (green colour), as shown in Figure 33. Then, the double-positive of B220 and NgR population (R125) was selected to gate either IgG against IgM or IgD against IgM (Figure 33). Isotype controls and/or negative controls have been used to count the non-specific binding of antibodies accurately determining the negative cell population. At disease onset, the double-positive NgR and B220 B-cells localised in the spinal cord of the *ngr1*^{+/+} mice were shown to be mainly IgG-positive (undergoing class-switching), and there was a significant increase in IgM B-cells expressing NgR, when compared to IgD-positive populations (Figure 33). The double-positive of B-cells and NgR was mainly expressed IgG (96.23%) in the spinal cord that was not positive to Ki-67, as shown in flow cytometric analysis (Figure 34A). The follicle-like cells of B-cell positive NgR were shown to be a few double-labelled with Ki-67 in the spinal cord of *ngr1*^{+/+} EAE-induced (Figure 34B). However, there was double-labelled for Ki-67 and NgR in the spleen tissues of *ngr1*^{+/+} EAE-induced (Figure

34C), suggesting that B-cells positive for NgR may be proliferative and maturing, defined by their Ig class switching.

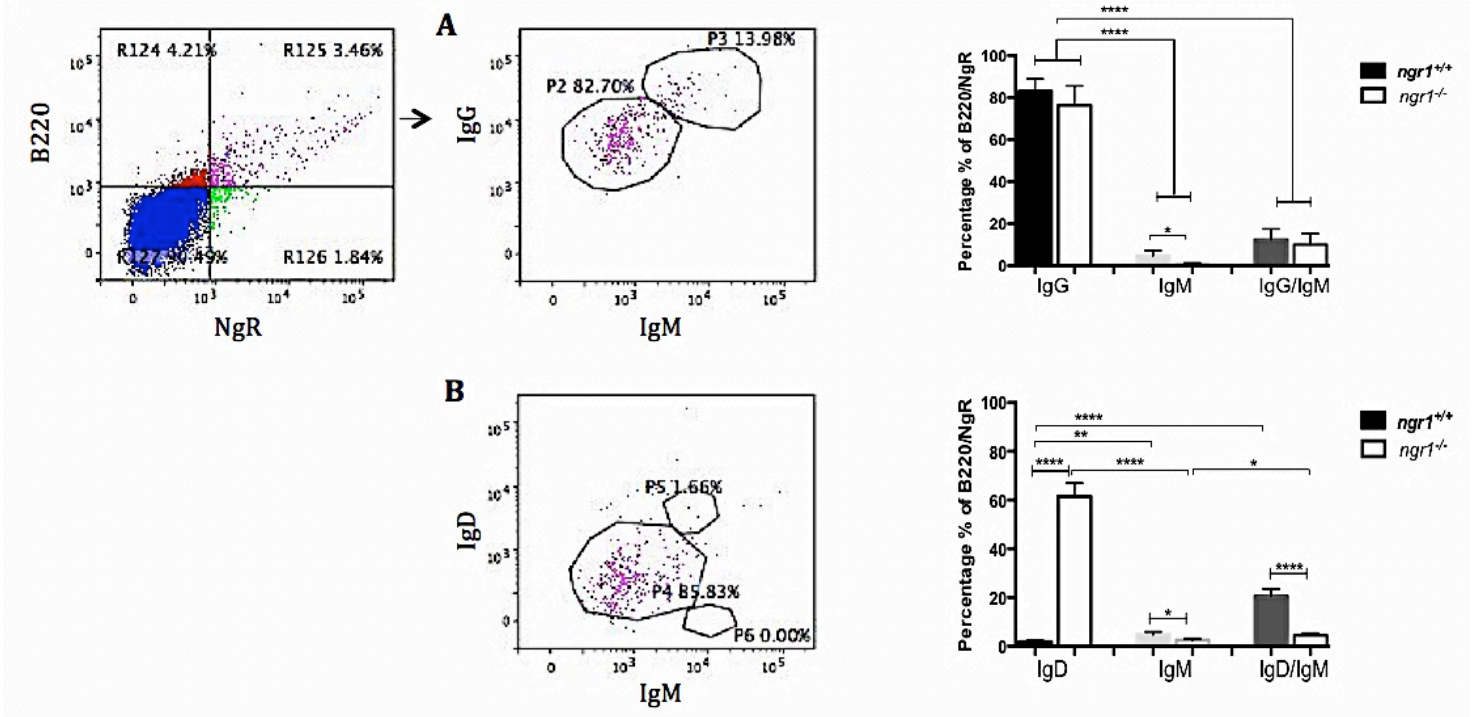


Figure 33. Phenotype of B-cells that were immunopositive for NgR1 from the spinal cord EAE-induced at the disease onset. **A.** B-cells that were positive NgR expressed IgG more than IgM in both of *ngr1*^{+/+} and *ngr1*^{-/-}. **B.** There was a significant increase in IgM B-cells expressing NgR, when compared to IgD populations in *ngr1*^{+/+}. Results represent mean ± SEM (n=6). *p<0.05, ** p<0.01, ****p<0.0001, t-test.

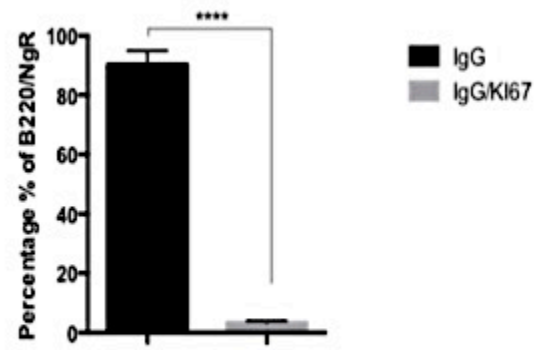
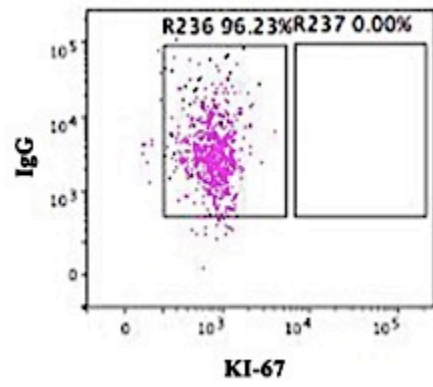
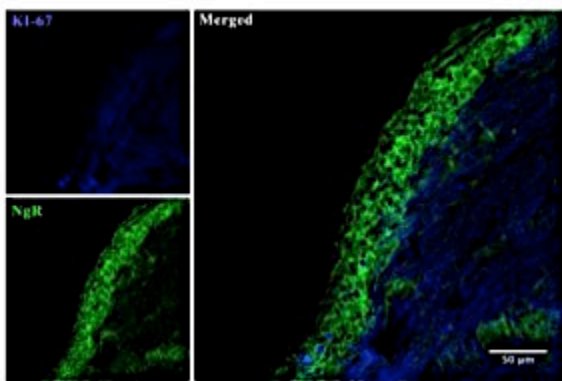
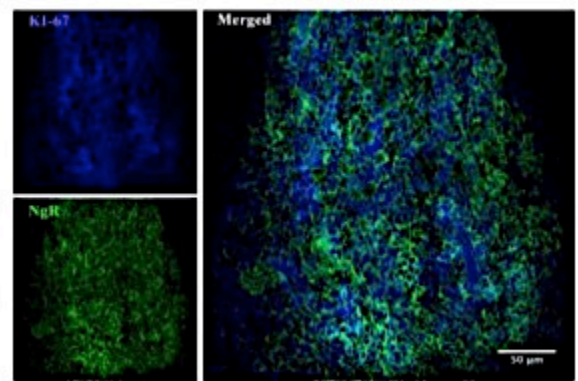
A**B****Spinal cord****C****Spleen**

Figure 34. Phenotype of B-cells and NgR double-positive populations from *ngr1*^{+/+} EAE-induced at clinical score 1. A. The double-positive of B-cells and NgR was expressed IgG in the spinal cord with 96.23% but was not positive for Ki-67. **B.** There was a few double-labelling of Ki-67 (blue) and NgR (green) in the spinal cord tissue of *ngr1*^{+/+} EAE-induced. **C.** Ki-67 was positive for NgR in the spleen tissue of *ngr1*^{+/+} EAE-induced. Results represent mean \pm SEM (n=4). ***p<0.0001, t-test

3.8 Discussion

The experiments outlined in chapter 3 have defined that NgR1 and NgR3 are expressed on populations of immune cells during CNS inflammation. This definition has been achieved experimentally through several analyses by inducing EAE with MOG₃₅₋₅₅ and rMOG, in both *ngr1*^{+/+} and *ngr1*^{-/-} mice. The former is B-cell independent but the later is B-cell dependent (Weber et al., 2010, Bernard et al., 1997, Lyons et al., 1999). Our results demonstrated that immunisation with MOG₃₅₋₅₅ peptide resulted in *ngr1*^{-/-} mice having a significant delay in EAE onset and a decrease in the severity of clinical signs when compared to *ngr1*^{+/+} mice, *ngr1*^{-/-} mice also showed an associated decrease in CNS tissue demyelination at disease onset and significantly decreased axonal damage at the chronic stage of disease. These results are consistent with our recent findings that the prevention and/or reduction of axonal degeneration in the optic nerve and spinal cord of EAE-induced mice by MOG₃₅₋₅₅ is associated with lower levels of the phosphorylated form of collapsin response mediator protein-2 (CRMP-2), pThr555CRMP-2, which is an important tubulin-associated protein that regulates the dynamics of axonal growth (Petratos et al., 2012). However, our results are not in line with a previous study that demonstrated no enhanced axonal sprouting in *ngr1/2*^{-/-} mice compared to the wild-type mice (Steinbach et al., 2011). On the other hand, our data showed a significant delay in EAE onset and decrease in clinical severity for the *ngr1*^{-/-} mice using rMOG, suggesting that NgR1 may affect B-cell function in the acute phase. However, this finding may be inconsistent with that reported by Litwak *et al.* (2013), who found that NgR1 did not play a role in B-cell expression when EAE was provoked by rMOG.

Flow cytometric analysis of immunological parameters during EAE progression provided vital information on the potential role of NgR1 and NgR3 in regulating the immune response in the MS model. *ngr1*^{-/-} mice, induced by either MOG₃₅₋₅₅ or rMOG peptides, presented an immune profile with and without NgR in the spleen and lymph nodes under both naïve and pathological conditions. This suggests that other NgR homologues (NgR2 and NgR3) may be detected with our monoclonal antibody with and without EAE, since *ngr1*^{-/-} mice demonstrated immunoreactivity. Thus, specific anti-NgR2 and anti-NgR3 antibodies were used with immune cell markers during EAE. Importantly, the B-cell population positive for NgR1 and NgR3 in the spinal cord of the *ngr1*^{+/+} mice were elevated significantly at disease onset and did not increase in *ngr1*^{-/-} mice. Indeed, knocking out the NgR1 gene in mice resulted in no modification in the infiltration of B-cells during disease progression. These findings suggest for the first time that NgR1 and NgR3 have a role as signalling molecules in regulating B-cell function during EAE-induction. These results were similar to what we observed in mice that were immunised with rMOG, although given differences in the pathogenesis of EAE induced by the encephalitogenic MOG₃₅₋₅₅ peptide against rMOG-induced EAE (Weber et al., 2010, Bettadapura et al., 1998). Moreover, our data are not consistent with those reported by Steinbach *et al.* (2011) and Litwak *et al.* (2013), who demonstrated a slight elevation in leukocyte infiltration into the CNS of EAE-induced mice. Nevertheless, neither of these receptors impacted the distribution or size of inflammatory lesions within the CNS, nor did they have any significant influence on the severity and development of EAE (Steinbach et al., 2011). Furthermore, the double-positive cells of NgR and B220 B-cells

in the spinal cord of *ngr1*^{+/+} mice were mainly IgG positive (class switching) not Ki-67, and there was a significant increase in IgM positive for B-cells expressing NgR, when compared to IgD populations, suggesting these infiltrates are a cluster of maturing B-cells.

Immunohistochemistry results showed that within EAE-induced *ngr1*^{+/+} spinal cord tissue, NgR1- and NgR3-positive cells could be detected in B-cells, which seemed to be clustered in FLS abutting the meninges and surrounding venules in the white matter at the disease onset. These results are in line with a recent finding demonstrated that B-cells are a prominent feature in the neurodegenerative process that localised and presented in follicles at the meninges of SP-MS patients (Howell et al., 2011); this finding supported that of a previous study (Serafini et al., 2004). Furthermore, TROY has been expressed on these B-cells positive for NgR1 and NgR3, suggesting a unique requirement for potential trimeric interactions to occur, although no physical binding of soluble NgR3 to TROY has also been reported (Dickendesher et al., 2012). Dickendesher *et al.* (2012) then demonstrated that NgR1 and NgR3 are part of the same receptor complex that co-expressed in HEK293T cells (Dickendesher et al., 2012).

From our data, we can now hypothesise and extrapolate that the role of NgR signalling in the differentiation and maturation of B-cells in EAE may be a pertinent mechanism to elucidate during EAE; NgR1 may play a role in B-cell aggregation within the CNS during neuro-inflammation, important in the formation a dispersion of meningeal follicles observed in EAE and, by extension, in MS. Therefore, the natural question that can now

be posited is whether or not NgR expression and signalling govern the formation of these FLS in the CNS during progressive disease. In the following chapters, we will identify if BAFF is a potential ligand for NgR during EAE onset and how it relates to B-cell physiology that may be NgR-dependent.

**CHAPTER 4: BAFF as an alternate ligand for NgR during the
induction of EAE**

4.1 Introduction

Recently, our laboratory has identified that NgR1 may ultimately potentiate neurodegeneration in EAE potentially via a direct neurobiological mechanism, in EAE-induced mice (Petratos et al., 2012). It is able to transduce its signals inside the cell via activating the intracellular RhoA-GTPase, causing inhibition of axonal outgrowth, or modulation of motility and cell adhesion when Nogo-A binds with high affinity to NgR1, expressed in conjunction with the LINGO-1 and either, TROY or p75^{NTR} signalling receptors (Pernet and Schwab, 2012, Fournier et al., 2003). Furthermore, alternate ligands of NgR1 are NgR2 and NgR3 and both paralogues are expressed in the developing and adult CNS. They share similar protein structures with NgR1, including the GPI-anchored domain and LRR motif, however, they have different gene loci to NgR1; NgR2 and NgR3 are located at chromosome 17 but NgR1 is located at 22q11 (Zhang et al., 2011). A very recent study identified that NgR family members (NgR1 and NgR3) as shared receptors for CSPG and MAIFs in regulating regeneration failure in the CNS provides new insights into how a diverse group of inhibitory cues regulates neuronal function and structure under physiological conditions after injury (Dickendesher et al., 2012). Since NgR1 and NgR3 bind directly and with high-affinity to the chondroitin sulphate glycosaminoglycan and participate as functionally redundant CSPG receptors (Dickendesher et al., 2012).

Despite clear evidence demonstrating that the deletion of NgR1 can protect against axonal degeneration and thus progression of EAE (Petratos et al., 2012), an

immunological role for this receptor is yet to yield mechanistic evidence. However, recently NgR has been suggested as an alternate receptor for BAFF in the CNS. Zhang *et al.* (2009) identified that BAFF may act as a potential ligand for NgR1 to inhibit neurite outgrowth (at least *in vitro*), thereby signalling independently of the putative MAIFs. Besides that fact that BAFF has the ability to bind to variable receptors, such as BCMA, TACI and BR3 (also known as BAFF-R) on the B-cell surface, it produced as type II transmembrane protein, then cleaved by furin protease activity to release BAFF as a soluble, biologically active molecule (17 kDa) (Schneider *et al.*, 1999, Zhou *et al.*, 2011). Therefore, it is plausible that NgR1 may interact with BAFF to elicit a signal transduction cascade regulating B-cell activity. It is tantalising to hypothesise that NgR1 and its homologues localised on B-cells may interact with BAFF on neighbouring B-cells within a follicular structure stimulating their development, thereby propagating the neurodegenerative disease through the development of immunocompetent B-cells that target neural autoantigens. Such a theory requires thorough molecular dissection but may be of significant in identifying CNS-localised B-cell pathophysiological mechanism that may govern inflammatory demyelination. By extension, if such theory is validated, targeting the molecular mechanism of axonal degeneration in EAE as we previously reported may be also applicable in regulating the adaptive immunological (humoral and cellular) mechanism that can mediate neurodegeneration in EAE.

4.2 Expression of NgR and BAFF in the spinal cord tissue of *ngr1*^{+/+} EAE-induced mice at clinical score 1

It has been identified *in vitro* that the B-lymphocyte stimulator BLYS or BAFF (the tumour necrosis factor superfamily protein involved in the development of B-cells) may act as a ligand for NgR1 to inhibit neurite outgrowth, thereby signalling independently of the putative MAIFs (Zhang et al., 2009). However, it is plausible that a BAFF/NgR1 mechanism may be also operational during EAE induction, with BAFF playing in a role in the purported FLS formed in the CNS of MS patients and these recently identified in EAE mice (Serafini et al., 2004, von Budingen et al., 2011). Thus, spinal cord sections from EAE-induced *ngr1*^{+/+} mice were stained with NgR1 and BAFF, along with positive control spleen sections (n=6), (BAFF arbitrates splenic B-cell and antibody responses and elevate the plasma cells number) (Bermejo et al., 2010). Figure 35 shows huge numbers of clustered immune cell infiltrates that labelled for BAFF and NgR1 within the spinal cord of *ngr1*^{+/+} EAE-induced mice at disease onset, and these populations were positive for both B220 and NgR1 within the spinal cord of *ngr1*^{+/+} EAE-induced mice at clinical score 1. Similarly, these double-positive populations were found within the spleen of EAE-induced *ngr1*^{+/+} mice at clinical score 1, present in the white pulp and follicle, as shown in Figure 35 and 36 respectively. Furthermore, there was occasional double-positive immunostaining of BAFF with NgR3 at the meninges of the spinal cord and within follicles in the spleen of *ngr1*^{+/+} mice at clinical score 1 (Figure 37).

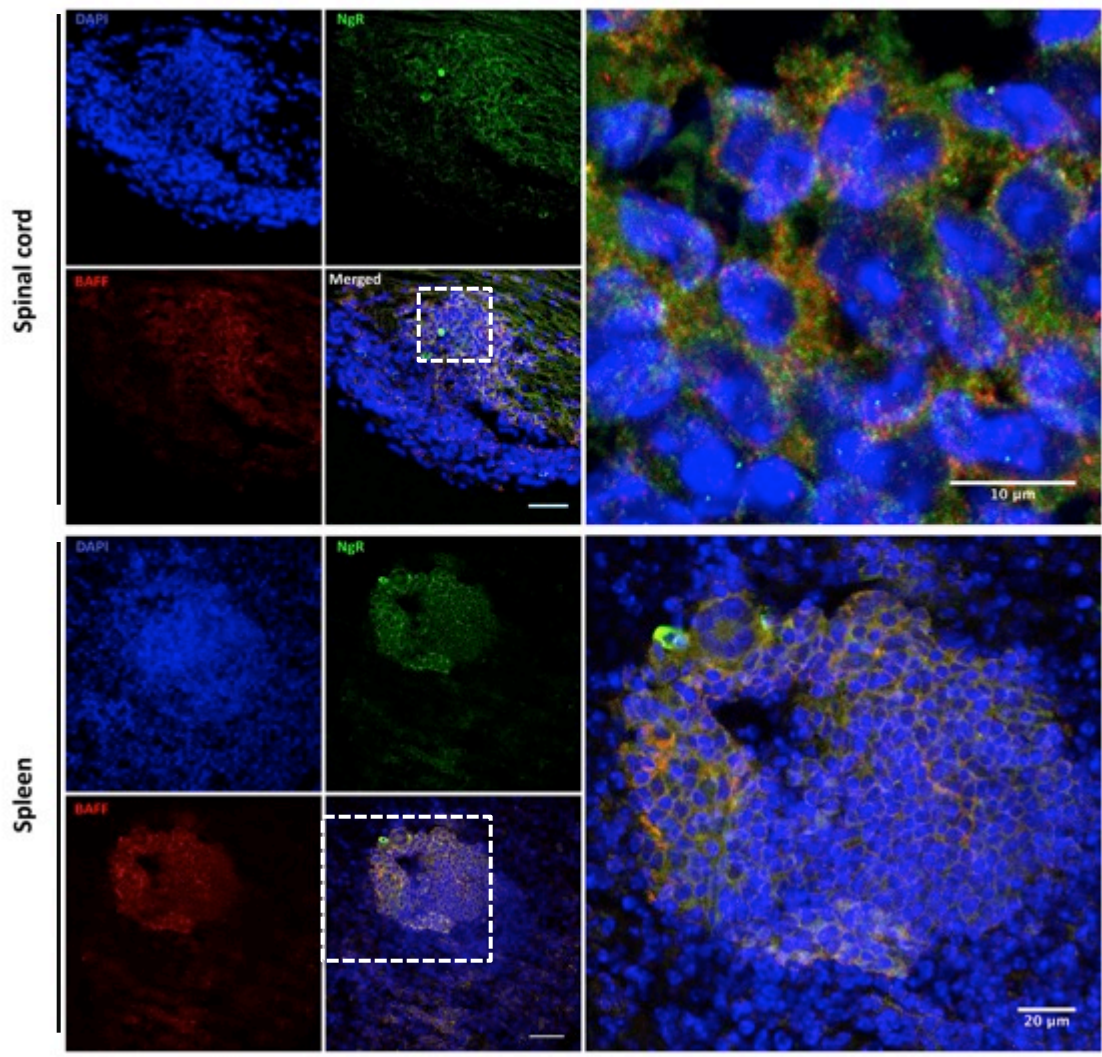


Figure 35. Expression of NgR in conjunction with BAFF in *ngr1*^{+/+} EAE-induced mice at the clinical score 1. BAFF was expressed in a green fluorescence and NgR was expressed in a red fluorescence within follicles in the spinal cord and within white pulp in the spleen. The nuclei of cells stained with DAPI. Magnification 40x, unlabelled scale bar = 50 μ m.

Spleen

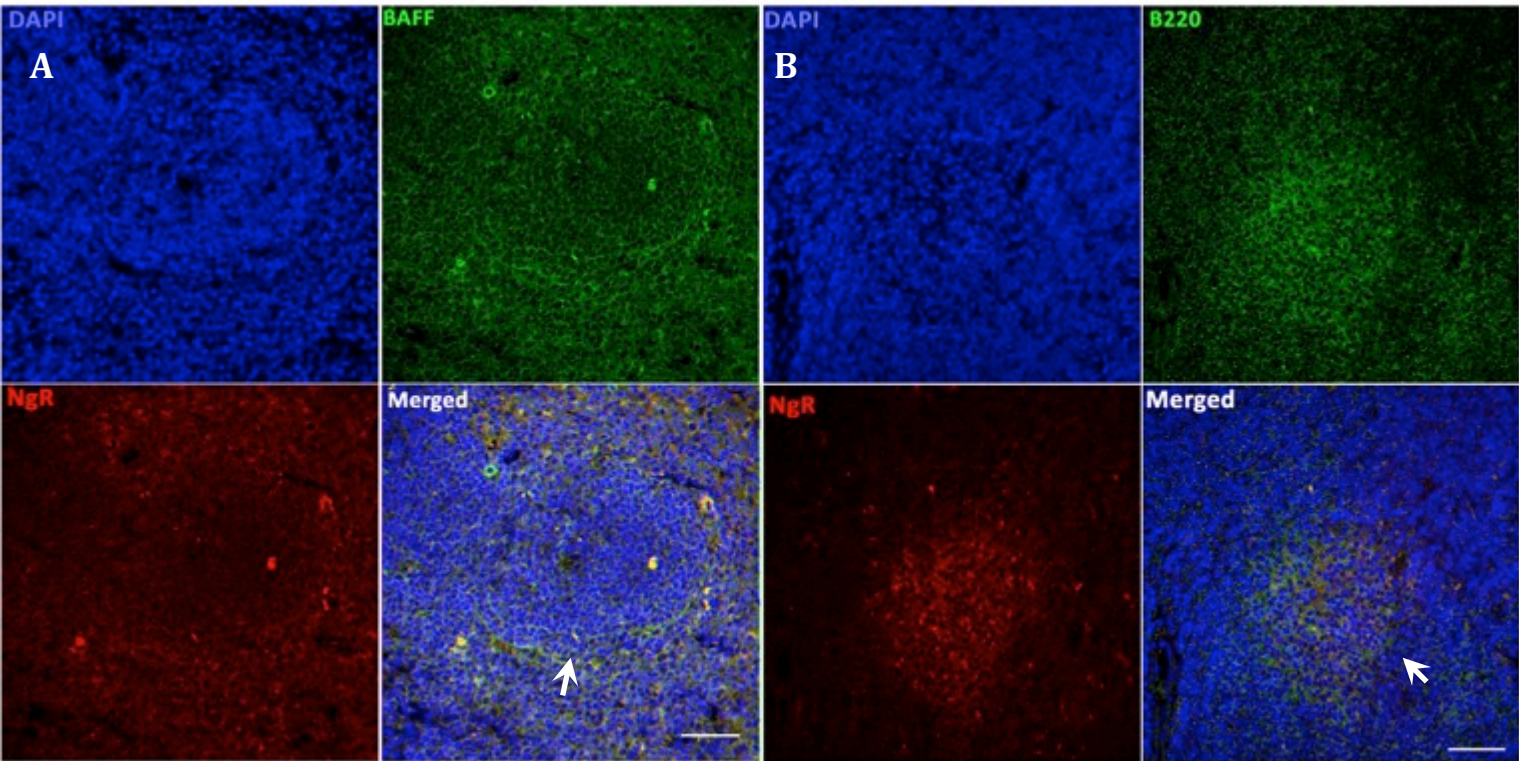


Figure 36. Expression of either NgR in conjunction with BAFF or B-cells in follicles of *ngr1*^{+/+} EAE-induced spleen at the clinical score 1. A. BAFF was expressed in a green fluorescence and NgR was expressed in a red fluorescence within follicles in the spleen (the white arrow). **B.** There was double-positive immunostaining of B-cells with NgR within follicles in the spleen (the white arrow). The nuclei of cells stained with DAPI. Magnification 40x, scale bar = 50 μ m.

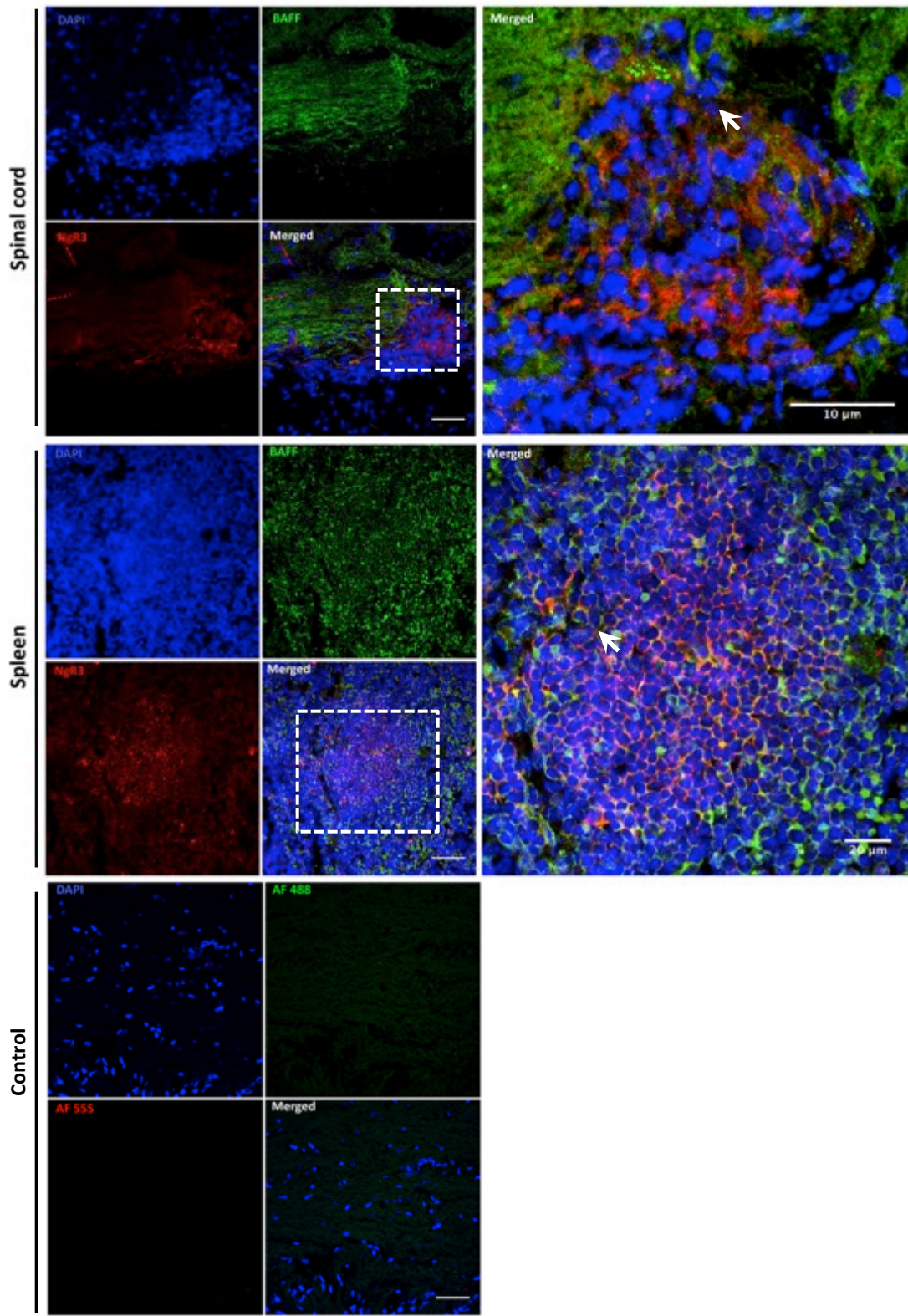


Figure 37. Expression of BAFF in conjunction with NgR3 on immune cells in *ngr1*^{+/+} EAE-induced at the clinical score 1. There was occasional co-localisation of BAFF (red fluorescence) and NgR (green fluorescence) at the meninges of the spinal cord and within follicles in the spleen of *ngr1*^{+/+} mice at disease onset (the white arrows). The nuclei of cells stained with DAPI. There was no staining with Alex Fluor 488 (green) and 555 (red) secondary antibodies, negative control.

4.3 Expression of BAFF-R and NgR on immune cells in the spleen

In order to elucidate the potential co-localisation between of NgR and BAFF-R as the other cognate receptor for BAFF in these follicles, immunostaining was performed within the spinal cord tissues of the *ngr1*^{+/+} mice at EAE onset and within spleen of BAFF^{-/-} mice and *ngr1*^{+/+} mice at EAE pre-onset (control). Zhou *et al.* (2011) identified that the development of EAE was significantly delayed and severity of disease was reduced in BAFF^{-/-} mice when compared to *ngr1*^{+/+} mice. Figure 38 illustrates that there was single-staining of NgR and BAFF-R on immune cells, but no double-stained co-expression. Furthermore, the spleen of the BAFF^{-/-} mice showed only few immune cells with NgR staining, but as expected no BAFF-R since BAFF^{-/-} mice lack the capacity for an autoimmune response (Schiemann *et al.*, 2001) (Figure 39A). There were occasional single-positive labelled cells for BAFF-R and NgR within the spleen of EAE-induced *ngr1*^{+/+} mice at pre-onset (Figure 39B).

Consequently, these results may indicate that there exists a strong correlation between NgR1 and BAFF during EAE induction. It is tantalising to hypothesise that NgR1 localised on B-cells may interact with BAFF on neighbouring B-cells within a follicular structure stimulating their development, thereby propagating the neurodegenerative disease through the development of immunocompetent B-cells that target neural autoantigens. This line of investigation was therefore further interrogated as a possible pathogenetic mechanism.

Spinal cord

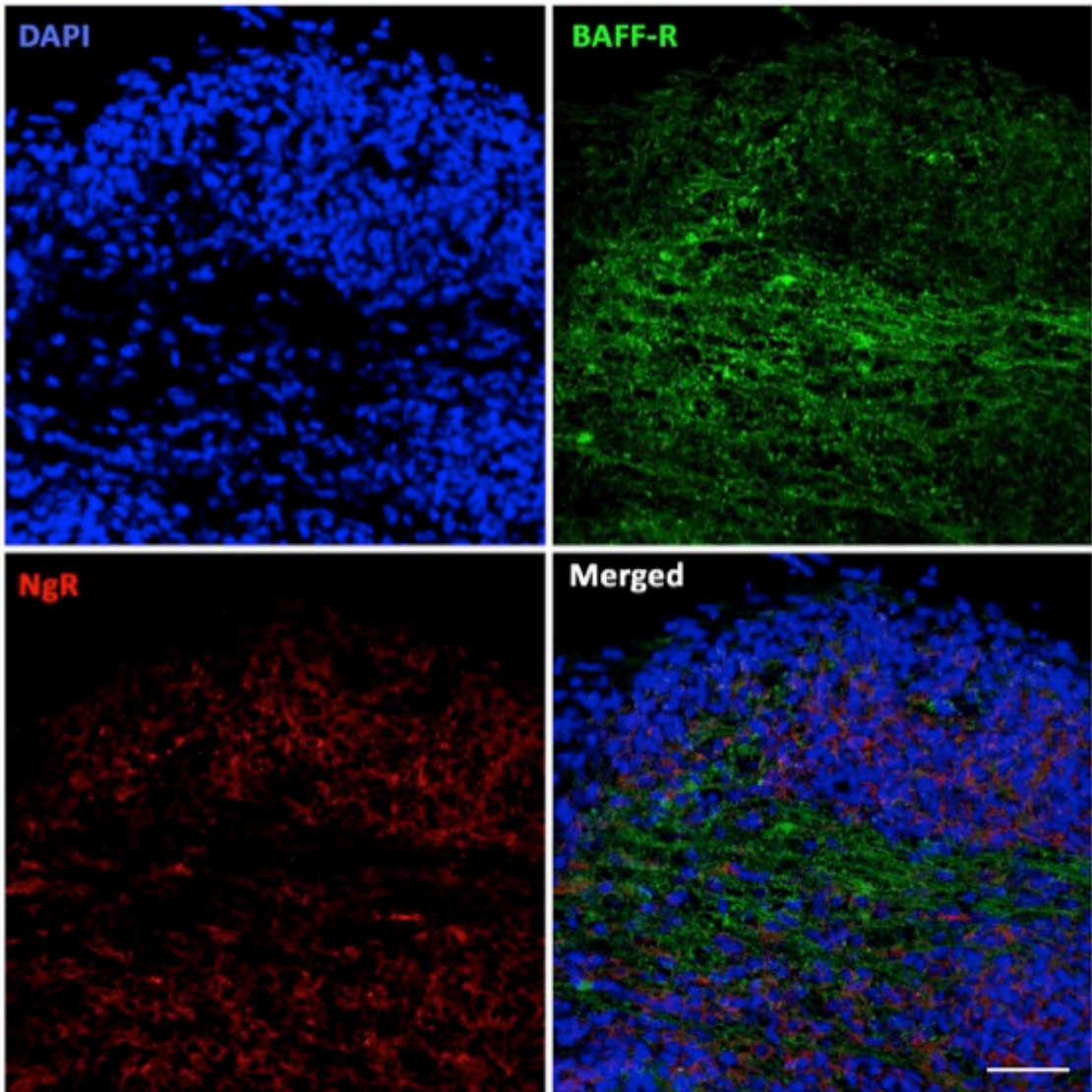


Figure 38. Expression of BAFF-R and NgR on immune cells in the spinal cord of *ngr1*^{+/+} EAE-induced mice at the clinical score 1. A. BAFF-R (green fluorescence) and NgR (red fluorescence) were not co-localised in the spinal cord of *ngr1*^{+/+} EAE-induced mice at disease onset. The nuclei of cells stained with DAPI, Magnification 40x, scale bar= 50 μ m.

Spleen

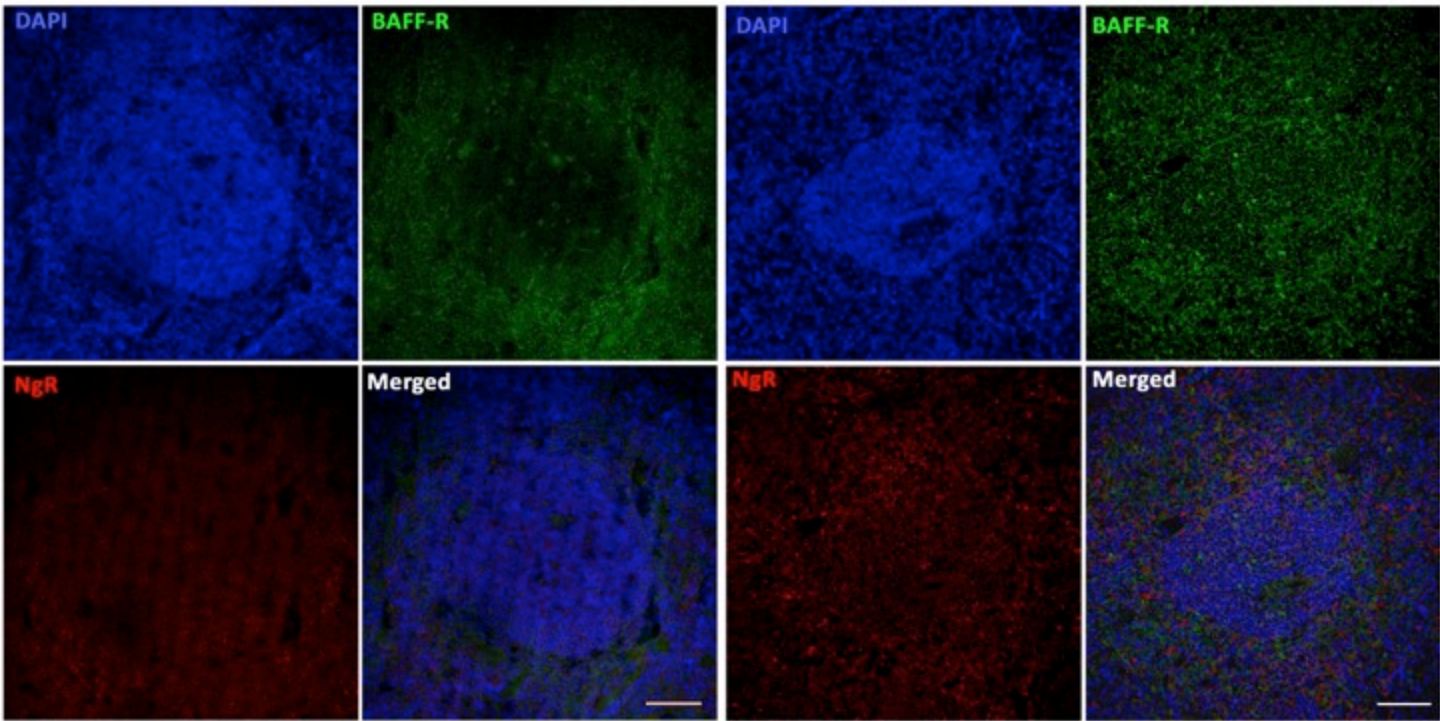


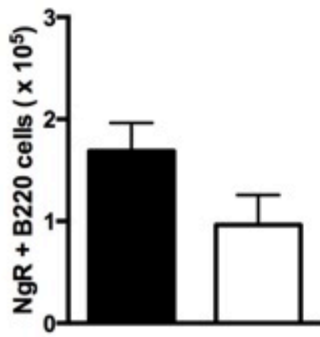
Figure 39. Expression of BAFF-R and NgR on immune cells within follicle in the spleen. **A.** There was not double-positive of BAFF-R and NgR in the spleen of *BAFF*^{-/-} KO mice. **B.** There was occasional double-positive immunostaining of BAFF-R and NgR at the pre-onset. The nuclei of cells stained with DAPI, magnification 40x, scale bar= 50 μm .

4.4 BAFF may play a role in stimulating B-cells that express NgR1 and NgR3 during the disease onset of EAE

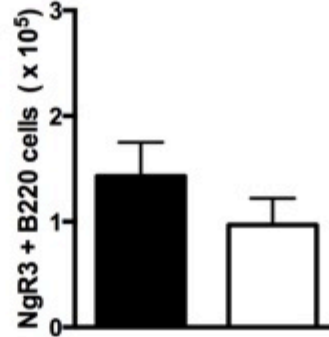
In order to define the physiological activity of BAFF with B-cells expressing NgR1 and NgR3 during the disease onset of EAE, these cells (n=36) were sorted using the BD FACS ARIA or BD Influx sorter at the FLOW core facility (AMREP). Figure 40 demonstrated the number of NgR and B220 positive cells in both the spleen and spinal cord of the *ngr1^{+/+}* (n=26) and *ngr1^{-/-}* mice (n=10). The number of double-positive cells was slightly increased in the spleen of *ngr1^{+/+}* mice compared to the *ngr1^{-/-}* mice (around 2×10^5 and 1.5×10^5 respectively), although this did not reach statistical significance (p=0.4, unpaired student's t-test) (Figure 40A). In addition, there was a significant increase in the number of B-cells expressing NgR1 within the spinal cord of *ngr1^{+/+}* mice compared to *ngr1^{-/-}* mice (0.8×10^5 and 0.2×10^5 respectively) (Figure 40B). However, the number of B-cells expressing NgR3 was almost the same in the spinal cord of *ngr1^{+/+}* mice compared to *ngr1^{-/-}* mice (0.8×10^5 and 0.7×10^5 respectively, p=0.78, unpaired student's t-test) (Figure 40B), suggesting that there may be compensation in the *ngr1^{-/-}* mice with other receptor homologues. Isolated and cultured spinal cord B-cells expressing either NgR1 or NgR3, were shown to form large clusters only seen in the cells of *ngr1^{+/+}* mice compared with those isolated from *ngr1^{-/-}* mice. However, all cells isolated from the spleen did not show similar clumping (Figure 41).

A

Spleen



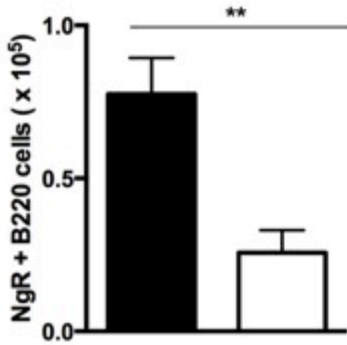
■ *ngr1*^{+/+}
□ *ngr1*^{-/-}



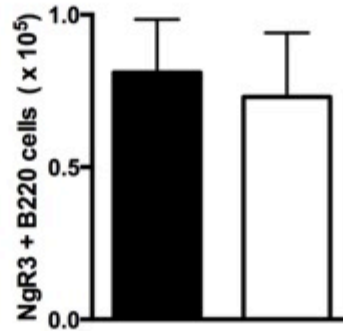
■ *ngr1*^{+/+}
□ *ngr1*^{-/-}

B

Spinal Cord



■ *ngr1*^{+/+}
□ *ngr1*^{-/-}



■ *ngr1*^{+/+}
□ *ngr1*^{-/-}

Figure 40. The number of B-cells expressing NgR1 and NgR3 from either spleen or spinal cord of EAE mice at disease onset. **A.** The number of double-positive cells in the spleen of *ngr1*^{+/+} mice is higher than *ngr1*^{-/-} (p=0.4, unpaired student's t-test). **B.** The number of B220 positive NgR1 in the spinal cord of *ngr1*^{+/+} mice is higher than *ngr1*^{-/-} (** p<0.01, unpaired student's t-test) but there was no significant in the number of B220 positive NgR3 (p=0.78, unpaired student's t-test). Results represent mean ± SEM.

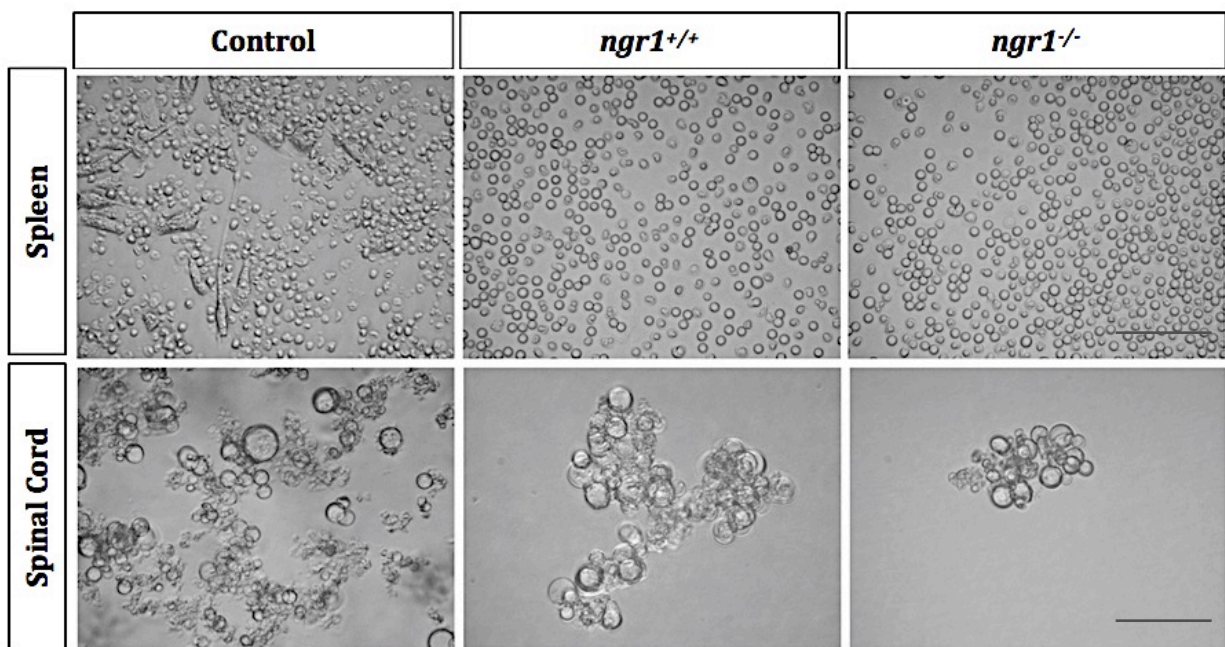


Figure 41. Isolated B-cells expressing NgR from spleen and spinal cord of *ngr1*^{+/+} and *ngr1*^{-/-} mice at clinical score 1. From the spinal cord of *ngr1*^{+/+} mice, these B-cells expressing either NgR1 or NgR3 were clumping together and their morphology was enlarged, comparing to isolates from the spleen. Magnification 40x, scale bar= 50 μ m.

In order to determine the ability of BAFF to stimulate B-cells expressing NgR in the spleen and spinal cord of *ngr1*^{+/+} mice (n=12) at disease onset, these isolated cells were analysed with the presence and absence of BAFF (50 ng/mL) *in vitro*. Interestingly, the stimulation of B-cells positive for either NgR or NgR3 with recombinant BAFF (rBAFF) in the spleen of *ngr1*^{+/+} mice led to a significant increase in DNA synthesis (S phase) (Figure 42A). However, these isolated cells from *ngr1*^{+/+} mice remained in the G0/G1 phase in the absence of BAFF, and no significant differences in the percentage of apoptosis with and without BAFF stimulation (p=0.59, unpaired student's t-test) (Figure 42A). Significantly, these isolated cells also remained in G0/G1 phase from those of the spleens of *ngr1*^{+/+} mice when BAFF activity was blocked by pre-incubating with either rBAFF-R (n=8), or, NgR3-peptide (n=6), or, NgR-Fc (n=6) peptides (Figure 42A). The NgR3 and NgR-Fc peptides were highly efficacious at blocking the cell cycle-dependent BAFF activity (~ 90%) than what could be demonstrated by pre-incubation with rBAFF-R (~ 50%) (Figure 42A). These data may suggest that both NgR1 and NgR3 are active contributory to B-cell maturation during EAE and in fact may contribute to the signal transduction stimulated by BAFF. Furthermore, the apoptosis of these isolated cells, which were blocked with rBAFF-R, increased significantly in *ngr1*^{+/+} mice when compared to isolated cells without BAFF stimulation (Figure 42A). In addition, cells isolated from the spleen of *ngr1*^{-/-} mice also were in S and G2/M phases after stimulation with BAFF but at a lower percentage (~ 60% and 40% respectively) compared to the *ngr1*^{+/+} mice (~ 80% and 20% respectively) (Figure 42B). These data demonstrate that BAFF can stimulate B-cells positive for NgR1 and NgR3 to proliferate, especially those cells that have infiltrated the CNS during EAE of *ngr1*^{+/+} mice, and those isolated cells

were pushed to proliferate and differentiate in *ngr1^{-/-}* mice. Furthermore, there were not any significant differences between the apoptotic phases in the cells isolated from *ngr1^{+/+}* mice compared to those from *ngr1^{-/-}* mice, with and without BAFF stimulation (($p=0.15$ and $p=0.12$ respectively, unpaired student's t-test) (Figure 42B). Moreover, there were significant differences between the G0/G1 and S phases in the cells isolated from *ngr1^{+/+}* mice compared to those from *ngr1^{-/-}* mice ($p<0.05$, $p<0.01$ respectively); double-positive cells were mainly residing in S phase, amongst those isolated from the spleens of *ngr1^{-/-}* mice (Figure 42B).

Stimulation of isolated B-cells From the spinal cord of *ngr1^{+/+}* mice positive for either NgR or NgR3 with rBAFF led to a significant increase in numbers of cells within S phase (Figure 43A). Interestingly, after blocking BAFF activity by either rBAFF-R, or, NgR3-peptide, or, NgR-Fc, double-positive cells isolated from the spinal cord of *ngr1^{+/+}* mice also remained in the G0/G1 phase (~ 50%, ~ 60% and ~ 60% respectively) (Figure 43A). Therefore, these results suggest that blockade of B-cell proliferation can be achieved with either rBAFF-R, NgR3-P and NgR-Fc, with the NgR3 and NgR peptides demonstrating greatest efficacy in modulating the B-cell cycle. However, there was a significant difference in growth G0/G1 (~ 20%) and DNA replication (~ 80%) phases in the B-cell populations isolated from spinal cords of *ngr1^{+/+}* mice after stimulation with BAFF when compared to those cells isolated from *ngr1^{-/-}* mice (~ 50% and ~ 40% respectively) (Figure 43B). Remarkably, the double-positive cells remained in G0/G1 phase (~ 60%) in the spinal cords of *ngr1^{+/+}* and *ngr1^{-/-}* mice in the absence of BAFF (Figure 43B). These data reveal that B-cells expressing NgR1 and its homologue, which have infiltrated the

CNS during EAE of *ngr1*^{+/+} mice, can be stimulated with BAFF to proliferate that may contribute to the signal transduction stimulated by BAFF, although the direct signal transduction effects within these B-cells are yet to be elucidated.

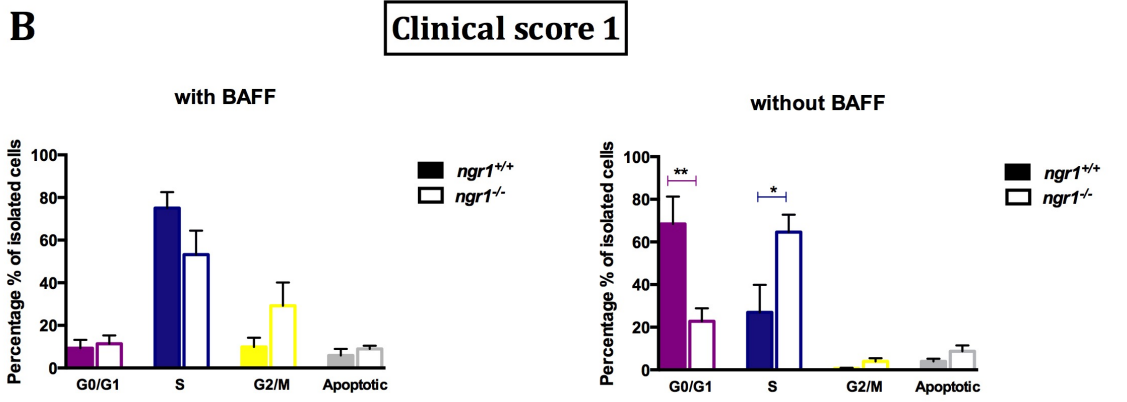
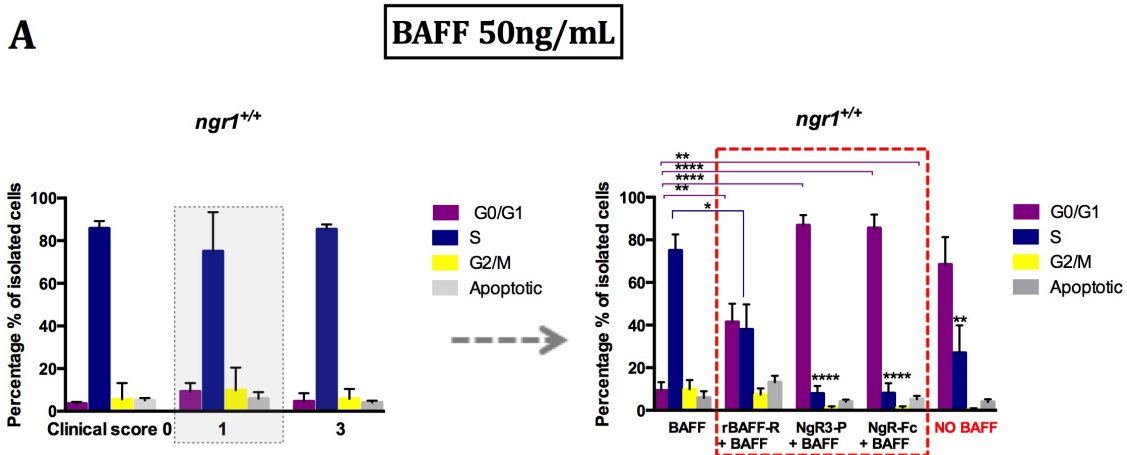
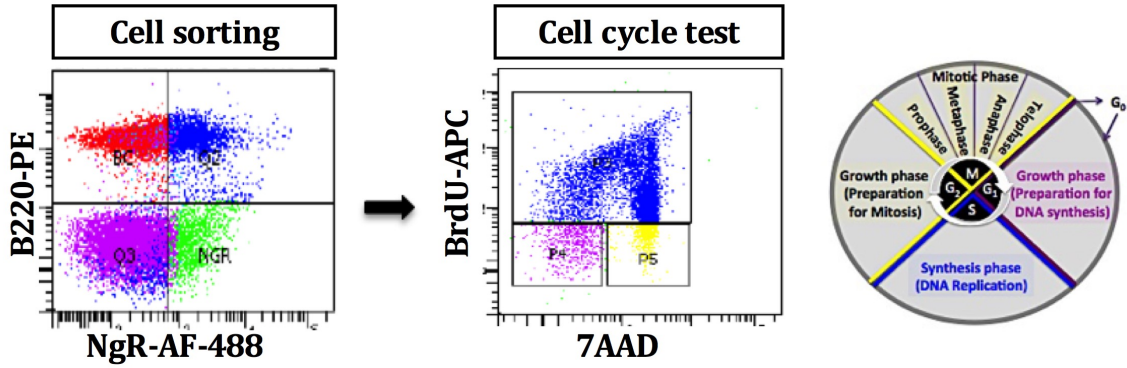
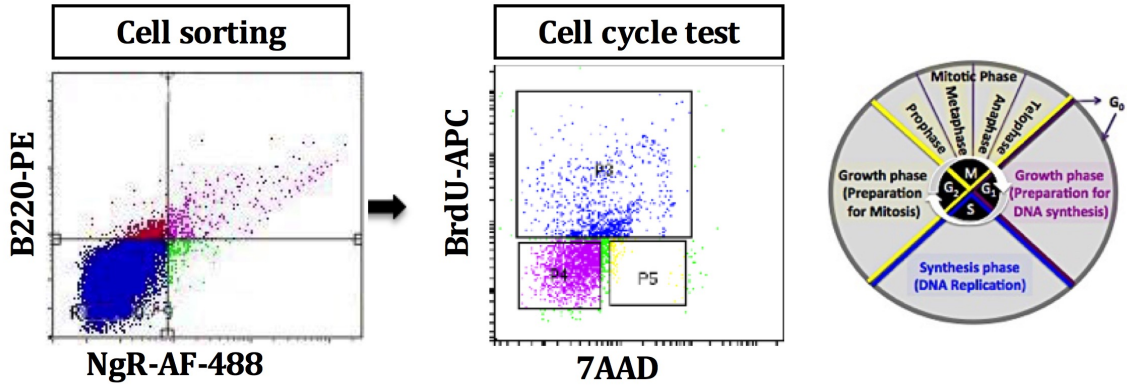
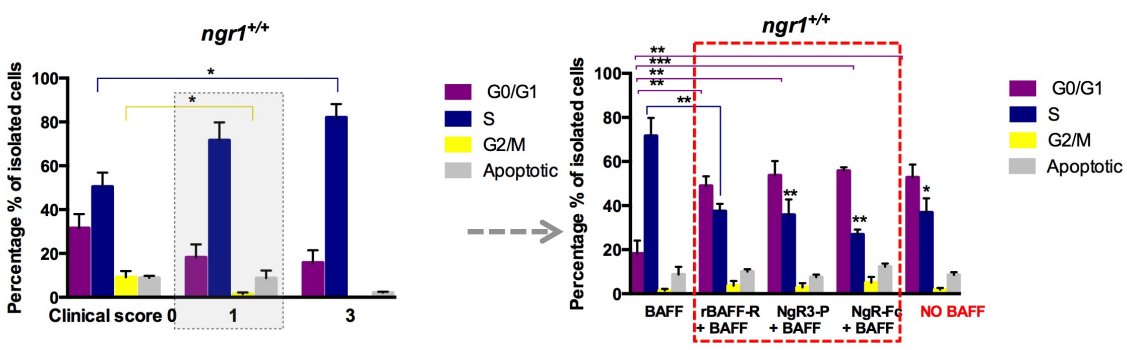


Figure 42. The association of BAFF as a ligand for NgR in the B-cells isolated from spleens of EAE-induced mice at the disease onset, identification and modulation cell cycle events. The double-positive of B220 and NgR population was selected to analyse the cell cycle phases; G0/G1 phase (purple colour), S phase (Blue), G2/M phase (yellow), as well as apoptosis (grey). **A.** Stimulation of B-cells positive for either NgR or NgR3 with exogenous BAFF (50 ng/mL) led to increase in S phase (around 90%) in the spleen of the *ngr1*^{+/+} and *ngr1*^{-/-} mice at clinical score 1. Nevertheless, the cells were observed to drive into G0/G1 phase rather than the S phase, when we blocked BAFF signalling using an excess amount of either rBAFF-R, NgR1-Fc or NgR3-P. **B.** Cells isolated from the spleen of *ngr1*^{-/-} mice were in S and G2/M phases with and without BAFF stimulation compared to the *ngr1*^{+/+} mice. Results represent mean \pm SEM. *p<0.05, ** p<0.01, ****p<0.0001, t-test.



A BAFF 50ng/mL



B Clinical score 1

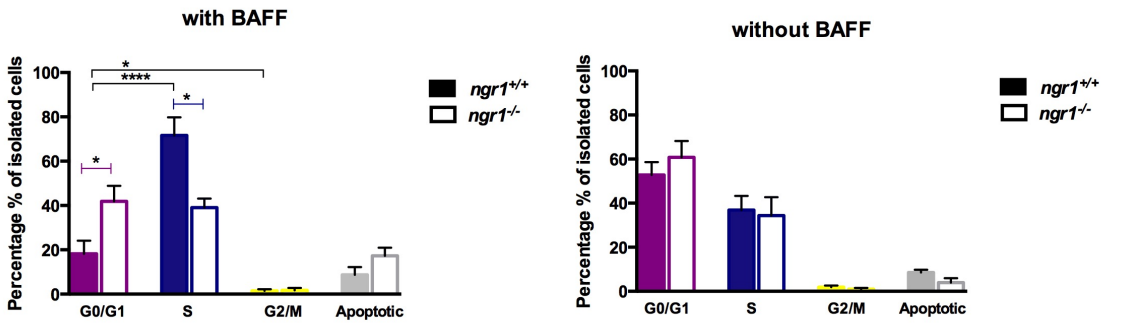


Figure 43. The association of BAFF as a ligand for NgR in the B-cells isolated from spinal cords of EAE-induced mice at clinical score 1, using cell cycle analysis. Flow cytometric analysis showed the gating for the cell cycle phases (G0/G1 (purple colour), S (Blue), G2/M (yellow) phase) of the double-labelling cells (B-cells and NgR). **A.** There was a significant increase in numbers of cells within S phase but after blocking BAFF activity by either rBAFF-R, or, NgR3-peptide, or, NgR-Fc, double-positive cells isolated from the spinal cord of *ngr1*^{+/+} mice remained in the G0/G1 phase. **B.** There was a significant difference in growth G0/G1 and DNA replication phases in *ngr1*^{+/+} mice after stimulation with BAFF when compared to *ngr1*^{-/-} mice. However, the double-positive cells remained in G0/G1 phase in both *ngr1*^{+/+} and *ngr1*^{-/-} mice in the absence of BAFF. Results represent mean ± SEM. *p<0.05, ** p<0.01, ****p<0.0001, t-test.

4.5 Phenotype of immune cells from spleen and spinal cord isolates, during EAE at clinical score 1

In order to identify if the secretory form of the double-labelled cell suspensions (B-cells positive for NgR1 and NgR3) are pathogenic, supernatant from the spleen and spinal cord of *ngr1*^{+/+} and *ngr1*^{-/-} EAE-induced mice at disease onset was collected from sorted and cultured cells before BAFF stimulation and Ig phenotype was examined using ELISA, immunohistochemistry and western blot.

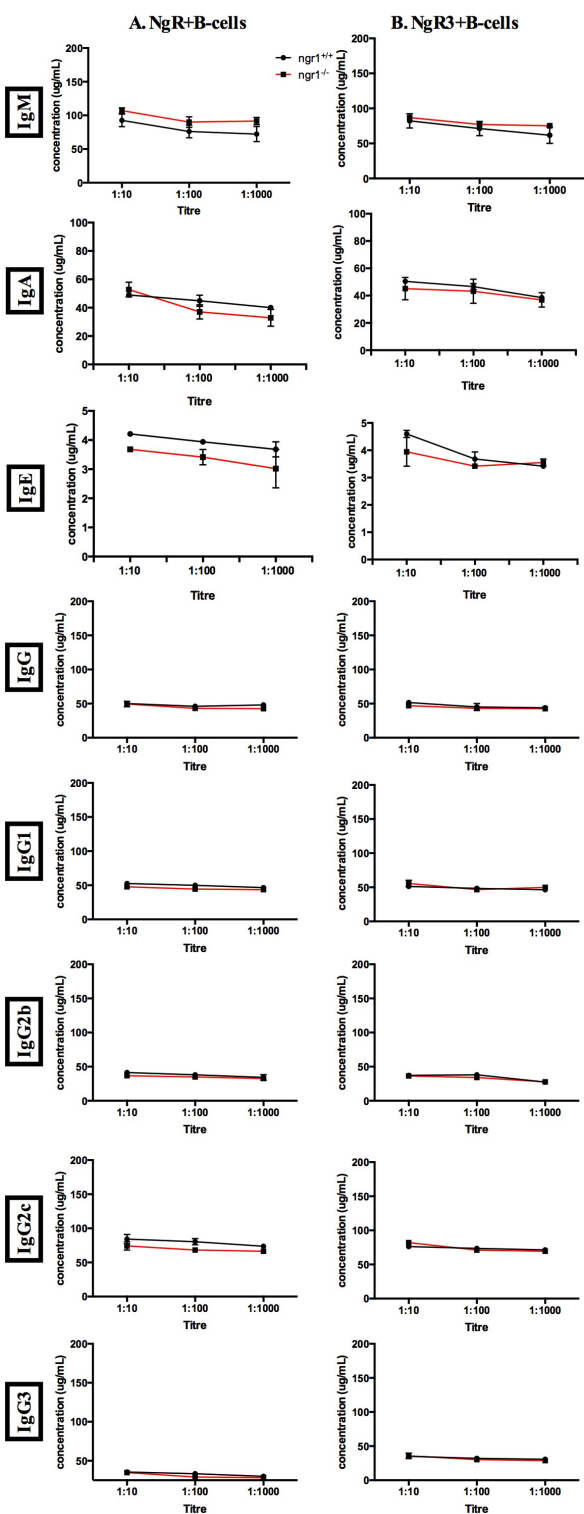
4.5.1 The immunoglobulin response in isolated cells measured by ELISA

As reported in Figure 44, the responses of IgM, IgA, IgE, IgG and IgG subclasses (IgG1, IgG2b, IgG2c and IgG3) were detected in the supernatant of isolated cells from the spleen and spinal cord of *ngr1*^{+/+} and *ngr1*^{-/-} mice at clinical score 1. According to the concentration of control antibodies utilised in a 1:10 titre, IgM, IgG, IgA and IgE responses turned positivity at ~ 90, 50, 50, and 4 µg/mL respectively in spinal cord and ~ 120, 190, 70, and 4 µg/mL respectively in spleen (Figure 44). Furthermore, the distribution of IgG subclasses in the supernatant from the spleen and spinal cord of *ngr1*^{+/+} and *ngr1*^{-/-} mice indicated that B-cells expressing NgR1 and NgR3 produced higher concentrations of specific IgG2c, IgG1, and IgG2b, compared to IgG3. There was a significant difference in these Ig observed between isolated cells (B-cells positive for NgR1) from the spleen of *ngr1*^{+/+} and *ngr1*^{-/-} mice, but no difference was found between B-cells positive for NgR3 from either the spleen or spinal cord of *ngr1*^{+/+} and *ngr1*^{-/-}

mice (Figure 44). These results demonstrated that B-cells expressing NgR produced more IgM, IgG and IgA respectively, and IgG subclasses (IgG2c, IgG1, and IgG2b) as well in the CNS of *ngr1^{+/+}* and *ngr1^{-/-}* mice at clinical score 1. This suggests that IgG subclasses are associated with T_h-response and that T_{h1}-cells help to switch IgG2b and IgG2c while T_{h2}-cells are associated with T_{h2}-cell reactivity (Finkelman et al., 1990). Based on these findings, B-cells expressing NgR1 and NgR3 have the capacity to develop antibody production, suggesting that these B-cell infiltrates are actually maturing B-cells and undergoing a class switch. Taken together, the BAFF responses of these cells has the propensity to stimulate immunoregulatory responses in the B-cell population; however, the contribution to disease immune modulation, and further demyelination and axonal degeneration need to be examined.

Key:
 Black=*ngr1*^{+/+}
 Red=*ngr1*^{-/-}

Spinal cord isolates



Spleen isolates

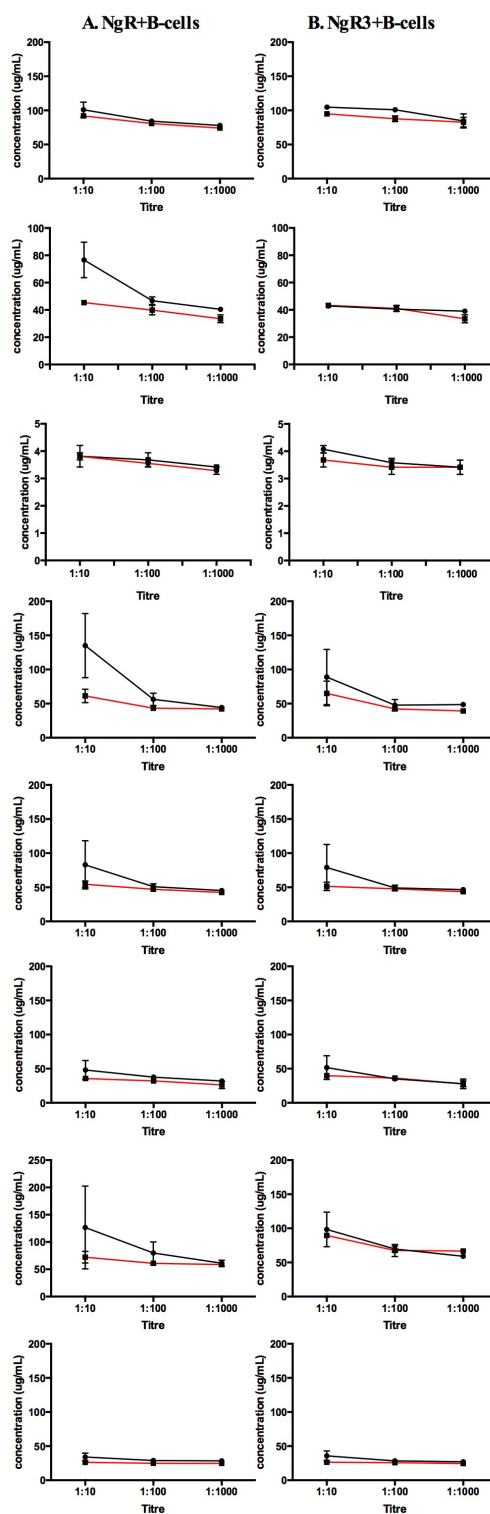


Figure 44. The responses of immunoglobulin in the supernatant of isolated cells from the spleen and spinal cord of *ngr1*^{+/+} and *ngr1*^{-/-} mice at clinical score 1. IgM, IgG, IgA, IgE, IgG1, IgG2b, IgG2c and IgG3 responses are positive at 1:10 titre. However, B-cells expressing NgR produced more IgM, IgG and IgA respectively, and IgG2c, IgG1, and IgG2b in the supernatant of isolated cells. Results represent mean ± SEM.

4.5.2 The immunoglobulin localisation detected by IHC

In order to elucidate the potential localisation of secretory IgG and IgM in supernatant from isolated cells (B-cells positive for either NgR1 or NgR3), immunostaining was performed within the spinal cord and optic nerve tissues of the *ngr1*^{+/+} mice (control). Figures 45 and 46 illustrate a cluster of cells positive for IgG in the spinal cord and optic nerve tissues of the *ngr1*^{+/+} mice, suggesting that these cells are oligodendrocytes from their morphological appearance. This cell type, which has the ability to differentiate into astrocytes and neurons, is reactive in EAE demyelination lesions in the spinal cord (Reynolds et al., 2002) and cerebral cortex (Di Bello et al., 1999, Girolamo et al., 2011). Moreover, isolated cells were positive for IgM within the optic nerve tissue of the *ngr1*^{+/+} mice as well (Figure 47). Recently, Sádaba *et al.* (2012) demonstrated that IgG and IgM co-localised on oligodendrocytes in MS lesions, suggested that they can induce axonal injury, causing disability in MS (Sadaba et al., 2012). As consequence of this staining, Nogo-A, which is an oligodendroglial component, was used in the same tissues to identify and confirm IgG localisation. As showed in Figure 48, Nogo-A was positive for the secretory form of IgG in the supernatant from isolated cells from the spinal cord tissues of *ngr1*^{+/+} mice. The white arrow indicates the presence of macrophages/microglia (morphological appearance), which are positive to IgG. Interestingly, IgG immunoreactivity (green) and Nogo-A immunoreactivity (red) were detected at paranodal myelin, where macrophages commonly induce myelin stripping, within the spinal cord tissues of *ngr1*^{+/+} mice (white arrow; Figure 49). This result demonstrates that isolated cells and Nogo-A may be enriched in the paranode region and are components of the

paranodal protein complex that may play a role in the degradation of the myelin sheath in demyelinating disease. Consistent with this, it has been found that Nogo-A is localised to paranodes, where it interacts with the paranodal junction of myelin and is distributed at the interface between oligodendrocytes and neurons (Nie et al., 2003). However, further qualifications of oligodendrocytes, macrophages/microglia and paranode junction are required by using NG2, Iba1 and caspr markers respectively.

Supernatant from spleen isolates

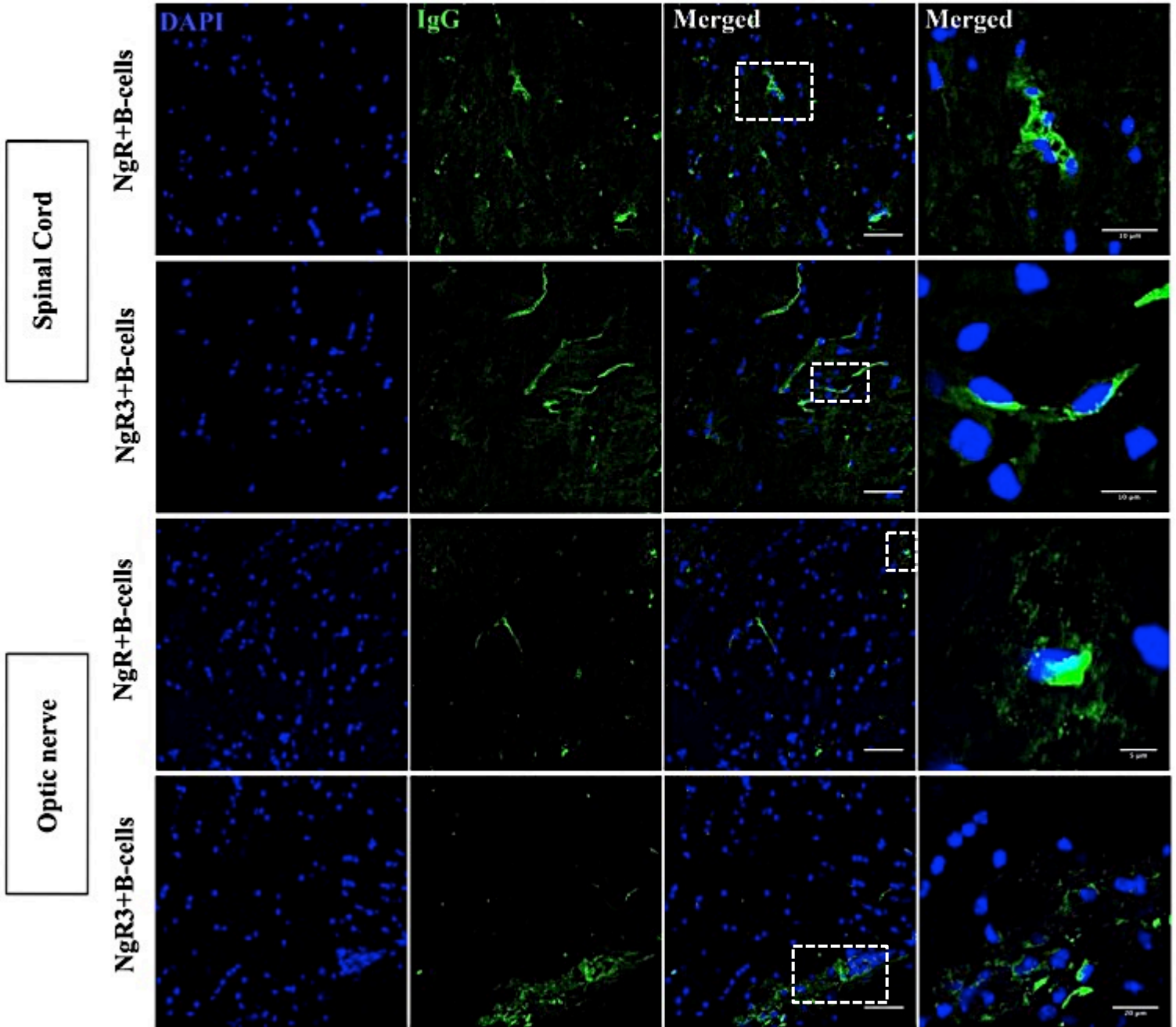


Figure 45. Immunostaining of secretory IgG in the supernatant from isolated cells (B-cells positive for either NgR1 or NgR3) from the spleen of *ngr1*^{+/+} mice. A cluster of oligodendrocytes positive for IgG presented in the lateral white matter of spinal cord and optic nerve tissues of the *ngr1*^{+/+} mice. The nuclei of cells stained with DAPI, magnification 40x, scale bar= 50 μ m, 10 μ m, and 5 μ m.

Supernatant from Spinal cord isolates

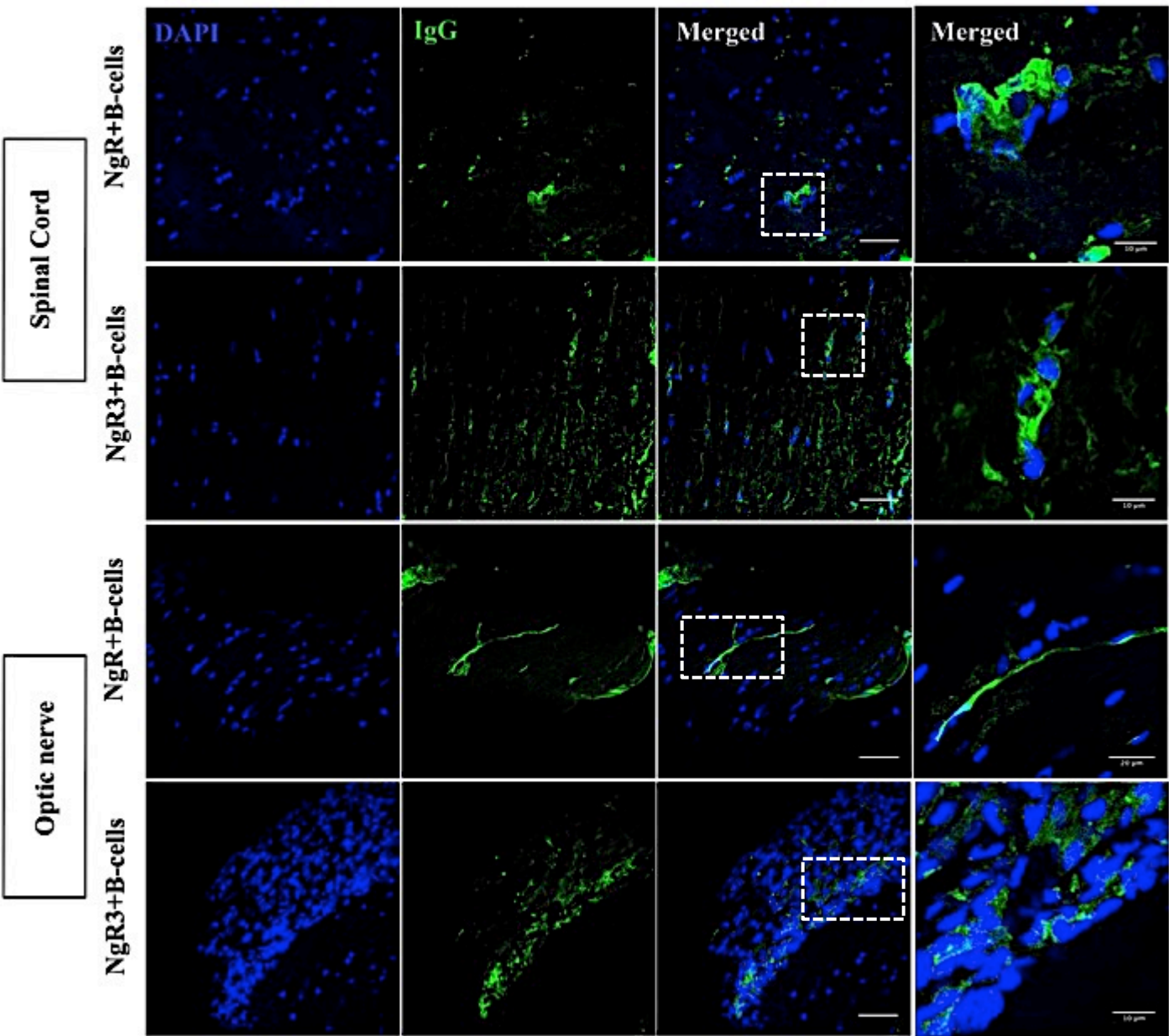


Figure 46. Immunostaining of secretory IgG in the supernatant from spinal cord isolates within the spinal cord and optic nerve tissues of the *ngr1*^{+/+} mice (control).

There was a cluster of cells positive for IgG presented in the spinal cord and optic nerve tissues of the *ngr1*^{+/+} mice. The nuclei of cells stained with DAPI, magnification 40x, scale bar= 50 μm , 10 μm , and 5 μm .

Supernatant from spinal cord isolates

Optic nerve

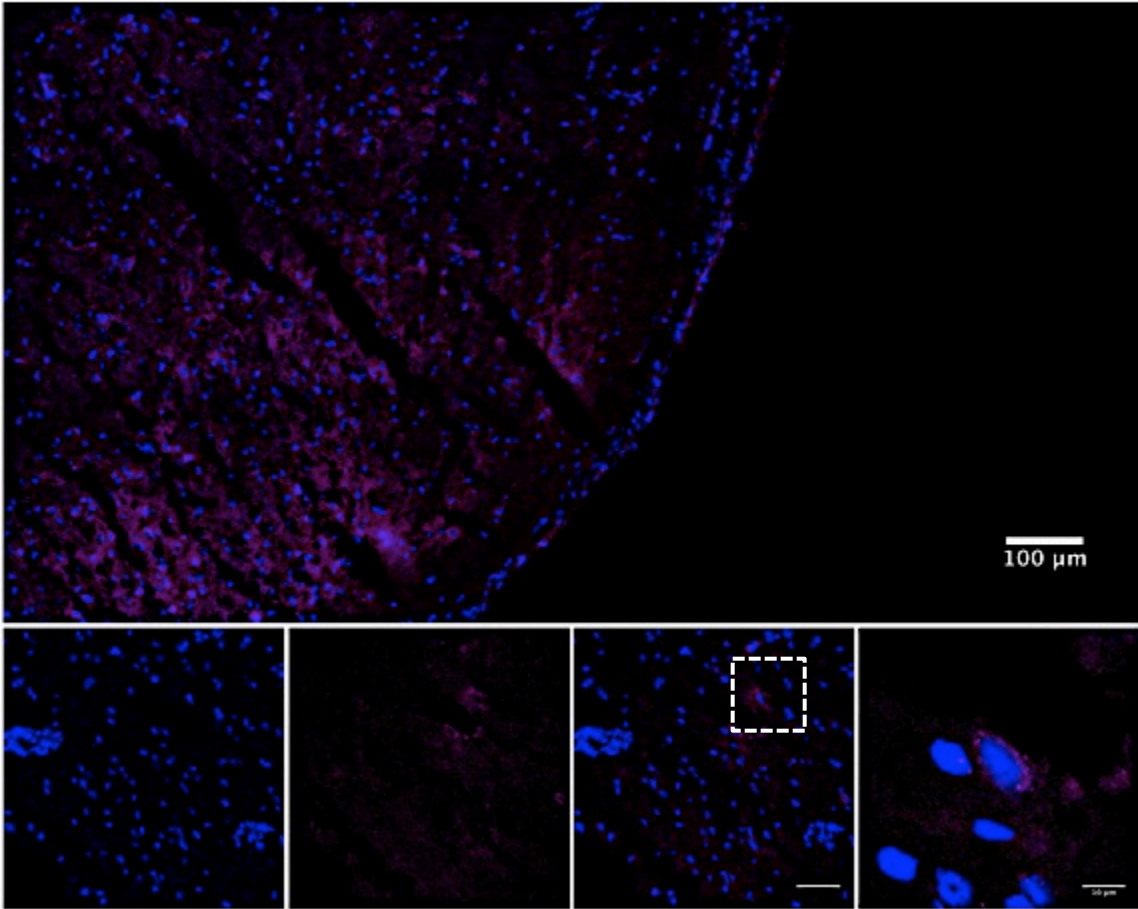


Figure 47. Immunostaining of IgM in the supernatant from spinal cord isolates within the optic nerve tissues of the *ngr1*^{+/+} mice (control). Supernatant from isolated cells was positive for IgM. The nuclei of cells stained with DAPI, magnification 40x. scale bar= 100 μm, 50 μm, and 10 μm.

Supernatant from Spinal cord isolates

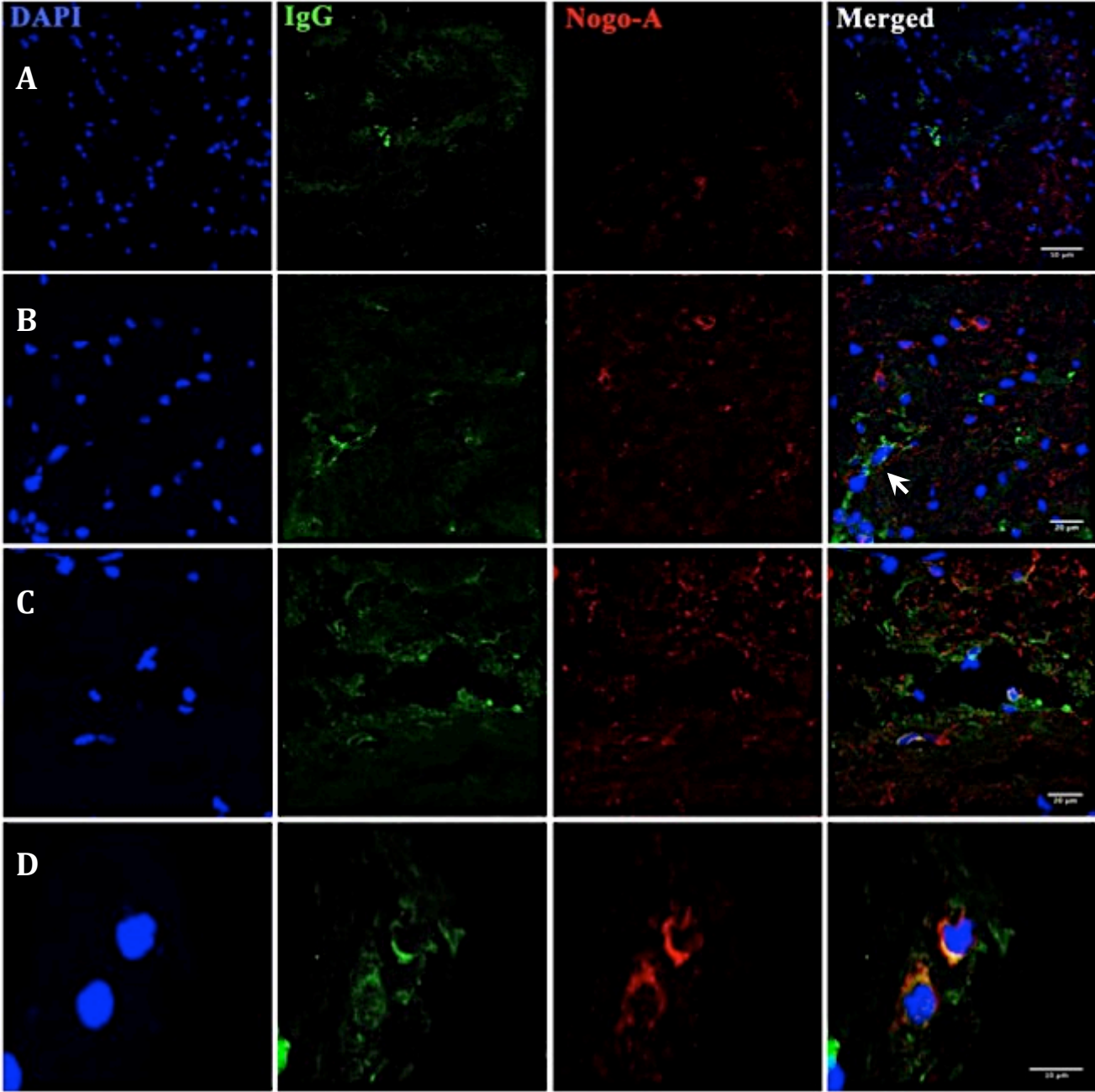


Figure 48. Immunostaining of Nogo-A and IgG from the supernatant of spinal cord isolated cells within the spinal cord tissue of the *ngr1*^{+/+} mice. **A.** Nogo-A was expressed in a red fluorescence and IgG was expressed in a green fluorescence within the tissue and the nuclei of cells stained with DAPI. **B.** Double-positive immunostaining of macrophage/microglia and IgG (white arrow). **C.D.** Double-labelling of Nogo-A and IgG in the spinal cord tissue. Magnification 40x, scale bar= 50 μm , 20 μm , and 10 μm .

Supernatant from Spinal cord isolates

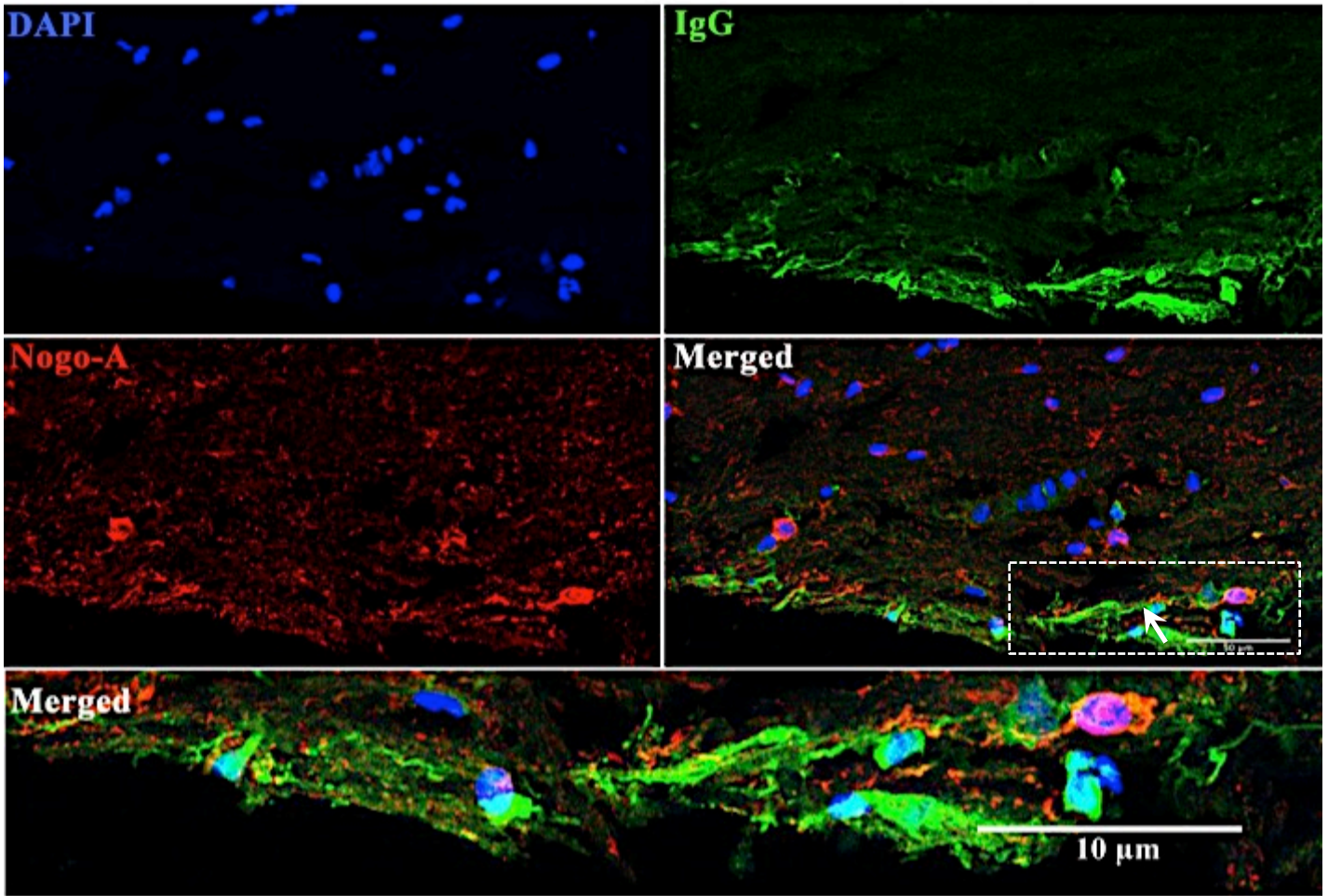


Figure 49. Immunostaining of Nogo-A and IgG from the supernatant of spinal cord isolated cells within the spinal cord tissue of the *ngr1*^{+/+} mice. IgG (green fluorescence) and Nogo-A (red fluorescence) were presented at paranodal region (white arrow). The nuclei of cells stained with DAPI. Magnification 40x, unlabelled scale bar = 50 μ m.

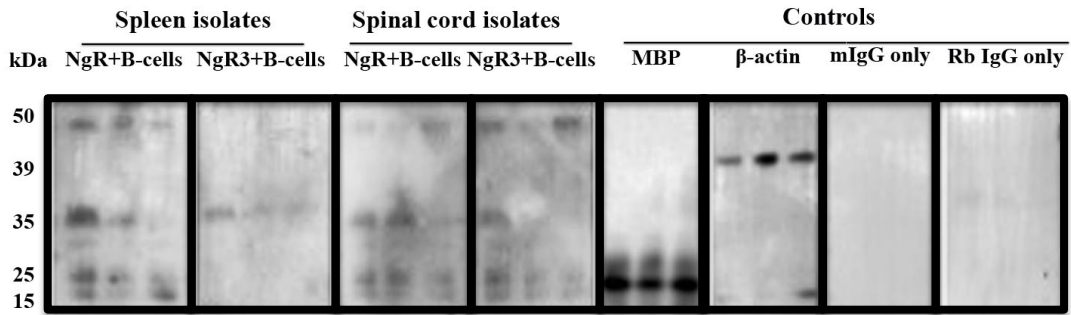
4.5.3 The immunoglobulin response against myelin

The ability of these isolates to bind to the myelin of naïve *ngr1*^{+/+} mice (n=3) was also examined. Our results indicated that IgG from isolated cells from either the spleen or spinal cord of *ngr1*^{+/+} mice at clinical score 1 could bind directly to myelin (Figure 50A). The myelin also reacted strongly with MBP (the positive control; Figure 50A). MBP is the most abundant protein component of the myelin membrane in the CNS (Lemke, 1988). Along with this, there were no immunoreactive bands detected for naïve *ngr1*^{+/+} mice, either in the spleen or spinal cord when secondary antibodies were used as negative controls (Figure 50A). Figure 50B showed silver stain, which used as positive control to visualised myelin proteins. These results highlight that our secretory form of IgG from isolated cells bound directly to myelin that evidence of actively persuade to promote demyelination.

W. Blot: supernatant from either spleen or spinal cord isolates of EAE-induce at clinical score 1

Myelin from *ngr1*^{+/+}

A



B

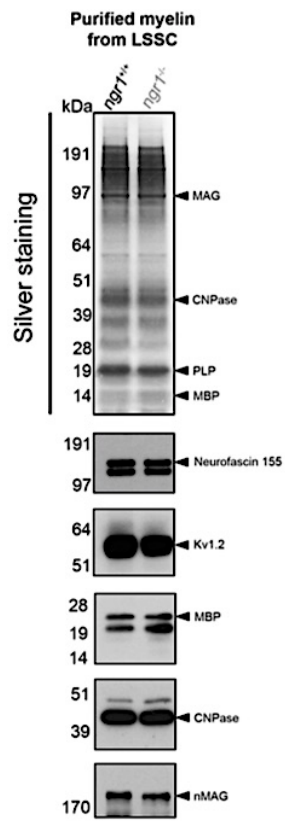


Figure 50. Immunoblot analysis of secretory IgG in the supernatant from isolated cells. Purified myelin from lumbo-sacral spinal cord of *ngr1*^{+/+} and *ngr1*^{-/-} were differentiated one-dimensionally on a 4-12% Bis-Tris gel using a MOPs buffer system. **A.** IgG presented in supernatant diluted 1:10 could bind directly to myelin lysate of naïve *ngr1*^{+/+} mice, which also reacted strongly with MBP. The three lanes per box are replicates. No immunoreactive bands detected when secondary antibodies were used as negative controls. **B.** Proteins were visualized by silver staining. Bands consisted of major myelin proteins, which are annotated. Representative immunoblot using anti-MBP, anti-Neurofascin 155, anti- CNPase, anti-Kv1.2, and anti-nMAG were shown.

4.6 Discussion

This study aimed to outline whether BAFF is a potential ligand for NgR during EAE onset and how it relates to B-cell physiology that may be NgR-dependent. The experiments outlined in chapter 4 have identified that BAFF can stimulate B-cells that express NgR1 and NgR3 demonstrated through *in vitro* analysis. Co-localisation of BAFF and NgR1 was identified in FLS at the meninges of the spinal cord of *ngr1^{+/+}* mice following EAE induction at the disease onset. As a consequence, it was hypothesised that these B-cells may be involved in the pathogenesis of inflammatory-mediated damage to neural tissue during EAE. These data are consistent with our finding from chapter 3 that B-cells expressing NgR1 are aggregated and presented at the meninges of the spinal cord of *ngr1^{+/+}* EAE-induced mice at the disease onset and may support the hypothesis that NgR is an alternate ligand. Our investigations of EAE-induced mice uncovered that, B-cells expressing NgR were present within the white pulp in the spleens of *ngr1^{+/+}* EAE-induced mice at the disease onset. Along with this, we found that the spleen of the BAFF^{-/-} mice showed only occasional NgR expressions cells in the spleen of BAFF^{-/-} mice. It is of importance that BAFF^{-/-} mice lack the capacity to autoimmunity (Schiemann et al., 2001, Zhou et al., 2011). Therefore, the potential loss of BAFF may lead to the down regulation of a BAFF-R and NgR dependent response. Recently, Kim *et al.* (2011) found that the number of mature B-cells decreased significantly and antibody production was impaired in BAFF-R^{-/-} mice, suggesting that the effect of BAFF on the survival of B-cells can be arbitrated through BAFF-R. Thus, it can be concluded that there is a potential role for BAFF-R to mediate its effect on T-cell regulation and macrophage function in EAE

that has been immunised with MOG₃₅₋₅₅. This occurs independently of mature B-cells through the generation of high levels of BAFF, which may act through other receptors to promote the responses of pro-inflammatory T-cells and macrophages in MS. Taken together, these data may suggest that BAFF has a prominent affect when NgR is expressed on pathogenic B-cells.

The most profound effects of BAFF upon NgR-expressing B-cells were identified during cell cycle analysis of isolated cultured cells. We found that upon rBAFF stimulation of the B-cell cultures, from either the spleens or spinal cords of EAE-induced mice, enhanced their DNA synthesis stage, suggesting it sent the cells into proliferation. Remarkably, when we blocked BAFF signalling *in vitro* using either rBAFF-R or NgR1-Fc or NgR3-P, the cells were observed to be primarily driven into G0/G1 phase (resting phase) rather than the S phase (DNA replication), suggesting that these peptides can effectively limit B-cell BAFF-dependent proliferation. Importantly, these findings suggest for the first time that there is an interaction of BAFF with NgR1 and NgR3 during EAE at the disease onset, especially in B-cells, although the direct signal transduction effects within these B-cells are yet to be elucidated. In agreement with our results, it has been suggested that BAFF, which is a signalling molecule on B-cells that potentiate the proliferation and differentiation of this population of lymphocytes, is highly expressed in FLS during EAE and may potentiate neuronal tissue damage. However, this needs to be investigated. The data presented in chapter 4 may provide a platform to determine how the expression of NgR1 and NgR3 in conjunction with BAFF in B-cells localised within the CNS during EAE, can further potentiate

neurodegeneration. Therefore, using either NgR1-Fc or NgR3-P or rBAFF-R peptides as potential biological disease modifying agents may be a viable therapeutic approach to be trialled in MS.

Beside the important role of BAFF on B-cells expressing NgR in EAE, it will be crucial to identify the biological consequences of secretory immunoglobulin and its participation in the effector function leading to demyelination. Since 1992, the roles of B-cells and antibodies in the immunoregulation and induction of EAE has been demonstrated (Myers et al., 1992). Interestingly with a direct relevant to our study, this study included an exceptional series of experiments that demonstrated the pathogenicity of the secretory form of double-labelled cell suspensions from the spleen and spinal cord of EAE-induced mice at disease onset by measuring Ig phenotype, using ELISA, immunohistochemistry and western blot analysis. We previously identified IgM, IgG and IgD on the surface of B-cells expressing NgR, which is discussed in chapter 3, but now we identified the secretory form of the supernatant. Our results demonstrated that these supernatants produced more IgM, IgG, IgA and IgE respectively, and IgG2c, IgG1, IgG2b and IgG3 in the CNS of *ngr1^{+/+}* and *ngr1^{-/-}* mice at clinical score 1. On the basis of these findings, B-cells expressing NgR1 and NgR3 have the capacity to develop antibody production, suggesting that these B-cell infiltrates are maturing B-cells and undergo class switching. Regarding B-cells undergoing a class switch, IgG2b switching is associated with the severity of EAE-induced by MOG₃₅₋₅₅ in non-obese diabetic mice, while other types of Ig (IgM, IgA, IgG1, IgG2a and IgG3) do not seem to influence the severity of EAE (Ichikawa et al., 1999), suggesting that IgG subclasses are associated with T_h-response

that T_{h1}-cells help to switch IgG2b and IgG2c but T_{h2}-cells are associated with T_{h2}-cell reactivity (Finkelman et al., 1990). Additionally, the role of IgG in the destruction of tissue components has been suggested in MS patients investigated by identifying demyelination and axonopathic IgG from patient sera, observing complement activation and Ig deposition in CNS tissue with subsequent successful plasma exchange in patient subsets with high titres (Keegan et al., 2005, Dau, 1995). Oligoclonal bands are present in CSF, in combination with elevated intrathecal IgG production, in around 90% of MS patients at the first clinical event, and approximately 40% of patients demonstrate oligoclonal IgM (Villar et al., 2010, Krumbholz et al., 2012). In fact, Villar *et al.* (2010) reported that B-cells responsible for the secretion of intrathecal IgM in MS may be related to the aggressive course of MS. Therefore, both the clinicopathological picture from MS patients and fundamental scientific data generated from animal models advocate a central role for antibody-dependent neurodegeneration during progressive MS, and during trials, this may now be directed to limit B-cell/antibody-dependent neural damage. In addition, BAFF has been reported to induce IgA switching in human B-cells, demonstrating that elevated levels of BAFF leads to the B-cell maturation, which subsequently causes IgA class switching in mixed connective tissue diseases complicated by intestinal lung disease (Kaneko et al., 2014). Taken together, BAFF responsive B-cells expressing NgR1 and NgR3 has the propensity to stimulate immunoregulatory responses in B-cell populations; however, their contribution to the disease immunomodulatory effect during disease, and further demyelination and axonal degeneration need to be elucidated.

As a consequence, immunostaining of these supernatants in the spinal cord and optic nerve tissues of *ngr1^{+/+}* mice has revealed a cluster of cells immunolabelled for bound IgG and IgM, with morphological appearance of oligodendrocytes and Nogo-A co-labelled confirmed this. Consistently, it has been reported that IgG and IgM are co-localised on oligodendrocytes in MS lesions, which suggests that they can propagate axonal injury following their death or dystrophy, causing disability in MS (Sadaba et al., 2012). As already stated, the current study detected IgG and Nogo-A immunoreactivity at paranodal myelin within the spinal cord tissue of *ngr1^{+/+}* mice, which agrees with a study by Nie *et al.* (2003) that found Nogo-A to be localised to paranodes, where it interacts with the paranodal junction of myelin and is distributed at the interface between oligodendrocytes and neurons (Nie et al., 2003). These results indicate that IgG from isolated cells from either the spleen or spinal cord of *ngr1^{+/+}* mice at clinical score 1 bind directly to myelin, which reacts strongly with MBP (as positive control). The results of this study reveal that the secretory form of IgG from isolated cells bound directly to myelin and may be evidence of active promotion of antibody-mediated demyelination. However, further markers (e.g NG2, Iba1 and caspr) are required to confirm the results. In the next chapter, NgR1-specific ligand will be targeted using a novel HSC-based delivery of a therapeutic protein as a means of limiting the immune-mediated degeneration of axons in EAE.

**CHAPTER 5: Transplantation of genetically modified HSCs to
deliver the therapeutic NgR(310)-Fc protein into the active
demyelinating lesion.**

5.1 Introduction

Currently there is no cure for MS, however a number of therapeutic agents are being used to treat specific symptoms and sequelae of the disease, with most designed to prevent relapse rates thereby potentially limiting the progression to disability, ostensibly by targeting immune activation and inflammation (Fassas and Mancardi, 2008). NgR may play a role in the modulation of the adaptive immune response during the progression of EAE in the maturation and differentiation of B-cells within follicles that are localized within the CNS due to the fact that NgR1 has an effect on the immune cells behaviour, as well as its role in preventing axonal regrowth. Several studies demonstrated that NgR1 can be expressed on circulating immune cells from MS demyelinating lesions and it has the ability to change the motility of these cells exposed to myelin (as substrate), demonstrating that it may impact on immune cell infiltration and migration, and/or modulating adherence through an alternate signalling mechanism may play a role in driving neuroinflammation (Pool et al., 2009, David et al., 2008, Fry et al., 2007). Additionally, it has been illustrated that BAFF interacts with NgR1 to inhibit dorsal root ganglion neuron outgrowth *in vitro*, thereby signalling independently of the putative MAIFs cascade (Zhang et al., 2009). Nevertheless, the physiological mechanisms and its role on immune cells are yet to be illuminated. However, we identified that NgR1 localised on B-cells may interact with BAFF on neighbouring B-cells within a follicular structure stimulating their development, thereby propagating the neurodegenerative disease through the development of immunocompetent B-cells that target neural autoantigens. Therefore, blockade of NgR1-ligand signalling is considered one such

promising approach. NgR1-specific ligand has targeted using a novel HSC-based delivery of a therapeutic protein because differentiated HSCs have the ability to cross the BBB and still produce consistent protein levels making them attractive vehicles for novel EAE/MS therapy. Consequently, the Nogo-receptor ectodomain fused to the mouse Fc peptide of IgG1 (NgR(310)-Fc), which was designed by the Strittmatter group (Li et al., 2004), was utilised as a means of limiting the immune-mediated degeneration of axons in a MS model. Given that studies using the NgR(310)ecto-Fc have recently shown enhanced neurological improvement in injury and disease models of the CNS by blocking the binding of the MAIFs (Wang et al., 2006b, Li et al., 2004, Lee et al., 2004). It is now imperative to attempt a similar therapeutic regime within the CNS active neuroinflammatory lesions of EAE-induced mice (Figure 51). Furthermore, through the utility of lentiviral transduced HSCs, we investigated whether the NgR1-Fc can possibly be a therapeutic approach for the inactivation of BAFF signalling in B-cells localised in spinal cord, along with limiting degeneration and inflammatory demyelination during EAE.

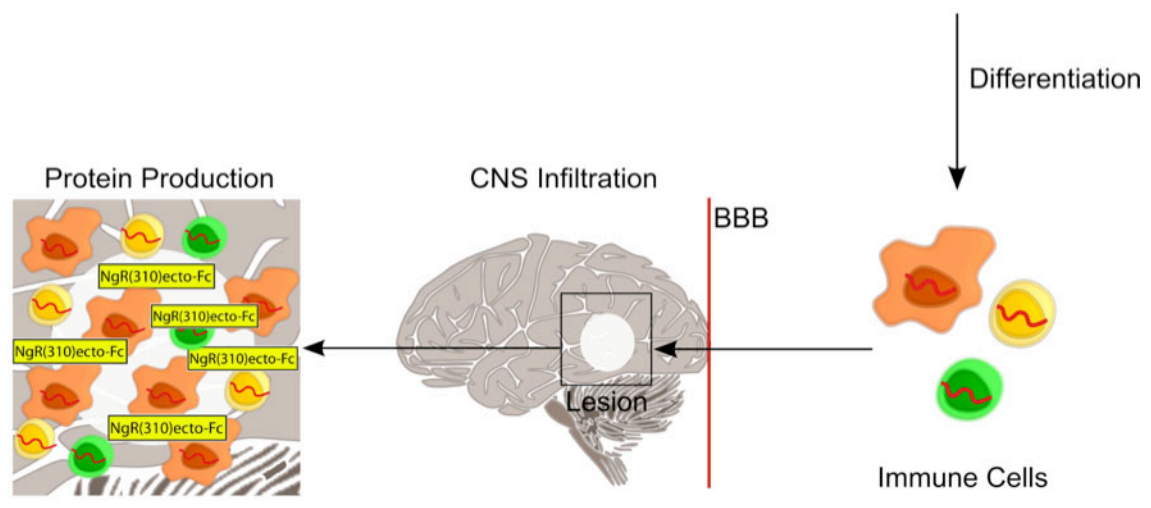
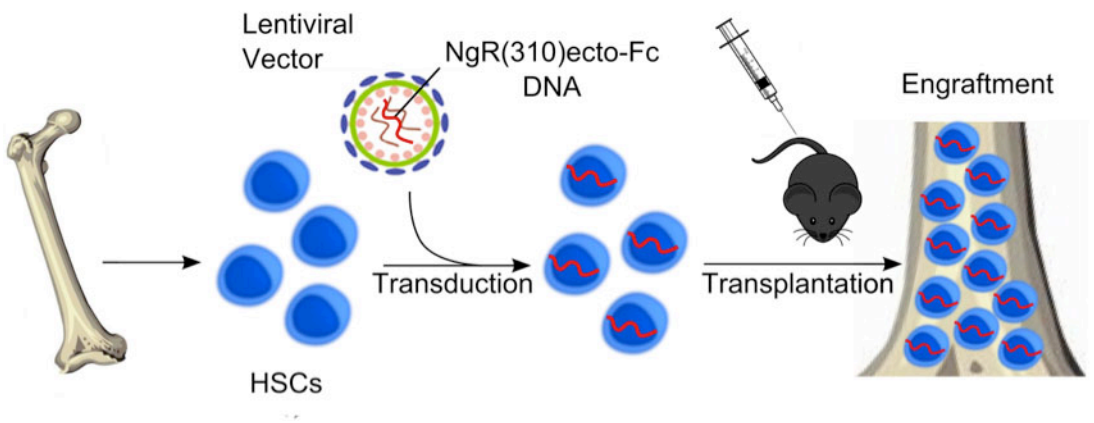


Figure 51. **Haematopoietic stem cell transplantation paradigm in EAE.** Insertion of NgR(310)ecto-Fc DNA into mouse HSCs followed by transplantation may lead to differentiation of immune cells carrying NgR(310)ecto-Fc, migrating via blood brain barrier and localising within the EAE lesions, where they can produce the NgR(310)ecto-Fc therapeutic fusion protein.

5.2 Production of lentivirus

The production of LV vectors was the main step in developing a successful transplant paradigm. pLVX-EF1 α -NgR(310)-Fc-IRES-ZsGreen1 vector, which produced in 293T cells, were subsequently quantified and tested through HeLa cells transduction. Initially, HeLa cells showed *Zoanthus sp.* Green1 fluorescent protein (ZsGreen) expression sequence under fluorescent confocal microscope, after collecting supernatant from the transfection and a neat sample used to transduce HeLa cells (Figure 52A and B). The expression of ZsGreen is controlled by an internal ribosomal entry site (IRES). This result confirmed the fact that the LV vectors are capable of transducing mammalian cell lines, however, we could not perform a successful titration using viral supernatant. Therefore, the LV was concentrated by ultracentrifugation in further experiments. Our flow cytometric analysis of concentrated LV demonstrated successful transduction of mammalian cells with sufficient efficiency to perform a titration, which showed the empty vector to have much higher concentration than the NgR(310)ecto-Fc vector at 1.5×10^6 versus 1.9×10^5 particles per μL respectively (Figure 52C). These results suggest that concentrated LV vectors have successfully transduced of mammalian cells at acceptable efficiency, and their use will be validated in the subsequent transplantation experiments.

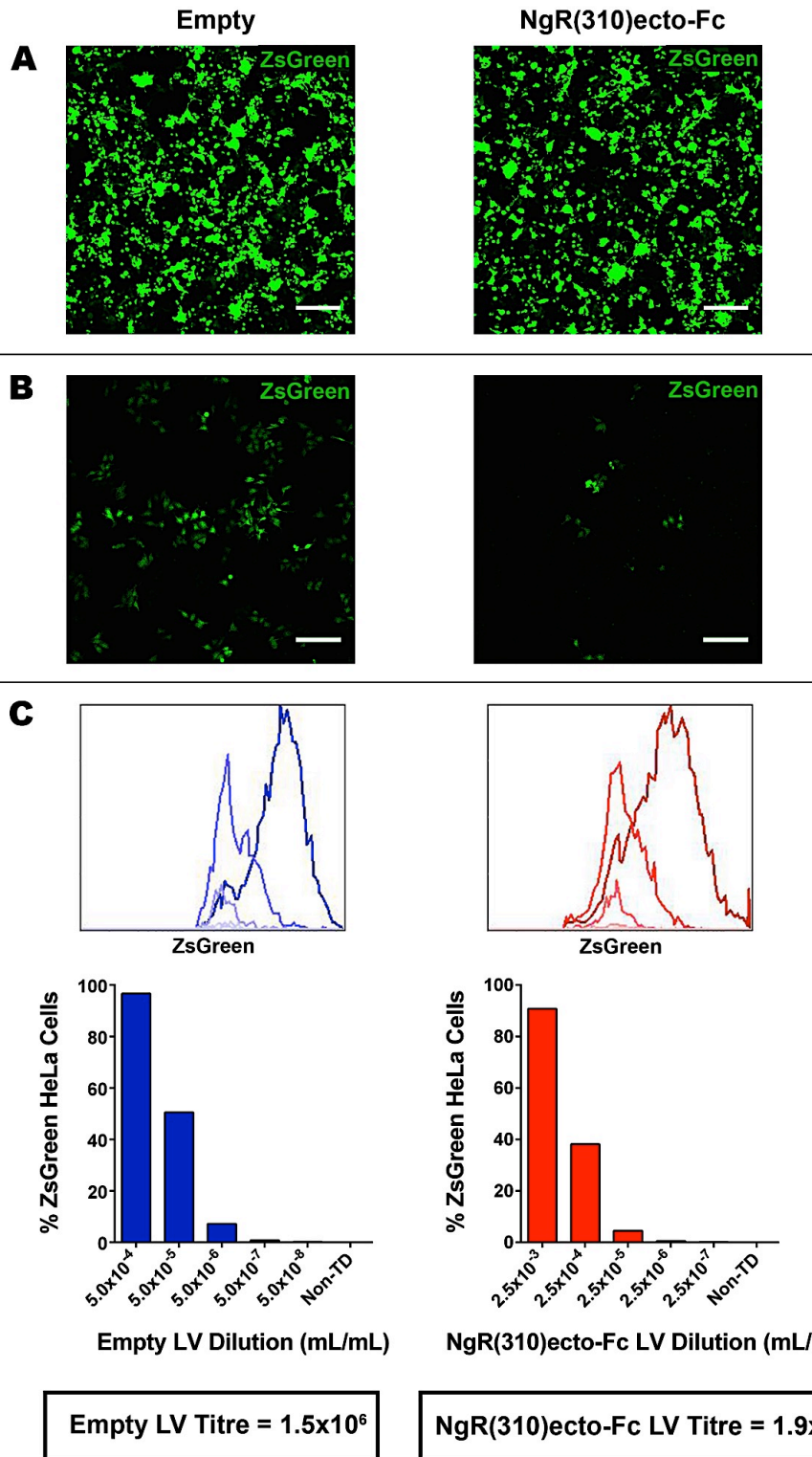


Figure 52. Lentiviral vector production and quantification. **A.** ZsGreen positive 293T cells 72 hours post-transfection with either pLVX (empty) or pLVXNgR(310)ecto-Fc-myc plasmids, magnification 10x, scale bar = 200 μ m. **B.** ZsGreen and HeLa cells 72 hours post-transduction with empty or NgR(310)ecto-Fc transfection supernatant, magnification 10x, scale bar = 200 μ m. **C.** Flow cytometric determination of virus titre shows percentage of ZsGreen positive HeLa cells for serial virus dilutions 72 hours post-transduction.

5.3 Lineage negative enrichment of bone marrow cells

In order to deliver the therapeutic NgR(310)ecto-Fc protein into the active demyelinating lesion, the formation of BM chimeric mice that have engrafted HSCs carrying the NgR(310)ecto-Fc construct was required. Therefore, it was important that the donor BM cells destined for transplantation was lin^- enriched. This was achieved through removal of lineage-differentiated cells (B220^+ , CD3^+ , ter119^+ , Mac1^+ , and Gr1^+) to yield a greater percentage of $\text{lin}^- \text{ckit}^+ \text{sca1}^+$ (LSK) HSCs. Furthermore, it was a requirement that lin^- enriched cells were cultured for 72 hours after isolation while they were transduced with the LV constructs. HSC supportive factors including IL-6, IL-3, Flt-3 and SCF was added to help stimulate LSK cells during the culture period. The conditions for enrichment and HSC culture were tested in order to demonstrate optimal maintenance of the LSK population throughout this process. Our enrichment protocol yielded a 4-fold elevate in the lin^- proportion (Figure 53A and C). Whilst culturing the cells for 72 hours lead to lineage differentiation and a decline in the proportion of lin^- cells, the conditions also resulted in an increase in the LSK population to 13.0% of the total cells (Figure 53B and C). Given these data, this protocol for lin^- enrichment for HSC culture was adopted before transplantation into irradiated recipients.

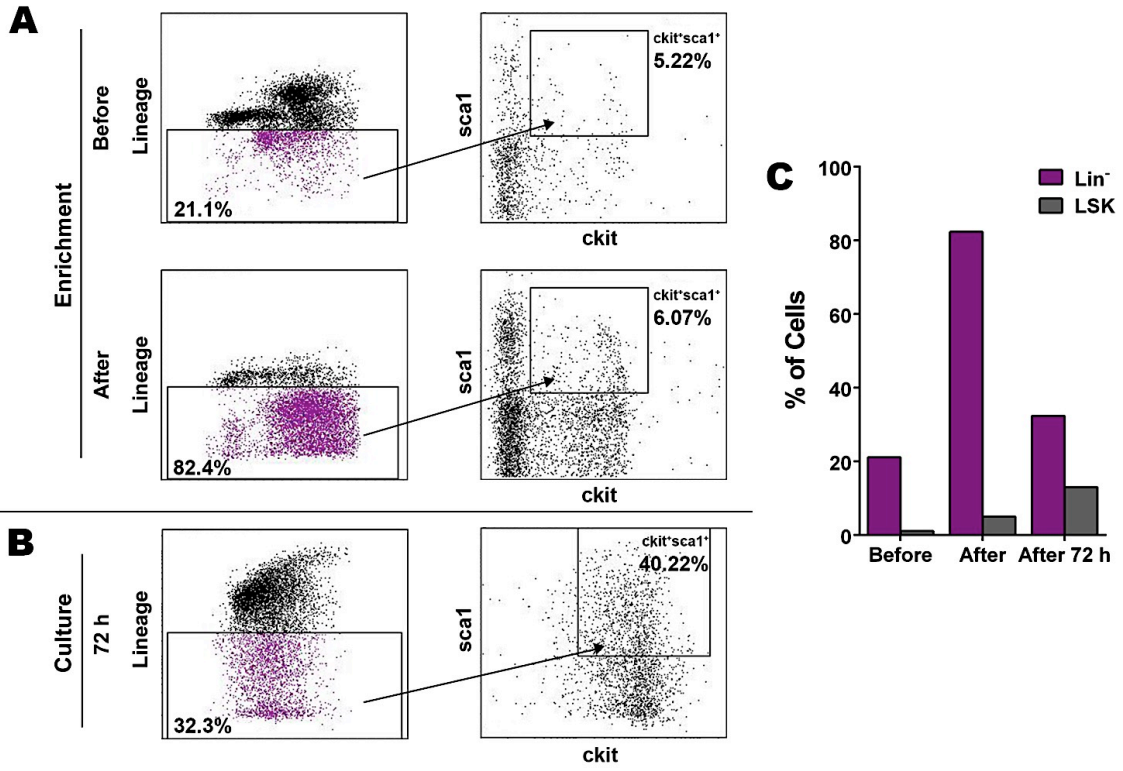
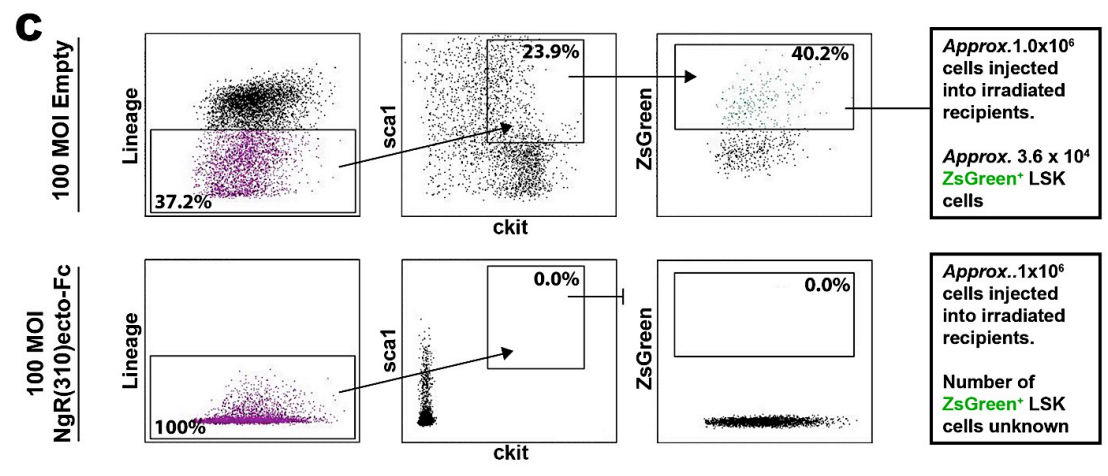
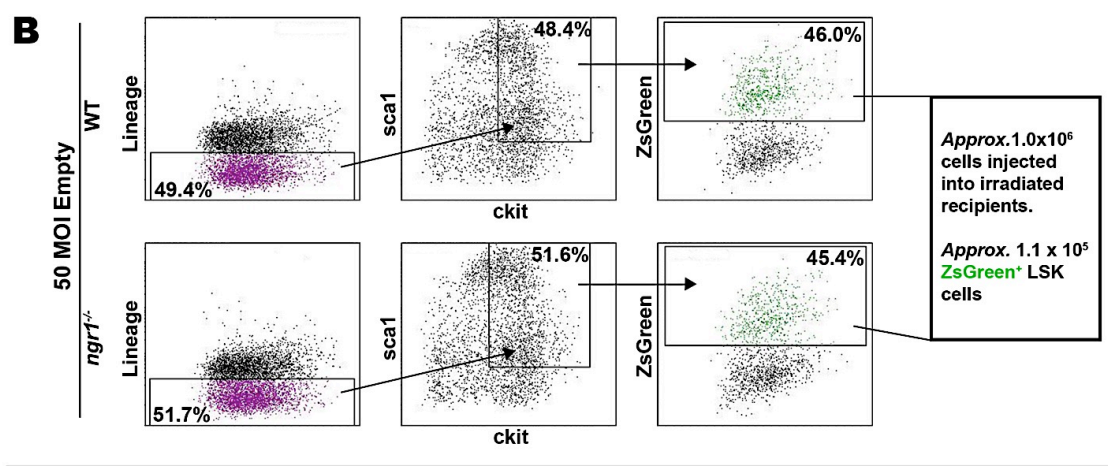
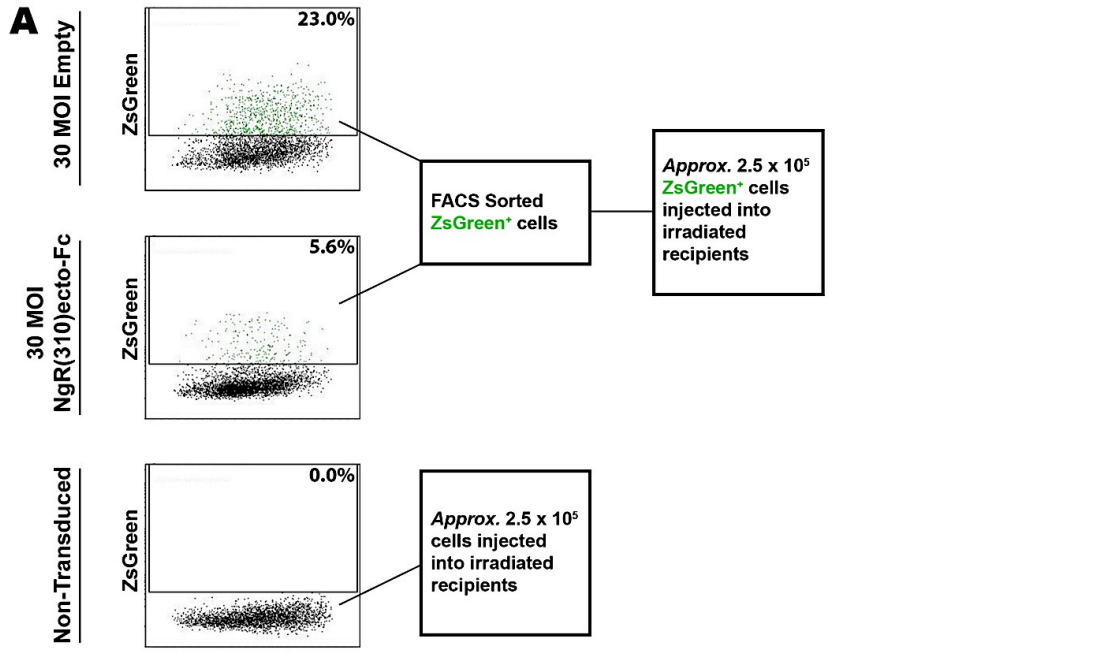


Figure 53. Lineage negative enrichment of BM cells. **A.** Analysis was performed on BM cells isolated from male *ngr1*^{+/+} mice, before and after lineage negative enrichment. *lin*⁻ cells were assessed on their *ckit* and *sca1* expression. **B.** Lineage, *ckit* and *sca1* expression analysis of *lin*⁻ enriched cells after 72 hours culture. **C.** Representation of *lin*⁻ cells and LSK cells as a percentage of the total live cells as determined by flow cytometric analysis of BM derived cells before and after enrichment and after 72 hours in culture.

5.4 Transduction of lineage negative bone marrow cells with lentiviral vector

Prior transplantation, lin^- enriched BM cells from either male C57Bl/6 ($\text{ngr1}^{+/+}$ or $\text{ngr1}^{-/-}$) donors were transduced with LV containing either empty or NgR(310)ecto-Fc constructs. We utilised $\text{ngr1}^{+/+}$ donor cells as the destined transplant recipients were also $\text{ngr1}^{+/+}$ and we aimed to mimic an autologous HSC transplant. The $\text{ngr1}^{-/-}$ cells were utilised as a control to delineate the potential endogenous expression of NgR1 in immune cells from the expression of the NgR(310)ecto-Fc fusion protein. Transduction efficiency in the donor cells was determined by flow cytometric detection of ZsGreen 72 hours post-transduction. In the first experiment, $\text{ngr1}^{+/+}$ lin^- enriched BM cells were either non-transduced or transduced with 30 MOI of either empty or NgR(310)ecto-Fc vectors. After 72 hours post-transduction, the cells were FACS sorted into ZsGreen⁺ cells, which represented 23.0% of the total cultured cells for empty vector, and 5.6% for NgR(310)ecto-Fc vector (Figure 54A). This suggests that NgR(310)ecto-Fc LV has much lower transduction efficiency in lin^- enriched BM cells than empty vector. In the second experiment, $\text{ngr1}^{+/+}$ or $\text{ngr1}^{-/-}$ lin^- enriched BM cells were transduced with 50 MOI empty vector. A sample of these cells was taken for flow cytometric analysis, revealing a transduction efficiency of 45.3% in live $\text{ngr1}^{+/+}$ cells and 46.6% in $\text{ngr1}^{-/-}$ cells (Figure 54B). Therefore, using 50 MOI shows a substantial improvement in transduction efficiency of the empty LV vector. Furthermore, it was of particular interest to determine the proportion of genuine ZsGreen⁺ LSK HSCs, as these are the precursor cells that, once engrafted, would give rise to ongoing vector positive immune cells. Thus, transduced cells were also analysed for their lineage, *ckit* and *sca1* expression. This showed that

11.1% and 11.3% of the total cultured and subsequently transplanted *ngr1*^{+/+} and *ngr1*^{-/-} cells were ZsGreen⁺ LSK HSCs (Figure 54B). In the third transplant, male donor *ngr1*^{+/+} *lin*⁻ enriched BM cells were transduced with 100 MOI of either NgR(310)ecto-Fc vector or empty vector. Figure 54C illustrates that there was an expression of lineage, ckit, sca1 and ZsGreen in empty or NgR(310)ecto-Fc vector transduced *lin*⁻ cells, 72 hours post-transduction. The transduction efficiency of these transduced cells was 51.2% ZsGreen⁺ cells and 3.6% ZsGreen⁺ LSK HSCs out of the total empty vector-transduced cells (Figure 54C). A confocal imaging shows the expression of ZsGreen in non-transduced *lin*⁻ cells, empty vector transduced *ngr1*^{+/+} *lin*⁻ cells, and empty vector-transduced *ngr1*^{-/-} *lin*⁻ cells, empty vector-transduced *lin*⁻ cells, and NgR(310)ecto-Fc vector-transduced *lin*⁻ cells, 72 hours post-transduction (Figure 54D).



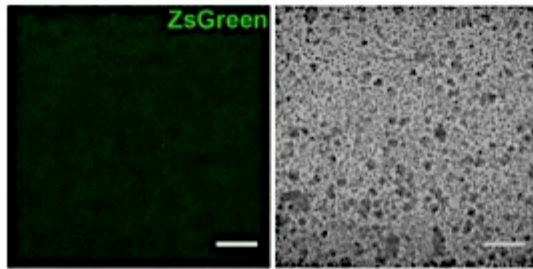
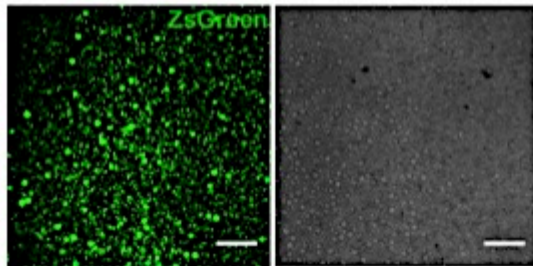
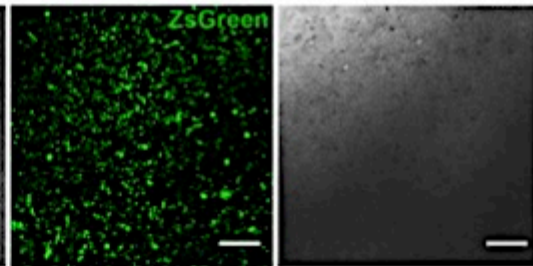
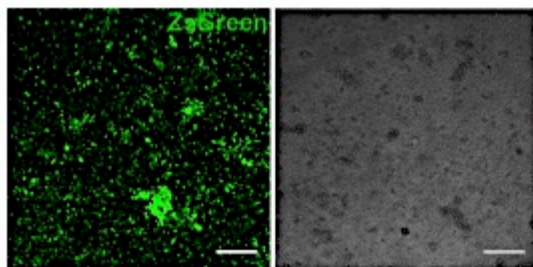
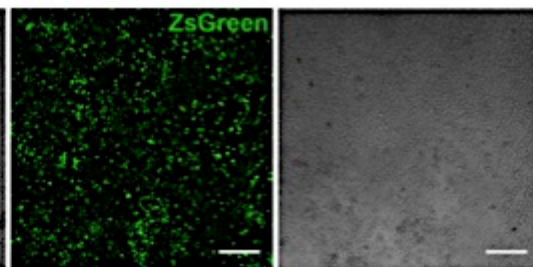
D**Non-Transduced WT HSC****30 MOI Empty in WT HSC****30 MOI Empty in *ngr1*^{-/-} HSC****100 MOI Empty in WT HSC****100 MOI NgR(310)ecto-Fc in WT HSC**

Figure 54. Qualification of vector-transduced cells used for transplantation. A. ZsGreen expression of empty or NgR(310)ecto-Fc vector-transduced, or non-transduced lineage-negative cells 72 hours post-transduction. In the first transplantation experiment, these ZsGreen⁺ cells were isolated using FACS and 2.5×10^5 transplanted into irradiated recipients. **B.** Empty vector-transduced *ngr1*^{+/+} and *ngr1*^{-/-} *lin*⁻ cells are assessed for expression of lineage markers B220, CD3, ter119, Mac1, and Gr1 and ckit, sca1 and ZsGreen, 72 hours post-transduction. For the second transplant experiment, 1.0×10^6 unsorted cells were transplanted into irradiated recipients. **C.** Lineage, ckit, sca1 and ZsGreen expression in empty or NgR(310)ecto-Fc vector transduced *lin*⁻ cells, 72 hours post-transduction. 1.0×10^6 unsorted cells were transplanted into irradiated recipients. **D.** ZsGreen expression in non-transduced *lin*⁻ cells, empty vector transduced *ngr1*^{+/+} *lin*⁻ cells, and empty vector-transduced *ngr1*^{-/-} *lin*⁻ cells, empty vector-transduced *lin*⁻ cells, and NgR(310)ecto-Fc vector-transduced *lin*⁻ cells, 72 hours post-transduction, magnification 10x, scale bar = 200 μ m.

5.5 Confirmation of NgR(310)ecto-Fc protein production upon pLVX-EF1 α

NgR(310)-Fc-myc-IRES-ZsGreen1 transfection

Following transfection of Chinese hamster ovarian (CHO) cells with the pLVX-EF1 α -NgR(310)-Fc-myc-IRES-ZsGreen1 vector and full-length NgR1 cDNA (pCMV-Sport 6 vector; NgR1-FL), cell lysate and conditioned media were collected. Western blotting was probed for mouse NgR1, Fc, and α -tubulin. No transfection (DNA vector alone) and lipofectamine alone (no DNA) controls were included. The data demonstrating the presence of secreted NgR(310)-Fc protein in the cell culture medium (Figure 55).

W.Blot: Secretion of NgR(310)-Fc protein

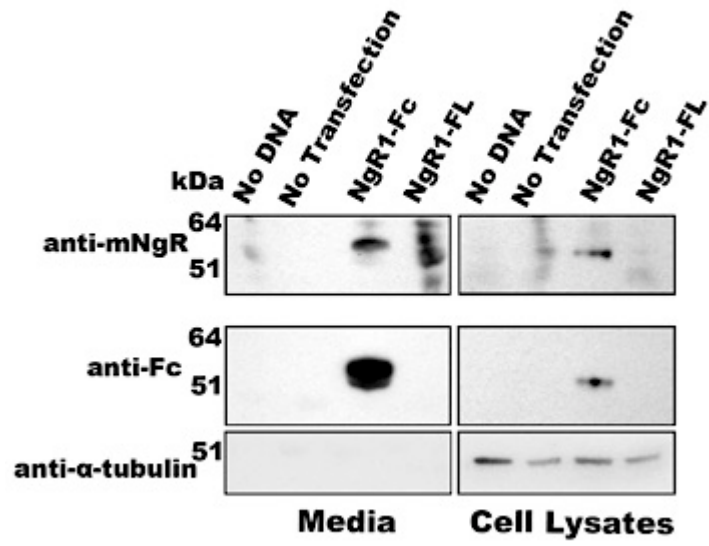


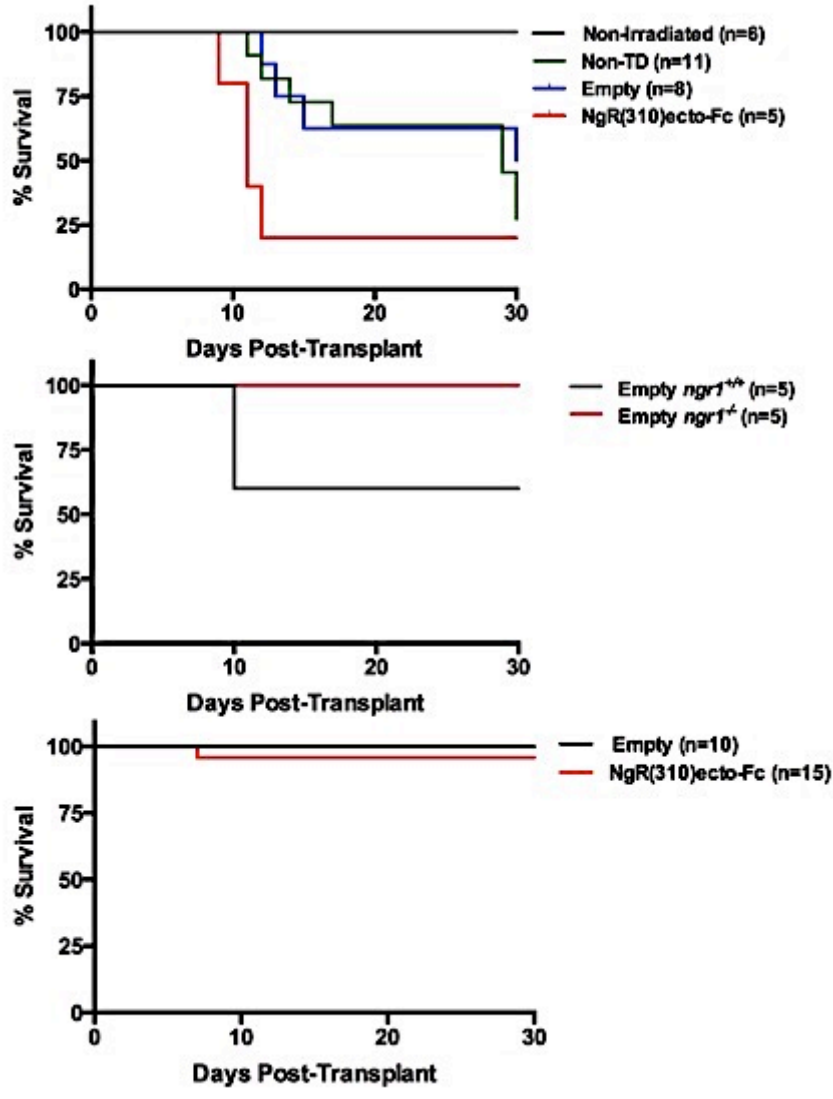
Figure 55. Confirmation of NgR(310)-Fc protein production upon pLVX-EF1 α -NgR(310)-Fc-myc-IRES-ZsGreen1 bicistronic vector transfection. CHO cells were transfected with LV vector and full-length NgR1 cDNA (pCMV-Sport 6 vector; NgR1-FL), or lipofectamine alone (no DNA) or no transfection. Cell lysates and medium were collected, run on an SDS-PAGE and probed for either NgR1(310) or Fc immunoreactivity after western blotting.

5.6 Transplantation of genetically manipulated HSCs to deliver therapeutic protein

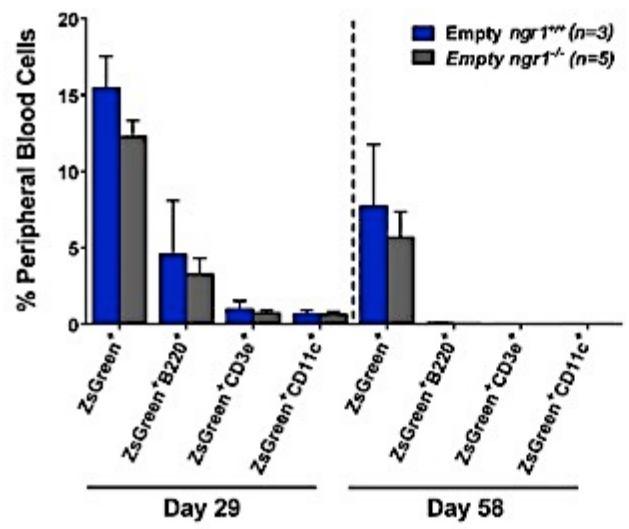
H SCT is the selected delivery method of NgR(310)ecto-Fc into the CNS, as has been highlighted extensively throughout this chapter. Optimisation post-transplant survival and engraftment of construct carrying HSCs were a critical outcome required of this pilot study. In first transplantation experiment, female *ngr1^{+/+}* mice, ages 6-8 weeks were subjected to 950 cGy caesium source gamma radiation as mentioned by Guirguis *et al.* (2016) in preparation for transplantation (Guirguis et al., 2016). The mice were then tail vein injected with 2.5×10^5 FACS sorted ZsGreen⁺ transduced lin⁻ cells after a 3 hours recovery period (Figure 54A). Figure 56A shows survival for 40 days following transplantation, revealing 75% mortality for irradiated mice: 81.8% in non-transduced HSC recipients, 62.5% in empty vector transduced HSC recipients, and 80.0% in NgR(310)ecto-Fc transduced recipients. Symptoms that prompted euthanasia included significant weight loss, reduced alertness and activity, isolation from cage mates and pale paws. Sub-mandibular bleeds at 4 and 8 weeks post-transplantation were performed and engraftment assessed through flow cytometry, however these experiments were unsuccessful and we were unable to record results, due to difficulties with the identification of ZsGreen expression. Given the high rate of mortality in the first transplantation experiment, we addressed the irradiation protocol for subsequent transplants. In the second transplant experiment, female *ngr1^{+/+}* mice, ages 6-8 weeks were irradiated with 2 doses of 550 gamma radiation separated by a 3 hours period of recovery, as utilised by Chung *et al.* (2014) (Chung et al., 2014). Moreover, we hypothesised that FACS sorting not only diminished cell numbers, but also cell viability

and sterility, so we opted to transplant unsorted cells. Hence, 3 hours following irradiation, we transplanted 1×10^6 of empty vector-transduced *ngr1*^{+/+} or *ngr1*^{-/-} cells. Survival for 40 days post-transplantation was improved with a reduced mortality of 20%: 40% in empty vector-transduced *ngr1*^{+/+} recipients (empty *ngr1*^{+/+} group), and 0% in empty vector-transduced *ngr1*^{-/-} recipients (empty *ngr1*^{-/-} group) (Figure 56A). In a third transplant, there was a greater improvement in mice survival with only 4% mortality, overall: 0% in the empty vector-transduced HSC recipients (empty group) and 6.7% in NgR(310)ecto-Fc vector-transduced HSC recipients (NgR(310)ecto-Fc group) (Figure 56A). After 4 weeks (day 29), submandibular bleeds were performed to provide a mean of 15.5% (\pm 2.1% SEM) ZsGreen⁺ cells in the peripheral blood for empty *ngr1*^{+/+}, and 12.3% (\pm 1.0% SEM) empty *ngr1*^{-/-} (Figure 56B). Another submandibular bleed after 8 weeks (day 58) revealed a reduction in ZsGreen⁺ cells to 7.7% (\pm 4.0% SEM) for empty *ngr1*^{+/+} and 5.7% (\pm 1.7% SEM) for empty *ngr1*^{-/-} (Figure 56B). Figure 56B also demonstrates the percentages of ZsGreen⁺ lineage-differentiated cells; day 58 analysis seems to show very low percentages of ZsGreen⁺ lineage-differentiated cells, however the percentages of lineage cells, positive or negative for ZsGreen are very low, suggesting an issue with the flow analysis. Flow cytometric analysis on the peripheral blood and BM of a mouse requiring euthanasia on day 10 post-irradiation indicated 34.8% ZsGreen⁺ cells in the blood and only 6.4% in BM (Figure 56C), suggesting that ZsGreen⁺ cells found in the blood in the earlier stages after transplant may be lineage-differentiated cells that were transplanted rather than being generated from engrafted HSCs.

A



B



C

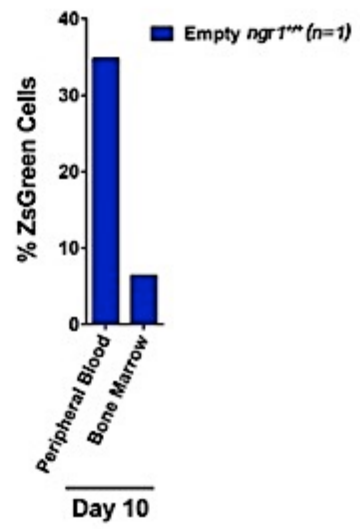


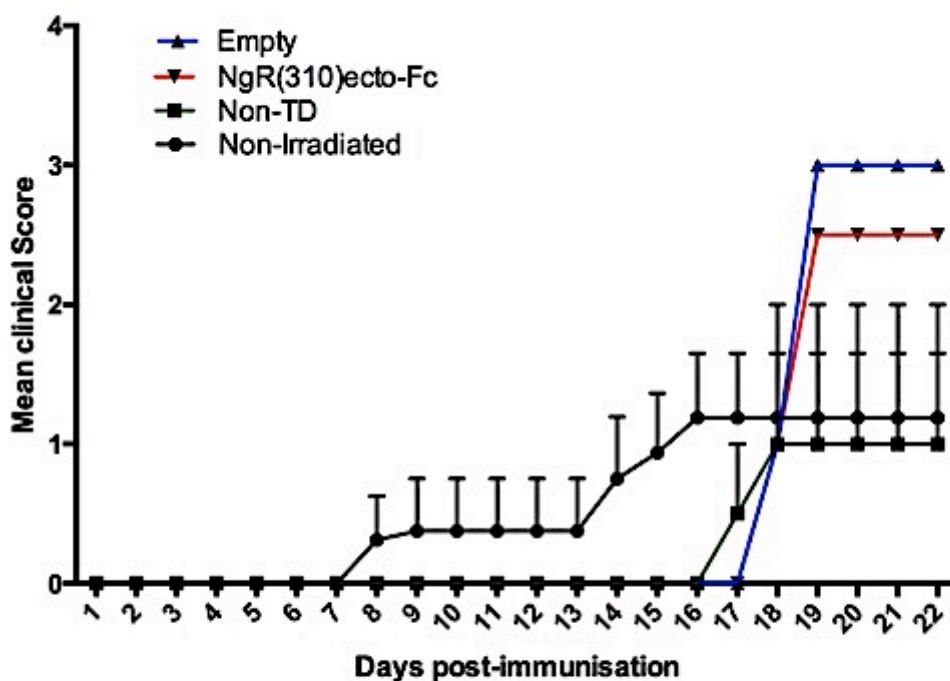
Figure 56. Post-HSCT monitoring. **A.** Kaplan-Meier plot of animal survival post-HSCT for the first, second and third transplant experiments. Non-irradiated no transplant controls (n=6), Non-transduced HSC recipients (n=11), empty vector-transduced HSC recipients (n=8), NgR(310)ecto-Fc vector-transduced HSC recipients (n=5), empty vector transduced *ngr1*^{+/+} HSC recipients (n=5), and empty vector-transduced *ngr1*^{-/-} HSC recipients (n=5), the second group of empty vector-transduced HSC recipients (n=10), and the second group of NgR(310)ecto-Fc vector-transduced HSC recipients (n=15). **B.** ZsGreen, B220, CD3e, and CD11c expression in peripheral blood collected by submandibular bleed from empty vector transduced *ngr1*^{+/+} HSC recipients (n=3) and empty vector-transduced *ngr1*^{-/-} HSC recipients (n=5) day 29 and day 58 post-transplant. **C.** ZsGreen expression in peripheral blood and BM of an empty vector-transduced *ngr1*^{+/+} HSC recipient euthanised on day 10.

5.7 Induce EAE post-transplantation

As we identified in chapter 3, immunisation with MOG₃₅₋₅₅ peptide resulted in *ngr1*^{-/-} mice having a significant delay in EAE onset and a decrease in the severity of clinical signs when compared to *ngr1*^{+/+} mice, and this result coincides with Petratos *et al.* (2012) findings. This is one of the fundamental bases for our confidence in the therapeutic potential of inhibiting NgR1 signalling using the NgR(310)ecto-Fc fusion protein. We induced EAE by immunisation with MOG₃₅₋₅₅ in our first transplant subjects and the non-irradiated control group, in order to test the impact of NgR(310)ecto-Fc on the clinical outcome and pathological features of EAE. The clinical progression of EAE in each group is represented in Figure 57A. Unfortunately, due to insufficient mice, no significant interpretation can be made about the difference in clinical progression between the groups. Figure 57B showed a significant delay in the onset of disease in the empty transduced *ngr1*^{-/-} HSC recipients' more than empty transduced *ngr1*^{+/+} HSC recipients compared to non-irradiated *ngr1*^{+/+} (no transplant controls) (p<0.0001) in the second transplant. The disease's clinical manifestations in these mice were determined by daily scoring.

A

Clinical scores of MOG35-55 EAE immunised for the first HSCT cohort



B

Clinical scores of MOG35-55 EAE immunised for the second HSCT cohort

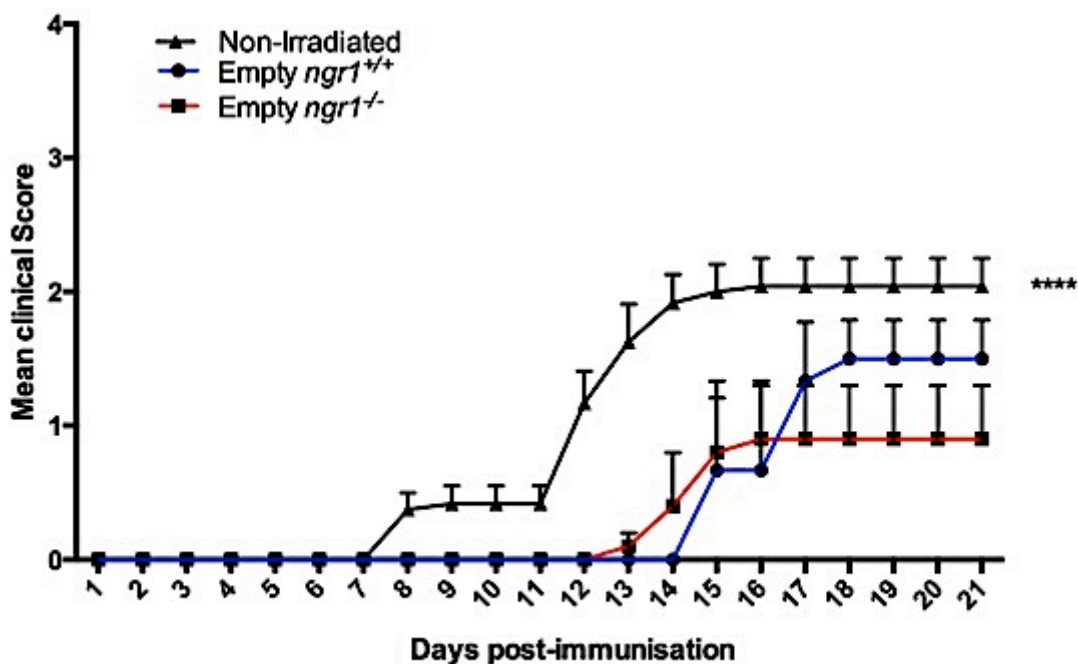


Figure 57. Clinical progression of EAE. Clinical scores (mean with SEM) of HSC-transplanted mice after induction of MOG₃₅₋₅₅ EAE. **A.** In the first transplant, non-irradiated no transplant controls (n=8), non-transduced HSC recipients (n=2), empty vector-transduced HSC recipients (n=1), NgR(310)ecto-Fc vector-transduced HSC recipients (n=1). **B.** In the second transplant, non-irradiated no transplant controls (n=13), empty transduced *ngr1*^{+/+} HSC recipients (n=3), and empty transduced *ngr1*^{-/-} HSC recipients (n=5). Their disease clinical manifestations were determined by daily scoring. Clinical scores represent mean ± SEM of diseased mice, **** p<0.0001, two-way ANOVA.

5.8 Peripheral localisation of vector–positive lineage differentiated cells

We next investigated the engraftment and chimerism in the vector-transduced HSCT post-EAE induction by analysing ZsGreen⁺ immune cells in the periphery of these mice. The mice were sacrificed at clinical score 2-3, and peripheral blood, spleen and lymph nodes were collected. Lymph nodes and peripheral blood were processed for flow cytometric analysis of immune lineage marker (CD3, B220, CD11c), myc and ZsGreen expression, while the spleen was paraffin embedded and analysed via immunohistochemistry. Flow cytometric analysis of peripheral blood (Figure 58A) showed low percentages of ZsGreen⁺ CD3e⁺, ZsGreen⁺ B220⁺ and ZsGreen⁺ CD11c⁺ cells: 0.67%, 0.23% and 1.5% respectively in an empty vector HSCT mouse; and 0.33%, 0.60% and 0.55% respectively in a NgR(310)ecto-Fc vector HSCT mouse. These levels are comparable with the levels of ZsGreen⁺ cells in the non-transduced HSCT animal. Moreover, myc⁺ cells percentage in the empty vector HSCT mice was 22.1%, while the NgR(310)ecto vector HSC-transplanted animal had a higher percentage of myc⁺ cells (52.17%), suggesting non-specificity of α -myc antibody or secondary antibody binding. In addition, the lymph node was only performed on the empty vector HSCT mouse and indicated no ZsGreen expression (Figure 58B). Figure 59 demonstrates the immunohistological analysis of the spleen, however, did reveal the existence ZsGreen⁺ CD3e⁺, ZsGreen⁺ B220⁺ and ZsGreen⁺ CD11c⁺ cells (arrowheads). This result suggests that the ZsGreen signal may have been compromised during the flow cytometry experiments. Overall, these data indicate the presence of ZsGreen⁺ cells in the periphery of transplanted mice and provide evidence their chimerism.

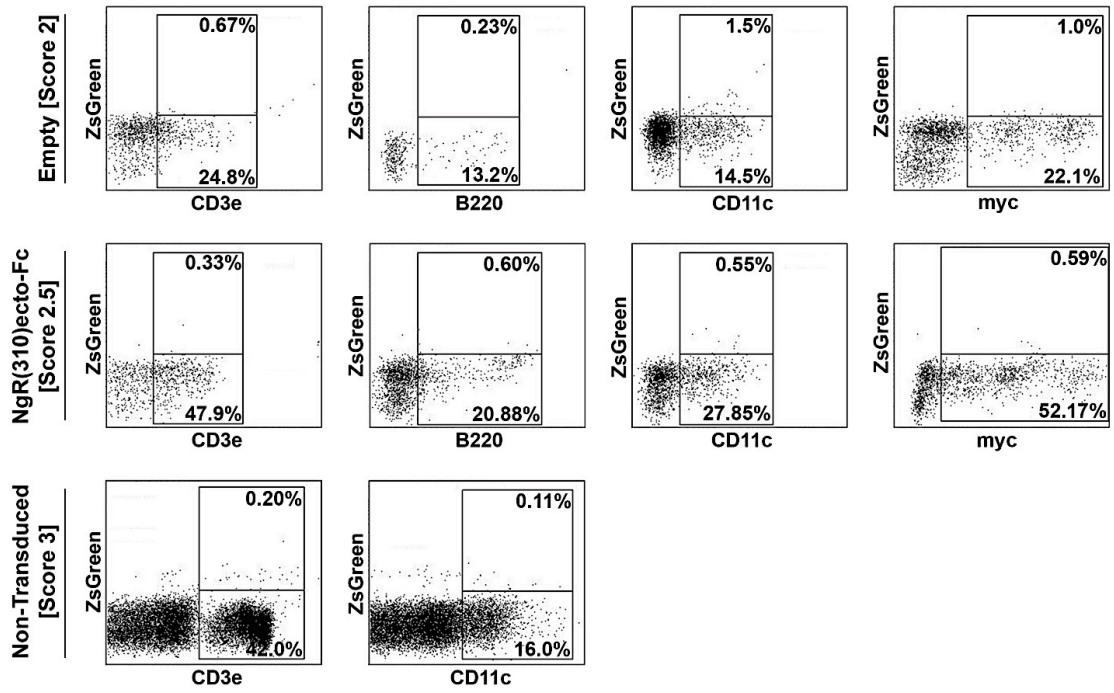
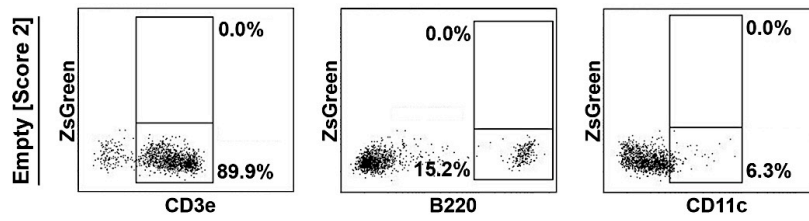
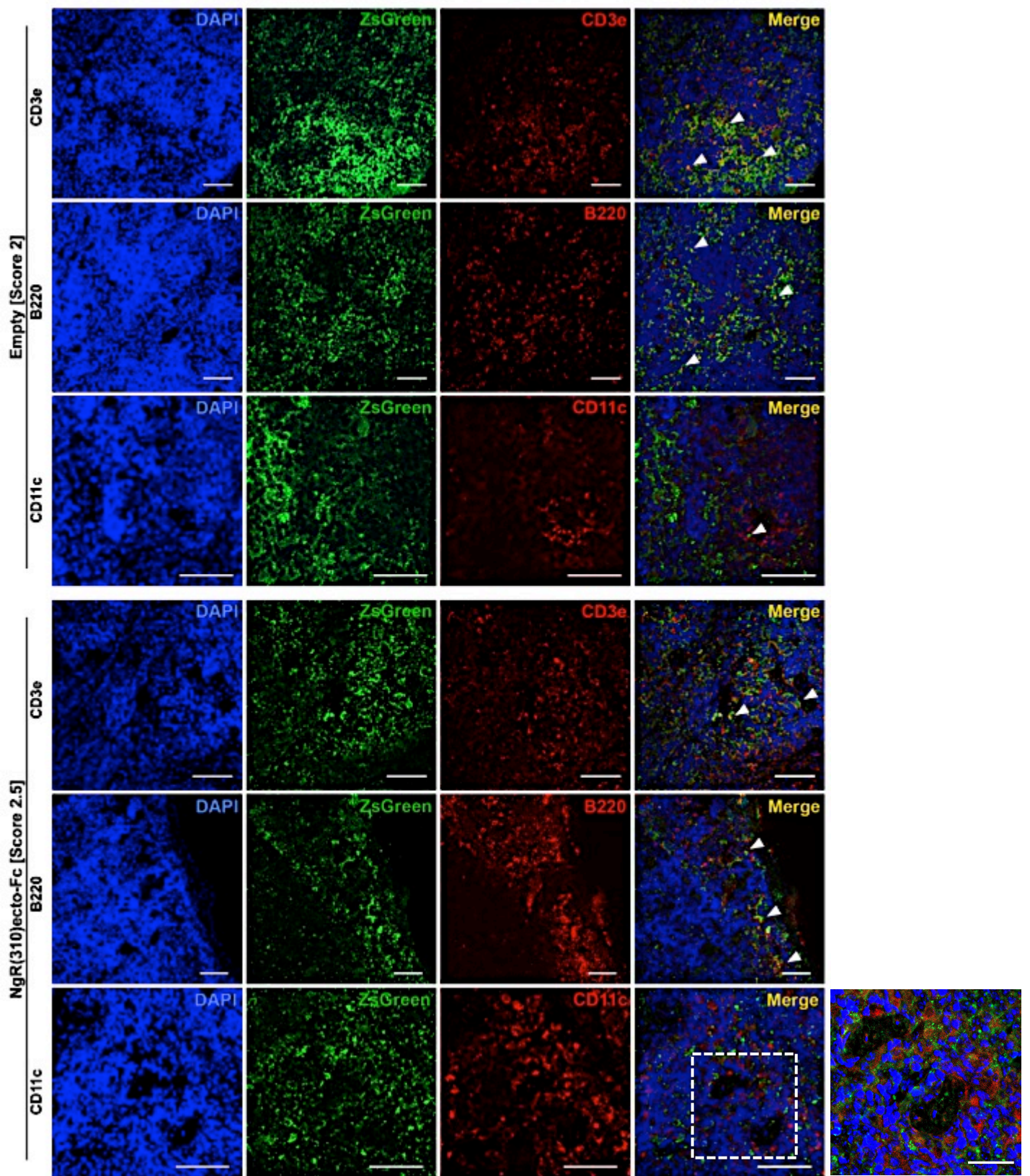
A**Peripheral Blood****B****Lymph Node**

Figure 58. Donor derived immune cells in HSC transplanted mice post-EAE. A. ZsGreen and CD3e, B220, CD11c or myc co-expression in the peripheral blood of either empty vector, NgR(310)ecto-Fc vector-transduced, or non-transduced HSC recipients. **B.** Co-expression of ZsGreen with CD3e, B220 or CD11c in the lymph node of either empty vector, NgR(310)ecto-Fc vector-transduced, or non-transduced HSC recipients.

Spleen



Spleen

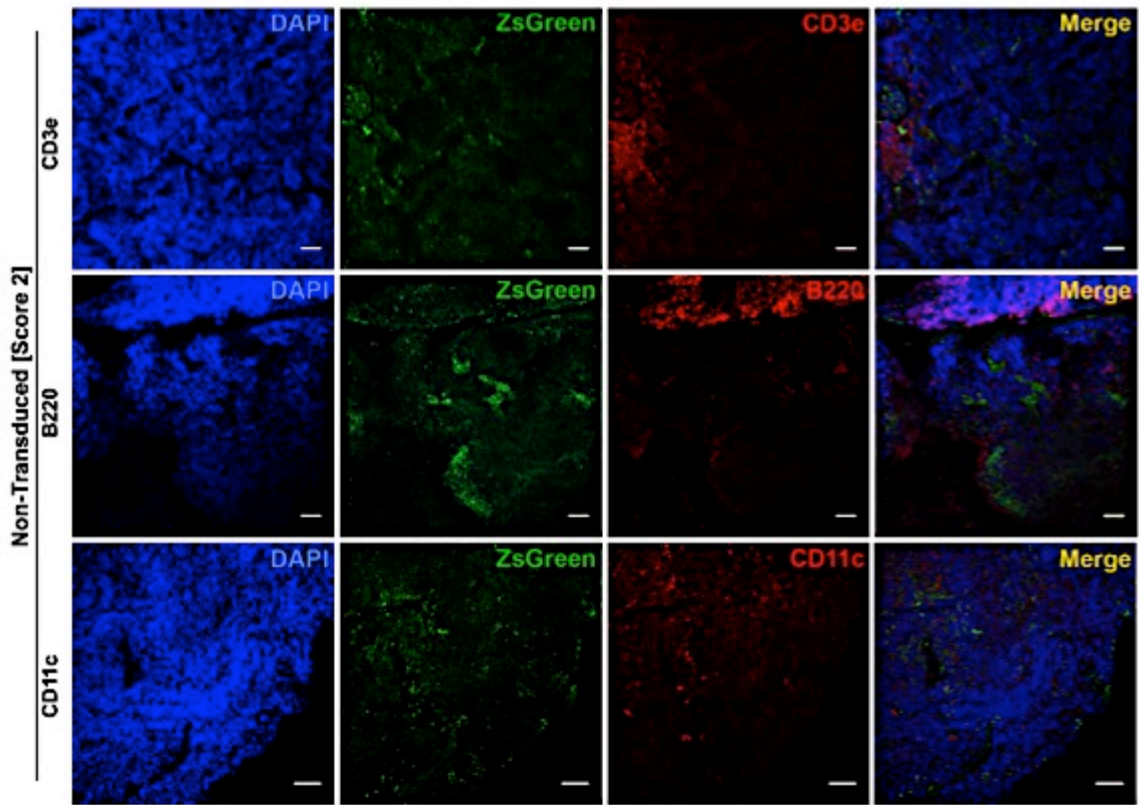


Figure 59. Donor derived immune cells in the spleen of HSC-transplanted mice post-EAE. ZsGreen and CD3e, B220, or CD11c co-expression (arrowheads) in the spleen of either empty vector, NgR(310)ecto-Fc vector-transduced, or non-transduced HSC recipients. Magnification 20x, scale bar = 50 μ m.

5.9 Infiltration of vector-positive lineage cells in the CNS post-EAE

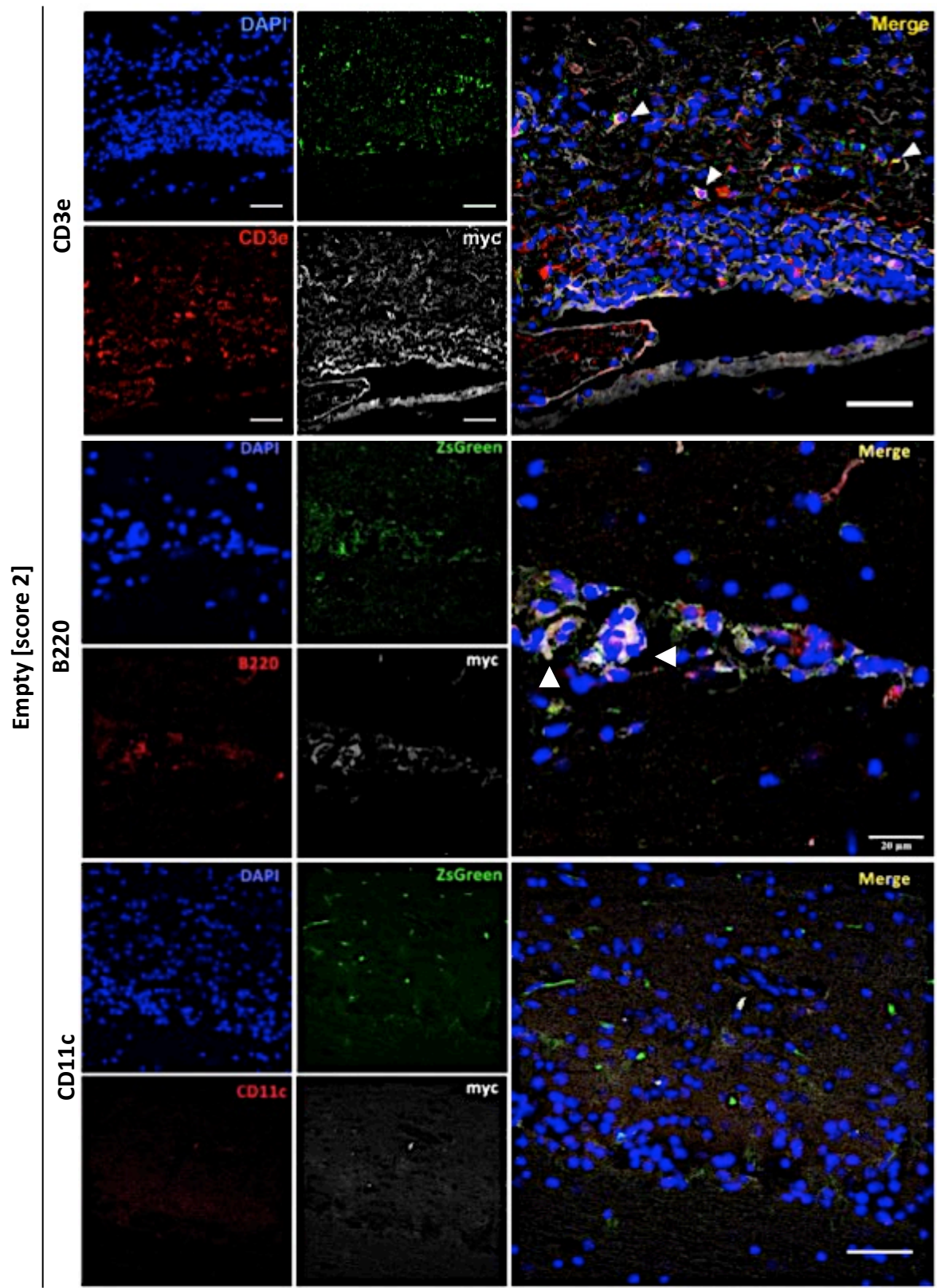
Based on the fact that immune cells are able to traverse the BBB and enter the CNS during EAE and MS, we harvested optic nerve and spinal cord from our transplanted mice following EAE, once they had reached clinical score 2–3. Consequently, we identified the localisation of myc-tagged NgR(310)ecto-Fc fusion protein and the localisation of ZsGreen⁺ lineage-differentiated cells (via immune markers; B220, CD3e, CD11c and Iba1) by immunohistochemistry. Spinal cord sections illustrate the presence of ZsGreen⁺CD3e⁺ cells and ZsGreen⁺B220⁺ cells throughout tissue from an empty vector HSCT mouse at clinical score 2-3 (Figure 60), although there was no co-expression of ZsGreen and Iba1, and ZsGreen and CD11c (Figure 60). The presence of ZsGreen⁺ CD3e⁺, ZsGreen⁺ B220⁺ and ZsGreen⁺ CD11c⁺ cells were also indicated in the spinal cord of a NgR(310)ecto-Fc vector HSCT mouse, and all these double-positive cells were also positive for myc (Figure 60, arrowheads). However, all sections in empty-vector and NgR(310)ecto-Fc vector-transduced, and non-transduced HSC transplanted mice show positive staining for myc, suggesting some non-specificity in the α -myc antibody, or the secondary antibody (Figure 60).

Immunohistochemical investigation of the optic nerve showed infiltration of ZsGreen⁺ cells in a NgR(310)ecto-Fc vector HSCT mouse (tailed arrowheads), however B220, CD11c and CD3e staining is inconclusive (Figure 61). We also investigated the presence of ZsGreen⁺ cell with regard to the pathological features of clinical score 2.5 in an NgR(310)-Fc vector HSCT mouse. Specifically, this included axonal degeneration as

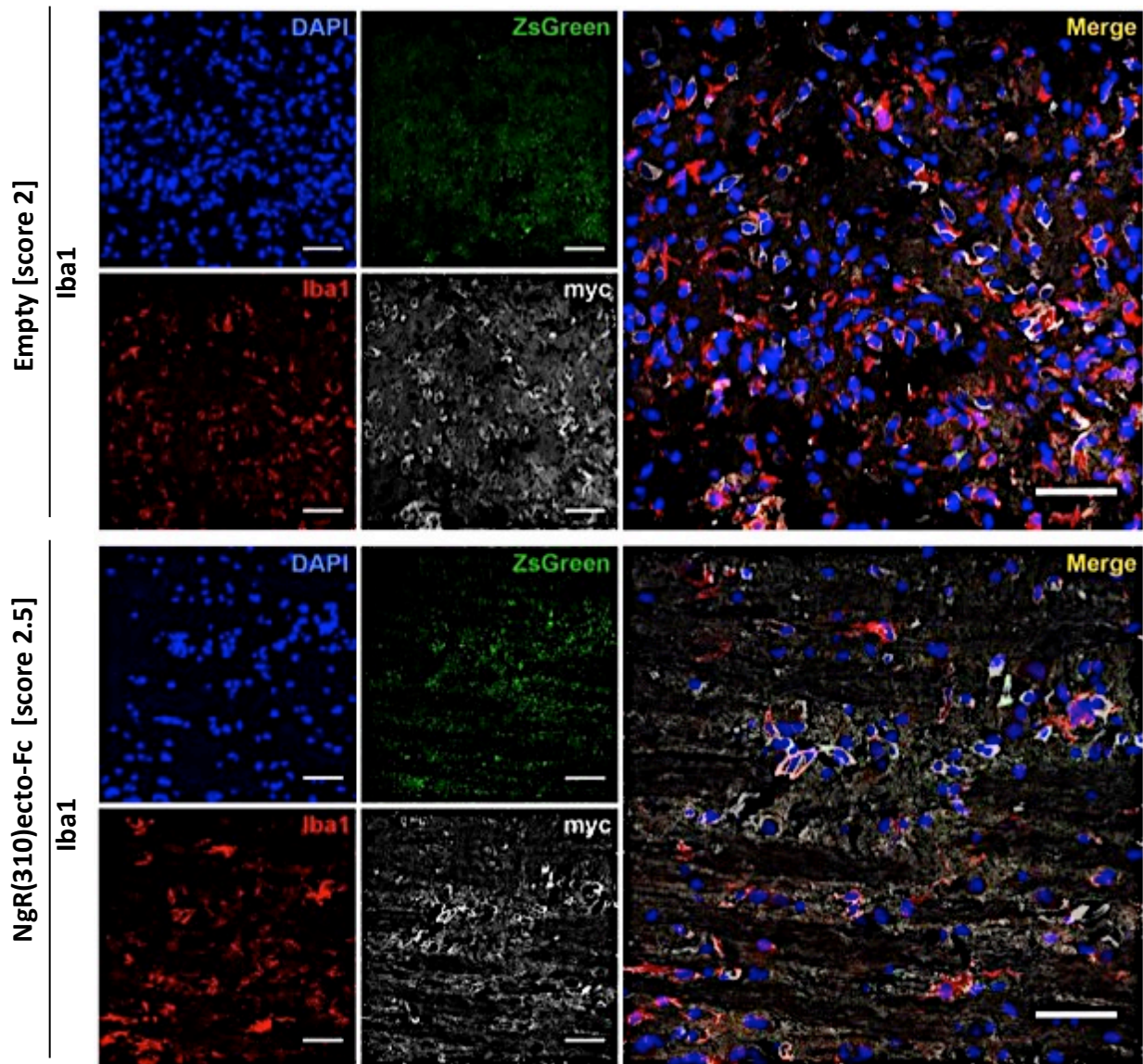
indicated by the presence of pThr555-CRMP-2, and demyelination as indicated by the disruption of MBP. ZsGreen⁺ cells in a fully demyelinated lumbosacral lesion presenting with axonal degeneration (yellow box), as well as in dorsal root entry infiltrates (white box) (Figure 62). Perivenule cuffing of ZsGreen⁺ cells (white dashed box) was also detected in a lumbosacral-demyelinating lesion, as well as close proximity of ZsGreen⁺ cells to the occasional pThr555-CRMP-2 positive axon (Figure 62).

Taken together, these data indicate that immune cells containing the vector construct are able to enter into the CNS during EAE and are present in key pathological areas during the peak stage of EAE. This confirms our hypothesis that immune cells are able to localise at demyelination lesions in order to deliver our therapeutic protein to the site where it is required.

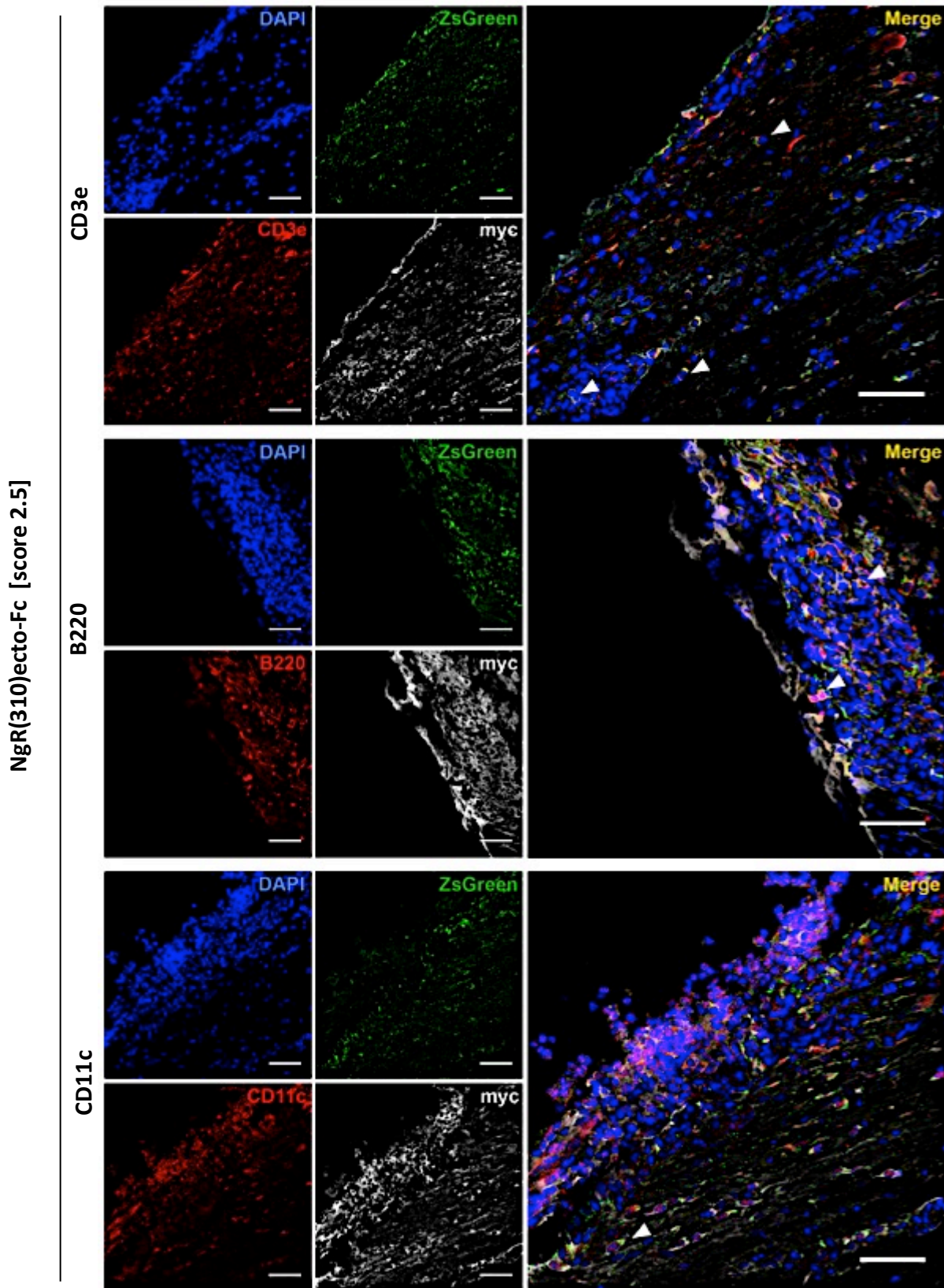
Spinal cord



Spinal cord



Spinal cord



Spinal Cord

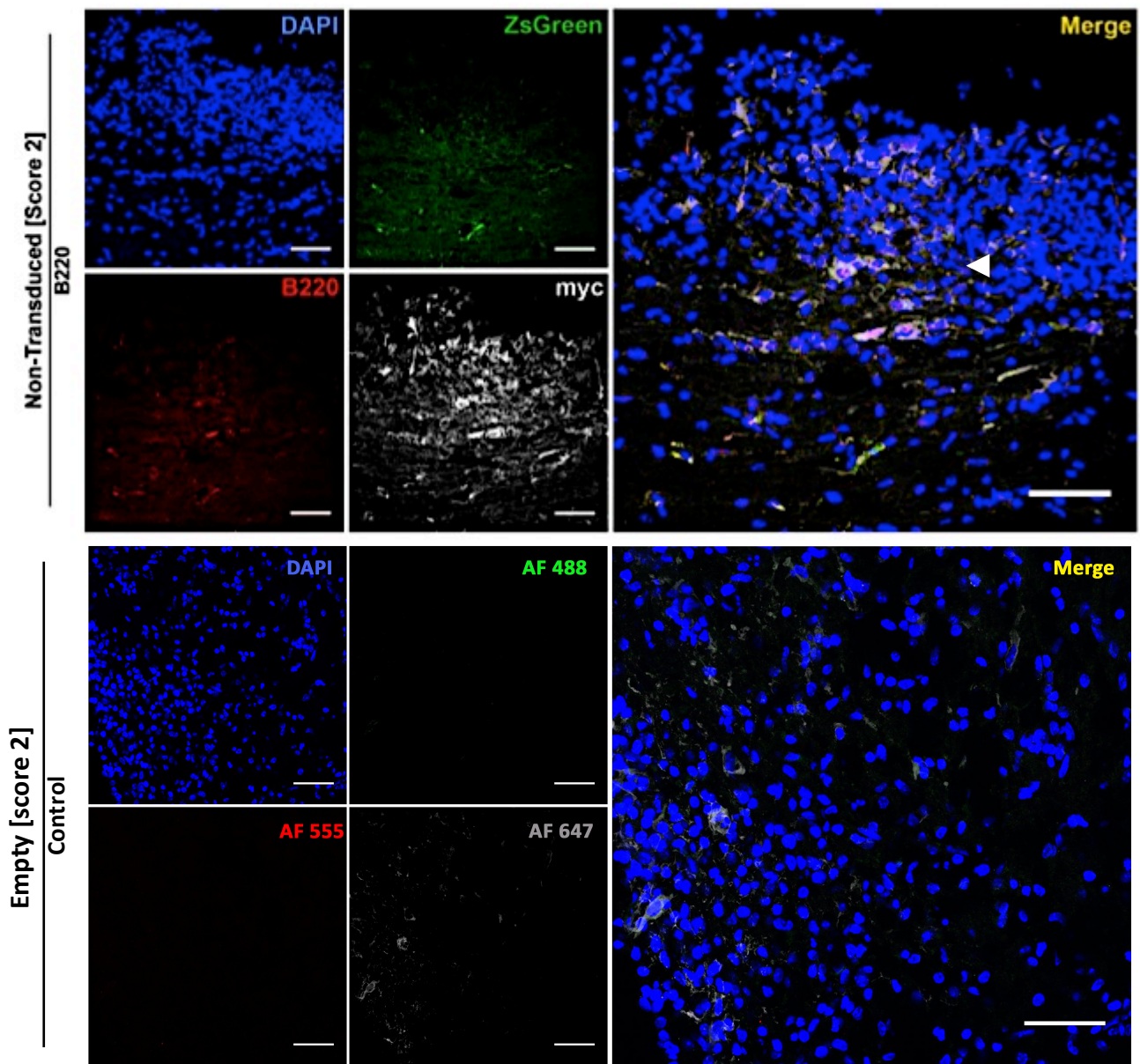


Figure 60. Infiltration of donor derived immune cells in the spinal cord of HSC-transplanted mice post-EAE. ZsGreen, myc and CD3e, B220 or CD11c co-expression (arrowheads) of spinal cord infiltrates at clinical score 2-3 in either empty vector, NgR(310)ecto-Fc vector-transduced, or non-transduced HSC recipients. Magnification 40x, scale bar = 50 μ m.

Optic Nerve

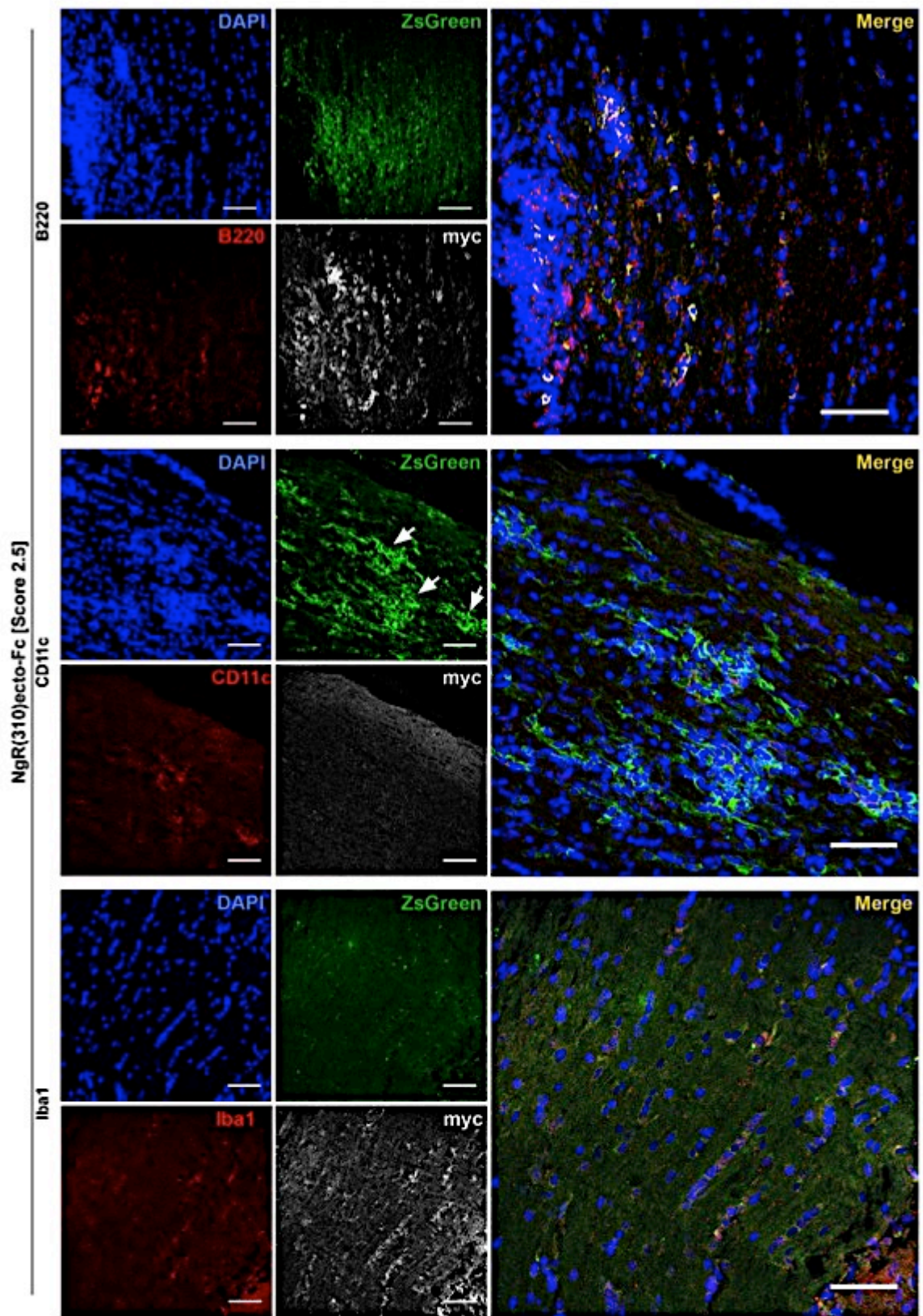


Figure 61. Donor derived immune cell infiltrates in the optic nerve of HSC-transplanted mice post-EAE. ZsGreen, myc and CD3e, B220 or CD11c co-expression (arrowheads) of optic nerve infiltrates at the peak stage of EAE in NgR(310)ecto-Fc-myc vector-transduced HSC recipients. Magnification 40x, scale bar = 50 μ m.

Spinal Cord

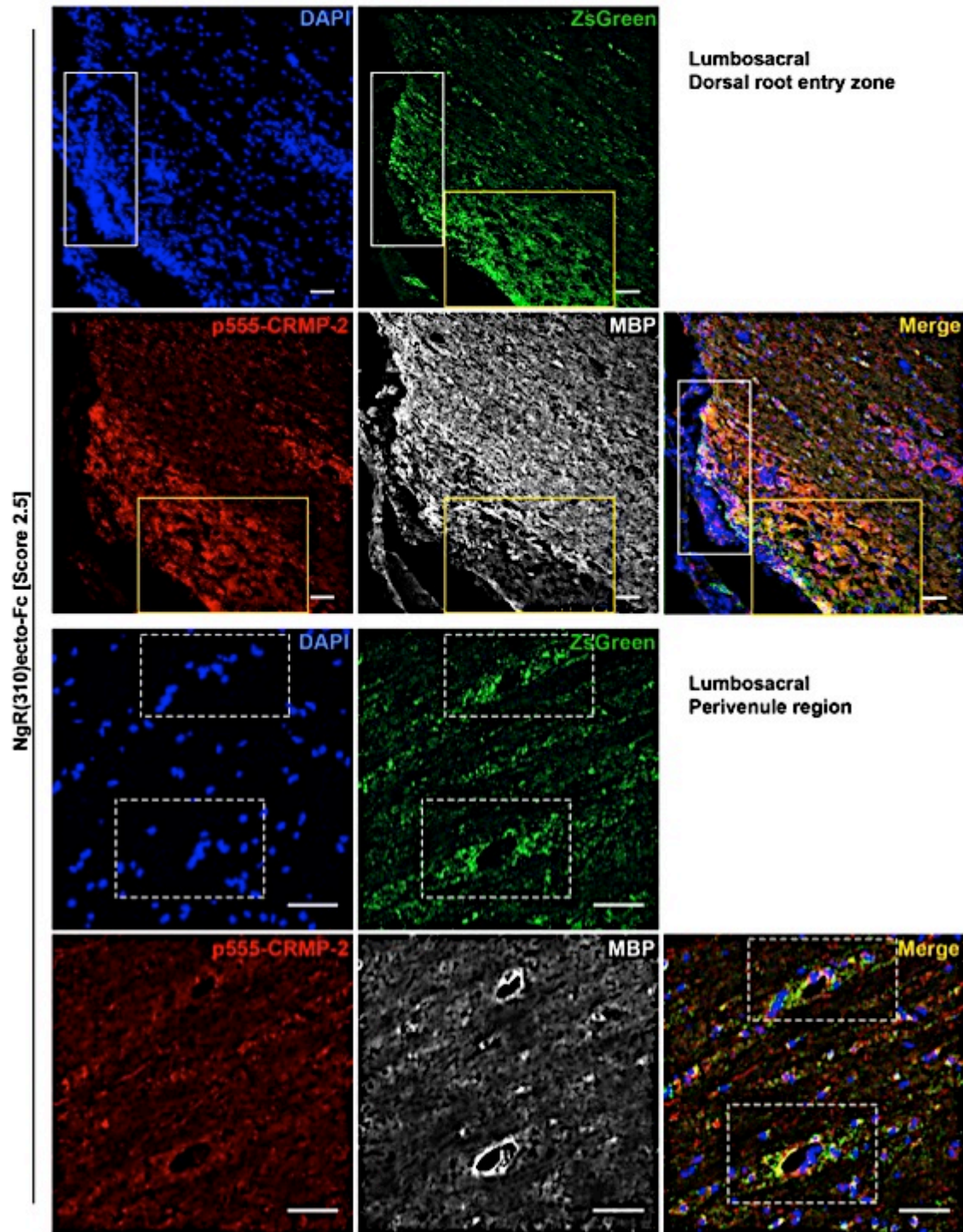


Figure 62. Localisation of transplant derived cells in pathologically significant regions of the CNS. Infiltration of ZsGreen⁺ cells in spinal cord lesions at the peak stage of EAE in a NgR(310)ecto-Fc vector-transduced HSC recipients. ZsGreen⁺ cells are present in areas of inflammation (white box), total demyelination and axonal degeneration (yellow box), and localised in lesion adjacent perivenule cuffing (white dotted box).

5.10 Discussion

In the current series of experiments, we have targeted the NgR1-specific ligands using a novel HSC-based delivery of a therapeutic protein that utilises NgR(310)ecto-Fc as a means of limiting the immune-mediated degeneration of axons in a MS model. As a corollary, ongoing studies will investigate whether the NgR1-Fc can bind and inactivate BAFF signalling in B-cells to localised in spinal cord to limit degeneration and inflammatory demyelination during EAE. In this chapter therefore, we have systematically compared the clinical and pathological outcome of EAE in NgR(310)ecto-Fc treated mice to various un-treated controls.

The use of retrovirally-transduced HSCs has been employed as a means to target specific mechanisms in the context of EAE (Xu et al., 2006, Chan et al., 2008). LV pLVX-EF1 α -IRES-ZsGreen1 was chosen for its safety and superior ability to transduce HSCs without the requirement for significant stimulation (Miyoshi et al., 1999, Kay et al., 2001), so as to minimise the likelihood of inducing excessive HSC differentiation. We successfully produced and quantified both NgR(310)ecto-Fc and empty construct containing LV vectors, which are capable of transducing mammalian cells including HSCs. It is of note that the NgR(310)ecto-Fc vector had a 10-fold lower titre than the empty vector, this may be due to either a reduced transduction capacity of this vector, which would subsequently reduce the percentage of transduced HeLa cells used in determining virus titre or packaging of the construct in the LV particle causing lower yield from 293T cell transfection. Overall, titres achieved for both NgR(310)ecto-Fc and empty vectors, which

were 10^3 – 10^5 fold less than predicted from 293T production (Pfeifer, 2004), demonstrating that the protocol can be further optimised to increase titre of both vectors.

In preparation of HSCT, we endeavoured to provide a maximal population of *bona fide* pluripotent LSK HSCs. In order to maximise this LSK HSC population, we were able to lin^- enrich donor BM cells and optimise culture conditions. Using these cells, we experimented with various transduction conditions to elucidate optimal transduction of lin^- cells, including HSCs, with both NgR(310)ecto-Fc and empty vectors, which could subsequently be transplanted into irradiated recipients. The reduced transductive capacity of NgR(310)ecto-Fc is supported by our finding that the percentage of NgR(310)ecto-Fc vector-transduced lin^- cells in HSC culture was approximately a quarter of that of empty vector-transduced cells in the first line lin^- BM transduction experiment. This finding was unable to be verified in a subsequent transduction experiment demonstrated by the failed flow cytometric analysis of the NgR(310)ecto-Fc vector-transduced cells. However, ZsGreen fluorescence was captured, using captured confocal microscopy images, demonstrating the occurrence of transduction that was not established via flow cytometry and ratifies our method for lin^- cell and HSC transduction with LV vector.

The secretion of fusion protein by transduced CHO cells was achieved using western blot analysis of cell lysate and culture supernatant. Consequently, a number of HSCTs were performed to verify the therapeutic rationale behind the use of transplantation as a specific delivery method for NgR(310)ecto-Fc into the CNS. Appropriate pre-conditioning of transplant recipients is a crucial component of a transplantation regime.

Ablation of the recipients' endogenous BM is required depletion of the HSC compartment to allow space for the engraftment of donor cells. Caesium source gamma irradiation is a common technique of myeloablation that has the potential for adverse side-effects, namely, irradiation sickness, which is common in the 14 day period following irradiation and characterised by malaise, lethargy, diarrhoea, dehydration, and lack of appetite (Duran-Struuck and Dysko, 2009). Moreover, complete myeloablation, while allowing maximal engraftment of donor cells, leaves the animals immunocompromised and susceptible to infection. We sought to achieve a high level of donor cell engraftment, therefore we opted for a radiation dose that would result in complete myeloablation, but was still deemed safe for C57Bl/6 mice (Hanson et al., 1987). In the first transplant, 950 cGy was used as recommended by collaborators (Guirguis et al., 2016). Despite our rationale, the transplant resulted in a high rate of mortality, the precise cause of which was not entirely clear. One alteration made in following transplants was adoption of a two-step irradiation protocol which would, in total, still deliver a myeloablative dose, but potentially cause less physiological strain to the animal; 2 doses of 550 cGy separated by a 3 hour period of recovery, a methodology successfully employed by another of our collaborators (Chung et al., 2014). Another important facet of HSCT is the quality and quantity of donor BM cells, as this is most likely to determine graft survival (Duran-Struuck and Dysko, 2009, Ema et al., 2007). With methods involving complete myeloablation, failure of engraftment leads to BM aplasia, which is fatal to the transplant recipient, causing continued immunodeficiency, anaemia, or thrombocytopenia (Duran-Struuck and Dysko, 2009). Before the first transplant, we elected to isolate the ZsGreen⁺ vector-transduced cells from our lin⁻

enriched culture using FACS to ensure increased engraftment of transduced cells. After sorting, however, there were a limited number of cells remaining for transplantation, thus only 2.5×10^5 were transplanted. Given the high rate of mortality that ensued, of which a high number presented as failure of engraftment with indications of anaemia and thrombocytopenia, we hypothesised that not enough pluripotent HSCs were provided for adequate engraftment, and additionally, the quality of these cells was diminished because of the FACS process. Thus, we refined our cell preparation protocol by eliminating FACS isolation of ZsGreen⁺ cells and increasing the number of cells for transplant to 1.0×10^6 . These changes were reflected in a decreased mortality rate in the second transplant experiment presumably due to increased provision of pluripotent HSCs.

For post-irradiation care, the mice were weighed and assessed for signs of illness to monitor their health. Furthermore, the provision of acidified water containing neomycin was used to diminish the risk of infection as a mean to monitor animal health. The second transplant resulted in 20% mortality and substantial weight loss that didn't recover until day 10 post-irradiation, although with the changes in cell preparation protocol and irradiation. Whilst the mortality was improved, we considered the possibility that the weight loss was due to radiation induced dehydration (Duran-Struuck and Dysko, 2009). It has also been reported that a decrease in fluid intake by mice treated with acidified water, and that simply increasing the pH of the water from 2.5 to 2.9 alleviated this issue while maintaining the anti-microbial benefits of acidified water (Duran-Struuck and Dysko, 2009). Therefore, the mice were treated with pH 2.9 acidified water containing

neomycin in our third transplant and observed faster weight recovery and further improvement in mortality rate.

Subsequent to HSCT, engraftment of donor HSCs was assessed by ZsGreen fluorescence in recipient peripheral blood samples, using flow cytometry. Further verification of engraftment was shown in flow cytometric and immunohistochemical analysis of the periphery in mice post-EAE. In the first transplantation cohort, sub-mandibular bleed, as well as post-EAE peripheral blood and lymph node samples from LV vector-transduced HSC recipients failed to display a signal for ZsGreen above the level of the non-transduced HSC recipients using flow cytometry. However, immunohistochemistry of the spleen post-EAE in non-transduced and vector-transduced HSC recipients did exhibit ZsGreen⁺ cells in the periphery and confirmed lineage-differentiation of engrafted HSCs. While sub-mandibular bleed samples for the second transplant cohort did show a signal for ZsGreen⁺ cells in peripheral blood on both days 29 and 58, it is clear there is a need for further refinement of the flow cytometric method employed for determining levels of ZsGreen⁺ in peripheral blood and lymph node samples to increase the consistency of results. An additional analysis that may be included to complement ZsGreen expression as a means of tracking engrafted cells is assessment of the male-specific histocompatibility antigen (H-Y), since a male-to-female transplantation was employed. This would give better quantification of engrafted cells, as all donor HSCs are H-Y⁺, yet only a percentage of these are ZsGreen⁺. Furthermore, BM cells should be examined at the experimental endpoint to fully characterise chimerism.

EAE was induced by immunisation with MOG₃₅₋₅₅ peptide in our HSCT mice and confirmed, through immunohistochemistry, that ZsGreen⁺ immune lineage-differentiated cells arising from engrafted transduced HSCs (referred to from here as vector-positive immune cells) could cross the BBB and localise in the CNS during EAE. Immunostaining of myc-tag peptide revealed the presence of NgR(310)ecto-Fc fusion protein in CNS tissue. There was, however, positive a few cells exhibiting anti-myc staining in an empty vector-transduced HSC recipient and a non-transduced HSC recipient, suggesting non-specificity of either the mouse anti-myc antibody, or the anti-mouse secondary antibody.

No significant difference could be detected in the clinical progression of the NgR(310)ecto-Fc treatment group because of the mortality associated with the first transplantation leading to low animal numbers available for analysis following EAE-induction. However, there was a significant difference observed in empty vector-transduced *ngr1*^{+/+} HSC recipients, empty vector-transduced *ngr1*^{-/-} HSC recipients and the control mice (non-transduced). Further studies with increased cohort sizes are required to confirm significant difference in the clinical progression of EAE. The demyelination and axonopathy study occurring in the spinal cord lesions of a NgR(310)ecto-Fc vector-transduced HSC recipient at clinical score 3 (acute stage of disease) revealed localisation of vector-positive immune cells in partially demyelinated and fully demyelinated lesions. Moreover, vector-positive immune cells were detected in proximity of pThr555-CRMP-2⁺ axons. As our laboratory has previously shown, phosphorylation of CRMP-2 at Thr 555 site is the downstream outcome of signalling through the NgR1 complex (Petratos et al., 2012), thus the pThr555-CRMP-2 expression

suggests NgR1 complex signalling is still occurring despite the presence of NgR(310)ecto-Fc fusion protein. Comparison with non-treated mice is required to elucidate whether pThr555-CRMP-2 is decreased due to inhibition of NgR1 by NgR(310)ecto-Fc or merely unaffected. As pThr555-CRMP-2⁺ is an indicator of axonal degeneration, the existence of pThr555-CRMP-2⁺ axons in spite of proximal vector-positive immune cells may be supported in studies of NgR(310)ecto-Fc treatment in spinal cord injury. It has been previously shown that treatment does not afford neuroprotection in acute injury as evidenced by similar levels of neuronal damage in treated and untreated animals, but rather it's affect is seen in enhancement of neuroregeneration (Wang et al., 2011, Wang et al., 2006b, Li et al., 2004).

Taken together, this pilot study has added advantage of demonstrating the utility of gene delivery technologies in pre-clinical research for future therapeutic adaptation in progressive MS. Despite the preliminary nature of our data, we have shown LV transduction of lin⁻ enriched BM cells, engraftment into irradiated recipients, lineage-differentiation, and trafficking of these cells into the CNS during acute EAE. Further rigorous studies are required to evaluate the clinical and mechanistic effects of NgR(310)ecto-Fc in EAE, which may in turn, be extended to MS. It has been extensively established that this fusion protein has the ability to promote axonal regeneration in spinal cord injury models, and remyelination has been exhibited in EAE with anti-LINGO-1 treatment (Mi et al., 2007). However, the similarities inferred between NgR(310)ecto-Fc and anti-LINGO-1 therapy are limited because of the potential non-exclusivity of LINGO-1 to the NgR1 signalling complex.

Full investigation of the regenerative potential of NgR(310)ecto-Fc in the CNS in the context of EAE, larger cohorts of HSCT mice extending to 40 days after EAE induction should be used to elucidate the effect of this treatment on the longer-term clinical progression of EAE. This would allow for better analysis of the impact of this fusion protein in the chronic stages of disease, thus as to fully investigate the ability of NgR(310)ecto-Fc to potentiate CNS repair by remyelination and axonal regeneration in CNS tissue collected from the chronic progressive stages of disease. An example of additional studies will include the investigation of axonal regeneration and distinguishing it from axonal preservation achieved by immunohistochemical analysis of growth associated protein 43 (GAP-43) expression, present in regenerating axons (Basi et al., 1987). LFB staining of myelin can be used to examine remyelination. On the basis of these finding, HSCT is a promising avenue for delivering specific, targeted therapeutic protein into the CNS in EAE and MS. The clinical relevance of NgR(310)ecto-Fc is yet to be determined through robust murine studies. It is evident there is a requirement for in-depth assessment of how NgR(310)ecto-Fc mediates degeneration and/or regeneration in CNS in the context of neurological injury induced by EAE and by extension, MS.

CHAPTER 6: Discussion

Current MS treatments predominantly target the inflammatory aspects of the disease, however, chronic-active MS lesions do not respond effectively to monotherapies (Fitzner, 2010). This highlights the critical need to develop novel disease modifying agents that can address the gap in treating progressive MS with profound neurodegenerative changes. A previous study from our laboratory has clearly demonstrated that deletion of NgR1 can protect against axonal degeneration, and thus progression of disease, in EAE-induced mice (Petratos et al., 2012). These data were further supported with signal transduction evidence to show that NgR1 may ultimately potentiate neurodegeneration in EAE via a direct neurobiological mechanism. Moreover, Nogo-A gene deletion or small interfering RNA (siRNA) knockdown, along with passive immunisation against the protein, have all been reported to confer disease-modifying activity during the course of EAE (Yang, 2010, Petratos et al., 2012), suggesting that Nogo-A may well be a plausible therapeutic target for neuroinflammatory disease, as seen in MS. Despite clear evidence demonstrating that the deletion of NgR1 can protect against axonal degeneration and thus progression of EAE, an immunological role for this receptor is yet to yield mechanistic evidence (McDonald et al., 2011).

Emerging evidence demonstrates that disease pathogenesis has been attributed to certain adaptive mechanisms through a combination of environmental and genetic factors that contribute to auto-reactive T-cells, entering the CNS and attacking myelin and oligodendrocytes and as such, the animal models of MS lack these heterogeneous risk factors. One hypothesis is that intracellular neuronal proteins are exposed to the immune system and eventually produce antibodies, which cause further neurodegeneration, by

releasing a great number of IgG antibodies (Weber et al., 2010, Hemmer et al., 2002). However, another plausible hypothesis during neuroinflammation is that NgR1 may be signalling in immune-competent cells during the inflammatory induction of EAE propagating pathology by immune damage to neural tissue. It has been shown that NgR1 has an effect on immune cell behaviour. Indeed, NgR1 can be expressed on circulating immune cells, such as rat macrophages, human monocytes and T-cells, and some inflammatory cells, from MS demyelinating lesions and may be involved in the induction of pro-inflammatory cytokines (Pool et al., 2009, David et al., 2008, Fry et al., 2007). Furthermore, NgR1 has the ability to change the motility of these cells exposed to myelin (as substrate), demonstrating that it may impact on immune cell infiltration and migration, and/or modulating adherence through an alternate signalling mechanism and thereby play a role in driving neuroinflammation (Pool et al., 2009, David et al., 2008). Moreover, a unique study revealed that the components of non-neuronal NgR1 are expressed on astrocytes and macrophages/microglia in MS brain lesions (Sato et al., 2007). However, the physiological mechanisms and a potential role of NgR1 on immune cells are yet to be illuminated.

In this project, we investigated the immunological mechanisms in EAE by cellular phenotyping to partially identify the role of NgR1 and its homologues, especially during B-cell maturation and differentiation, along with the identification of FLS localised in the CNS during inflammation. B-cells play a significant role in MS, in addition to their ability for processing and presenting antigen (von Budingen et al., 2011). To address the main question, EAE was induced by immunisation with MOG₃₅₋₅₅ and rMOG, in both

ngr1^{+/+} and *ngr1*^{-/-} mice. Recently, it has been suggested that the adherence capacity of human and mouse DCs to myelin substrate may be regulated by the expression of NgR1 and NgR2. This physiological mechanism may serve important in the processing of myelin for antigen presentation in EAE and MS. Recently, it was shown that when EAE was induced by rMOG, B-cells can play a role as sophisticated and highly selective antigen-presenting cells that promote the differentiation of pro-inflammatory T_{h1}- and T_{h17}- cells (Weber et al., 2010). Consistently, as we present in this study, immunisation with both peptides resulted in *ngr1*^{-/-} mice having a significant delay in EAE onset and a decrease in the severity of clinical signs when compared to *ngr1*^{+/+} mice, demonstrating the role of NgR1 in the B-cell populations at the acute stage of disease. Although these outcomes are consistent with our recent findings that the prevention and/or reduction of axonal degeneration in the optic nerve and spinal cord of EAE-induced mice by MOG₃₅₋₅₅ is associated with lower levels of pThr555CRMP-2 (Petratos et al., 2012, Litwak et al., 2013), they are not in line with previous studies that reported by Steinbach *et al.* (2011), who identified that combined genetic deletion of NgR1 and NgR2 did not enhance axonal sprouting in a chronic model of EAE-induced by MOG₃₅₋₅₅ (Steinbach et al., 2011). Moreover, it has been found that NgR1 deletion may dysregulate B-cell numbers when EAE is induced by rMOG (Litwak et al., 2013).

In the current study, we found that B-cells expressing NgR1 and NgR3 in the spinal cord of *ngr1*^{+/+} mice were significantly elevated at the acute stage of the disease compared to *ngr1*^{-/-} mice that were immunised with either MOG₃₅₋₅₅ or rMOG. This finding emphasises that NgR1 and NgR3 may signal in B-cells during the onset of EAE since the

signalling co-receptor TROY, was also identified in these cells, and suggest the existence of an association between NgR1 and NgR3 in the receptor-signalling complex. Although, our results are not in line with previous studies that demonstrated no significant influence of leukocyte infiltration into the CNS on the severity and development of EAE (Steinbach et al., 2011, Litwak et al., 2013), the Litwak *et al.* (2013) study implies that NgR1 may influence the APC function of B-cells or the production of potentially pathogenic humoral immune responses. There are several reasons for this discrepancy, including the source of the MOG peptide, the condition of animal facilities and/or the strength of the encephalitogenic challenge (Teuscher et al., 2004). Furthermore, our data has for the first time interrogated the expression of NgR1 and its homologues in B-cells localised within the spinal cord of EAE induced mice. Additionally, these double-positive B-cell populations, expressing NgR1 and NgR3 were clustered in FLS at the meninges of lumbosacral spinal cords of the of *ngr1*^{+/+} EAE-induced mice at the disease onset. From these data, we can now extrapolate that the role of NgR signalling in the differentiation and maturation of B-cells in EAE may be a pertinent mechanism to elucidate during EAE. Consistent with this, recent histopathological observations have demonstrated that B-cells are indeed presented in follicles at the meninges of MS patients (Howell et al., 2011, Serafini et al., 2004). Moreover, a very recent study demonstrated that NgR1 and NgR3, which are co-expressed in 293T cells, are part of the same receptor complex (Dickendesher et al., 2012).

Therefore, the question that we posited is whether or not NgR expression and potentially signalling govern the formation of these FLS in the CNS during progressive disease.

Taken together, these data may provide a platform to determine how the expression of NgR1 and NgR3 in B-cells localised within the CNS, during EAE, can further potentiate neurodegeneration and axonal degeneration, or alternatively, as reported by Pool *et al.* (2009) and David *et al.* (2008) govern their egress from the CNS. Even though the exact mechanism of the B-cell contribution to the cellular and humoral mechanisms of MS pathogenesis is still not fully understood, B-cell-targeted therapies have shown promising outcomes in clinical trials (Fassas and Mancardi, 2008) and so if NgR1 and NgR3 are also possible therapeutic targets, then they may be novel pathways of disease specific B-cell modulation.

With the emerging view that BAFF is a known stimulator of B-cell activation (Mackay *et al.*, 1999, Schneider *et al.*, 1999, Thompson *et al.*, 2000), we also investigated its role during NgR activation. This is due to the fact that BAFF has been highlighted as a potential target in MS because it is produced endogenously in the CNS by astrocytes during the pathogenesis; it is also importantly associated with BAFF-R expressing cells, which are up-regulated within the meninges in ectopic lymphoid follicles (Krumbholz *et al.*, 2005, Magliozzi *et al.*, 2004). It may also act as an alternate ligand for NgR1 to inhibit DRG neurite outgrowth *in vitro*, however no data were shown to correspond with to B-cell pathophysiology (Zhang *et al.*, 2009). Our finding indicated co-localisation of BAFF and NgR1 and NgR3 was identified in FLS at the meninges of the spinal cord of *ngr1*^{+/+} mice following EAE induction at the disease onset, confirming that fact that B-cells are a prominent feature in the neurodegenerative process in MS patients, as reported by Howell *et al.* (2011) and Serafini *et al.* (2004). On the basis of these findings, we

hypothesised that an alternate mechanism may also be operative with BAFF playing a role in the purported FLS formed in the CNS of MS patients and EAE mice, regulated possibly through NgR1 and NgR3 interactions.

In vitro studies performed whereby NgR-expressing B-cells were stimulated with BAFF have shown remarkable enhancement of their DNA synthesis stage at disease onset in the spleen and spinal cords of EAE-induced mice, demonstrating the ability of BAFF to direct the cells into proliferation. These findings were supported by blocking BAFF signalling *in vitro* using several peptides (e.g. rBAFF-R, NgR1-Fc and NgR3), causing replenishment of the isolated cells into the G0/G1 phase in the spleen and spinal cord of *ngr1*^{-/-} mice. These data showed for the first time that both NgR1 and NgR3 are active contributors to B-cell maturation during EAE and may participate in the signal transduction events elicited through BAFF ligation, although the direct signal transduction effects within these B-cells are yet to be elucidated. Consequently, we identified the biological consequences of secretory immunoglobulins from these cells and its participation in the effector function leading to demyelination, and we found that there was a significant elevation of secreted immunoglobulins from these cells in the spinal cord of *ngr1*^{-/-} mice at disease onset, suggesting these CNS-infiltrates are maturing B-cells and have the ability to develop antibody production. Furthermore, we identified that the secretory form of IgG from isolated cells immunoreacted with oligodendrocyte epitopes in the spinal cord tissues of *ngr1*^{+/+} mice and bound directly to myelin, providing possible evidence of active promotion of antibody-mediated demyelination.

These findings coincide with Sadaba *et al.* (2012) who reported that IgG and IgM are co-localised on oligodendrocytes leading to disability in MS (Sadaba *et al.*, 2012).

Blockade of NgR1-ligand signalling using a novel HSC-based delivery of a therapeutic protein is considered one such promising approach in EAE, as we identified that NgR1 localised on B-cells may interact with BAFF on neighbouring B-cells within a FLS stimulating their development, thereby propagating the neurodegenerative disease through the development of immunocompetent B-cells that target neural autoantigens. Given that a series of studies using the NgR(310)ecto-Fc have recently shown enhanced neurological improvement in injury and disease models of the CNS by blocking the binding of the MAIFs (Wang *et al.*, 2006b, Li *et al.*, 2004, Lee *et al.*, 2004). In this project, we attempted to investigate whether the NgR1-Fc can bind and inactivate BAFF signalling in B-cells localised in the spinal cord, along with limiting degeneration and inflammatory demyelination during EAE. Therefore, we have systematically compared the clinical and pathological outcome of EAE in NgR(310)ecto-Fc treated mice to various un-treated controls. Our preliminary results confirmed that a successful transplantation, as we found that ZsGreen positive immune lineage-differentiated cells and fusion protein were trafficking into the CNS during EAE. These outcomes demonstrate a promising aspect for delivering therapeutic fusion protein into the CNS in EAE and by extension, MS. However, appropriate validation of NgR(310)ecto-Fc utility as a therapeutic paradigm remains to be achieved. In particular, this will also require the elucidation of the appropriate pathogenic ligand(s), BAFF and/or MAIFs/CSPGs.

Study Limitations and future directions

In this project, we aimed to answer a critical question in neuroimmunology regarding the existence of a prominent immunological role for NgR, which may in fact play a role in the maturation and differentiation of B-cells within the follicles that are localised within the CNS during neuroinflammation, exhibited in the animal model of MS, EAE. We systematically dissected the immune function of NgR1 and NgR3 during CNS inflammation, initially in *ngr1*^{+/+} mice following EAE induction. We then compared this repertoire with the *ngr1*^{-/-} mutant mice, to elucidate how the expression of NgR1 and NgR3 on specific immune cell lineages can effect their infiltration and activation in the CNS. In particular, future work has been planned to identify how NgR1 and NgR3 can propagate neurodegeneration by blocking the inflammatory-mediated effect of degeneration in the CNS by virtue of a novel gene delivery system of the therapeutic fusion protein, NgR1-Fc. As a potential therapeutic strategy, we have shown LV transduction of lin⁻ enriched BM cells, engraftment into irradiated recipients, lineage-differentiation, and trafficking of these cells into the CNS during acute EAE but the efficacy of NgR1-Fc in the limitation of neurodegenerative or repair process along with limitation of B-cell activity are yet to be demonstrated. In addition, further qualifications of oligodendrocytes, macrophages/microglia and paranode junction, which demonstrated in a cluster of cells positive for IgG in the spinal cord and optic nerve tissues of the *ngr1*^{+/+} mice at disease onset, are required, using specific markers.

Future Directions

A. Utilising an immune cell adoptive transfer technique to identify the role of NgR1 in EAE disease onset

Rationale: In EAE, myelin-specific T_{H1} -cells can be adoptively transferred to induce EAE into recipient animals and are directly related to the immunopathology of the disease (Martinez et al., 2012). What we need to establish now is if the expression or deletion of NgR1 can modulate the T-cell responsiveness by utilising an adoptive transfer paradigm. Currently, our laboratory has transferred HSCs *ngR1*^{-/-} mice into *ngR1*^{+/+} mice, thus the disease onset and progression can be assessed.

B. A conditional Knock down of NgR1 in B-cells by crossing NgR1-floxed mice with the Mb1-Cre transgenic mice, B-cell specific Cre-mouse line.

Rationale: The Cre-loxP site specific recombination system allows us to control gene activity in space and time in any mouse tissue, opening new avenues for studying the role of genes and for creating sophisticated mouse models of human diseases (Feil, 2009). In our study, we identified that NgR1 and its homologue localised on B-cells may interact with BAFF on neighbouring B-cells within a follicular structure stimulating their development, thereby propagating the neurodegenerative disease through the development of immunocompetent B-cells that target neural autoantigens. Therefore, we hypothesise that a conditional gene deletion of NgR1 on these B-cells may ameliorate disease progression.

C. Large cohort of HSCT animals to deliver NgR(310)ecto-Fc into the lesion-specific that can attenuate axonal degeneration during EAE.

Rational: Full investigation of the regenerative potential of NgR(310)ecto-Fc in the CNS in the context of EAE, larger cohorts of HSCT mice extending to 40 days after EAE induction should be used to elucidate the effect of this treatment on the longer-term clinical progression of EAE. This would allow for better analysis of the impact of this fusion protein in the chronic stages of disease, thus as to fully investigate the ability of NgR(310)ecto-Fc to potentiate CNS repair by remyelination and axonal regeneration in CNS tissue collected from the chronic progressive stages of disease. An example of additional studies, we will perform to investigate axonal regeneration and distinguish it from axonal preservation is immunohistochemical analysis of growth associated protein 43 (GAP-43), present in regenerating axons (Basi et al., 1987). Electronmicroscopy and MRI (diffusion weighted imaging) of myelin can be used to examine remyelination, or limitation of demyelination. On the basis of these findings, HSCT is a promising avenue for delivering specific, targeted therapeutic protein into the CNS in EAE and MS. The clinical relevance of NgR(310)ecto-Fc is yet to be determined through robust murine studies. It is evident there is a requirement for in-depth assessment of how NgR(310)ecto-Fc limits degeneration and/or enhances regeneration in CNS in the context of neurological injury induced by EAE and by extension, MS.

References

- ALDERUCCIO, F., NASA, Z., CHUNG, J., KO, H. J., CHAN, J. & TOH, B. H. 2011. Hematopoietic stem cell gene therapy as a treatment for autoimmune diseases. *Mol Pharm*, 8, 1488-94.
- ALIX, J. J., BLACKBURN, D. J., SOKHI, D., CRAVEN, I., SHARRACK, B. & SNOWDEN, J. A. 2013. Autologous hematopoietic stem cell transplantation following pulsed cyclophosphamide in a severely disabled patient with malignant multiple sclerosis. *J Neurol*, 260, 914-6.
- ATKINS, H. L. & FREEDMAN, M. S. 2013. Hematopoietic stem cell therapy for multiple sclerosis: top 10 lessons learned. *Neurotherapeutics*, 10, 68-76.
- ATKINS, H. L., MURARO, P. A., VAN LAAR, J. M. & PAVLETIC, S. Z. 2012. Autologous hematopoietic stem cell transplantation for autoimmune disease--is it now ready for prime time? *Biol Blood Marrow Transplant.*, 18, S177-83.
- BABBE, H., ROERS, A., WAISMAN, A., LASSMANN, H., GOEBELS, N., HOHLFELD, R., FRIESE, M., SCHRODER, R., DECKERT, M., SCHMIDT, S., RAVID, R. & RAJEWSKY, K. 2000. Clonal expansions of CD8(+) T cells dominate the T cell infiltrate in active multiple sclerosis lesions as shown by micromanipulation and single cell polymerase chain reaction. *J Exp Med*, 192, 393-404.
- BASI, G. S., JACOBSON, R. D., VIRÁG, I., SCHILLING, J. & SKENE, J. P. 1987. Primary structure and transcriptional regulation of GAP-43, a protein associated with nerve growth. *Cell*, 49, 785-791.
- BERMEJO, D. A., AMEZCUA-VESELY, M. C., MONTES, C. L., MERINO, M. C., GEHRAU, R. C., CEJAS, H., ACOSTA-RODRIGUEZ, E. V. & GRUPPI, A. 2010. BAFF mediates splenic B cell response and antibody production in experimental Chagas disease. *PLoS Negl Trop Dis*, 4, e679.
- BERNARD, C. C., JOHNS, T. G., SLAVIN, A., ICHIKAWA, M., EWING, C., LIU, J. & BETTADAPURA, J. 1997. Myelin oligodendrocyte glycoprotein: a novel candidate autoantigen in multiple sclerosis. *J Mol Med (Berl)*, 75, 77-88.
- BETTADAPURA, J., MENON, K. K., MORITZ, S., LIU, J. & BERNARD, C. C. 1998. Expression, purification, and encephalitogenicity of recombinant human myelin oligodendrocyte glycoprotein. *J Neurochem*, 70, 1593-9.
- BETTELLI, E. 2007. Building different mouse models for human MS. *Ann N Y Acad Sci.*, 1103, 11-8.
- BOURQUIN, C., VAN DER HAAR, M. E., ANZ, D., SANDHOLZER, N., NEUMAIER, I., ENDRES, S., SKERRA, A., SCHWAB, M. E. & LININGTON, C. 2008. DNA vaccination efficiently induces antibodies to Nogo-A and does not exacerbate experimental autoimmune encephalomyelitis. *Eur J Pharmacol*, 588, 99-105.
- BOWEN, J. D., KRAFT, G. H., WUNDES, A., GUAN, Q., MARAVILLA, K. R., GOOLEY, T. A., MCSWEENEY, P. A., PAVLETIC, S. Z., OPENSHAW, H., STORB, R., WENER, M., MCLAUGHLIN, B. A., HENSTORF, G. R. & NASH, R. A. 2012. Autologous hematopoietic cell transplantation following high-dose immunosuppressive

- therapy for advanced multiple sclerosis: long-term results. *Bone Marrow Transplant*, 47, 946-51.
- BURT, R. K., BALABANOV, R., HAN, X., SHARRACK, B., MORGAN, A., QUIGLEY, K., YAUNG, K., HELENOWSKI, I. B., JOVANOVIĆ, B., SPAHOVIĆ, D., ARNAUTOVIĆ, I., LEE, D. C., BENEFIELD, B. C., FUTTERER, S., OLIVEIRA, M. C. & BURMAN, J. 2015. Association of nonmyeloablative hematopoietic stem cell transplantation with neurological disability in patients with relapsing-remitting multiple sclerosis. *JAMA*, 313, 275-84.
- BURT, R. K., BURNS, W. & HESS, A. 1995. Bone marrow transplantation for multiple sclerosis. *Bone Marrow Transplant*, 16, 1-6.
- BURT, R. K., COHEN, B., ROSE, J., PETERSEN, F., OYAMA, Y., STEFOSKI, D., KATSAMAKIS, G., CARRIER, E., KOZAK, T., MURARO, P. A., MARTIN, R., HINTZEN, R., SLAVIN, S., KARUSSIS, D., HAGGIAG, S., VOLTARELLI, J. C., ELLISON, G. W., JOVANOVIĆ, B., POPAT, U., MCGUIRK, J., STATKUTE, L., VERDA, L., HAAS, J. & ARNOLD, R. 2005. Hematopoietic stem cell transplantation for multiple sclerosis. *Arch Neurol*, 62, 860-4.
- BURT, R. K., COHEN, B. A., RUSSELL, E., SPERO, K., JOSHI, A., OYAMA, Y., KARPUS, W. J., LUO, K., JOVANOVIĆ, B., TRAYNOR, A., KARLIN, K., STEFOSKI, D. & BURNS, W. H. 2003. Hematopoietic stem cell transplantation for progressive multiple sclerosis: failure of a total body irradiation-based conditioning regimen to prevent disease progression in patients with high disability scores. *Blood*, 102, 2373-8.
- BURT RK, T. A., CRAIG R, COHEN B, SUFFIT R, BARR W 2008. Hematopoietic stem cell transplantation for autoimmune diseases: what have we learned? *J Autoimmun.*, 30, 116-20.
- BUSS, A. & SCHWAB, M. E. 2003. Sequential loss of myelin proteins during Wallerian degeneration in the rat spinal cord. *Glia*, 42, 424-32.
- CARBONATTO, M., YU, P., BERTOLINO, M., VIGNA, E., STEIDLER, S., FAVA, L., DAGHERO, C., ROATTINO, B., ONIDI, M., ARDIZZONE, M., PEANO, S., VISICH, J., JANSZEN, D., DILLON, S. & PONCE, R. 2008. Nonclinical safety, pharmacokinetics, and pharmacodynamics of atacicept. *Toxicol Sci*, 105, 200-10.
- CARRERAS, E., SAIZ, A., MARIN, P., MARTINEZ, C., ROVIRA, M., VILLAMOR, N., AYMERICH, M., LOZANO, M., FERNANDEZ-AVILES, F., URBANO-IZPIZUA, A., MONTSERRAT, E. & GRAUS, F. 2003. CD34+ selected autologous peripheral blood stem cell transplantation for multiple sclerosis: report of toxicity and treatment results at one year of follow-up in 15 patients. *Haematologica*, 88, 306-14.
- CASTIGLI, E., WILSON, S. A., SCOTT, S., DEDEOGLU, F., XU, S., LAM, K. P., BRAM, R. J., JABARA, H. & GEHA, R. S. 2005. TACI and BAFF-R mediate isotype switching in B cells. *J Exp Med*, 201, 35-9.
- CHALLEN, G. A., BOLES, N., LIN, K. K. & GOODELL, M. A. 2009. Mouse hematopoietic stem cell identification and analysis. *Cytometry A*, 75, 14-24.
- CHAN, J., BAN, E., CHUN, K., WANG, B., BACKSTROM, B., BERNARCD, C. & ET, A. 2008. Transplantation of Bone Marrow transduced to Express Self-Antigen

- Establishes Deletional Tolerance and Permanently Remits Autoimmune Disease. *J Immunol.*, 181, 7571-7580.
- CHUN, J., HARTUNG HP 2010. Mechanism of action of oral fingolimod (FTY720) in multiple sclerosis. *Clin Neuropharmacol*, 33, 91-101.
- CHUNG, J. Y., FIGGETT, W., FAIRFAX, K., BERNARD, C., CHAN, J., TOH, B. H., MACKAY, F. & ALDERUCCIO, F. 2014. Gene therapy delivery of myelin oligodendrocyte glycoprotein (MOG) via hematopoietic stem cell transfer induces MOG-specific B cell deletion. *J Immunol*, 192, 2593-601.
- COMPSTON, A. & COLES, A. 2002. Multiple sclerosis. *Lancet*, 359, 1221-31.
- CRAWFORD, M. P., YAN, S. X., ORTEGA, S. B., MEHTA, R. S., HEWITT, R. E., PRICE, D. A., STASTNY, P., DOUEK, D. C., KOUP, R. A., RACKE, M. K. & KARANDIKAR, N. J. 2004. High prevalence of autoreactive, neuroantigen-specific CD8+ T cells in multiple sclerosis revealed by novel flow cytometric assay. *Blood*, 103, 4222-31.
- CUKER, A., COLES, A. J., SULLIVAN, H., FOX, E., GOLDBERG, M., OYUELA, P., PURVIS, A., BEARDSLEY, D. S. & MARGOLIN, D. H. 2011. A distinctive form of immune thrombocytopenia in a phase 2 study of alemtuzumab for the treatment of relapsing-remitting multiple sclerosis. *Blood.*, 118, 6299-305.
- DAIKELER, T., LABOPIN, M., DI GIOIA, M., ABINUN, M., ALEXANDER, T., MINIATI, I., GUALANDI, F., FASSAS, A., MARTIN, T., SCHWARZE, C. P., WULFFRAAT, N., BUCH, M., SAMPOL, A., CARRERAS, E., DUBOIS, B., GRUHN, B., GUNGOR, T., POHLREICH, D., SCHUERWEGH, A., SNARSKI, E., SNOWDEN, J., VEYS, P., FASTH, A., LENHOFF, S., MESSINA, C., VOSWINKEL, J., BADOGLIO, M., HENES, J., LAUNAY, D., TYNDALL, A., GLUCKMAN, E., FARGE, D. & PARTY, E. A. D. W. 2011. Secondary autoimmune diseases occurring after HSCT for an autoimmune disease: a retrospective study of the EBMT Autoimmune Disease Working Party. *Blood.*, 118, 1693-8.
- DAU, P. C. 1995. Increased antibody production in peripheral blood mononuclear cells after plasma exchange therapy in multiple sclerosis. *J Neuroimmunol*, 62, 197-200.
- DAVID, S., FRY, E. J. & LOPEZ-VALES, R. 2008. Novel roles for Nogo receptor in inflammation and disease. *Trends Neurosci*, 31, 221-6.
- DAVID, S. & LACROIX, S. 2003. Molecular approaches to spinal cord repair. *Annu Rev Neurosci*, 26, 411-40.
- DEV, K. K., MULLERSHAUSEN F, MATTES H, KUHN RR, BILBE G, HOYER D, ET AL 2008. Brain sphingosine-1-phosphate receptors: implication for FTY720 in the treatment of multiple sclerosis. *Pharmacol Ther.*, 117, 77-93.
- DI BELLO, I. C., DAWSON, M. R., LEVINE, J. M. & REYNOLDS, R. 1999. Generation of oligodendroglial progenitors in acute inflammatory demyelinating lesions of the rat brain stem is associated with demyelination rather than inflammation. *J Neurocytol*, 28, 365-81.
- DICKENDESHER, T. L., BALDWIN, K. T., MIRONOVA, Y. A., KORIYAMA, Y., RAIKER, S. J., ASKEW, K. L., WOOD, A., GEOFFROY, C. G., ZHENG, B., LIEPMANN, C. D., KATAGIRI, Y., BENOWITZ, L. I., GELLER, H. M. & GIGER, R. J. 2012. NgR1 and NgR3 are receptors for chondroitin sulfate proteoglycans. *Nat Neurosci*, 15, 703-12.

- DORNER, T. & BURMESTER, G. R. 2008. New approaches of B-cell-directed therapy: beyond rituximab. *Curr Opin Rheumatol*, 20, 263-8.
- DURAN-STRUUCK, R. & DYSKO, R. C. 2009. Principles of Bone Marrow Transplantation (BMT): Providing Optimal Veterinary and Husbandry Care to Irradiated Mice in BMT Studies. *Journal of the American Association for Laboratory Animal Science : JAALAS*, 48, 11-22.
- EMA, H., MORITA, Y., YAMAZAKI, S., MATSUBARA, A., SEITA, J., TADOKORO, Y., KONDO, H., TAKANO, H. & NAKAUCHI, H. 2007. Adult mouse hematopoietic stem cells: purification and single-cell assays. *Nat. Protocols*, 1, 2979-2987.
- FAGIUS, J., LUNDGREN, J. & OBERG, G. 2009. Early highly aggressive MS successfully treated by hematopoietic stem cell transplantation. *Mult Scler*, 15, 229-37.
- FARGE, D., LABOPIN, M., TYNDALL, A., FASSAS, A., MANCARDI, G. L., VAN LAAR, J., OUYANG, J., KOZAK, T., MOORE, J., KOTTER, I., CHESNEL, V., MARMONT, A., GRATWOHL, A. & SACCARDI, R. 2010. Autologous hematopoietic stem cell transplantation for autoimmune diseases: an observational study on 12 years' experience from the European Group for Blood and Marrow Transplantation Working Party on Autoimmune Diseases. *Haematologica*, 95, 284-92.
- FASSAS A, ANAGNOSTOPOULOS A, KAZIS A, KAPINAS A, SAKELLARI I, KIMISKIDIS V & TSOMPANAKOU A 1997. Peripheral blood stem cell transplantation in the treatment of progressive multiple sclerosis: first results of a pilot study. *Bone Marrow Transplant*, 20, 631-8.
- FASSAS A, ANAGNOSTOPOULOS A, KAZIS A, KAPINAS K, SAKELLARI I, KIMISKIDIS V, SMIAS C, ELEFThERIADIS N & V., T. 2000. Autologous stem cell transplantation in progressive multiple sclerosis--an interim analysis of efficacy. *J Clin Immunol*, 24-30.
- FASSAS, A., KIMISKIDIS, V. K., SAKELLARI, I., KAPINAS, K., ANAGNOSTOPOULOS, A., TSIMOURTOU, V., SOTIRAKOGLU, K. & KAZIS, A. 2011. Long-term results of stem cell transplantation for MS: a single-center experience. *Neurology*, 76, 1066-70.
- FASSAS, A. & MANCARDI, G. L. 2008. Autologous hemopoietic stem cell transplantation for multiple sclerosis: is it worthwhile? *Autoimmunity*, 41, 601-10.
- FASSAS, A. & NASH, R. 2004. Multiple sclerosis. *Best Practice & Research Clinical Haematology*, 17, 247-262.
- FEIL, S., VALTCHEVA N, FEIL R 2009. Inducible Cre mice. *Methods Mol Biol*, 530, 343-63.
- FILIP, S., MOKRÝ, J., VÁVROVÁ, J., CÍZKOVÁ, D., SINKOROVÁ, Z., TOSNEROVÁ, V. & BLÁHA, M. 2009. Homing of lin-/CD117+ hematopoietic stem cells. *Transfusion and Apheresis Science*, 41, 183-190.
- FINKELMAN, F. D., HOLMES, J., KATONA, I. M., URBAN, J. F., JR., BECKMANN, M. P., PARK, L. S., SCHOOLEY, K. A., COFFMAN, R. L., MOSMANN, T. R. & PAUL, W. E. 1990. Lymphokine control of in vivo immunoglobulin isotype selection. *Annu Rev Immunol*, 8, 303-33.

- FITZNER, D., SIMONS M 2010. Chronic Progressive Multiple Sclerosis – Pathogenesis of Neurodegeneration and Therapeutic Strategies. *Curr Neuropharmacol.*, 8, 305-315.
- FONTOURA, P., HO, P. P., DEVOSS, J., ZHENG, B., LEE, B. J., KIDD, B. A., GARREN, H., SOBEL, R. A., ROBINSON, W. H., TESSIER-LAVIGNE, M. & STEINMAN, L. 2004. Immunity to the extracellular domain of Nogo-A modulates experimental autoimmune encephalomyelitis. *J Immunol*, 173, 6981-92.
- FOURNIER, A. E., TAKIZAWA, B. T. & STRITTMATTER, S. M. 2003. Rho kinase inhibition enhances axonal regeneration in the injured CNS. *J Neurosci*, 23, 1416-23.
- FRY, E. J., HO, C. & DAVID, S. 2007. A role for Nogo receptor in macrophage clearance from injured peripheral nerve. *Neuron*, 53, 649-62.
- GECZY, C. L., ROBERTS, I. M., MEYER, P. & BERNARD, C. C. 1984. Susceptibility and resistance to experimental autoimmune encephalomyelitis and neuritis in the guinea pig correlate with the induction of procoagulant and anticoagulant activities. *J Immunol*, 133, 3026-36.
- GIGER, R. J., HOLLIS, E. R., 2ND & TUSZYNSKI, M. H. 2010. Guidance molecules in axon regeneration. *Cold Spring Harb Perspect Biol*, 2, a001867.
- GIROLAMO, F., FERRARA, G., STRIPPOLI, M., RIZZI, M., ERREDE, M., TROJANO, M., PERRIS, R., RONCALI, L., SVELTO, M., MENNINI, T. & VIRGINTINO, D. 2011. Cerebral cortex demyelination and oligodendrocyte precursor response to experimental autoimmune encephalomyelitis. *Neurobiol Dis*, 43, 678-89.
- GOSELIN, D. & RIVEST, S. 2011. Immune mechanisms underlying the beneficial effects of autologous hematopoietic stem cell transplantation in multiple sclerosis. *Neurotherapeutics*, 8, 643-9.
- GRESS, R. E., EMERSON, S. G. & DROBYSKI, W. R. 2010. Immune reconstitution: how it should work, what's broken, and why it matters. *Biol Blood Marrow Transplant.*, 16, S133-7.
- GROSS, J. A., JOHNSTON, J., MUDRI, S., ENSELMAN, R., DILLON, S. R., MADDEN, K., XU, W., PARRISH-NOVAK, J., FOSTER, D., LOFTON-DAY, C., MOORE, M., LITTAU, A., GROSSMAN, A., HAUGEN, H., FOLEY, K., BLUMBERG, H., HARRISON, K., KINDSVOGEL, W. & CLEGG, C. H. 2000. TACI and BCMA are receptors for a TNF homologue implicated in B-cell autoimmune disease. *Nature*, 404, 995-9.
- GUERMONPREZ, P., VALLADEAU J, ZITVOGEL L, THÉRY C, AMIGORENA S 2002. Antigen presentation and T cell stimulation by dendritic cells. *Annu Rev Immunol*, 20, 621-67.
- GUIMARÃES FA, O.-C. E., MASTROPIETRO AP, ET AL 2010. Impact of autologous hematopoietic stem cell transplantation on the quality of life of patients with multiple sclerosis. *Arg Neuropsiquiatr*, 68, 522-7.
- GUIRGUIS, A., SLAPE, C., FAILLA, L., SAW, J., TREMBLAY, C., POWELL, D., ROSSELLO, F., WEI, A., STRASSER, A. & CURTIS, D. 2016. PUMA promotes apoptosis of hematopoietic progenitors driving leukemic progression in a mouse model of myelodysplasia. *Cell Death & Differentiation*.
- HAILE, Y., SIMMEN, K. C., PASICHNYK, D., TOURET, N., SIMMEN, T., LU, J. Q., BLEACKLEY, R. C. & GIULIANI, F. 2011. Granule-derived granzyme B

- mediates the vulnerability of human neurons to T cell-induced neurotoxicity. *J Immunol*, 187, 4861-72.
- HANSON, W., FRY, R., SALLESE, A., FRISCHER, H., AHMAD, T. & AINSWORTH, E. 1987. Comparison of Intestine and Bone Marrow Radiosensitivity of the BALB/c and the C57BL/6 Mouse Strains and Their Offspring. *Radiation research*, 110, 340-352.
- HARTUNG, H. P. & KIESEIER, B. C. 2010. Atacicept: targeting B cells in multiple sclerosis. *Ther Adv Neurol Disord*, 3, 205-16.
- HAUSER, S. L., WAUBANT, E., ARNOLD, D. L., VOLLMER, T., ANTEL, J., FOX, R. J., BAROR, A., PANZARA, M., SARKAR, N., AGARWAL, S., LANGER-GOULD, A., SMITH, C. H. & GROUP, H. T. 2008. B-cell depletion with rituximab in relapsing-remitting multiple sclerosis. *N Engl J Med*, 358, 676-88.
- HEDEGAARD, C. J., SELLEBJERG, F., KRAKAUER, M., HESSE, D., BENDTZEN, K. & NIELSEN, C. H. 2011. Interferon-beta increases systemic BAFF levels in multiple sclerosis without increasing autoantibody production. *Mult Scler*, 17, 567-77.
- HEMMER, B., ARCHELOS, J. J. & HARTUNG, H. P. 2002. New concepts in the immunopathogenesis of multiple sclerosis. *Nat Rev Neurosci*, 3, 291-301.
- HOLLOMAN, J., HO, CC, HUKKI A, ET AL 2013. The development of hematopoietic and mesenchymal stem cell transplantation as an effective treatment for multiple sclerosis. *Am J Stem Cell*, 2, 95-107.
- HOWELL, O. W., REEVES, C. A., NICHOLAS, R., CARASSITI, D., RADOTRA, B., GENTLEMAN, S. M., SERAFINI, B., ALOISI, F., RONCAROLI, F., MAGLIOZZI, R. & REYNOLDS, R. 2011. Meningeal inflammation is widespread and linked to cortical pathology in multiple sclerosis. *Brain*, 134, 2755-71.
- HUNTINGTON, N. D., TOMIOKA, R., CLAVARINO, C., CHOW, A. M., LINARES, D., MANA, P., ROSSJOHN, J., CACHERO, T. G., QIAN, F., KALLED, S. L., BERNARD, C. C. & REID, H. H. 2006. A BAFF antagonist suppresses experimental autoimmune encephalomyelitis by targeting cell-mediated and humoral immune responses. *Int Immunol*, 18, 1473-85.
- ICHIKAWA, M., KOH, C. S., INABA, Y., SEKI, C., INOUE, A., ITOH, M., ISHIHARA, Y., BERNARD, C. C. & KOMIYAMA, A. 1999. IgG subclass switching is associated with the severity of experimental autoimmune encephalomyelitis induced with myelin oligodendrocyte glycoprotein peptide in NOD mice. *Cell Immunol*, 191, 97-104.
- JARIUS, S. & WILDEMANN, B. 2010. AQP4 antibodies in neuromyelitis optica: diagnostic and pathogenetic relevance. *Nat Rev Neurol*, 6, 383-92.
- JEON, S. T., KIM, W. J., LEE, S. M., LEE, M. Y., PARK, S. B., LEE, S. H., KIM, I. S., SUK, K., CHOI, B. K., CHOI, E. M., KWON, B. S. & LEE, W. H. 2010. Reverse signaling through BAFF differentially regulates the expression of inflammatory mediators and cytoskeletal movements in THP-1 cells. *Immunol Cell Biol*, 88, 148-56.
- JUOPPERI, T. A., SCHULER, W., YUAN, X., COLLECTOR, M. I., DANG, C. V. & SHARKIS, S. J. 2007. Isolation of Bone Marrow-Derived Stem Cells using Density-Gradient Separation. *Exp Hematol.*, 35, 335-341.

- KANEKO, T., AMANO, H., KAWANO, S., MINOWA, K., ANDO, S., WATANABE, T., NAKANO, S., SUZUKI, J., MORIMOTO, S., TOKANO, Y. & TAKASAKI, Y. 2014. Increased serum concentration of BAFF/APRIL and IgA2 subclass in patients with mixed connective tissue disease complicated by interstitial lung disease. *Mod Rheumatol*, 24, 310-5.
- KANNEL, K., ALNEK, K., VAHTER, L., GROSS-PAJU, K., UIBO, R. & KISAND, K. V. 2015. Changes in Blood B Cell-Activating Factor (BAFF) Levels in Multiple Sclerosis: A Sign of Treatment Outcome. *PLoS One*, 10, e0143393.
- KAPPOS, L., LI, D., CALABRESI, P. A., O'CONNOR, P., BAR-OR, A., BARKHOF, F., YIN, M., LEPPERT, D., GLANZMAN, R., TINBERGEN, J. & HAUSER, S. L. 2011. Ocrelizumab in relapsing-remitting multiple sclerosis: a phase 2, randomised, placebo-controlled, multicentre trial. *Lancet*, 378, 1779-87.
- KARNEZIS, T., MANDEMAKERS, W., MCQUALTER, J. L., ZHENG, B., HO, P. P., JORDAN, K. A., MURRAY, B. M., BARRES, B., TESSIER-LAVIGNE, M. & BERNARD, C. C. 2004. The neurite outgrowth inhibitor Nogo A is involved in autoimmune-mediated demyelination. *Nat Neurosci*, 7, 736-44.
- KAY, M. A., GLORIOSO, J. C. & NALDINI, L. 2001. Viral vectors for gene therapy: the art of turning infectious agents into vehicles of therapeutics. *Nature medicine*, 7, 33-40.
- KEBIR, H., KREYMBORG, K., IFERGAN, I., DODELET-DEVILLERS, A., CAYROL, R., BERNARD, M., GIULIANI, F., ARBOUR, N., BECHER, B. & PRAT, A. 2007. Human TH17 lymphocytes promote blood-brain barrier disruption and central nervous system inflammation. *Nat Med*, 13, 1173-5.
- KEEGAN, M., KONIG, F., MCCLELLAND, R., BRUCK, W., MORALES, Y., BITSCH, A., PANITCH, H., LASSMANN, H., WEINSHENKER, B., RODRIGUEZ, M., PARISI, J. & LUCCHINETTI, C. F. 2005. Relation between humoral pathological changes in multiple sclerosis and response to therapeutic plasma exchange. *Lancet*, 366, 579-82.
- KIM, S. S., RICHMAN, D. P., ZAMVIL, S. S. & AGIUS, M. A. 2011. Accelerated central nervous system autoimmunity in BAFF-receptor-deficient mice. *J Neurol Sci*, 306, 9-15.
- KIMISKIDIS, V., SAKELLARI, I., TSIMOURTOU, V., KAPINA, V., PAPAGIANNPOULOS, S., KAZIS, D., VLAIKIDIS, N., ANAGNOSTOPOULOS, A. & FASSAS, A. 2008. Autologous stem-cell transplantation in malignant multiple sclerosis: a case with a favorable long-term outcome. *Mult Scler.*, 14, 278-83.
- KRUMBHOLZ, M., DERFUSS, T., HOHLFELD, R. & MEINL, E. 2012. B cells and antibodies in multiple sclerosis pathogenesis and therapy. *Nat Rev Neurol*, 8, 613-23.
- KRUMBHOLZ, M., DERFUSS T, HOHLFELD R, MEINL E 2012. B cells and antibodies in multiple sclerosis pathogenesis and therapy. *Nat Rev Neurol*, 8, 613-23.
- KRUMBHOLZ, M., FABER, H., STEINMEYER, F., HOFFMANN, L. A., KUMPFEL, T., PELLKOFER, H., DERFUSS, T., IONESCU, C., STARCK, M., HAFNER, C., HOHLFELD, R. & MEINL, E. 2008. Interferon-beta increases BAFF levels in multiple sclerosis: implications for B cell autoimmunity. *Brain*, 131, 1455-63.
- KRUMBHOLZ, M., THEIL, D., CEPOK, S., HEMMER, B., KIVISAKK, P., RANSOHOFF, R. M., HOFBAUER, M., FARINA, C., DERFUSS, T., HARTLE, C., NEWCOMBE, J.,

- HOHLFELD, R. & MEINL, E. 2006. Chemokines in multiple sclerosis: CXCL12 and CXCL13 up-regulation is differentially linked to CNS immune cell recruitment. *Brain*, 129, 200-11.
- KRUMBHOLZ, M., THEIL, D., DERFUSS, T., ROSENWALD, A., SCHRADER, F., MONORANU, C. M., KALLED, S. L., HESS, D. M., SERAFINI, B., ALOISI, F., WEKERLE, H., HOHLFELD, R. & MEINL, E. 2005. BAFF is produced by astrocytes and up-regulated in multiple sclerosis lesions and primary central nervous system lymphoma. *J Exp Med*, 201, 195-200.
- KUTZELNIGG, A., LUCCHINETTI, C. F., STADELMANN, C., BRUCK, W., RAUSCHKA, H., BERGMANN, M., SCHMIDBAUER, M., PARISI, J. E. & LASSMANN, H. 2005. Cortical demyelination and diffuse white matter injury in multiple sclerosis. *Brain*, 128, 2705-12.
- LEE, J. K., KIM, J. E., SIVULA, M. & STRITTMATTER, S. M. 2004. Nogo receptor antagonism promotes stroke recovery by enhancing axonal plasticity. *J Neurosci*, 24, 6209-17.
- LEE, J. Y., BIEMOND, M. & PETRATOS, S. 2015. Axonal degeneration in multiple sclerosis: defining therapeutic targets by identifying the causes of pathology. *Neurodegener Dis Manag*, 5, 527-48.
- LEMKE, G. 1988. Unwrapping the genes of myelin. *Neuron*, 1, 535-43.
- LI, S., LIU, B. P., BUDEL, S., LI, M., JI, B., WALUS, L., LI, W., JIRIK, A., RABACCHI, S., CHOI, E., WORLEY, D., SAH, D. W., PEPINSKY, B., LEE, D., RELTON, J. & STRITTMATTER, S. M. 2004. Blockade of Nogo-66, myelin-associated glycoprotein, and oligodendrocyte myelin glycoprotein by soluble Nogo-66 receptor promotes axonal sprouting and recovery after spinal injury. *J Neurosci*, 24, 10511-20.
- LITWAK, S. A., PAYNE, N. L., CAMPANALE, N., OZTURK, E., LEE, J. Y., PETRATOS, S., SIATSKAS, C., BAKHURAYSAH, M. & BERNARD, C. C. 2013. Nogo-receptor 1 deficiency has no influence on immune cell repertoire or function during experimental autoimmune encephalomyelitis. *PLoS One*, 8, e82101.
- LOH, Y., OYAMA, Y., STATKUTE, L., TRAYNOR, A., SATKUS, J., QUIGLEY, K., YAUNG, K., BARR, W., BUCHA, J., GHEORGHIADE, M. & BURT, R. K. 2007. Autologous hematopoietic stem cell transplantation in systemic lupus erythematosus patients with cardiac dysfunction: feasibility and reversibility of ventricular and valvular dysfunction with transplant-induced remission. *Bone Marrow Transplant*, 40, 47-53.
- LOVATO, L., WILLIS, S. N., RODIG, S. J., CARON, T., ALMENDINGER, S. E., HOWELL, O. W., REYNOLDS, R., O'CONNOR, K. C. & HAFLER, D. A. 2011. Related B cell clones populate the meninges and parenchyma of patients with multiple sclerosis. *Brain*, 134, 534-41.
- LYONS, J. A., SAN, M., HAPP, M. P. & CROSS, A. H. 1999. B cells are critical to induction of experimental allergic encephalomyelitis by protein but not by a short encephalitogenic peptide. *Eur J Immunol*, 29, 3432-9.
- MA, N., XIAO, H., MARRERO, B., XING, C., WANG, X., ZHENG, M., HAN, G., CHEN, G., HOU, C., SHEN, B., LI, Y., WANG, R. & JIANG, Z. 2014a. Combination of TACI-IgG and anti-IL-15 treats murine lupus by reducing mature and memory B cells. *Cell Immunol*, 289, 140-4.

- MA, N., XING, C., XIAO, H., HE, Y., HAN, G., CHEN, G., HOU, C., MARRERO, B., WANG, Y., ZHANG, S., SHEN, B., LI, Y. & WANG, R. 2014b. BAFF suppresses IL-15 expression in B cells. *J Immunol*, 192, 4192-201.
- MACKAY, F., WOODCOCK, S. A., LAWTON, P., AMBROSE, C., BAETSCHER, M., SCHNEIDER, P., TSCHOPP, J. & BROWNING, J. L. 1999. Mice transgenic for BAFF develop lymphocytic disorders along with autoimmune manifestations. *J Exp Med*, 190, 1697-710.
- MADER, S., GREGLER, V., SCHANDA, K., ROSTASY, K., DUJMOVIC, I., PFALLER, K., LUTTEROTTI, A., JARIUS, S., DI PAULI, F., KUENZ, B., EHLING, R., HEGEN, H., DEISENHAMMER, F., ABOUL-ENEIN, F., STORCH, M. K., KOSON, P., DRULOVIC, J., KRISTOFERITSCH, W., BERGER, T. & REINDL, M. 2011. Complement activating antibodies to myelin oligodendrocyte glycoprotein in neuromyelitis optica and related disorders. *J Neuroinflammation*, 8, 184.
- MAETZIG, T., BRUGMAN, M. H., BARTELS, S. & ET, A. L. 2011. Polyclonal fluctuation of lentiviral vector-transduced and expanded murine hematopoietic stem cells. *Blood*, 117, 3053-64.
- MAGLIOZZI, R., COLUMBA-CABEZAS, S., SERAFINI, B. & ALOISI, F. 2004. Intracerebral expression of CXCL13 and BAFF is accompanied by formation of lymphoid follicle-like structures in the meninges of mice with relapsing experimental autoimmune encephalomyelitis. *J Neuroimmunol*, 148, 11-23.
- MAGLIOZZI, R., HOWELL O, VORA A, SERAFINI B, NICHOLAS R, PUOPOLO M, ET AL 2007. Meningeal B-cell follicles in secondary progressive multiple sclerosis associate with early onset of disease and severe cortical pathology. *Brain*, 130, 1089-1104.
- MAGLIOZZI, R., HOWELL, O. W., REEVES, C., RONCAROLI, F., NICHOLAS, R., SERAFINI, B., ALOISI, F. & REYNOLDS, R. 2010. A Gradient of neuronal loss and meningeal inflammation in multiple sclerosis. *Ann Neurol*, 68, 477-93.
- MALONEY, D. G., LILES, T. M., CZERWINSKI, D. K., WALDICHUK, C., ROSENBERG, J., GRILLO-LOPEZ, A. & LEVY, R. 1994. Phase I clinical trial using escalating single-dose infusion of chimeric anti-CD20 monoclonal antibody (IDEC-C2B8) in patients with recurrent B-cell lymphoma. *Blood*, 84, 2457-66.
- MANCARDI, G. L., SORMANI, M. P., GUALANDI, F., SAIZ, A., CARRERAS, E., MERELLI, E., DONELLI, A., LUGARESI, A., DI BARTOLOMEO, P., ROTTOLI, M. R., RAMBALDI, A., AMATO, M. P., MASSACESI, L., DI GIOIA, M., VUOLO, L., CURRO, D., ROCCATAGLIATA, L., FILIPPI, M., AGUGLIA, U., IACOPINO, P., FARGE, D., SACCARDI, R., ASTIMS HAEMATO-NEUROLOGICAL COLLABORATIVE GROUP, O. B. O. T. A. D. W. P. O. T. E. G. F. B., MARROW, T., BLOOD, A. H.-N. C. G. O. B. O. T. A. D. W. P. A. O. T. E. G. F. & MARROW TRANSPLANTATION, E. 2015. Autologous hematopoietic stem cell transplantation in multiple sclerosis: a phase II trial. *Neurology*, 84, 981-8.
- MARTINEZ, N. E., SATO, F., OMURA, S., MINAGAR, A., ALEXANDER, J. S. & TSUNODA, I. 2012. Immunopathological patterns from EAE and Theiler's virus infection: Is multiple sclerosis a homogenous 1-stage or heterogenous 2-stage disease? *Pathophysiology*.

- MCDONALD, C. L., STEINBACH, K., KERN, F., SCHWEIGREITER, R., MARTIN, R., BANDTLOW, C. E. & REINDL, M. 2011. Nogo receptor is involved in the adhesion of dendritic cells to myelin. *J Neuroinflammation*, 8, 113.
- MCMAHON, E. J., BAILEY SL, CASTENADA CV, WALDNER H, MILLER SD 2005. Epitope spreading initiates in the CNS in two mouse models of multiple sclerosis. *Nat Med*, 11, 335-9.
- METZ, I., LUCCHINETTI, C. F., OPENSHAW, H., GARCIA-MERINO, A., LASSMANN, H., FREEDMAN, M. S., ATKINS, H. L., AZZARELLI, B., KOLAR, O. J. & BRUCK, W. 2007. Autologous haematopoietic stem cell transplantation fails to stop demyelination and neurodegeneration in multiple sclerosis. *Brain*, 130, 1254-62.
- MEUTH, S. G., HERRMANN, A. M., SIMON, O. J., SIFFRIN, V., MELZER, N., BITTNER, S., MEUTH, P., LANGER, H. F., HALLERMANN, S., BOLDAKOWA, N., HERZ, J., MUNSCH, T., LANDGRAF, P., AKTAS, O., HECKMANN, M., LESSMANN, V., BUDDE, T., KIESEIER, B. C., ZIPP, F. & WIENDL, H. 2009. Cytotoxic CD8+ T cell-neuron interactions: perforin-dependent electrical silencing precedes but is not causally linked to neuronal cell death. *J Neurosci*, 29, 15397-409.
- MI, S., HU, B., HAHM, K., LUO, Y., KAM HUI, E. S., YUAN, Q., WONG, W. M., WANG, L., SU, H., CHU, T. H., GUO, J., ZHANG, W., SO, K. F., PEPINSKY, B., SHAO, Z., GRAFF, C., GARBER, E., JUNG, V., WU, E. X. & WU, W. 2007. LINGO-1 antagonist promotes spinal cord remyelination and axonal integrity in MOG-induced experimental autoimmune encephalomyelitis. *Nat Med*, 13, 1228-33.
- MILLER, N. M., SHRIVER, L. P., BODIGA, V. L., RAY, A., BASU, S., AHUJA, R., JANA, A., PAHAN, K. & DITTEL, B. N. 2013. Lymphocytes with cytotoxic activity induce rapid microtubule axonal destabilization independently and before signs of neuronal death. *ASN Neuro*, 5, e00105.
- MIYOSHI, H., SMITH, K. A., MOSIER, D. E., VERMA, I. M. & TORBETT, B. E. 1999. Transduction of human CD34+ cells that mediate long-term engraftment of NOD/SCID mice by HIV vectors. *Science*, 283, 682-686.
- MOISINI, I. & DAVIDSON, A. 2009. BAFF: a local and systemic target in autoimmune diseases. *Clin Exp Immunol*, 158, 155-63.
- MOORE, P. A., BELVEDERE, O., ORR, A., PIERI, K., LAFLEUR, D. W., FENG, P., SOPPET, D., CHARTERS, M., GENTZ, R., PARMELEE, D., LI, Y., GALPERINA, O., GIRI, J., ROSCHKE, V., NARDELLI, B., CARRELL, J., SOSNOVTSEVA, S., GREENFIELD, W., RUBEN, S. M., OLSEN, H. S., FIKES, J. & HILBERT, D. M. 1999. BLyS: member of the tumor necrosis factor family and B lymphocyte stimulator. *Science*, 285, 260-3.
- MURARO, P. A., DOUEK, D. C., PACKER, A., CHUNG, K., GUENAGA, F. J., CASSIANI-INGONI, R., CAMPBELL, C., MEMON, S., NAGLE, J. W., HAKIM, F. T., GRESS, R. E., MCFARLAND, H. F., BURT, R. K. & MARTIN, R. 2005. Thymic output generates a new and diverse TCR repertoire after autologous stem cell transplantation in multiple sclerosis patients. *J Exp Med*, 201, 805-16.
- MYERS, K. J., SPRENT, J., DOUGHERTY, J. P. & RON, Y. 1992. Synergy between encephalitogenic T cells and myelin basic protein-specific antibodies in the induction of experimental autoimmune encephalomyelitis. *J Neuroimmunol*, 41, 1-8.

- NASH, R. A., HUTTON, G. J., RACKE, M. K., POPAT, U., DEVINE, S. M., GRIFFITH, L. M., MURARO, P. A., OPENSHAW, H., SAYRE, P. H., STUVE, O., ARNOLD, D. L., SPYCHALA, M. E., MCCONVILLE, K. C., HARRIS, K. M., PHIPPARD, D., GEORGES, G. E., WUNDES, A., KRAFT, G. H. & BOWEN, J. D. 2015. High-dose immunosuppressive therapy and autologous hematopoietic cell transplantation for relapsing-remitting multiple sclerosis (HALT-MS): a 3-year interim report. *JAMA Neurol.*, 72, 159-69.
- NESBETH, Y., SCARLETT, U., CUBILLOS-RUIZ, J., MARTINEZ, D., ENGLE, X., TURK, M. J. & CONEJO-GARCIA, J. R. 2009. CCL5-mediated endogenous antitumor immunity elicited by adoptively transferred lymphocytes and dendritic cell depletion. *Cancer Res*, 69, 6331-8.
- NG, L. G., SUTHERLAND, A. P., NEWTON, R., QIAN, F., CACHERO, T. G., SCOTT, M. L., THOMPSON, J. S., WHEWAY, J., CHTANOVA, T., GROOM, J., SUTTON, I. J., XIN, C., TANGYE, S. G., KALLED, S. L., MACKAY, F. & MACKAY, C. R. 2004. B cell-activating factor belonging to the TNF family (BAFF)-R is the principal BAFF receptor facilitating BAFF costimulation of circulating T and B cells. *J Immunol*, 173, 807-17.
- NIE, D. Y., ZHOU, Z. H., ANG, B. T., TENG, F. Y., XU, G., XIANG, T., WANG, C. Y., ZENG, L., TAKEDA, Y., XU, T. L., NG, Y. K., FAIVRE-SARRAILH, C., POPKO, B., LING, E. A., SCHACHNER, M., WATANABE, K., PALLEN, C. J., TANG, B. L. & XIAO, Z. C. 2003. Nogo-A at CNS paranodes is a ligand of Caspr: possible regulation of K(+) channel localization. *EMBO J*, 22, 5666-78.
- NITSCH, R., POHL, E. E., SMORODCHENKO, A., INFANTE-DUARTE, C., AKTAS, O. & ZIPP, F. 2004. Direct impact of T cells on neurons revealed by two-photon microscopy in living brain tissue. *J Neurosci*, 24, 2458-64.
- OPENSHAW, H., STUVE O, ANTEL JP, NASH R, LUND BT, WEINER LP, ET AL 2000. Multiple sclerosis flares associated with recombinant granulocyte colony-stimulating factor. *Neurology*, 54, 2147-50.
- PASHENKOV, M., SODERSTROM, M. & LINK, H. 2003. Secondary lymphoid organ chemokines are elevated in the cerebrospinal fluid during central nervous system inflammation. *J Neuroimmunol*, 135, 154-60.
- PASQUINI, M. C., VOLTARELLI, J., ATKINS, H. L., HAMERSCHLAK, N., ZHONG, X., AHN, K. W., SULLIVAN, K. M., CARRUM, G., ANDREY, J., BREDESON, C. N., CAIRO, M., GALE, R. P., HAHN, T., STOREK, J., HOROWITZ, M. M., MCSWEENEY, P. A., GRIFFITH, L. M., MURARO, P. A., PAVLETIC, S. Z. & NASH, R. A. 2012. Transplantation for autoimmune diseases in north and South America: a report of the Center for International Blood and Marrow Transplant Research. *Biol Blood Marrow Transplant.*, 18, 1471-8.
- PAYNE, N. L., SUN, G., HERSZFELD, D., TAT-GOH, P. A., VERMA, P. J., PARKINGTON, H. C., COLEMAN, H. A., TONTA, M. A., SIATSKAS, C. & BERNARD, C. C. 2012. Comparative study on the therapeutic potential of neurally differentiated stem cells in a mouse model of multiple sclerosis. *PLoS One*, 7, e35093.
- PEARCE, D. J. & BONNET, D. 2007. The combined use of Hoechst efflux ability and aldehyde dehydrogenase activity to identify murine and human hematopoietic stem cells. *Experimental Hematology*, 35, 1437-1446.

- PERNET, V. & SCHWAB, M. E. 2012. The role of Nogo-A in axonal plasticity, regrowth and repair. *Cell Tissue Res*, 349, 97-104.
- PETRATOS, S., AZARI, M. F., OZTURK, E., PAPADOPOULOS, R. & BERNARD, C. C. 2010. Novel therapeutic targets for axonal degeneration in multiple sclerosis. *J Neuropathol Exp Neurol*, 69, 323-34.
- PETRATOS, S., OZTURK, E., AZARI, M. F., KENNY, R., LEE, J. Y., MAGEE, K. A., HARVEY, A. R., MCDONALD, C., TAGHIAN, K. & MOUSSA, L. 2012. Limiting multiple sclerosis related axonopathy by blocking Nogo receptor and CRMP-2 phosphorylation. *Brain*, 135, 1794-1818.
- PFEIFER, A. 2004. Lentiviral transgenesis. *Transgenic research*, 13, 513-522.
- PIKOR, N. & GOMMERMAN, J. L. 2012. B cells in MS: Why, where and how? *Multiple Sclerosis and Related Disorders*, 1, 123-130.
- POOL, M., NIINO, M., RAMBALDI, I., ROBSON, K., BAR-OR, A. & FOURNIER, A. E. 2009. Myelin regulates immune cell adhesion and motility. *Experimental Neurology*, 217, 371-377.
- RAGHEB, S., LI, Y., SIMON, K., VANHAERENTS, S., GALIMBERTI, D., DE RIZ, M., FENOGLIO, C., SCARPINI, E. & LISAK, R. 2011. Multiple sclerosis: BAFF and CXCL13 in cerebrospinal fluid. *Mult Scler*, 17, 819-29.
- REBOLDI, A., COISNE, C., BAUMJOHANN, D., BENVENUTO, F., BOTTINELLI, D., LIRA, S., UCCELLI, A., LANZAVECCHIA, A., ENGELHARDT, B. & SALLUSTO, F. 2009. C-C chemokine receptor 6-regulated entry of TH-17 cells into the CNS through the choroid plexus is required for the initiation of EAE. *Nat Immunol*, 10, 514-23.
- REINDL, M., KHANTANE, S., EHLING, R., SCHANDA, K., LUTTEROTTI, A., BRINKHOFF, C., OERTLE, T., SCHWAB, M. E., DEISENHAMMER, F., BERGER, T. & BANDTLOW, C. E. 2003. Serum and cerebrospinal fluid antibodies to Nogo-A in patients with multiple sclerosis and acute neurological disorders. *Journal of Neuroimmunology*, 145, 139-147.
- REYNOLDS, R., DAWSON, M., PAPADOPOULOS, D., POLITO, A., DI BELLO, I. C., PHAM-DINH, D. & LEVINE, J. 2002. The response of NG2-expressing oligodendrocyte progenitors to demyelination in MOG-EAE and MS. *J Neurocytol*, 31, 523-36.
- SACCARDI, R., KOZAK, T., BOCELLI-TYNDALL, C., FASSAS, A., KAZIS, A., HAVRDOVA, E., CARRERAS, E., SAIZ, A., LOWENBERG, B., TE BOEKHORST, P. A., GUALANDIO, F., OPENSHAW, H., LONGO, G., PAGLIAI, F., MASSACESI, L., DECONINK, E., OUYANG, J., NAGORE, F. J., BESALDUCH, J., LISUKOV, I. A., BONINI, A., MERELLI, E., SLAVINO, S., GRATWOHL, A., PASSWEG, J., TYNDALL, A., STECK, A. J., ANDOLINA, M., CAPOBIANCO, M., MARTIN, J. L., LUGARESI, A., MEUCCI, G., SAEZ, R. A., CLARK, R. E., FERNANDEZ, M. N., FOUILLARD, L., HERSTENSTEIN, B., KOZA, V., COCCO, E., BAURMANN, H., MANCARDI, G. L. & AUTOIMMUNE DISEASES WORKING PARTY OF, E. 2006. Autologous stem cell transplantation for progressive multiple sclerosis: update of the European Group for Blood and Marrow Transplantation autoimmune diseases working party database. *Mult Scler*, 12, 814-23.
- SADABA, M. C., TZARTOS, J., PAINO, C., GARCIA-VILLANUEVA, M., ALVAREZ-CERMENO, J. C., VILLAR, L. M. & ESIRI, M. M. 2012. Axonal and

- oligodendrocyte-localized IgM and IgG deposits in MS lesions. *J Neuroimmunol*, 247, 86-94.
- SAINAGHI PP, C. L., ALCIATO F, ET AL 2013. Growth arrest specific gene 6 protein concentration in cerebrospinal fluid correlates with relapse severity in multiple sclerosis. *Mediators Inflamm*, 2013, 406483.
- SAIZ, A., CARRERAS, E., BERENQUER, J., YAGUE, J., MARTINEZ, C., MARIN, P., ROVIRA, M., PUJOL, T., ARBIZU, T. & GRAUS, F. 2001. MRI and CSF oligoclonal bands after autologous hematopoietic stem cell transplantation in MS. *Neurology*, 56, 1084-9.
- SASAKI, Y., CASOLA, S., KUTOK, J. L., RAJEWSKY, K. & SCHMIDT-SUPPRIAN, M. 2004. TNF family member B cell-activating factor (BAFF) receptor-dependent and -independent roles for BAFF in B cell physiology. *J Immunol*, 173, 2245-52.
- SATO, J., TABUNOKI, H., YAMAMURA, T., ARIMA, K. & KONNO, H. 2007. TROY and LINGO-1 expression in astrocytes and macrophages/microglia in multiple sclerosis lesions. *Neuropathol Appl Neurobiol*, 33, 99-107.
- SCHIEGMANN, B., GOMMERMAN, J. L., VORA, K., CACHERO, T. G., SHULGA-MORSKAYA, S., DOBLES, M., FREW, E. & SCOTT, M. L. 2001. An essential role for BAFF in the normal development of B cells through a BCMA-independent pathway. *Science*, 293, 2111-4.
- SCHNEIDER, P., MACKAY, F., STEINER, V., HOFMANN, K., BODMER, J. L., HOLLER, N., AMBROSE, C., LAWTON, P., BIXLER, S., ACHA-ORBEA, H., VALMORI, D., ROMERO, P., WERNER-FAVRE, C., ZUBLER, R. H., BROWNING, J. L. & TSCHOPP, J. 1999. BAFF, a novel ligand of the tumor necrosis factor family, stimulates B cell growth. *J Exp Med*, 189, 1747-56.
- SCHWAB, M. E. 2004. Nogo and axon regeneration. *Curr Opin Neurobiol*, 14, 118-24.
- SCOLDING, N. 2011. Adult stem cells and multiple sclerosis. *Cell Prolif*, 44 Suppl 1, 35-8.
- SERAFINI, B., ROSICARELLI, B., MAGLIOZZI, R., STIGLIANO, E. & ALOISI, F. 2004. Detection of ectopic B-cell follicles with germinal centers in the meninges of patients with secondary progressive multiple sclerosis. *Brain Pathol*, 14, 164-74.
- SHEVCHENKO, J. L., KUZNETSOV, A. N., IONOVA, T. I., MELNICHENKO, V. Y., FEDORENKO, D. A., KURBATOVA, K. A., GORODOKIN, G. I. & NOVIK, A. A. 2015. Long-term outcomes of autologous hematopoietic stem cell transplantation with reduced-intensity conditioning in multiple sclerosis: physician's and patient's perspectives. *Ann Hematol*, 94, 1149-57.
- SKULINA, C., SCHMIDT, S., DORNMAIR, K., BABBE, H., ROERS, A., RAJEWSKY, K., WEKERLE, H., HOHLFELD, R. & GOEBELS, N. 2004. Multiple sclerosis: brain-infiltrating CD8+ T cells persist as clonal expansions in the cerebrospinal fluid and blood. *Proc Natl Acad Sci U S A*, 101, 2428-33.
- SORENSEN, P. S. & BLINKENBERG, M. 2016. The potential role for ocrelizumab in the treatment of multiple sclerosis: current evidence and future prospects. *Ther Adv Neurol Disord*, 9, 44-52.
- STEINBACH, K., MCDONALD, C. L., REINDL, M., SCHWEIGREITER, R., BANDTLOW, C. & MARTIN, R. 2011. Nogo-receptors Ngr1 and Ngr2 do not mediate

- regulation of CD4 T helper responses and CNS repair in experimental autoimmune encephalomyelitis. *PLoS One*, 6, e26341.
- SUREDA, A., BADER, P., CESARO, S., DREGER, P., DUARTE, R. F., DUFOUR, C., FALKENBURG, J. H., FARGE-BANCEL, D., GENNERY, A., KROGER, N., LANZA, F., MARSH, J. C., NAGLER, A., PETERS, C., VELARDI, A., MOHTY, M. & MADRIGAL, A. 2015. Indications for allo- and auto-SCT for haematological diseases, solid tumours and immune disorders: current practice in Europe, 2015. *Bone Marrow Transplant.*, 50, 1037-56.
- SVENSSON, L., ABDUL-MAJID, K. B., BAUER, J., LASSMANN, H., HARRIS, R. A. & HOLMDAHL, R. 2002. A comparative analysis of B cell-mediated myelin oligodendrocyte glycoprotein-experimental autoimmune encephalomyelitis pathogenesis in B cell-deficient mice reveals an effect on demyelination. *Eur J Immunol*, 32, 1939-46.
- TEUSCHER, C., BUNN, J. Y., FILLMORE, P. D., BUTTERFIELD, R. J., ZACHARY, J. F. & BLANKENHORN, E. P. 2004. Gender, age, and season at immunization uniquely influence the genetic control of susceptibility to histopathological lesions and clinical signs of experimental allergic encephalomyelitis: implications for the genetics of multiple sclerosis. *Am J Pathol*, 165, 1593-602.
- THEOTOKIS, P., LOURBOPOULOS, A., TOULOUMI, O., LAGOUDAKI, R., KOFIDOU, E., NOUSIOPOULOU, E., POULATSIDOU, K. N., KESIDOU, E., TASCOS, N., SPANDOU, E. & GRIGORIADIS, N. 2012. Time course and spatial profile of Nogo-A expression in experimental autoimmune encephalomyelitis in C57BL/6 mice. *J Neuropathol Exp Neurol*, 71, 907-20.
- THOMPSON, J. S., BIXLER, S. A., QIAN, F., VORA, K., SCOTT, M. L., CACHERO, T. G., HESSION, C., SCHNEIDER, P., SIZING, I. D., MULLEN, C., STRAUCH, K., ZAFARI, M., BENJAMIN, C. D., TSCHOPP, J., BROWNING, J. L. & AMBROSE, C. 2001. BAFF-R, a newly identified TNF receptor that specifically interacts with BAFF. *Science*, 293, 2108-11.
- THOMPSON, J. S., SCHNEIDER, P., KALLED, S. L., WANG, L., LEFEVRE, E. A., CACHERO, T. G., MACKAY, F., BIXLER, S. A., ZAFARI, M., LIU, Z. Y., WOODCOCK, S. A., QIAN, F., BATTEN, M., MADRY, C., RICHARD, Y., BENJAMIN, C. D., BROWNING, J. L., TSAPIS, A., TSCHOPP, J. & AMBROSE, C. 2000. BAFF binds to the tumor necrosis factor receptor-like molecule B cell maturation antigen and is important for maintaining the peripheral B cell population. *J Exp Med*, 192, 129-35.
- THOMPSON, S. A., JONES, J. L., COX, A. L., COMPSTON, D. A. & COLES, A. J. 2010. B-cell reconstitution and BAFF after alemtuzumab (Campath-1H) treatment of multiple sclerosis. *J Clin Immunol*, 30, 99-105.
- TSIFTSOGLOU, A. S., BONOVOLIAS, I. D. & TSIFTSOGLOU, S. A. 2009. Multilevel targeting of hematopoietic stem cell self-renewal, differentiation and apoptosis for leukemia therapy. *Pharmacol Ther.*, 122, 264-280.
- VAKNIN-DEMBINSKY, A., BRILL, L., ORPAZ, N., ABRAMSKY, O. & KARUSSIS, D. 2010. Preferential increase of B-cell activating factor in the cerebrospinal fluid of neuromyelitis optica in a white population. *Mult Scler*, 16, 1453-7.

- VAN BEKKUM, D. 2004. Stem cell transplantation for autoimmune disorders. Preclinical experiments. *Best Pract Res Clin Haematol.*, 17, 201-22.
- VAN GELDER M & VAN BEKKUM DW. 1996. Effective treatment of relapsing experimental autoimmune encephalomyelitis with pseudoautologous bone marrow transplantation. *Bone Marrow Transplant.*, 18, 1029-34.
- VAN WIJMEERSCH, B., SPRANGERS, B., DUBOIS, B., WAER, M. & BILLIAU, A. D. 2008. Autologous and allogeneic hematopoietic stem cell transplantation for Multiple Sclerosis: Perspective on mechanisms of action. *J Neuroimmunol.*, 197, 89-98.
- VILLAR, L. M., ESPINO, M., CAVANILLAS, M. L., ROLDAN, E., URCELAY, E., DE LA CONCHA, E. G., SADABA, M. C., ARROYO, R., GONZALEZ-PORQUE, P. & ALVAREZ-CERMENO, J. C. 2010. Immunological mechanisms that associate with oligoclonal IgM band synthesis in multiple sclerosis. *Clin Immunol.*, 137, 51-9.
- VON BUDINGEN, H. C., BAR-OR, A. & ZAMVIL, S. S. 2011. B cells in multiple sclerosis: connecting the dots. *Curr Opin Immunol*, 23, 713-20.
- VON BÜDINGEN, H. C., KUO, T. C., SIROTA, M., VAN BELLE, C. J., APELTSIN, L., GLANVILLE, J., CREE, B. A., GOURRAUD, P. A., SCHWARTZBURG, A., HUERTA, G., TELMAN, D., SUNDAR, P. D., CASEY, T., COX, D. R. & HAUSER, S. L. 2012. B cell exchange across the blood-brain barrier in multiple sclerosis. *Journal of Clinical Investigation*, 122, 4533-4543.
- VOSOUGHI, R. & FREEDMAN, M. S. 2010. Therapy of MS. *Clin Neurol Neurosurg.* , 112, 365-385.
- WANG, T., ALLIE, R., CONANT, K., HAUGHEY, N., TURCHAN-CHELOWO, J., HAHN, K., ROSEN, A., STEINER, J., KESWANI, S., JONES, M., CALABRESI, P. A. & NATH, A. 2006a. Granzyme B mediates neurotoxicity through a G-protein-coupled receptor. *FASEB J*, 20, 1209-11.
- WANG, T., LEE, M. H., CHOI, E., PARDO-VILLAMIZAR, C. A., LEE, S. B., YANG, I. H., CALABRESI, P. A. & NATH, A. 2012. Granzyme B-induced neurotoxicity is mediated via activation of PAR-1 receptor and Kv1.3 channel. *PLoS One*, 7, e43950.
- WANG, X., BAUGHMAN, K. W., BASSO, D. M. & STRITTMATTER, S. M. 2006b. Delayed Nogo receptor therapy improves recovery from spinal cord contusion. *Ann Neurol*, 60, 540-9.
- WANG, X., DUFFY, P., MCGEE, A. W., HASAN, O., GOULD, G., TU, N., HAREL, N. Y., HUANG, Y., CARSON, R. E. & WEINZIMMER, D. 2011. Recovery from chronic spinal cord contusion after Nogo receptor intervention. *Annals of neurology*, 70, 805-821.
- WANG, X., XIAO, H., WEI, Y., LIU, X., HAN, G., CHEN, G., HOU, C., SHEN, B., LI, Y. & WANG, R. 2015. Blockade of B-cell activating factor with TACI-IgG effectively reduced Th1 and Th17 cells but not memory T cells in experimental allergic encephalomyelitis mice. *Cent Eur J Immunol*, 40, 142-8.
- WATERHOUSE, N. J., SUTTON, V. R., SEDELIES, K. A., CICCONE, A., JENKINS, M., TURNER, S. J., BIRD, P. I. & TRAPANI, J. A. 2006. Cytotoxic T lymphocyte-induced killing in the absence of granzymes A and B is unique and distinct from both apoptosis and perforin-dependent lysis. *J Cell Biol*, 173, 133-44.

- WEBER, M. S. & HEMMER, B. 2010. Cooperation of B cells and T cells in the pathogenesis of multiple sclerosis.
- WEBER, M. S., PROD'HOMME, T., PATARROYO, J. C., MOLNARFI, N., KARNEZIS, T., LEHMANN-HORN, K., DANILENKO, D. M., EASTHAM-ANDERSON, J., SLAVIN, A. J., LININGTON, C., BERNARD, C. C., MARTIN, F. & ZAMVIL, S. S. 2010. B-cell activation influences T-cell polarization and outcome of anti-CD20 B-cell depletion in central nervous system autoimmunity. *Ann Neurol*, 68, 369-83.
- WEINSHENKER, B. G., BASS, B., RICE, G. P., NOSEWORTHY, J., CARRIERE, W., BASKERVILLE, J. & EBERS, G. C. 1989. The natural history of multiple sclerosis: a geographically based study. I. Clinical course and disability. *Brain*, 112 (Pt 1), 133-46.
- WOGNUM, A. W., EAVES, A. C. & THOMAS, T. E. 2003. Identification and isolation of hematopoietic stem cells. *Arch Med Res*, 34, 461-75.
- XU, B., HAVIERNIK, P., WOLFRAIM, L. A., BUNTING, K. D. & SCOTT, D. W. 2006. Bone marrow transplantation combined with gene therapy to induce antigen-specific tolerance and ameliorate EAE. *Molecular Therapy*, 13, 42-48.
- YANG, Y., LIU, Y., WEI, P., PENG, H., WINGER, R., HUSSAIN, R. Z., BEN, L. H., CRAVENS, P. D., GOCKE, A. R., PUTTAPARTHI, K., RACKE, M. K., MCTIGUE, D. M. & LOVETT-RACKE, A. E. 2010. Silencing Nogo-A promotes functional recovery in demyelinating disease. *Ann Neurol*, 67, 498-507.
- YANG, Y., LIU, Y., WEI, P., PENG, H., WINGER, R., HUSSAIN, RZ, ET AL 2010. Silencing Nogo-A promotes functional recovery in demyelinating disease. *Ann Neurol*, 67, 498-50.
- ZHANG, L., KUANG, X. & ZHANG, J. 2011. Nogo receptor 3, a paralog of Nogo-66 receptor 1 (NgR1), may function as a NgR1 co-receptor for Nogo-66. *J Genet Genomics*, 38, 515-23.
- ZHANG, L., ZHENG, S., WU, H., WU, Y., LIU, S., FAN, M. & ZHANG, J. 2009. Identification of BLYS (B Lymphocyte Stimulator), a non-myelin-associated protein, as a functional ligand for Nogo-66 receptor. *Journal of Neuroscience*, 29, 6348-6352.
- ZHOU, X., XIA, Z., LAN, Q., WANG, J., SU, W., HAN, Y. P., FAN, H., LIU, Z., STOHL, W. & ZHENG, S. G. 2011. BAFF promotes Th17 cells and aggravates experimental autoimmune encephalomyelitis. *PLoS One*, 6, e23629.

Appendix 1

Table 8. Reagents and their preparations.

Name	Ingredients
4% Paraformaldehyde (PFA) (in Hood)	20g PFA 250mL dH ₂ O 10 drops 1M NaOH until clear 250 mL 0.2M phosphate buffer 1.2g NaH ₂ PO ₄ .H ₂ O 6.5g Na ₂ HPO ₄ .2H ₂ O store at 4°C
Fluorescence Activated Cell Sorting (FACS) wash	500mL of 1XPBS 1mL of 10% sodium Azide (10g sodium azide in 100mL PBS, in hood) 5mL of 10% BSA (10g BSA and 100 mL dH ₂ O) store at 4°C
Fluorescence Activated Cell Sorting (FACS) wash for cell culture	500mL of DPBS 2% of FCS (Heat inactivate at 55-65°C for 45-1 hours) store at 4°C
10X Phosphate Buffered Saline (PBS) pH7.4	160g NaCL 4g KCL 4.8g KH ₂ PO ₄ 23g Na ₂ HPO ₄ .2H ₂ O top up to 1600mL dH ₂ O (2L) store at room temperature
20X MOPS	1M MOPS (104.6g) 1M Tris base (60.6g) 2% w/v SDS (10g) 20mM EDTA (3g) omit if using Bolt system from life tech pH should be ~ 7.7 (do not adjust pH) Filter store at room temperature
Western blot running Buffer	47.5 mL Nupage MOPS SDS running buffer (Life technology) 2.4 antioxidant 902.5 dH ₂ O store at room temperature

10X Western transfer buffer	30g Tris 148g Glycine 1L M.H ₂ O store at room temperature
10X Tris Buffered Saline Tween (TBST) pH7.4	12.1g tris 88g NaCl 5mL Tween20 1L M.H ₂ O. store at room temperature
Stripping Buffer pH6.8	2.5 mM Tris (0.3g) 2% SDS (20g) make up to 1L M.H ₂ O store at room temperature
Coomassie blue dye	2g coomassie blue in 250mL dH ₂ O add slowly 75mL of glacial acetic acid 500mL ethanol top up to 1000 mL dH ₂ O store at room temperature
De-stain for Coomassie blue dye	200mL of 20% methanol 100mL of 10% acetic acid 700mL dH ₂ O store at room temperature
Western blot blocking buffer (5% skim milk) pH7.4	2.5g of skim milk powder 50mL of 1X TBST
Immunohistochemistry blocking buffer	5% FBS 5% normal goat serum 0.1% triton X 50 mL 1X PBS
50X TAE	121g of 2M Tris base 28.55mL 1M glacial acetic acid 9.3g of 50mM disodium EDTA Make up to 500ml with dH ₂ O The pH of this buffer was not adjusted. Dilute 1:50. store at room temperature
10X Agarose gel	10g agarose powder 100mL 1X TAE
Recombinant Myelin oligodendrocyte Glycoprotein (rMOG) Purification	rMOG was produced in the Escherichia coli strain DH5alpha using the pQE9 expression vector (QIAGEN) load Bacterial lysate containing rMOG onto a Ni-NTA Superflow column (QIAGEN) under denaturing conditions (6M Guanidine-HCl, 20 mM Tris, 500 mM NaCl, 5 mM Imidazole, pH 8.0)

Appendix 2

Table 9. rMOG purification.

Name	Ingredients
<p>Purification of Recombinant MOG</p>	<p>The extracellular domain of rMOG was produced in the <i>Escherichia coli</i> (<i>E.coli</i>) strain DH5alpha using the pQE9 expression vector (QIAGEN). A clarified bacterial lysate containing rMOG was loaded onto a Ni-NTA Superflow column (QIAGEN) under denaturing conditions (6 M Guanidine-HCl, 20 mM Tris, 500 mM NaCl, 5 mM Imidazole, pH 8.0) using a BioLogic LP chromatography system (BioRad). Bound protein was then washed sequentially with Buffer A (8M Urea, 100 mM NaH₂PO₄, 10 mM Tris) at different pH levels (8.0, 6.3, and 8.0) before it was finally washed with Buffer B (10 mM Tris-Cl, pH 8). The protein was washed by alternating between Buffer C (60% iso-propanol/ 10 mM Tris-Cl, pH 8) and Buffer B (2x) to remove endotoxin. Buffer A was then used again to wash the protein. A linear gradient of Buffer A, which included 14 mM 2-mercaptoethanol (100%–0%) against Buffer D (100 mM NaH₂PO₄, 10 mM Tris, pH 8.0, 1 mM reduced glutathione, 0.1 mM oxidised glutathione) (0%–100%) was used to carry out of refolding of the bound protein. Following this step, a</p>

second linear gradient of Buffer D (100%–0%) against Buffer E (100 mM NaH₂PO₄, 10 mM Tris, pH 8.0) (0%–100%) was used. Buffer E, which contained 300 mM Imidazole, was used to elute the bound protein; the buffer was then extensively dialysed over 72 hours against 200 mM NaCl/10 mM Tris, pH 8.0. The purity and protein concentration were assessed using an A280 nm measurement and SDS-PAGE, respectively. The protein produced was verified as rMOG by western blotting, using antibodies specific for native MOG (Payne et al., 2012).